REPORT NO. CASD-NSC-75-002
CONTRACT NAS9-14095
NASA CR-
144519

SPACE SHUTTLE ORBITER REACTION CONTROL SYSTEM JET INTERACTION STUDY

FINAL REPORT

GENERAL DYNAMICS
Convair Division

FOREWORD

The present study was undertaken by the Convair Division of General Dynamics under NASA contract NAS9-14095 and this report covers work undertaken from 15 June 1974 through 15 June 1975. The contract monitor was Mr. Barney Roberts of the NASA Johnson Space Center, Houston, Texas and the author wishes to acknowledge his very valuable assistance, direction and contributions to the successful completion of this study. The OA82 test data used in this program was generated in the NASA Langley Research Center CFHT hypersonic tunnel under the capable direction of Mr. Tom Blackstock to whom we wish to express our appreciation for his interest in and thorough efforts toward obtaining precise data required in this study.

TABLE OF CONTENTS

TABLE OF CONTENTS (Cont'd)

TABLE OF CONTENTS (Cont'd)

LIST OF FIGURES

LIST OF FIGURES (Cont'd)

LIST OF FIGURES (Cont'd)

LIST OF FIGURES (Cont'd)

LIST OF FIGURES (Cont'd)

LIST OF TABLES

NOMENCLATURE

Symbol	Definition
A	area (ft^2)
b	lateral-directional reference length (ft)
$\bar{c}$	wing chord reference length (ft)
C_ℓ	body axis rolling moment coefficient = (rolling moment)/$q\, S_{ref}\, b$
C_m	body axis pitching moment coefficient = (pitching moment)/$q\, s_{ref}\, \bar{c}$
C_N	body axis normal force coefficient = (normal force)/$q\, S_{ref}$
C_n	body axis yaw moment coefficient = (yawing moment)/$q\, S_{ref}\, b$
C_P	pressure coefficient = $(P - P_\infty)/q$
C_t	thrust coefficient = $T/q\, S_{ref}$
C_y	body axis side force coefficient = (side force)/$q\, S_{ref}$
d	diameter (ft)
h	kinetic energy parameter (ft^2/sec^2)
K	force or moment amplification factor
ℓ_{ref}	longitudinal reference length (ft)
ℓ_B	body length (ft)
$\dot{m}$	mass flow (lbm/sec)
M	Mach number
n	number of jets in cluster
P	pressure (lbf/ft^2)
q	dynamic pressure (lbf/ft^2)
R	gas constant (ft^2/sec^2-°R)
r	radius (ft)
R_e	Reynolds number
S_{ref}	wing reference area (ft^2)
t	time (sec)

NOMENCLATURE (cont'd)

Symbol	Definition
T	thrust (lb)
T	temperature (°R)
V	velocity (ft/sec)
x	radial distance (ft)
α	angle of attack (deg)
β	angle of yaw (deg); also $\sqrt{M^2 - 1}$
θ_N	nozzle angle (deg)
θ	angular orientation in jet (deg)
ρ	density (lbm/ft^3)
γ	ratio of specific heat
Φ	momentum parameter (lbf) = $\gamma P M^2 A$
Subscripts	
amb	ambient conditions
c	rocket chamber condition
i	initial condition or conditions at point i
j	jet exit conditions
ℓ	local condition or rolling moment
MAC	mean aerodynamic chord
M	any force or moment coefficient
m	pitching moment
n	yawing moment
N	normal force
o	total conditions
y	side force
p	peak
∞	free stream condition
interaction	increment due to plume interaction

Symbol	Definition
Subscripts (cont'd)	
impingement	increment due to plume impingement
cross coupling	increment due to combined jets interacting
thrust	thrust terms
total	sum of all terms
Superscripts	
$\bar{}$	mean value or averaged value
*	throat condition

SUMMARY

This report is the final technical report and documents the work performed through 15 June 1975 under NASA Contract NAS9-14095.

The space shuttle orbiter has forward mounted and rear mounted Reaction Control Systems (RCS) which are used for orbital maneuvering and also provide control during entry and abort maneuvers in the atmosphere. RCS control effectiveness is critical to orbiter flight performance and safety. The effects of interaction between the RCS jets and the flow over the vehicle in the atmosphere is the subject of this study. This report presents the analysis of test data obtained in the NASA Langley Research Center 31 inch continuous flow hypersonic tunnel at a nominal Mach number of 10.3. The data was obtained with a 0.01 scale force model with aft mounted RCS nozzles mounted on the sting off of the force model balance. The plume simulations were accomplished primarily using air in a cold gas simulation through scaled nozzles, however, various cold gas mixtures of Helium and Argon were also tested to obtain (RT) ratio effects. The effect of number of nozzles was tested as were limited tests of combined controls.

The data shows that RCS nozzle exit momentum ratio is the primary correlating parameter for effects where the plume impinges on an adjacent surface and mass flow ratio is the parameter where the plume interaction is primarily with the external stream. An analytic model of aft mounted RCS units was developed in which the total reaction control moments are the sum of thrust, impingement, interaction, and cross-coupling terms.

1

INTRODUCTION

The space shuttle orbiter has two reaction controls systems (RCS), as shown in Figure 1-1, which are used for orbital maneuvering . The rear RCS provides control during entry until the aerodynamic surfaces have sufficient effectiveness to assume full control of the vehicle as shown in Figure 1-2. Both the front and rear RCS units are also used during abort maneuvers to separate the orbiter from the tank, to pitch it to entry attitude, and to control it until aerodynamic control is established. Thus RCS control effectiveness is critical to the space shuttle orbiter flight performance and safety.

The study performed in reference 1 and wind tunnel data on the present baseline orbiter have shown that the control effectiveness of the RCS system is appreciably changed by the presence of air flow over and around the vehicle. These RCS - flow interactions have acted in directions such that the net RCS system effectiveness is much lower than the thrust moments alone and it is critical to flight safety and performance to know what the induced RCS - flow interaction moments are caused by and to develop methods to predict them. These are the basic purposes of this study conducted under NASA contract NAS9-14095. This report is the final report of this contract and documents the data analysis and analytic model development for RCS flow interference prediction. The data used for these analyses came principally from the space shuttle orbiter test designated OA82 which was documented in the interim technical report (reference 2) of this contract. These data were obtained from tests conducted by Rockwell International personnel within NASA test facilities, primarily the NASA-LRC 31 inch continuous flow hypersonic tunnel (CFHT) at a nominal Mach number of 10.3. The data was obtained primarily with a 0.010 scale force model with the RCS nozzles mounted on the sting of the force model balance. The plume simulations were accomplished primarily using air in a cold gas simulation through scaled nozzles, however, various cold gas mixtures of Helium and Argon were also tested to obtain (RT) ratio effects. The effect of number of nozzles was tested as were limited tests of combined controls.

The thermal analysis task was also documented in the interim report (reference 2) and will not be presented in this report.

This report will concentrate primarily on the data analyses and analytic model development and contains 5 parts:

a) Test Data Summary
b) Data Analysis
c) Analytic Model Development
d) Representative Full Scale Results
e) Study Conclusions

The data presented in this report is data for the aft RCS unit only. No test data has been obtained on forward RCS unit effectiveness at the time of preparation of this report.

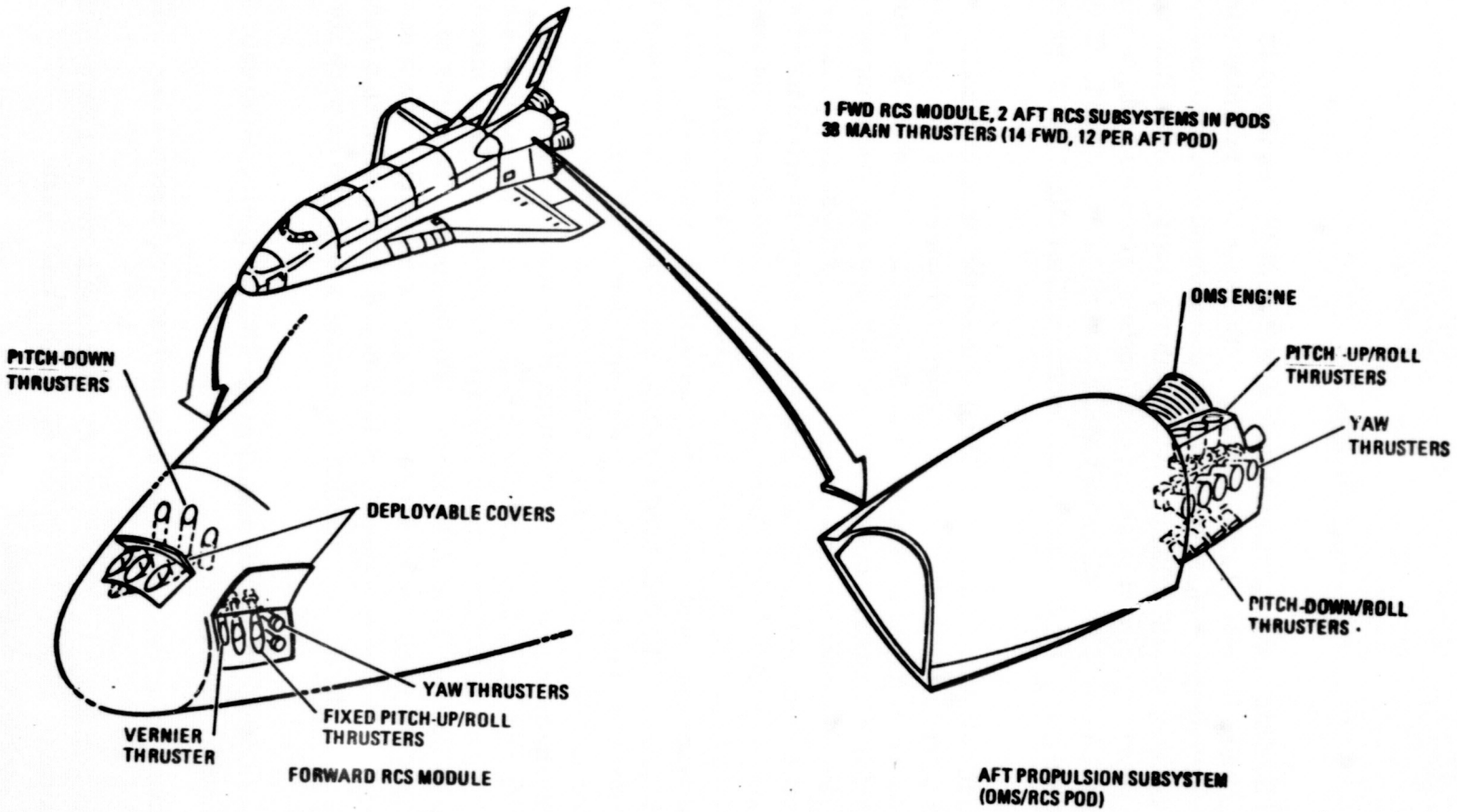

Figure 1-1. Reaction Control Systems on Space Shuttle Orbiter

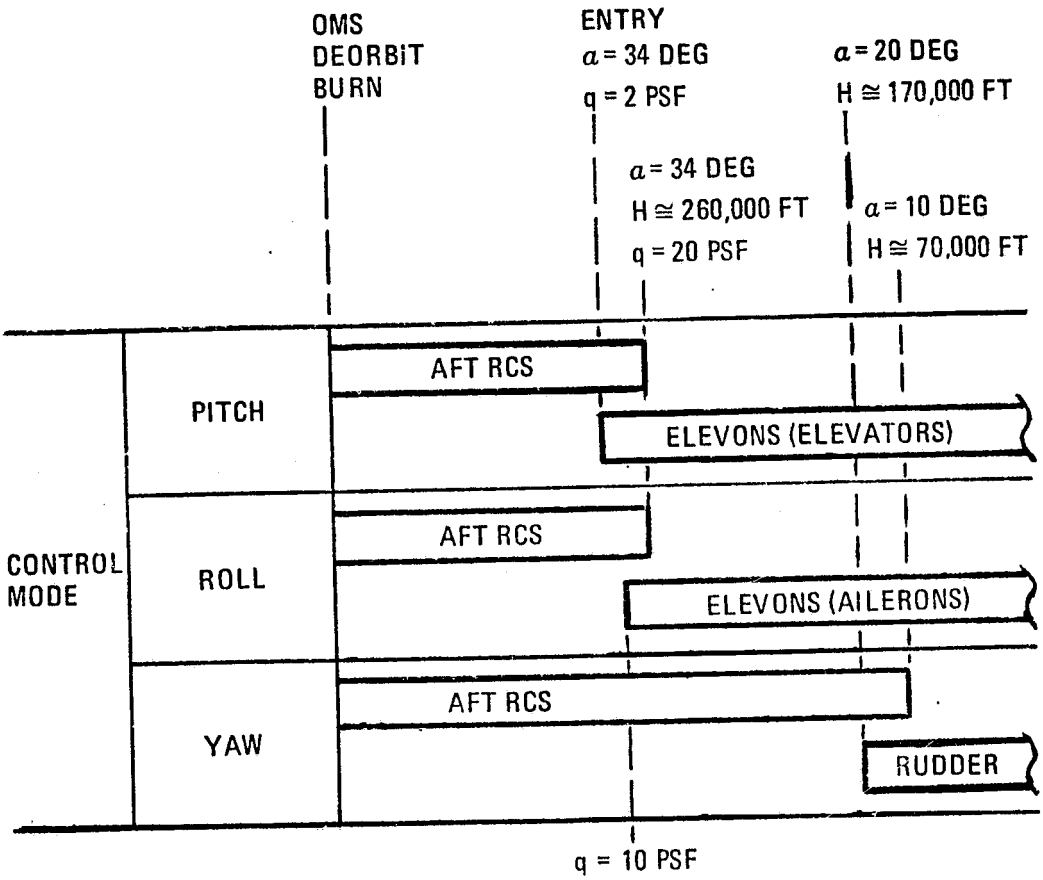

Figure 1-2. Aft RCS Operation During Entry

2

TEST SUMMARY

2.1 REAR MOUNTED RCS DATA BASE

Data from all rear mounted RCS tests was provided to Convair by NASA-JSC for compilation and analysis under this contract. This rear mounted RCS data base represents 10 tests as summarized in table 1. The PRR configuration data was obtained by General Dynamics/Convair in the test program reported in reference 1 and all of the remaining test data has been obtained in tests conducted by Rockwell International as part of the space shuttle orbiter development and the data for each test has been or will be reported in the DATAMAN reporting system for the shuttle. The OA82 test data documented in reference 2 is the principal source of data used in this study.

2.2 TEST MODEL AND RCS NOZZLES

Figure 2-1 presents the 139B orbiter configuration used in these tests. The model was a 0.010 scale model constructed from aluminum. The model was attached to a force balance mounted on a sting up through the base of the model as shown in Figure 2-2. The plenum chamber and nozzle block assembly was also mounted on the sting close to the base of the model but not attached to it. Thus the force balance measured model forces and moments and the loads induced by RCS operation but not the RCS jet moments. Grounding strips were mounted in the gap between the plenum and the model to insure that the model did not ground on the nozzles during the tests.

A number of different nozzles were used throughout the tests and tables 2 to 4 present the nozzle code numbers and a brief summary of the nozzle characteristics. All nozzles were tested using cold gas supplies located external to the tunnel and piped in through a pressure regulation system which was used to control the pressure in the plenum chamber manually during a tunnel data run. The pressure in the plenum chamber was measured by a pressure tap in the chamber connected to a pressure transducer mounted externally to the tunnel in most tests. The test gas used was air for all tests except for 12 runs on test OA82 where helium and Argon mixtures were used to vary the gas constant (R) of the test gas.

2.3 REFERENCE DIMENSIONS

All data used in the analysis was reduced to common reference dimensions using the orbiter wing area as the reference area, the wing mean aerodynamics chord ($\bar{c}$) as the longitudinal reference length, and the wing span (b) as the lateral-directional reference length. The model scale for all tests but OA73 was .010 and the scale dimensions are:

$$S_{ref} = S_{wing} = 0.02499 \text{ Meters}^2 \ (0.269 \text{ Ft}^2)$$

$$\ell_{ref} = \bar{c} = 12.06 \text{ cm } (4.748 \text{ in})$$

$$b_{ref} = b = 23.79 \text{ cm } (9.367 \text{ in})$$

The moment reference center used for all model data reduction is located at 65% of the body length aft of the nose (full scale station 1076.7) on the fuselage reference line (full scale waterline 400). In .010 model scale

X_{CG} = 21.303 cm (8.387 in) from nose

Y_{CG} = 0

Z_{CG} = 10.160 cm (4.0 in) from bottom reference plane

2.4 OA82 TEST PROGRAM SUMMARY

The aft RCS test designated OA82 was perfomed at the NASA Langley Research Center Continous Flow Hypersonic Tunnel (CFHT) where it carried the test number CFHT113. The test was performed at a nominal Mach number of 10.3 using a .01 scale model of 139B orbiter to obtain 6 component force and moment data using a cold gas simulation of the RCS exhaust flow. The major test variables included:

a) tunnel dynamic pressure (q = 75, 100, 125, 150, 200 PSIA)

b) RCS chamber pressure (P_{oj} = 0 to 700 PSIA)

c) test gas (air, He, Argon, .85 He.15A, .90 He.10A)

d) RCS control direction (pitch down N_{49}, pitch up N_{52}, yaw N_{84})

e) number of RCS nozzles

I	Pitch down	1,2,3
II	Pitch up	1,2,3
III	Yaw	2,4

All aerodynamic control surfaces were kept at zero degree deflection throughout the test.

Reference 3 presents the error analysis performed on the PRR configuration data generated in the Unitary Plan Wind Tunnel at NASA-Langley Research Center. This data showed the advantages of obtaining repeat runs for the RCS off data in order to obtain a mean value for computing induced jet effects. A similar approach was taken during test OA82 where 6 repeat jet-off runs were obtained at a tunnel dynamic pressure (q_∞) of 150 PSF and 4 repeat runs were obtained at q_∞ of 125 PSF. These data were used to generate mean value jet-off coefficients for the two dynamic pressures by selecting a base run and interpolating the 6 component data from all the other jet-off repeat runs to the base run angle of attack. The mean values were then computed for each force and moment component at each angle of attack.

Reference 2 documents the error analysis based on the OA82 test data which showed that there were systematic errors in the pitch axis jet off data at higher angles of attack as well as the statistical random errors in all data. This systematic error was interpreted as being caused by differences in upper surface pressures acting on the wing due to differences in the way the wing flow separates (reference 2). These data also show that the total error in amplification factor (Figure 2-3) is less than 20% for all moments except at the very lowest thrust coefficient tested and for normal force amplification where it is never better than 20%.

2.5 OA82 DATA SUMMARY

2.5.1 DATA REDUCTION PROCEDURE - The measured balance data from test OA82 included the basic vehicle aerodynamic forces and moments plus an induced loads resulting either from RCS jet impingement or from changes to the vehicle flow caused by the RCS jet plumes. The RCS jets were mounted on the non-metric sting so direct thrust forces were not measured on the balance. Therefore, the incremental induced effects are computed by removing the basic vehicle characteristics from the jet-on data:

$$\Delta C_{M_i} = C_{M_j} - C_{M_o} \tag{1}$$

where

ΔC_{M_i} = induced force or moment increment

C_{M_j} = measured force or moment coefficient with jet on

C_{M_o} = measured force or moment coefficient with jet off

Because the incremental values can be very small and thus sensitive to data scatter, the mean values of the jet off coefficient data were used as the best estimates of the data.

$$\Delta C_{M_i} = C_{M_j} - \bar{C}_{M_o} \tag{2}$$

where

$\bar{C}_{M_o}$ = mean value of jet off force or moment coefficient

Angle of attack differences between the jet-on data and the mean jet-off data were accounted for by passing a 3rd degree polynominal through the jet-off mean data with the nearest mean value angle of attack data as the midpoint of the curve fit and the interpolation is made to the jet-on angle of attack. The interpolation of the mean

value jet-off curves was done because it was assumed that these mean curves are less likely to have scatter to fit the curve through and better difference curves would result. Difference data was generated for all six aerodynamic components but axial force difference data was not analyzed.

During the data analysis the induced data increment was broken into an impingement component and a flow interaction component where the interaction component was obtained by

$$\Delta C_{M_{interaction}} = C_{M_j} - \bar{C}_{M_o} - C_{M_{impingement}} \quad (3)$$

where $\Delta C_{M_{interaction}}$ = induced force or moment resulting from RCS flow/flow field interactions

$C_{M_{impingement}}$ = predicted force or moment due to plume impingement

and where the plume impingement of the model nozzles was predicted using the model to be discussed in Section 4.

Nozzle thrust was computed using the calibration data on the model nozzles while the other nozzle flow parameters were computed using ideal nozzle equations.

2.5.2 PITCH DOWN JET INDUCED DATA - The pitch down jet data was generated primarily with the nozzle set designated N_{49} whose principal characteristics are defined in table 2. This nozzle was mounted on the left side of the model as were all the other pitch nozzles used in this test except for one run of symmetric pitch down jets. The thrust moments thus would be nose down pitch (-) and right wing down roll(+) in the body axis data sign convention. The nominal values of the RCS thrust moments are tabulated with the run symbols on each plot.

Figure 2-4 presents the effect of supply pressure for nozzle N_{49} for freestream dynamic pressures of 125 PSF. These data show that the induced pitch and roll oppose the thrust moment and they are large compared to the control moment; therefore, the total control amplification factor will be low. The lowest pressure data on Figure 2-4 cluster very close together indicating a non-linearity in the induced effects and the data shows very little sensitivity or change with angle of attack. These data are typical of the pitch down jet incremental data shown in reference 2.

Figure 2-5 shows that symmetric firing of the pitch down jets results in an induced moment which is greater than twice the value for one side by a significant amount indicating plume/plume flow interaction in the base region of the model around the sting mount.

These data indicate that a better representation of the base region is needed for the pitch down RCS simulation. The roll jet data Figure 2-6, shows that the normal force and pitching moment effects are derived primarily from the pitch down jet, the side force and yawing moment are derived from the pitch up jet, and the induced roll increment as the sum of the single jet induced effects.

2.5.3 PITCH UP JET INDUCED DATA - The pitch-up RCS data was generated primarily with the nozzle designated as N_{52} whose principal characteristics are defined in Table 3. This nozzle block was mounted on the right side of the model and contains a two nozzle set exhausting vertically upward past the vertical fin which is approximately 9 nozzle diameters laterally from the nozzle centerlines. Figure 2-7 presents typical data of the induced forces and moments resulting from RCS jets firing upward. The pitch axis data shows some jet interaction effects at negative angle of attack where the upper surface is completely exposed to the flow but very little at higher angles of attack. The trends are much clearer in the lateral-directional data which shows strong interactions at negative angles decreasing as the angle of attack increases to approximately 10 degrees. Above this angle the induced effects become relatively insensitive to angle of attack. This data could be interpreted to show that a jet interaction type of flow occurs as long as the free stream flow is attached to the fin and when this is no longer true the interaction is primarily plume impingement on the fin where the plume shape is modified by freestream flow over the vehicle.

The only run of symmetric pitch up data obtained in the RCS test program to this time is presented in Figure 2-8. No difference can be seen in the induced pitching moment between the single side and the symmetric RCS cases in this figure.

2.5.4 YAW JET INDUCED DATA - The yaw jet data obtained in test OA82 was obtained with the nozzle set designated N_{85} whose characteristics are defined in Table 4. These nozzles were mounted on the left side of the model and exhausted perpendicular to the fuselage centerline in a plane parallel to the wing and approximately 13 nozzle diameters above it. This test concentrated on RCS pitch problems so that fewer yaw runs were obtained. Figure 2-9 presents yaw RCS data at two supply pressures and these data show little flow interaction at angles of attack below 5 degrees except in yaw where there appears to be some amplification of the thrust moment due to jet interaction. At higher angles of attack, pitch up and wing down moments are induced by the yaw jet but the effect appears to be non-linear in that the initial thrust created a larger change in moments than that caused by increasing thrust.

2.5.5 PITCH UP PLUS YAW JET COMBINED CONTROL - One nozzle set designated N_{84} was tested which contained both pitch-up and yaw nozzles. The nozzle characteristics are similar to those of nozzles N_{52} and N_{85}. This nozzle set was mounted on the right side of the model firing upward and over the right wing. Figure 2-10 shows the effect

of supply pressure on induced forces and moments. At angles of attack below 10 degrees only the highest supply pressure shows any induced pitching moment but it is greater than the comparable data for the pitch up jet alone while at angles of attack above 10 degrees the pitching moment data looks quite close to the nearest comparable yaw jet case. The rolling moment at high angles appears to be due primarily to the yaw jet while at low angles it appears to be due to the pitch up/roll jet. Thus it appears for this combination of RCS controls that the pitch up/roll nozzles effects dominate at low angles of attack and yaw nozzle effects at high angles of attack.

TABLE 1

RCS TESTS

Test Number	Test Type	Model	Scale	Facility	Date Received	Other
-	Force + Heat Transfer	PRR	.015	UPWT	Tape	Original PRR Data
OA70	Force	139B	.015	UPWT	Tape	Yaw RCS Data Only
OA73	Force	139B	.015	ARC 3.5	Tape	
OA85	Force + Limited Press.	139B	.010	CFHT	Tape	Tabulated Pressure Only
OA105	Force	"	"	"	"	
IA60	Force	"	"	"	"	Orbiter + Tank
OA83	Press.	"	"	ARC 3.5	Plots	Plotted Data Only
LA25	Force	"	.010	CFHT	Tape	
OA82	Force	"	"	CFHT	Tape	
OA99	Force + Limited Press.	"	.0175	Vacuum	Report	Vacuum Impingement

TABLE 2

PITCH DOWN NOZZLES

Test	Nozzle	Expansion Ratio	Exit Diameter	Number in Set	Aft Angle	Outboard Angle	Side	Exit Angle
OA73	N_{21}	1.159	.144 in	2	12°	20°	Left	5°
	N_{22}	"	"	"	0	0	"	"
IA60	N_{49}	4.43	.141	2	12	20	Left	34.25
	N_{50}	"	"	"	"	"	Right	"
OA105	Same as IA 60							
LA25	N_{31}	1.155	.0990	2	12	20	Left	5
	N_{34}	2.851	.0878	"	"	"	"	9
	N_{35}	"	"	"	"	"	Right	"
	N_{38}	"	"	"	30	"	"	"
OA85	N_{49}	4.43	.141	2	12	20	Left	34.25
	N_{50}	"	"	"	"	"	Right	"
	N_{46}	6.332	.117	"	"	"	Right	"
	N_{47}	"	"	"	"	"	Left	"
	N_{43}	7.697	.129	"	"	"	"	"
	N_{45}	"	"	"	30	"	"	"
	N_{42}	"	"	"	"	"	Right	"
	N_{60}	"	"	"	12	"	"	"
OA82	N_{49}	4.43	.141	2	12	20	Left	"
	N_{50}	"	"	"	"	"	Right	"
	N_{79}	"	"	1	"	"	Left	"
	N_{83}	"	"	3	"	"	Left	"

TABLE 3

PITCH UP NOZZLES

Test	Nozzle	Expansion Ratio	Exit Diam.	Number in Set	Aft Angle	Outboard Angle	Side	Exit Angle
OA73	N_{23}	1.159	.144 in	2	0°	0°	Right	5°
IA60	N_{52}	4.43	.141	2	0	0	Right	34.25
OA105	Same as IA 60							
LA25	N_{32}	1.155	.099	2	0	0	Right	5
	N_{36}	2.851	.0878	"	"	"	Right	9
OA85	N_{52}	4.43	.141	2	0	0	Right	34.25
	N_{48}	6.332	.117	"	"	"	"	"
	N_{44}	7.697	.129	"	"	"	"	"
OA82	N_{52}	4.43	.141	2	0	0	Right	34.25
	N_{81}	"	"	"	"	"	Left	"
	N_{82}	"	"	3	"	"	Right	"
	N_{78}	"	"	1	"	"	Right	"
	N_{80}	"	"	2	12	20	Right	"
	N_{84}	"	"	2+2 Yaw	0	0	"	"

TABLE 4

YAW NOZZLES

Test	Nozzle	Expansion Ratio	Exit Diam.	Number in Set	Aft Angle	Outboard Angle	Side	Exit Angle
OA70	N_{19}	10.81	.144	2	0	0	Left	5°
OA73	N_{19}	10.81	.144	2	0	0	Left	5
	N_{20}	1.159	"	"	"	"	"	"
IA60	N_{51}	4.43	.141	4	0	0	Left	34.25
OA105	Same as IA 60							
LA25	N_{33}	1.159	.099	2	0	0	Left	5
	N_{37}	2.85	.0878	"	"	"	"	9
OA85	N_{51}	4.43	.141	4	0	0	Left	34.25
	N_{61}	7.697	.129	2	"	"	"	"
OA82	N_{51}	4.43	.141	4	0	0	Left	34.25
	N_{85}	"	"	2	"	"	"	"
	N_{84}	"	"	2+2 Pitch	"	"	Right	"

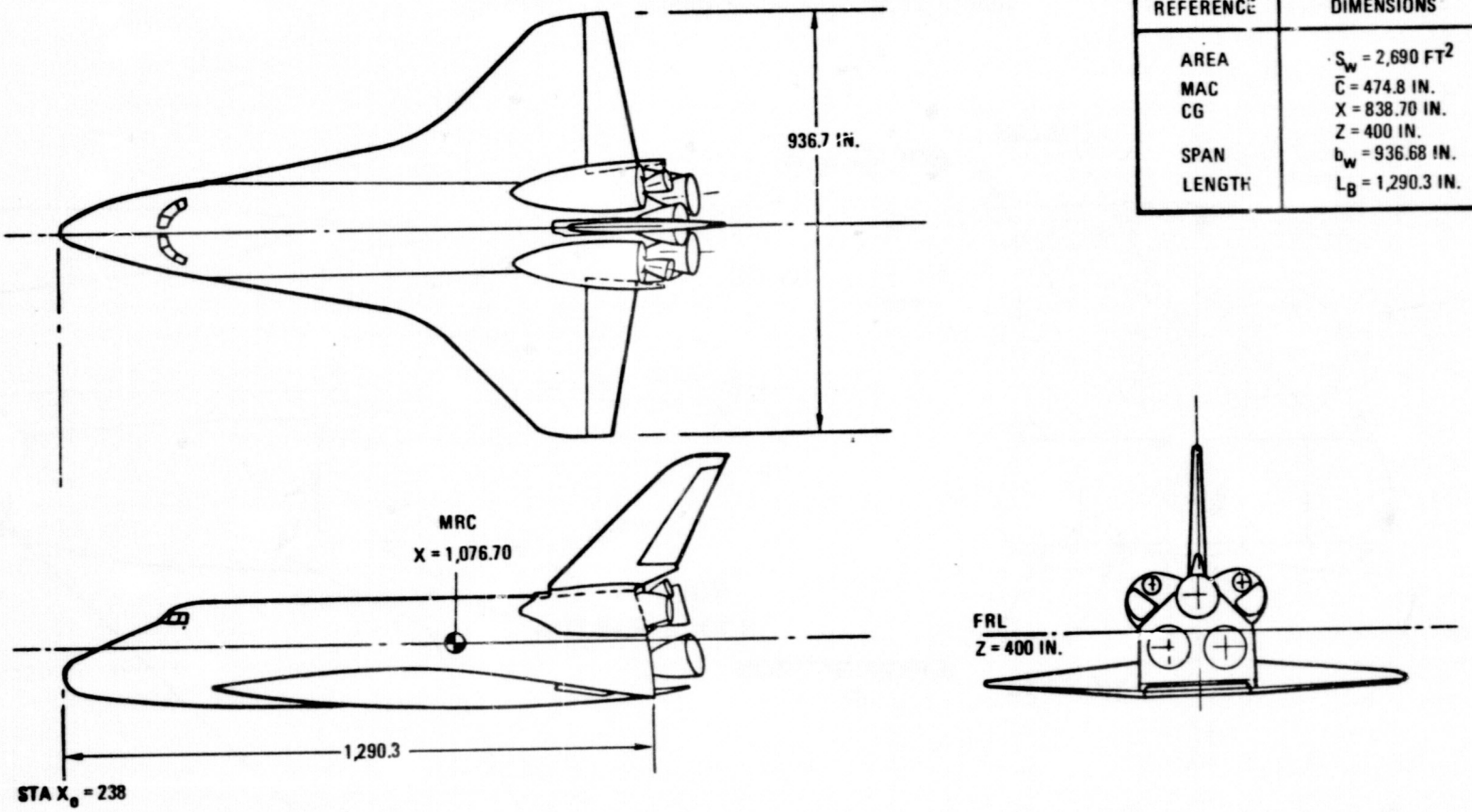

REFERENCE	DIMENSIONS
AREA	S_w = 2,690 FT^2
MAC	$\bar{C}$ = 474.8 IN.
CG	X = 838.70 IN.
	Z = 400 IN.
SPAN	b_w = 936.68 IN.
LENGTH	L_B = 1,290.3 IN.

Figure 2-1. 139B Orbiter Configuration

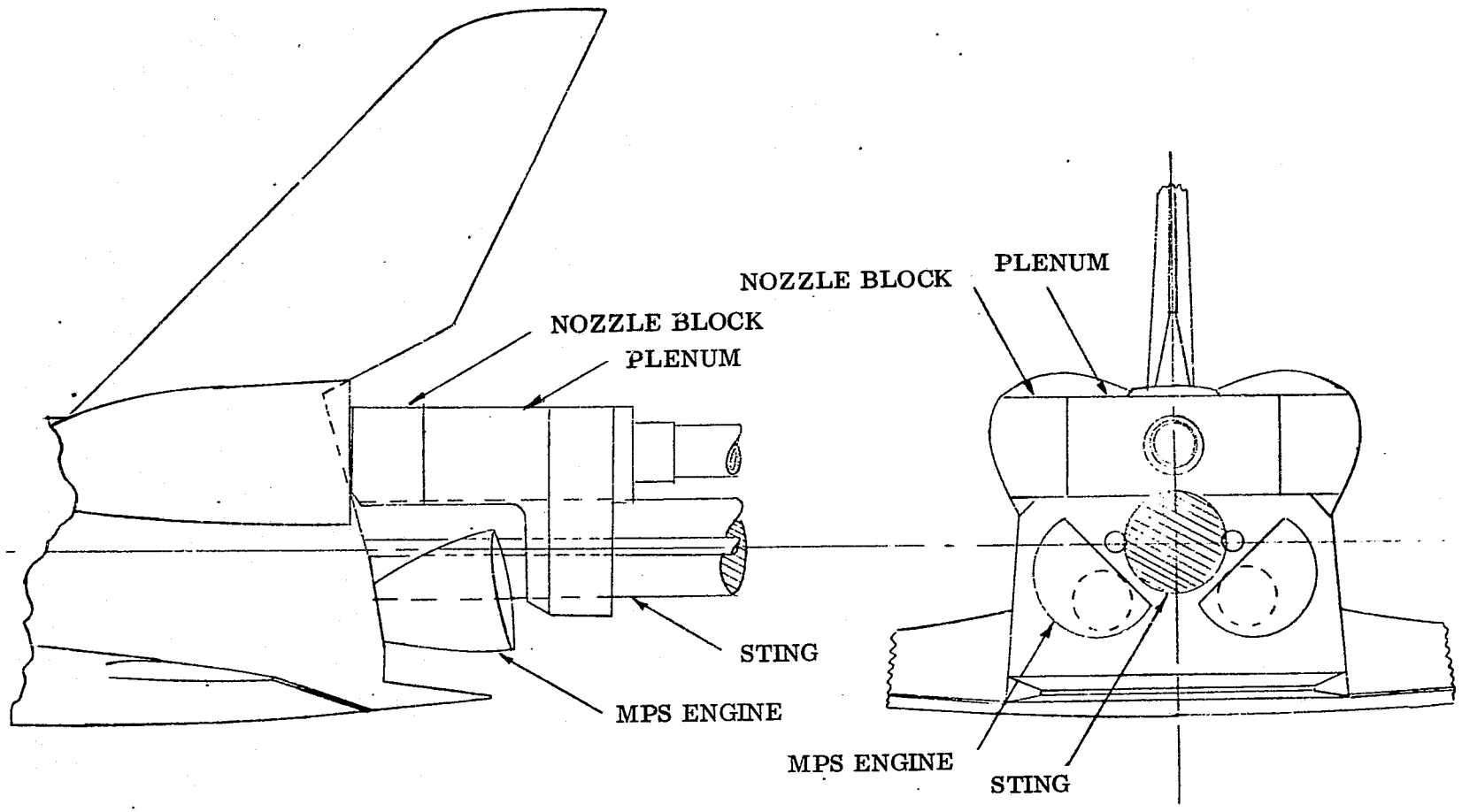

Figure 2-2. Model Base with Sting Mount

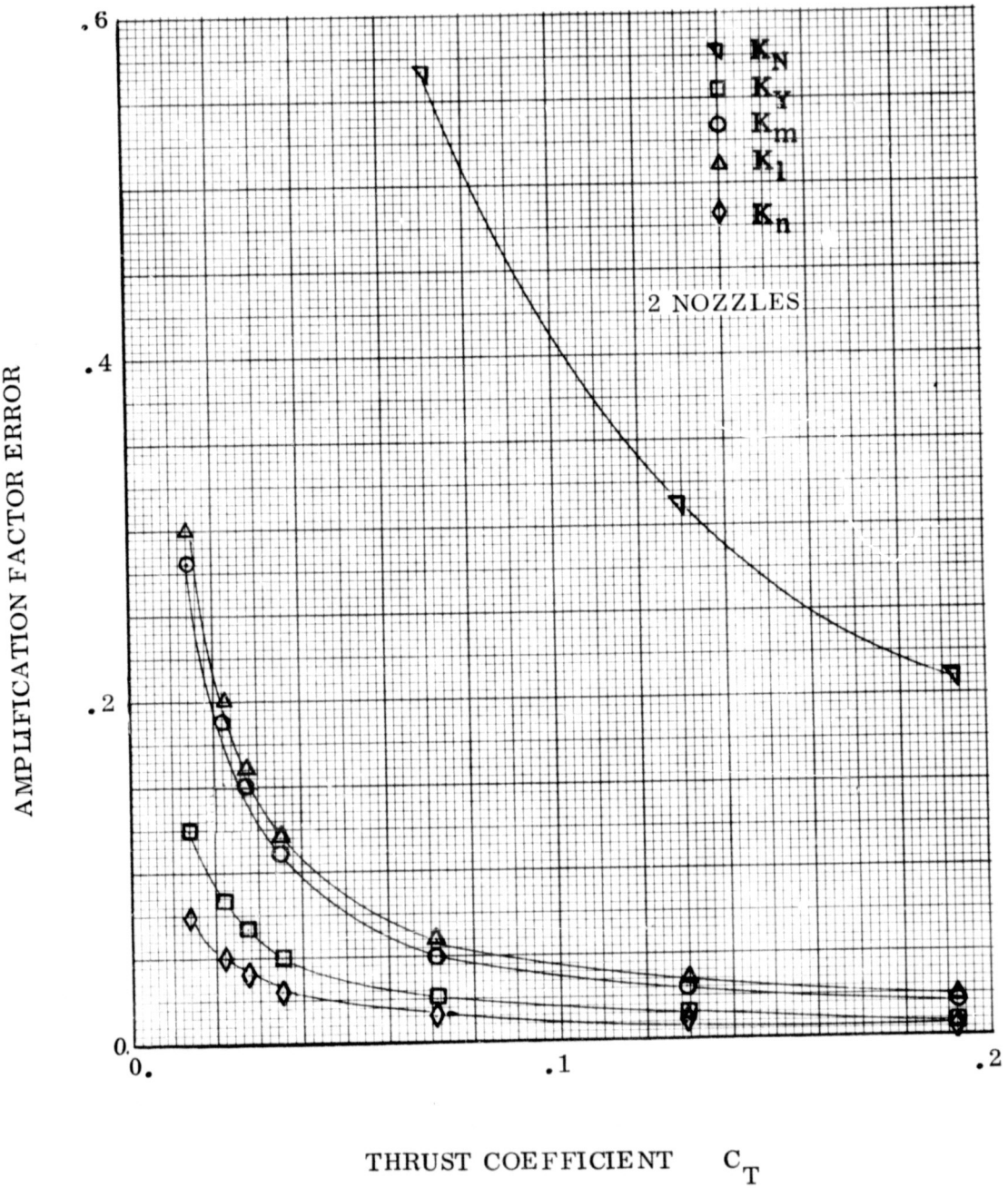

Figure 2-3: Expected Error in Amplification Factor

SYMBOL	RUN	P_{oj}	C_m	C_l
O	59	78	-.01885	.00224
X	60	98	-.02368	.00307
□	64	129	-.03117	.00404
Y	61	261	-.06307	.00517
+	62	473	-.1143	.01481
*	63	702	-.1696	.02199

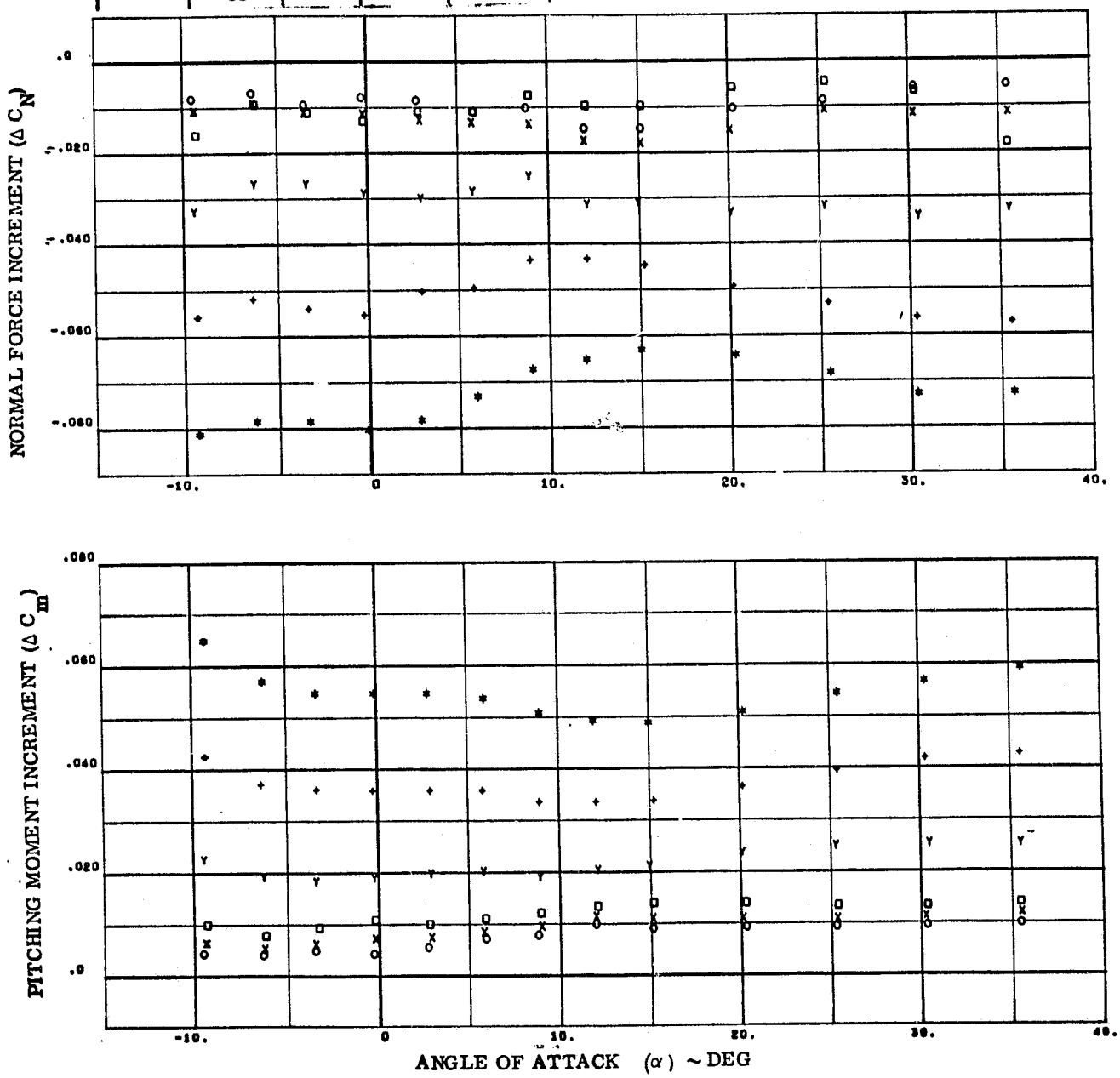

Figure 2-4a. N_{49} Effect of Supply Pressure at Q=125 PSF

SYMBOL	RUN	P_{oj}	C_m	C_l
O	59	78	-.01885	.00224
X	60	98	-.02368	.00307
□	64	129	-.03117	.00404
Y	61	261	-.06307	.00817
+	62	473	-.1143	.01481
*	63	702	-.1696	.02199

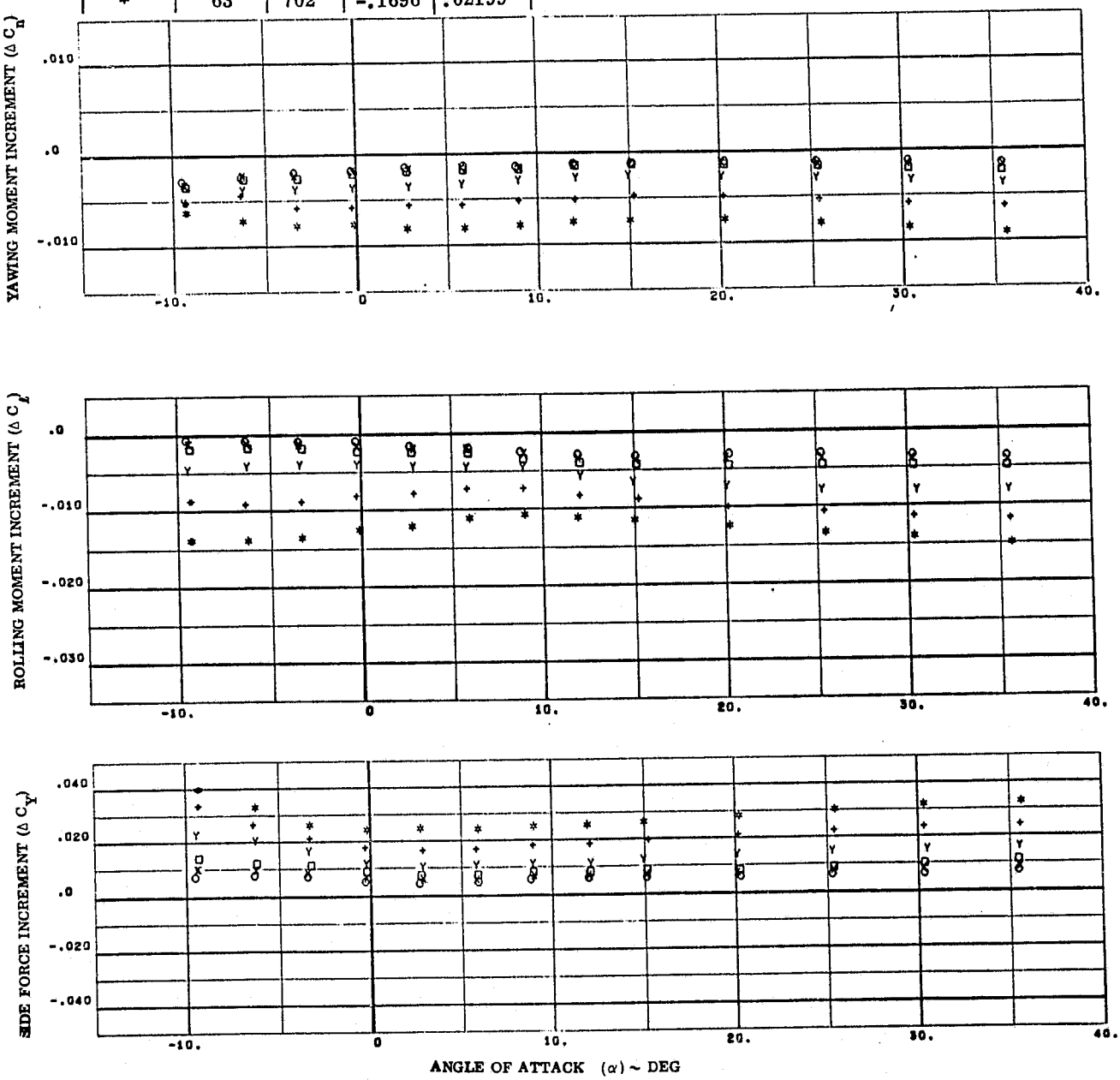

Figure 2-4b. N_{49} Effect of Supply Pressure at Q=125 PSF

SYMBOL	RUN	P_{oj}	C_m	C_l	NOZ
O	6	155	-.03121	.00404	Left
X	8	164	-.06121	0	Both

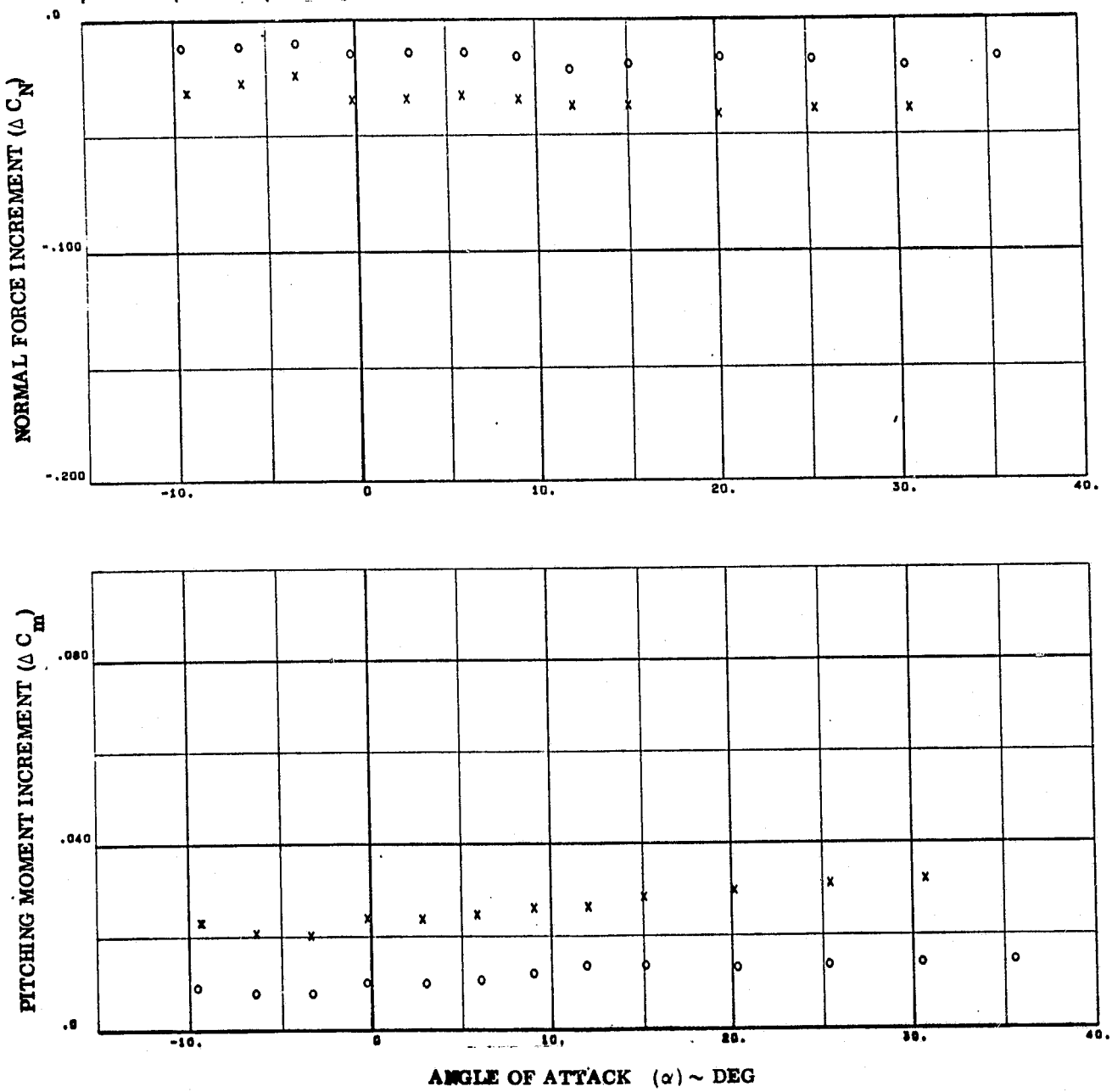

Figure 2-5. $N_{49}N_{50}$ Symmetric Pitch Down, Q=150 PSF

SYMBOL	RUN	P_{oj}	C_m	C_l	NOZ
O	6	155	-.03121	.00404	Down
X	14	157	+.03305	.00440	Up
□	10	155	0	.00845	Roll

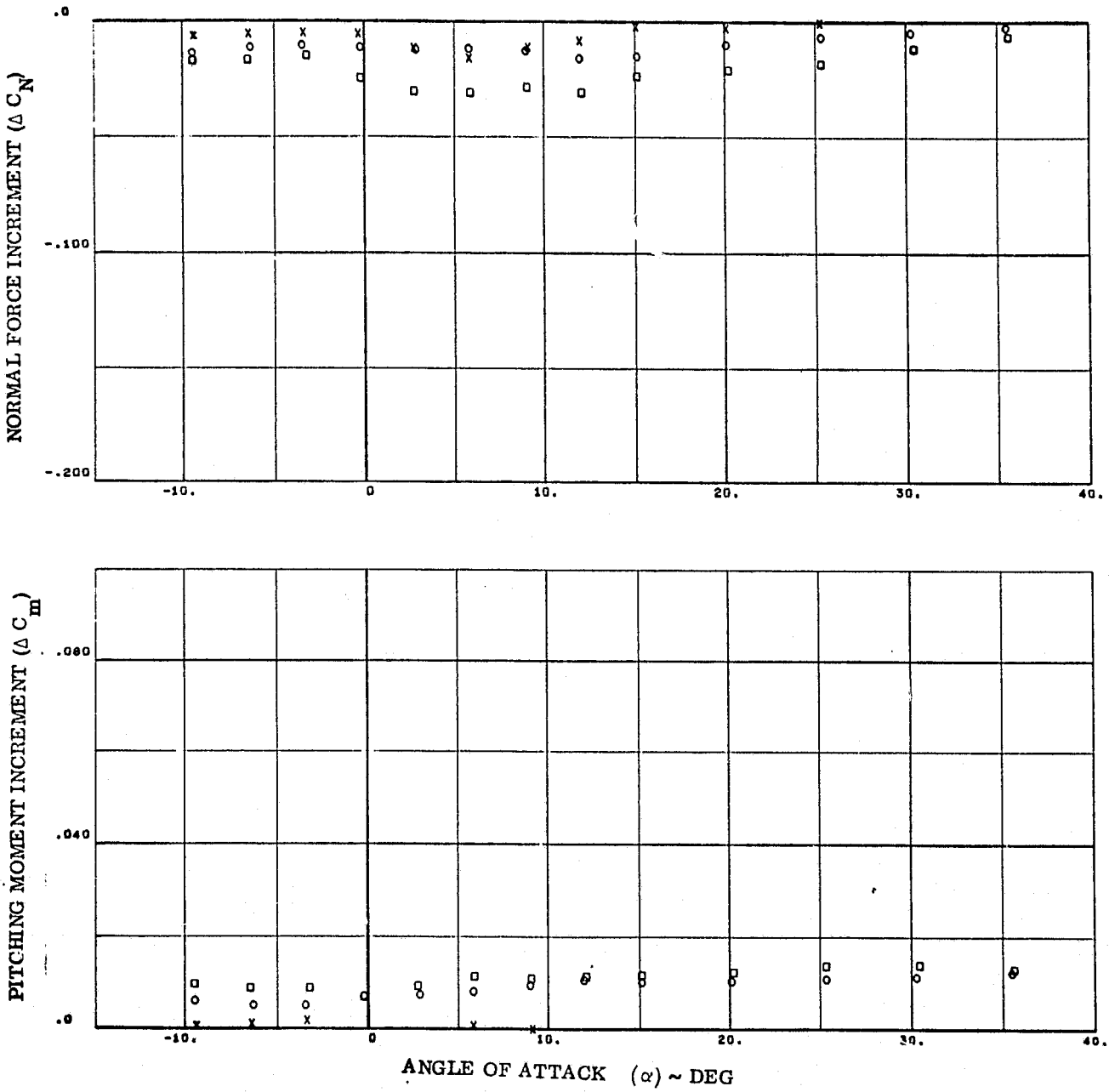

Figure 2-6a. $N_{49}N_{52}$ Asymmetric Roll Jet at Q=150 PSF

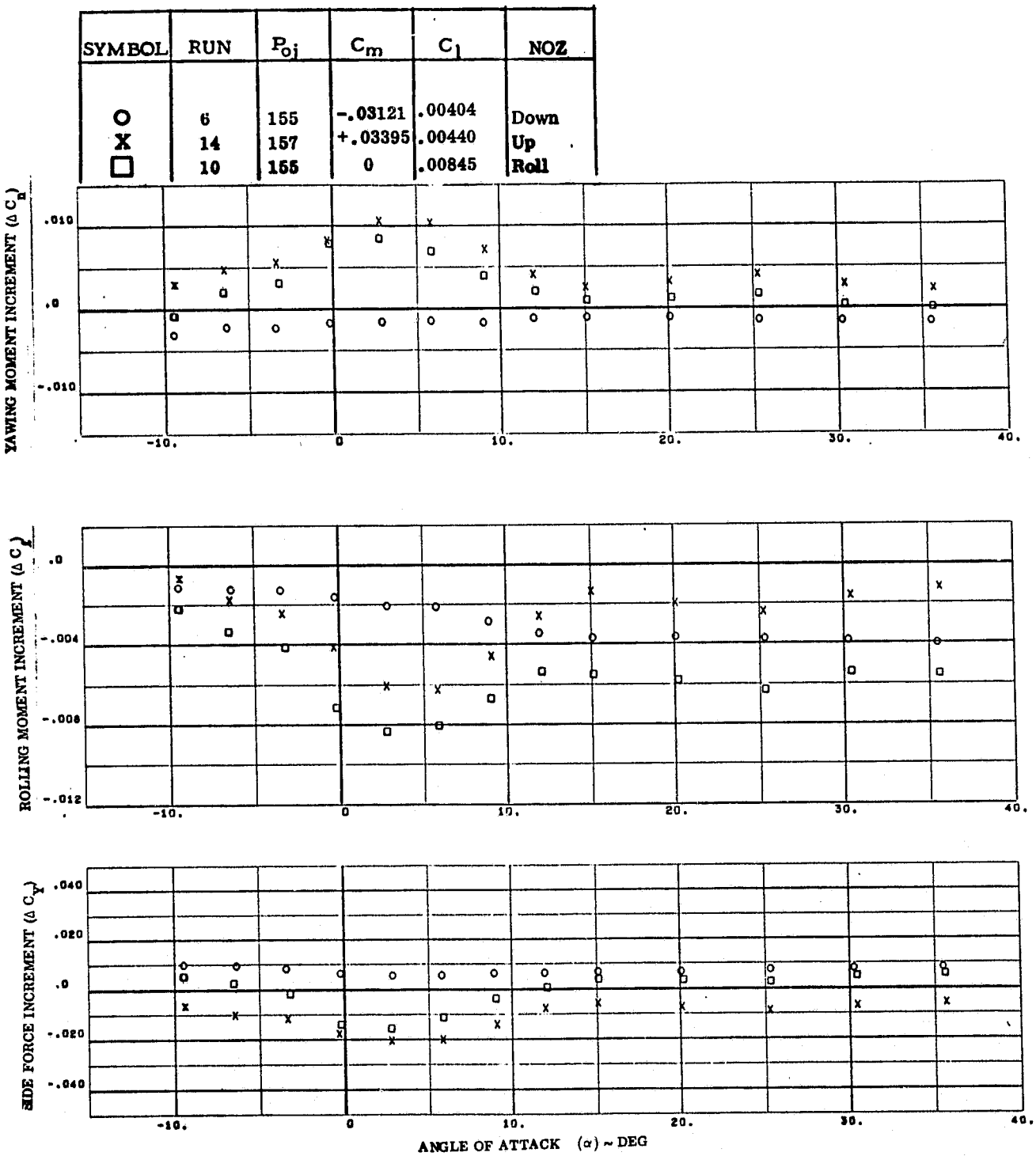

Figure 2-6b. $N_{49}N_{52}$ Asymmetric Roll Jet at Q=150 PSF

SYMBOL	RUN	P_{oj}	C_m	C_l
O	53	78	.02051	.00266
X	54	98	.02576	.00334
□	34	129	.03391	.00439
Y	55	261	.06861	.00889
+	56	473	.12434	.01612
*	57	702	.1845	.02392

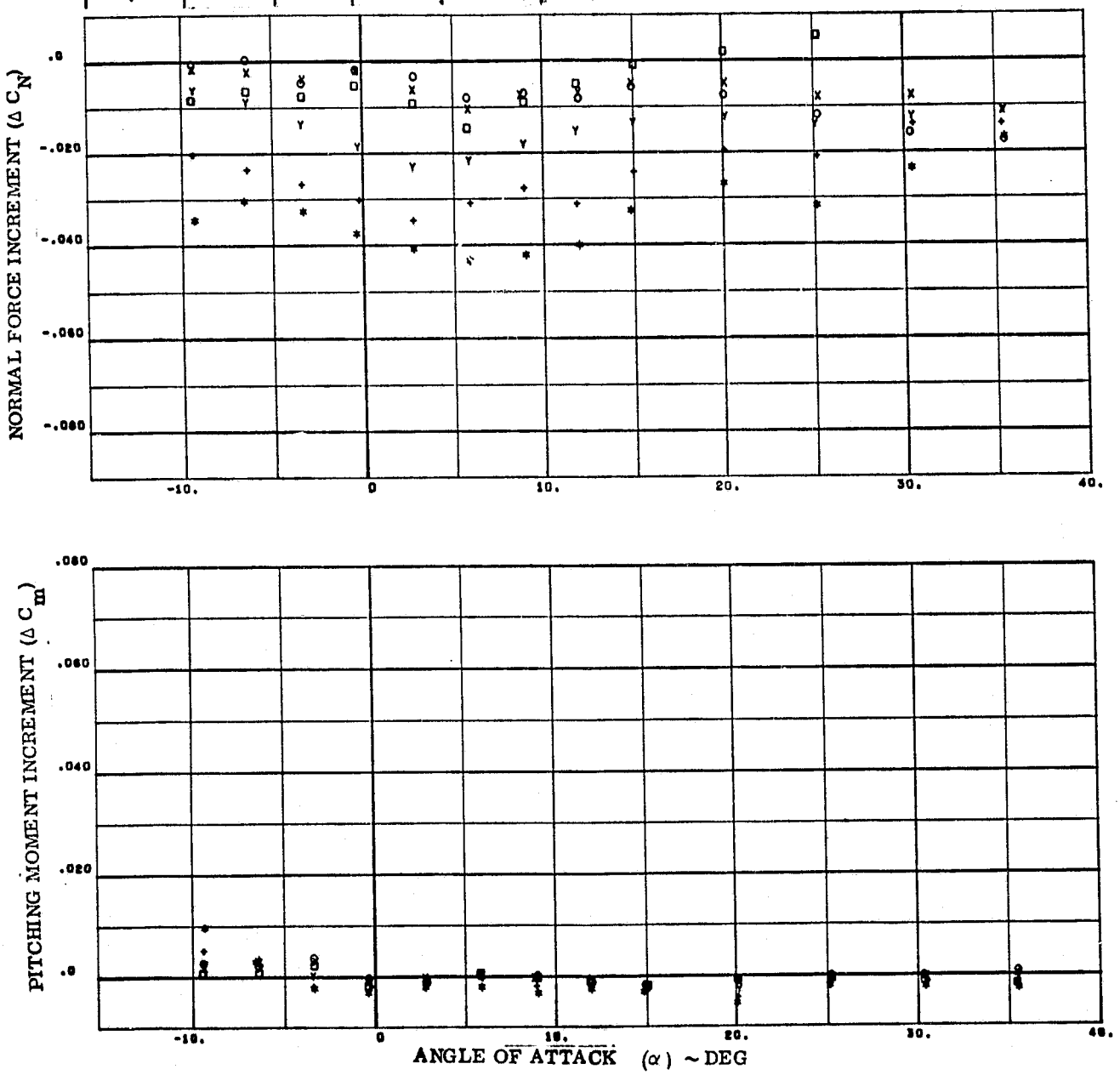

Figure 2-7a. N_{52} Effect of Supply Pressure at Q=125 PSF

SYMBOL	RUN	P_{oj}	C_m	C_l
O	53	78	.02051	.00266
X	54	98	.02576	.00334
□	34	129	.03391	.00439
Y	55	261	.06861	.00889
+	56	473	.12434	.01612
*	57	702	.1845	.02392

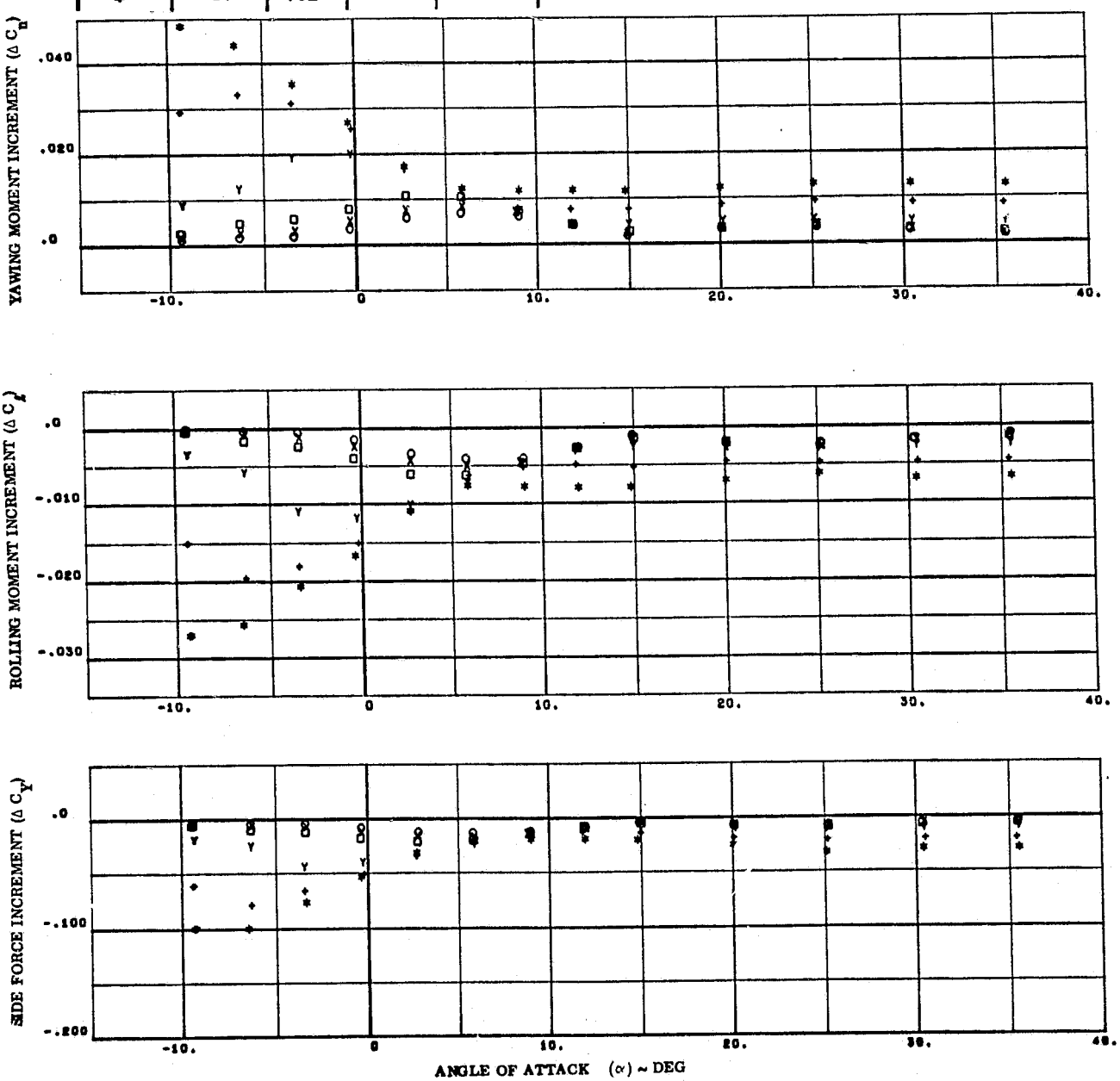

Figure 2-7b. N_{52} Effect of Supply Pressure at Q=125 PSF

SYMBOL	RUN	P_{oj}	C_m	C_ℓ
O	14	157	.03305	.00440
X	12	157	.0679	0

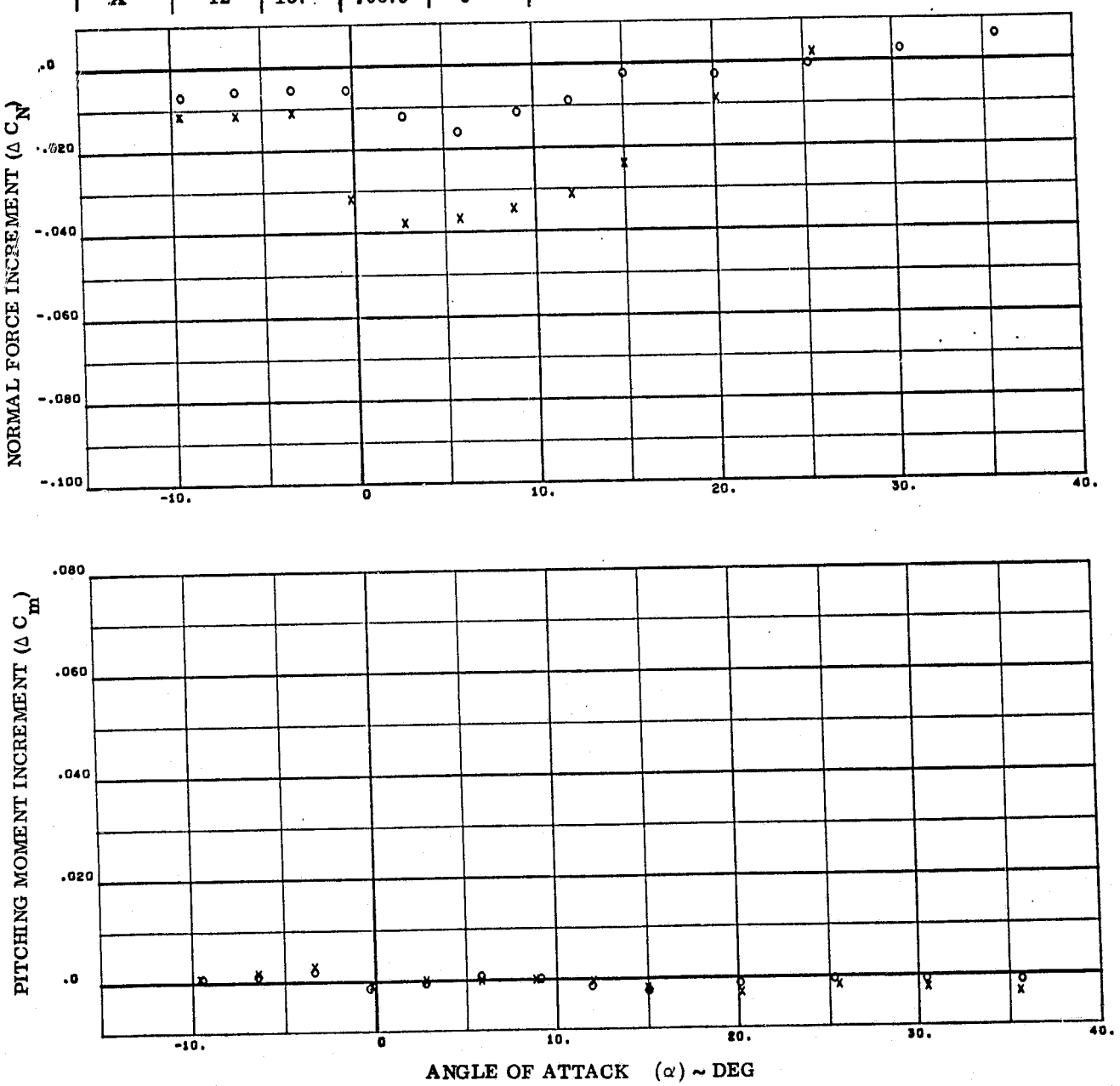

Figure 2-8. $N_{52}N_{81}$ Symmetric Pitch Up at Q=150 PSF

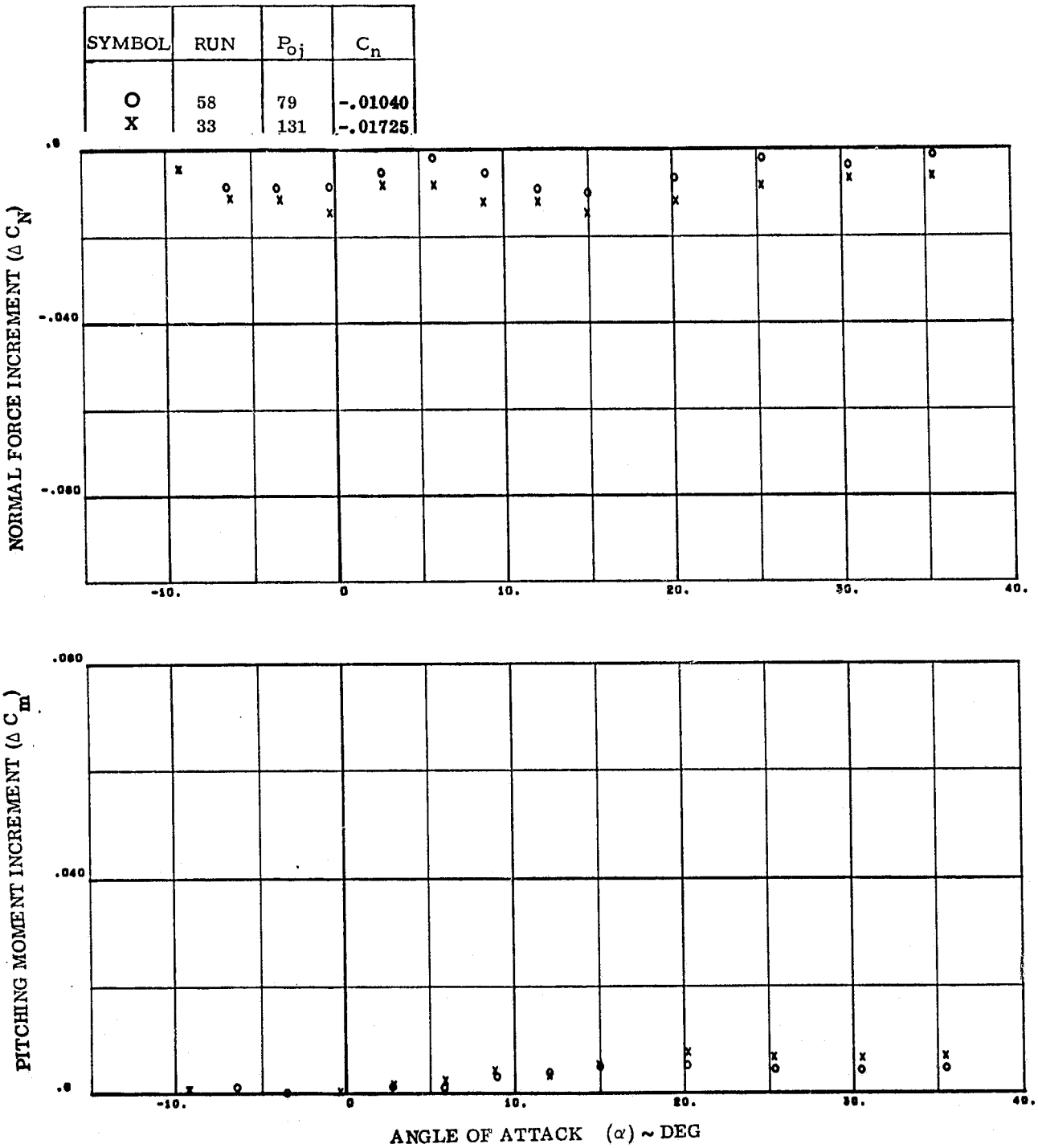

Figure 2-9a. N_{85} Effect of Supply Pressure at Q=125 PSF

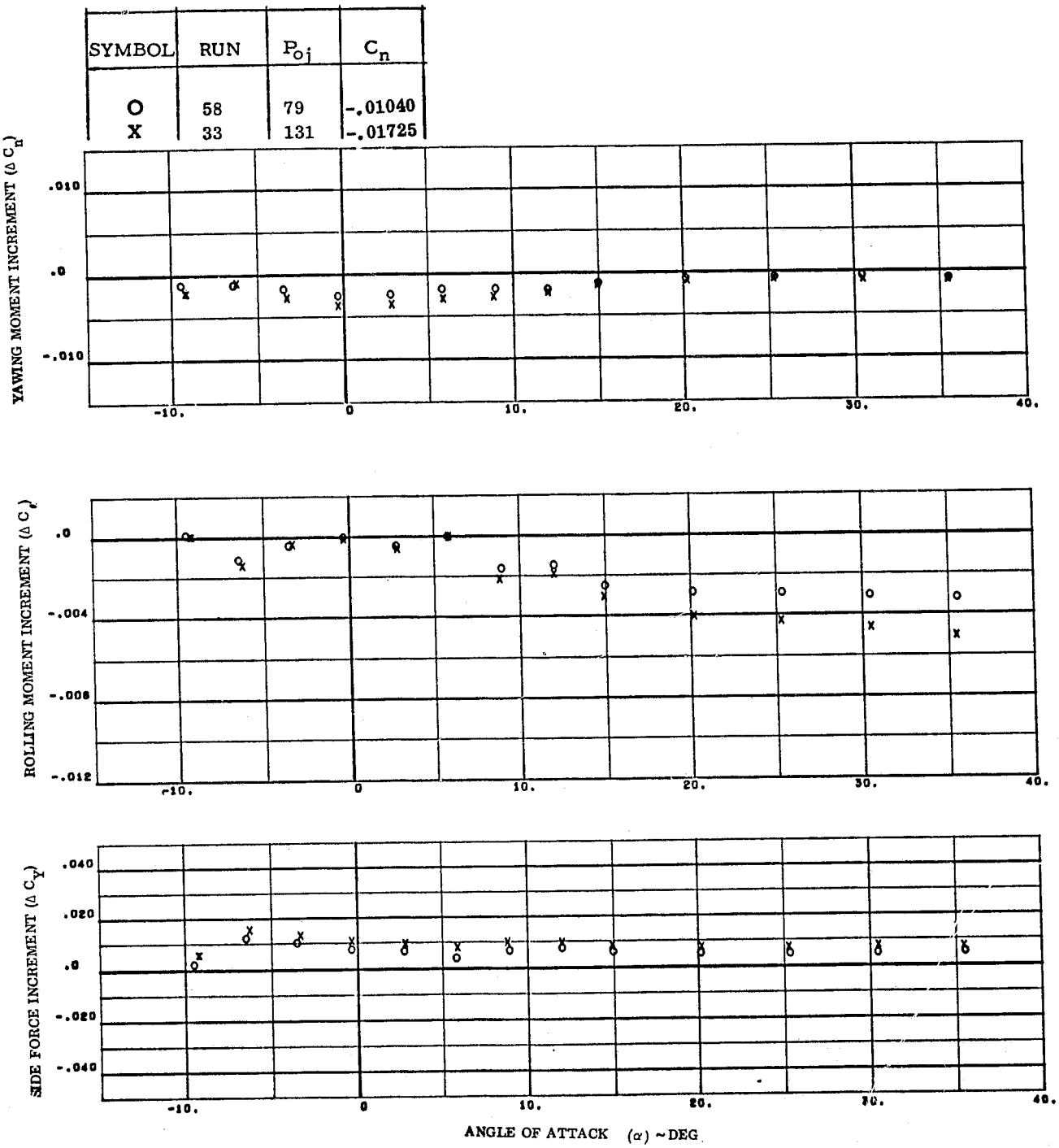

Figure 2-9b. N_{85} Effect of Supply Pressure at Q=125 PSF

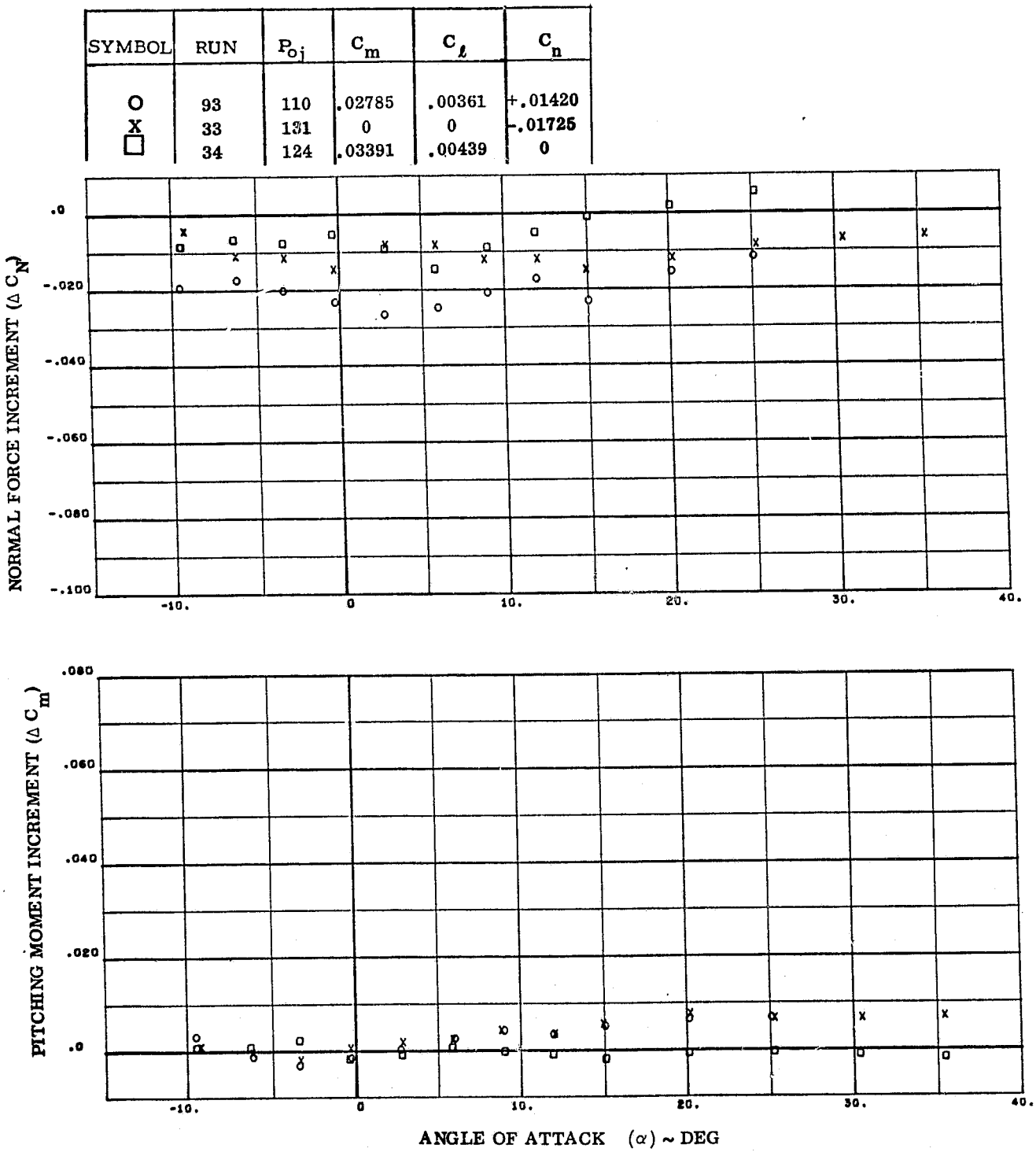

Figure 2-10a. N_{84} Comparison of Control Additivity at Q=125 PSF

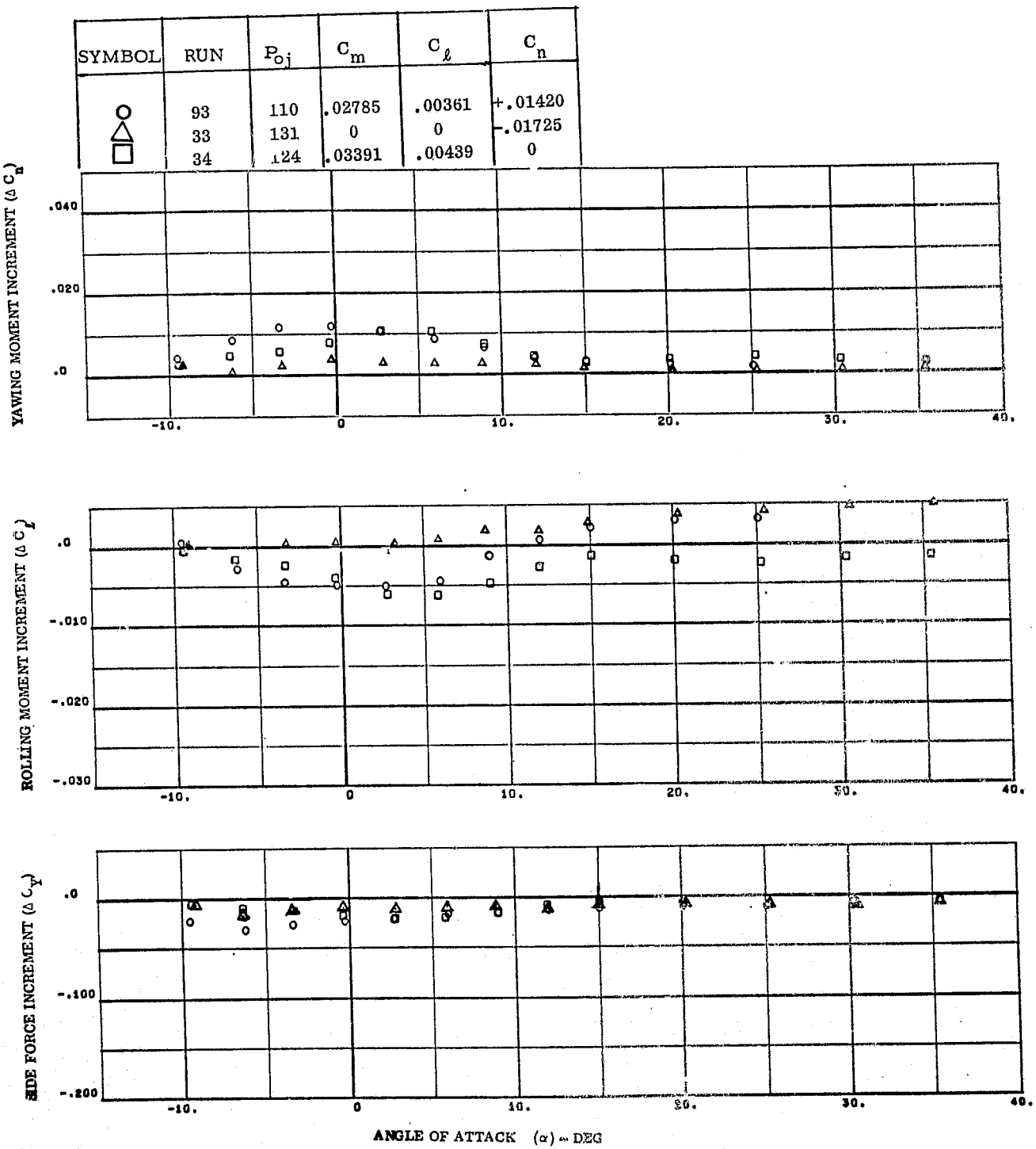

Figure 2-10b. N_{84} Comparison of Control Additivity at Q = 125 PSF

3. DATA ANALYSIS

3.1 SUMMARY OF PREVIOUS RESULTS

Reference 1 presents the final report analyzing the RCS data on the PRR configuration. That analysis showed that any nozzle parameter which was directly related to nozzle exit momentum ratio

$$\frac{\Phi_j}{\Phi_\infty} = \frac{\gamma_j P_j M_j^2 A_j}{\gamma_\infty P_\infty M_\infty^2 A_\infty} \tag{1}$$

was a good parameter with which to correlate the total induced effects of the RCS controls. That study could not show which of all the nozzle parameters was the best since only one nozzle shape was used to generate the data. In addition that data could not answer questions concerning the effects of number of nozzles firing in a given direction combining controls in other two directions, and the importance of gas temperature ratio as a parameter. Thus the purpose of this study was to obtain data on a more current orbiter base line configuration and to update the analytic models to this configuration. In addition, data on the effects of temperature ratio,numbers of nozzles, and combined control were to be obtained and added to the models.

Thayer's dimensional analysis model (Ref. 1) for jet interaction problems shows that energy ratio

$$\frac{h_{oj}}{h_\infty} = \frac{R_j T_{o_j}}{R_\infty T_\infty} \tag{2}$$

is a parameter for these types of flow interaction although he showed little effect if the ratio is below 9. The applicability of cold gas simulation techniques to simulate RCS effects and the extrapolation to full scale results depends on knowledge of how strong a parameter the energy ratio is and helium/argon gas mixtures were tested during test OA82 to vary the gas constant (R) in order to answer this question.

The data of Reference 1 were generated with two RCS nozzles being used in all control planes and the model was developed on a unit area ratio basis

$$A_\infty = A_j \tag{3}$$

However, the Shuttle control system determines the control requirements and uses varying numbers of nozzles to obtain the desired control moment. Thus a major test

parameter on test OA82 was to vary the number of nozzles in each control plane to determine the addivity of numbers of nozzles. Also a limited amount of combined control testing was performed to determine the cross-coupling effects on RCS flow-interaction.

The analytic model developed in Reference 1 assumes that the total control force or moment of a RCS control is the linear sum of the jet force or moment and an induced force or moment which is itself the sum of a term contributed by the direct impingement of the RCS plumes on adjacent surfaces and an interaction term which is the plume flow interacting with the external flow over the vehicle.

$$C_{M_{total}} = C_{M_{jet}} + C_{M_{impingement}} + C_{M_{interaction}} \quad (4)$$

where

$C_{M_{total}}$ = total control force or moment coefficient

$C_{M_{jet}}$ = RCS force or moment coefficient

$C_{M_{impingement}}$ = force or moment coefficient due to plume impingement on adjacent surfaces

$C_{M_{interaction}}$ = force or moment coefficient caused by plume interactions with the flow over the vehicle

The reasons for dividing the RCS induced effects into an impingement and an interaction component are that the vehicle geometry is such that the RCS jets exhaust toward many surfaces such as the wing upper surface, the body flap, the main propulsion engines, and vertical fin. The vacuum test data (Ref. 3) shows that there is plume impingement on these surfaces; but, the total induced forces and moments are larger than that which is predicted by plume impingement alone (Ref. 1), and this shows that there is a plume interaction with the flow field around the shuttle orbiter. In order to derive this interaction term, however, it is necessary to know or assume the impingement term and to subtract it from the total induced term. This was done in these analyses by using the analytic plume impingement model presented in Section 4 to predict the plume impingement for the model nozzle, test gas, and wind tunnel conditions and to remove it from the induced data as shown in Equation 3 of Section 2.

The analysis of the data will be presented by the direction of the control thrust and analysis includes the following topics:

3.2 Pitch Down/Roll RCS
3.3 Pitch Up/Roll RCS
3.4 Yaw RCS
3.5 Combined Control
3.6 Possible Sting Interference
3.7 Time Dependent Effects

3.2 PITCH DOWN/ROLL RCS

Section 2.5.2 presents a summary of the left side, pitch down/roll jet data obtained during test OA82 and Figure 3-1 presents typical pitching moment increments obtained from these data. This figure shows that there appears to be little angle of attack effects in the data and that it may be possible to treat the incremental data as a function of nozzle flow parameters only. Figure 3-2 to 3-4 present comparisons of data averaged at all angles of attack with the data averaged in a high angle and a low angle of attack range. These figures show that there is a difference in data particularly at the lower momentum ratios and as a result a high/low range breakdown was selected for the pitch down data correlations in which 15 degrees angle of attack is the crossover point between models.

3.2.1 HIGH ANGLE OF ATTACK CORRELATIONS. Having divided the data into two groups above and below 15 degrees angle of attack, the data correlations for the high angle of attack represent approximately 5 points per data run taken at 5 degree intervals from 15 degrees to 35 degrees angle of attack. These data were treated as a set containing no angle of attack effects.

These data showed some correlation with all nozzle parameters which are directly related to nozzle momentum ratio (for a fixed nozzle geometry) such as jet exit pressure ratio in Figure 3-5. This figure shows, however, that the number of nozzles is a parameter which must be accounted for in some way. It was found that by redefining momentum ratio (Equation 1) with wing area as A_∞ and the sum of the nozzle exit areas as the equivalent nozzle area A_j was the best method for accounting for numbers of nozzles: Thus, momentum ratio is defined as:

$$\frac{\Phi_j}{\Phi_\infty} = \frac{\gamma_j P_j M_j^2 \Sigma A_j}{\gamma_\infty P_\infty M_\infty^2 S_{wing}} \qquad (5)$$

The breakdown of the total induced moments into an impingement component and an interaction component still remains the best model of accounting for the differences between the flow in the base region of the model where the primary interactions should be impingement and that part of the plume which impinges on and interacts with wing flow. The plume impingement component of the pitch down data was generated using the model presented in Section 4 and the data was analyzed to determine the interaction term. Figure 3-6 presents the interaction pitching moment and rolling moment increments for the left side only pitch down jet ratioed to total jet moment. This data is very interesting because it shows that the interaction components are initially very large relative to the jet moments but becomes a smaller effect compared to the jet moment as jet moments increase. This is a new result compared to the PRR data (Ref. 1) due in part to higher jet momentum ratios achieved in these tests compared to the earlier results.

Figure 3-7 through 3-12 present the interaction increments for the pitch down jets firing on the left side only and these data show that the interaction terms increase very rapidly at low momentum ratios but tend to reach a constant level at higher momentum ratios. It was decided to develop the interaction model in terms of the interaction increments shown in these figures by curve fitting the data on these figures. The figures present average data for each run but the curve fits were generated as least square polynominal fits through all of the data.

The question of the need to simulate the exhaust gas energy ratio in addition to momentum ratio for the pitch down jets is answered by comparing Figure 3-9 with 3-8 where, for a fixed nozzle mass flow ratio is proportional to momentum ratio times energy ratio.

$$\frac{\dot{m}_j}{\dot{m}_\infty} = \left[\frac{\Phi_j}{\Phi_\infty} \cdot \frac{A_j P_j}{A_\infty P_\infty} \left(\frac{R_\infty T_\infty}{R_j T_j} \right) \right]^{1/2} \tag{6}$$

In Figure 3-8 the gas mixture data from helium (R = 386) to Argon (R = 38.6) agree well with the air data based on momentum ratio whereas in Figure 3-9 the data form a line which crosses the air data correlation. Thus, cold air simulations appear to be adequate and momentum ratio is the parameter for pitch down RCS.

The normal force data whose averages are shown on Figure 3-7 were fit with a 2nd order least squares curve fit whose equation is

$$\Delta C_{N_{interaction}} = -0.0021945 - 0.811385 \, (\Phi_j/\Phi_\infty) + 4.51527 \, (\Phi_j/\Phi_\infty)^2 \tag{7}$$

This curve has a minimum value at a momentum ratio of 0.08985 and the minimum value of incremental normal force is - 0.0386.

The incremental pitching moment (Figure 3-8) due to interaction curve fit is given by the equation

$$\Delta C_{m_{interaction}} = 0.004384 + 0.52205 \, (\Phi_j/\Phi_\infty) - 3.37717 \, (\Phi_j/\Phi_\infty)^2 \tag{8}$$

and has a maximum value of 0.024562 at a momentum ratio of 0.07729. The rolling moment data of Figure 3-10 curve fit is given by Equation 9

$$\Delta C_{\ell_{interaction}} = -0.0017358 - 0.1628144 \, (\Phi_j/\Phi_\infty) + 0.802611 \, (\Phi_j/\Phi_\infty)^2 \tag{9}$$

and this curve has a minimum value of -0.009993 at a momentum ratio of 0.1014.

The side force data (Figure 3-12) and yawing moment data (Figure 3-11) have different shapes than the previous curves and fourth order curve fits were made

through these data to get better representations of curve shape. The incremental yawing moment due to interaction is given by Equation 10 while the side force data was fit by Equation 11.

$$\Delta C_{n_{interaction}} = 0.00034372 - 0.221604\,(\Phi_j/\Phi_\infty) + 8.022016\,(\Phi_j/\Phi_\infty)^2 - 79.03936\,(\Phi_j/\Phi_\infty)^3 + 246.3438\,(\Phi_j/\Phi_\infty)^4 \quad (10)$$

$$\Delta C_{y_{interaction}} = 0.0067507 + 0.6925\,(\Phi_j/\Phi_\infty) - 17.07348\,(\Phi_j/\Phi_\infty)^2 + 157.52286\,(\Phi_j/\Phi_\infty)^3 - 477.3934\,(\Phi_j/\Phi_\infty)^4 \quad (11)$$

3.2.2 LOW ANGLE OF ATTACK CORRELATIONS. The low angle of attack data was analyzed in the same manner as the high angle data and the correlations are presented in Figure 3-13 to 3-17. The normal force due to interaction curve fit is given by Equation 12.

$$\Delta C_{N_{interaction}} = 0.000406927 - 0.795865\,(\Phi_j/\Phi_\infty) + 4.1104\,(\Phi_j/\Phi_\infty)^2 \quad (12)$$

which has a minimum value of -0.03812 at a momentum ratio of 0.096811. The pitching moment due to interaction equation is

$$\Delta C_{m_{interaction}} = 0.000999527 + 0.501729\,(\Phi_j/\Phi_\infty) - 3.0783998\,(\Phi_j/\Phi_\infty)^2 \quad (13)$$

and this curve has a maximum value of 0.02144292 at a momentum ratio of 0.08149. Equation 14 defines the rolling moment due to interaction as

$$\Delta C_{\ell_{interaction}} = -0.000033456 - 0.132110\,(\Phi_j/\Phi_\infty)^2 + 0.5691798\,(\Phi_j/\Phi_\infty)^2 \quad (14)$$

and this equation has a minimum value of -0.007699 at a momentum ratio of 0.11605. These maximum or minimum values show close agreement with the results of the high angle of attack curve fits as was expected from Figure 3-3 and 3-4.

The side force and yawing moment increments due to pitch down jet RCS interaction at low angles of attack are given by Equations 15 and 16.

$$\Delta C_{n_{interaction}} = 0.000057745 - 0.259978\,(\Phi_j/\Phi_\infty) + 9.05189\,(\Phi_j/\Phi_\infty)^2 - 86.79901\,(\Phi_j/\Phi_\infty)^3 + 265.0127\,(\Phi_j/\Phi_\infty)^4 \quad (15)$$

$$\Delta C_{Y_{interaction}} = -0.00017443 + 0.754012\,(\Phi_j/\Phi_\infty) - 18.2713\,(\Phi_j/\Phi_\infty)^2 + 163.014\,(\Phi_j/\Phi_\infty)^3 - 481.427\,(\Phi_j/\Phi_\infty)^4 \quad (16)$$

Comparing these curves with the high angle of attack models at a momentum ratio of 0.1 shows

high α $\quad \Delta C_n = 0.0039982, \quad \Delta C_Y = 0.0089138$

low α $\quad \Delta C_n = 0.0042811, \quad \Delta C_Y = 0.0073851$

a good agreement between curve fits.

3.3 PITCH UP/ROLL RCS

Section 2.5.3 presents a summary of the right side pitch up/roll jet data obtained during test OA82 and Figure 3-18 presents the rolling moment increments obtained as a function of angle of attack. Above 15 degrees, the data appears much like the pitch down data in that angle of attack effects are small. As angle of attack decreases below 15 degrees angle of attack, all the data appears to follow one curve until a peak value is reached and the data decays along separate curves. The peak values and the angles of attack at which they occur appear to be functions of supply pressure or some other nozzle related parameters. The pitch up RCS data was broken into three parts for analysis based on these observations which are

a) high angle of attack
b) peak values
c) below peak values

3.3.1 HIGH ANGLE OF ATTACK CORRELATIONS. The division between the high angle of attack data and the other regions was arbitrarily chosen as 15 degrees. There are approximately five data points on each tunnel run between 15 and 35 degrees angle of attack which were analyzed as a set independent of angle of attack. These data were treated in the same way as the pitch down data in which it was assumed that the total induced force or moment was the sum of an impingement term and an interaction term. A theoretically predicted impingement term was then subtracted from the induced terms in order to define the interaction terms for correlation with nozzle parameters. Figure 3-19 shows that the interaction terms are large relative to the thrust at low values of momentum ratio (and thrust) but decline in much the same way as the pitch down data of Figure 3-4 did.

Figure 3-20 to 3-23 present the incremental normal force and pitching moment due to interaction correlated to mass flow ratio and momentum ratio respectively. The scatter in these data makes it difficult to choose a correlating parameter but the case is much clearer for the peak value which demonstrates what Figure 3-20 hints at, that is that the energy ratio cannot be ignored as a parameter for these data and as a result mass flow ratio is the better parameter. Least square polynominal curve fits were made through the mass flow data and Equations 17 and 18 were obtained

$$\Delta C_{N_{interaction}} = 0.008828 - 0.156367\ (\dot{m}_j/\dot{m}_\infty) + 0.051909\ (\dot{m}_j/\dot{m}_\infty)^2 \quad (17)$$

$$\Delta C_{m_{interaction}} = -0.000421898 - 0.0168642\,(\dot{m}_j/\dot{m}_\infty) + 0.026014\,(\dot{m}_j/\dot{m}_\infty)^2 \quad (18)$$

The normal force curve has a minimum value of -0.118 at a mass flow ratio of 1.506 while the pitching moment curve has a maximum value of 0.021443 at a mass flow ratio of 0.3241 which is much closer to the actual range of the data. The normal force and pitching moments due to interaction are not consistent with each other at low mass flow ratios (i.e., a positive normal force increment and a negative moment increment) and this must be laid to the relative inaccuracies of the data in this range. At low mass flow ratios the impingement predictions were zero and did not add scatter to the interaction data.

Figure 3-24 presents the rolling moment resulting from plume interaction correlated against momentum ratio. The moment due to interaction is small at high angles of attack and the correlation was weak with any parameter tried. The data was curve fitted using momentum ratio as the parameter because the lower angle peak values correlate better with this parameter and because plume impingement on the fin will induce rolling moments. Equation 19 is the resulting curve fitted through the data of Figure 3-24.

$$\Delta C_{\ell_{interaction}} = -0.0010188 - 0.037801\,(\Phi_j/\Phi_\infty) - 0.147119\,(\Phi_j/\Phi_\infty)^2 \quad (19)$$

The side force and yawing moment correlations are presented in Figure 3-25 and 3-26. These data were found to correlate but with momentum ratio and Equations 20 and 21 present the least square curve fit polynominals fitted through the data.

$$\Delta C_{n_{interaction}} = 0.0013671 + 0.079588\,(\Phi_j/\Phi_\infty) + 0.26561\,(\Phi_j/\Phi_\infty)^2 \quad (20)$$

$$\Delta C_{Y_{interaction}} = -0.0030983 - 0.16962\,(\Phi_j/\Phi_\infty) - 0.639818\,(\Phi_j/\Phi_\infty)^2 \quad (21)$$

Equations 19 to 21 do not have maximum or minimum values for positive momentum ratios unlike the pitch down data correlations and caution must be used in extending these curves too far from the range of the fit.

3.3.2 PEAK VALUE CORRELATIONS. Figure 3-18 showed that the interaction data exhibited a range of peak values at lower angles of attack which are dependent on nozzle conditions as is the angle of attack at which the peak value occurred. Figure 3-27 and 3-28 present peak values of interaction rolling moment and yawing moment plotted against the angles of attack at which they occur to show that there is a range of angles of attack where the peak values of interaction moments occur and that the data at angles of attack above the peak value lies on the same curve. No curve fitting nor interpolating of data was used to determine peak values of the data and some scatter must result because of the fixed angles of attack tested over this region of angles of attack. The model for predicting the effects in the peak value region consists of the following steps:

a. predict peak value as a function of nozzle parameters,

b. predict peak angle of attack from peak value,

c. if the angle of attack is above that for the peak value, predict interaction value from angle of attack vs peak value curve

and the discussion will proceed in this stepwise fashion.

Figure 3-29 to 3-32 present correlations of peak value data as functions of momentum ratio. These data in general show very good correlation with momentum ratio with the exception of the longitudinal data whereas Figure 3-33 shows the gas mixture data shows better agreement when it is correlated on the basis of mass flow ratio. The peak interaction data for the lateral/directional increments was curve fitted with momentum ratio as the parameter and Equations 22 to 24 present the results.

$$\Delta C_{\ell_{peak}} = -0.0005544 - 0.2908833\,(\Phi_j/\Phi_\infty) + 0.4219384\,(\Phi_j/\Phi_\infty)^2 \quad (22)$$

$$\Delta C_{n_{peak}} = 0.0006995 + 0.5021707\,(\Phi_j/\Phi_\infty) - 0.718513\,(\Phi_j/\Phi_\infty)^2 \quad (23)$$

$$\Delta C_{Y_{peak}} = 0.00113266 - 1.1443836\,(\Phi_j/\Phi_\infty) + 1.868108\,(\Phi_j/\Phi_\infty)^2 \quad (24)$$

These curves all have a maximum or minimum value reasonably close to the data range; the rolling moment has a minimum value of -0.05068797 at a momentum ratio of 0.344699; the yawing moment peak has a maximum value of 0.08844 at a momentum ratio of 0.34945; and the side force has a minimum value of -0.174127 at a momentum ratio of 0.306295. The agreement between the values of momentum ratio at the curve maximums would indicate that the peak value curves are good fits of the data.

The normal force peak value data of Figure 3-32 and 3-33 clearly indicate that the energy ratio is an important parameter and must be accounted for by using mass flow ratio rather than momentum ratio as the curve fit parameter given in Equation 25.

$$\Delta C_{N_{peak}} = 0.008828114 - 0.1563674\,(\dot{m}_j/\dot{m}_\infty) + 0.0519091\,(\dot{m}_j/\dot{m}_\infty)^2 \quad (25)$$

and this curve has a minimum value of -0.11817 at a mass flow ratio of 1.506. The pitching moment peak values data was very erratic at low values of momentum ratio or mass flow ratio and while not an important term a curve fit (Equation 26) was made through it for completeness of the model.

$$\Delta C_{m_{peak}} = 0.00116665 + 0.0073166\,(\dot{m}_j/\dot{m}_\infty) + 0.114445\,(\dot{m}_j/\dot{m}_\infty)^2 \quad (26)$$

Equations 22 to 26 present curve fits which allow computation of the peak value of the coefficients as a function of nozzle parameters. The next step is to compute the angles of attack at which these peak values occur and the shape of the peak value versus angle of attack curve. Equations 27 to 31 were obtained by curve fitting the data of Figure

3-27, 3-28 and similar data for the remaining peak increments.

$$\Delta C_{\ell_{peak}} = -0.0435488\ (\alpha + 13.273)^{-1} + 0.00081505\ (\alpha) - 0.0082231 \quad (27)$$

$$\Delta C_{n_{peak}} = 0.588341\ (\alpha + 18.9366)^{-1} + 0.000111737\ (\alpha) + 0.0140611 \quad (28)$$

$$\Delta C_{Y_{peak}} = -6.06039\ (\alpha + 31.8419)^{-1} - 0.0017003\ (\alpha) + 0.154756 \quad (29)$$

$$\Delta C_{N_{peak}} = 42.9197\ (\alpha - 91.8437)^{-1} + 0.00822308\ (\alpha) + 0.435187 \quad (30)$$

$$\Delta C_{m_{peak}} = 0.0590783\ (\alpha + 16.9382)^{-1} + 0.000055711\ (\alpha) - 0.00208543 \quad (31)$$

Equations 27 to 31 can be solved for the angle of attack of peak increments determined from Equations 22 to 26 and if the vehicle angle of attack is higher than the peak angle the value of the induced increment is computed from Equations 27 to 31 directly as a function of vehicle angle of attack.

3.3.3 DATA AT ANGLES OF ATTACK BELOW PEAK VALUES. Figure 3-18 shows that the data below the angle of attack where the peak value occurred decays to a reduced level. A limited amount of analysis has been performed in this region because the number of data points is very small particularly for the higher jet pressures where the peak value was reached at or very near the lowest value of angle of attack tested and the curves depend on the lowest pressure data where error effects become significant. Figures 3-34 to 3-36 present typical results of these correlations. The data is presented as ratios of the peak value plotted against angle of attack measured from the peak value. These figures show the decline in the data below the peak value very clearly, however the scatter in the data is large and is introduced by all of the terms (α, α_{peak}, C_Y, $C_{Y_{peak}}$, for example). A model has been tentatively selected for this region which uses the peak value and assumes that the interaction increment goes to zero at 20 degrees below the peak. Equation 32 presents the model

$$C_M = C_{M_{peak}} \left\{ \sin \left[\frac{\pi}{2} \left(\frac{\alpha - \alpha_{peak} + 20}{20} \right) \right] \right\}^2 \quad (32)$$

where

C_M = pitch up force or moment coefficient

$C_{M_{peak}}$ = peak pitch up force or moment coefficient

The value of 20 degrees below the peak was chosen because of the rolling moment data (Figure 3-34) and is below the range of angles of attack of practical interest.

3.4 YAW RCS

Figure 3-37 presents the induced yaw and roll data from the left side mounted yaw jets of test OA82. The data shows differences between the values at high angles of attack and those at low angles but within each range the variation with angle of attack is small and a high angle/low angle model similar to the pitch down model of Section 3.2 was used at correlate this data. There was fewer yaw data runs on test OA82 than pitch runs so that the models have fewer conditions to correlate against.

3.4.1 HIGH ANGLE OF ATTACK DATA. The high angle of attack range was defined as angles of attack above 15 degrees and the data presented in Figure 3-38 to 3-44 are averages of all the data above this angle of attack. Figures 3-39 and 3-41 present the longitudinal data correlated to momentum ratio while Figures 3-38 and 3-40 show that RT ratio is important and mass flow ratio is the better correlating parameter. This result was true for all of the yaw RCS increments.

The least squares curve fits through the normal force and pitching moment are given in Equations 33 and 34.

$$\Delta C_{N_{interaction}} = 0.012030 - 0.443928\ (\dot{m}_j/\dot{m}_\infty) + 0.423644\ (\dot{m}_j/\dot{m}_\infty)^2 \quad (33)$$

$$\Delta C_{m_{interaction}} = 0.00153551 + 0.1525983\ (\dot{m}_j/\dot{m}_\infty) - 0.9910115\ (\dot{m}_j/\dot{m})^2 \quad (34)$$

The normal force curve fit has a minimum value of -0.1042558 at a mass flow ratio of 0.5239 while the pitching moment has a maximum value of 0.0074098 at a mass flow of 0.07699.

The lateral-directional interaction increments are shown in Figure 3-42 to 3-44. The rolling moment increments showed the poorest correlation to any of the nozzle parameters and more data is needed to refine this curve. Curves fitted through these increments are given in Equations 35 to 37.

$$\Delta C_{\ell_{interaction}} = -0.0017298 - 0.079945\ (\dot{m}_j/\dot{m}_\infty) + 0.575868\ (\dot{m}_j/\dot{m}_\infty)^2 \quad (35)$$

$$\Delta C_{n_{interaction}} = -0.00034818 - 0.0193889\ (\dot{m}_j/\dot{m}_\infty) + 0.0929347\ (\dot{m}_j/\dot{m}_\infty)^2 \quad (36)$$

$$\Delta C_{Y_{interaction}} = 0.00273838 + 0.157324\ (\dot{m}_j/\dot{m}_\infty) - 0.920077\ (\dot{m}_j/\dot{m}_\infty)^2 \quad (37)$$

Each of these curves has a maximum within the range of the test data. The rolling moment curve has a minimum value of -0.004504 at a mass flow ratio of 0.069413; the yawing moment has a minimum value of -0.001359 at a mass flow ratio of 0.1043; and the side force curve has a maximum value of 0.009464 at a mass flow ratio of 0.85495.

3.4.2 LOW ANGLE OF ATTACK YAW DATA. Figure 3-45 to 3-49 present similar data to that presented above with the exception that it is low angle of attack yaw data. The trends are very similar to the high angle of attack data and mass flow ratio was found to be the better parameter thus RT ratio simulation is important in the interaction. Equations 38 to 42 present the curve fits for these data:

$$\Delta C_{N_{interaction}} = 0.00340516 - 0.4768133\,(\dot{m}_j/\dot{m}_\infty) + 3.8111191\,(\dot{m}_j/\dot{m}_\infty)^2 \quad (38)$$

$$\Delta C_{m_{interaction}} = 0.000219195389 + 0.0251417\,(\dot{m}_j/\dot{m}_\infty) - 0.0637262\,(\dot{m}_j/\dot{m}_\infty)^2 \quad (39)$$

$$\Delta C_{\ell_{interaction}} = -0.00049126 - 0.00860359\,(\dot{m}_j/\dot{m}_\infty) + 0.0470322\,(\dot{m}_j/\dot{m}_\infty)^2 \quad (40)$$

$$\Delta C_{n_{interaction}} = -0.00017444 - 0.07711317\,(\dot{m}_j/\dot{m}_\infty) + 0.5407319\,(\dot{m}_j/\dot{m}_\infty)^2 \quad (41)$$

$$\Delta C_{Y_{interaction}} = 0.00111215 + 0.3044469\,(\dot{m}_j/\dot{m}_\infty) - 2.233286\,(\dot{m}_j/\dot{m}_\infty) \quad (42)$$

and the table presented below compares the peak values which result from these curves with those of the high angle of attack models of Section 3.4.1

	Low α Curve		High α Curve	
Increment	Peak Value	$\dot{m}_j/\dot{m}_\infty$	Peak Value	$\dot{m}_j/\dot{m}_\infty$
ΔC_N	-0.011507	0.06255	-0.1042558	0.5239
ΔC_m	0.002772	0.19726	0.0074098	0.0769911
ΔC_ℓ	-0.0008847	0.09146	-0.004504	0.069413
ΔC_n	-0.002924	0.07130	-0.0013595	0.10431
ΔC_Y	0.011488	0.06816	0.0094636	0.0855

These peak values show that the high angle of attack yaw RCS data showed much greater effects on the wing resulting in higher values of ΔC_N, ΔC_m, ΔC_ℓ while the lower angle data shows greater effects on the side of the fuselage and possibly the fin.

3.5 COMBINED CONTROL

All of the data presented in Section 3 have been devoted to RCS controls operating on a single side of the vehicle and not in combination with other controls. The possibility of combined control interference was shown in References 1 and 2, and these effects

must be accounted for in any model of RCS effects. A limited set of data was obtained during test OA82 on certain control combinations which include:

a. Symmetric pitch down RCS

b. Symmetric pitch up RCS

c. Roll RCS

d. Combined right side pitch up and yaw RCS

Because the data set is limited the measured effects must be considered preliminary only.

3.5.1 SYMMETRIC PITCH DOWN. Figure 2-5 presents the symmetric pitch down data obtained in test OA82 and Figure 3-50 presents the ratio of the symmetric jet data to that of a single side set. These data show that the symmetric pitch down RCS effects are significantly greater than twice that of a single side firing and although there is some scatter it does not appear to be related to angle of attack. The interaction between the plumes must occur in the base region of the model between the body flap and main propulsion engines and must be related primarily to the plume impingement component rather than the interaction component. The effect of the sting is unknown (see Section 3.6) in this plume/plume interaction but a preliminary model has been made by averaging the data of Figure 3-50.

$$\Delta C_{N_{\text{cross coupling}}} = 0.3\left(\Delta C_{N_{\text{impingement}}} + \Delta C_{N_{\text{interaction}}}\right)_{(1 \text{ side})} \quad (43)$$

$$\Delta C_{m_{\text{cross coupling}}} = 0.32\left(\Delta C_{m_{\text{impingement}}} + \Delta C_{m_{\text{interaction}}}\right)_{(1 \text{ side})} \quad (44)$$

where Equations 43 and 44 are additional terms to be added to the basic Equation 1.

3.5.2 SYMMETRIC PITCH UP RCS. Figure 2-8 presented the symmetric pitch up data obtained in test OA82 and this figure showed no difference in pitching moment between the single side and symmetric firing data. The normal force increment shows a very large difference in the range from zero angle of attack to 15° but a reversal occurs at higher angles of attack. While more data is needed to better define these effects, the pitching moment data should be more accurate and no effect of symmetric pitch up cross-coupling has been modeled.

3.5.3 ROLL RCS CROSS-COUPLING. Figure 2-6 presented a comparison of the roll jet increments with the two single side components which make up the roll jet combination. Figure 3-51 presents the roll combined control ratioed to the sum of

the individual components. There is large scatter in the normal force results at higher angles of attack but an average value taken through the data below 15° shows that there is a small increment

$$\Delta C_{N_{\text{cross coupling}}} = 0.124\ (\Sigma \Delta C_N)_{\text{components}} \tag{45}$$

while the pitch data shows a slightly greater effect which is

$$\Delta C_{m_{\text{cross coupling}}} = 0.211\ (\Sigma \Delta C_m)_{\text{components}} \tag{46}$$

The rolling moment data shows that it is very close to the sum of the two components ($1.057\ \Sigma \Delta C_\ell$) and no cross coupling term is used.

In the data presented above the components from the left and right sides act in the same direction and add together. The nozzles on opposite sides of the vehicle cause induced effects which oppose each other in the case of side force and yawing moment. Figure 3-51 shows that the resulting yawing moment is less than the difference of the two values and the average cross coupling term is

$$\Delta C_{n\ \text{cross coupling}} = -0.206\ (\Sigma \Delta C_n)_{\text{components}} \tag{47}$$

The side force components from both sides almost completely cancel each other except at the higher angles. Thus an average was taken for the data above 15° which relates the cross coupling to the pitch up force only

$$\Delta C_{Y_{\text{cross coupling}}} = -0.431\ (\Delta C_{Y_{\text{pitch up}}}) \tag{48}$$

3.5.4 RIGHT SIDE PITCH UP COMBINED WITH RIGHT SIDE YAW. Figure 2-10 presents a comparison of the combined right side pitch-up and yaw RCS incremental data compared with right side pitch up data and left side yaw data. There was no right side yaw RCS data generated to make the comparison and thus the signs of the yaw lateral-directional increments are reversed on this plot. The longitudinal data (Figure 2-10a) shows that the normal force is close to the sum of the pitch up and yaw components at angles of attack below 15° while the pitching moment shows very close agreement with the yaw induced component. Thus the present cross coupling model assumes no normal force effect and that the pitching moment cross coupling cancels the pitch-up RCS increment.

$$\Delta C_{m_{\text{cross coupling}}} = -\Delta C_{m_{\text{pitch up}}} \tag{49}$$

The side force and yawing moment increments should add to each other to obtain the combined pitch up/yaw data, however, the data shows that these increments from the

combined control follows the roll jet value at high angles and lies between the curves at the lowest angles. Thus the yaw cross coupling models were taken to be

$$\Delta C_{n_{\text{cross coupling}}} = -\Delta C_{n_{\text{yaw}}} \text{ for } \alpha > 0° \tag{50}$$

$$\Delta C_{n_{\text{cross coupling}}} = -0.6785\, \Sigma(\Delta C_n)_{\text{components}} \text{ for } \alpha < 0° \tag{51}$$

and the side force models are

$$\Delta C_{Y_{\text{cross coupling}}} = -\Delta C_{Y_{\text{yaw}}} \quad \alpha > 0° \tag{52}$$

$$\Delta C_{Y_{\text{cross coupling}}} = 0 \quad \alpha \leq 0° \tag{53}$$

The rolling moment induced effects should oppose each other, however, the data shows that the combined control tends to follow the yaw jet induced increment at high angles of attack and the pitch up jet increment at low angles. The models chosen give

$$\Delta C_{\ell_{\text{cross coupling}}} = -\Delta C_{\ell_{\text{pitch up}}} \quad \alpha > 15° \tag{54}$$

$$\Delta C_{\ell_{\text{cross coupling}}} = 0 \quad \alpha < 15° \tag{55}$$

3.6 POSSIBLE STING INTERFERENCE EFFECTS

All of the data presently available on rear RCS interference effects have been generated using a sting mounted model. The sting passes up through the base region of the model as is shown in Figure 2-2 with the nozzle block assembly used to simulate the RCS mounted to it. The net result is that only part of two MPS engines and the body flap were simulated and the sting and plenum act to restrict the plume flow across the model to the area between the sting and flap. Very highly underexpanded plumes, such as are needed for RCS simulation will expand to impinge on the sting and this impingement could be a significant factor in the RCS data obtained to date. Figure 3-50 showed that the RCS induced effects for the symmetric pitch down case are greater than twice the induced effect for a single side pitch down. This shows that there is plume-plume interaction occurring in the base region of the model and the sting's presence must influence this interaction. Other data presented in Reference 2 shows that the symmetric firing of pitch down jets causes a high pressure across the body flap under the sting. These data plus data on the effects of changing base geometry also given in Reference 2 present a good case for possible sting interference effects and for the need for a blade mounted model test.

3.7 TIME DEPENDENT EFFECTS

All of the data presented in this report were obtained from steady-state RCS jet testing, however, the RCS jets are not necessarily fired in this manner. The full scale vehicle jets are fired in a pulsed fashion where the duration of a pulse is determined by the vehicle response to the pulse and the minimum length pulse can be very short. The question then can be asked whether these induced effects could be time dependent and thus completely different for a rapidly pulsing control.

The answer to this question can only be obtained indirectly since no data is presently available to verify it. The interaction induced effects which use mass flow ratio as the correlating parameter have had little or no impingement correction taken from them so that it appears that they are caused by the plume acting on the external flow over the vehicle. This being the case there will be essentially no time delay between the rocket coming on and the interaction occurring. The forces and moments which were correlated to mass flow ratio included all of the yaw RCS interaction effects and the pitch up/roll RCS normal force and pitching moment. In addition, the other pitch up/roll RCS data had plume impingement corrections only at the highest nozzle pressure ratios. This coupled with the non-linearity of the incremental interaction data which shows a rapid increase in interaction at low values of jet momentum would argue for interaction occurring during the start of the RCS engine.

At high momentum ratios, the data shows that impingement dominates the pitch down data. The transit time of the RCS plume impinging on structure will be very short and thus the impingement terms will follow the thrust rise with essentially no delay.

In conclusion, it is not expected that there will be any difference between the pulsing control effectiveness and a steady state control.

SYMBOL	RUN	P_{oj} (10^6 N/M^2)	P_{oj} (PSI)
⊡	64	0.889423	129
⊙	61	1.799531	261
◇	62	3.261220	473
△	63	4.840119	702

$$\Delta C_m = C_{m_{jet\ on}} - \bar{C}_{m_{jet\ off}}$$

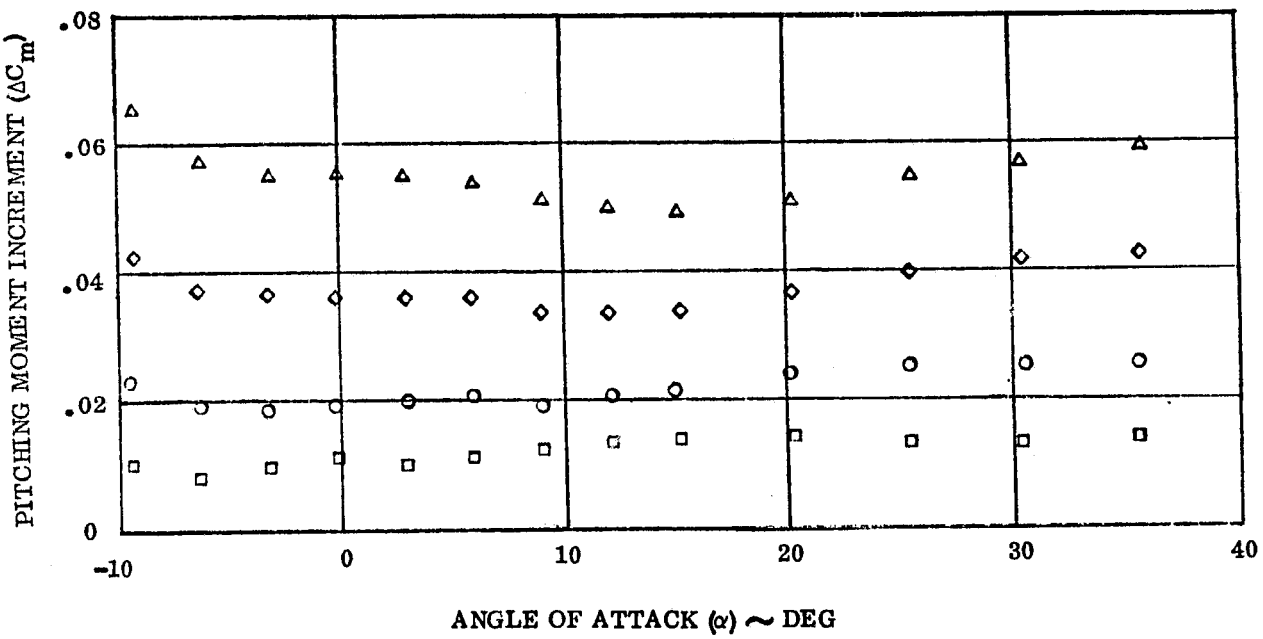

Figure 3-1. Typical Left Side Pitch Down RCS Pitching Moment

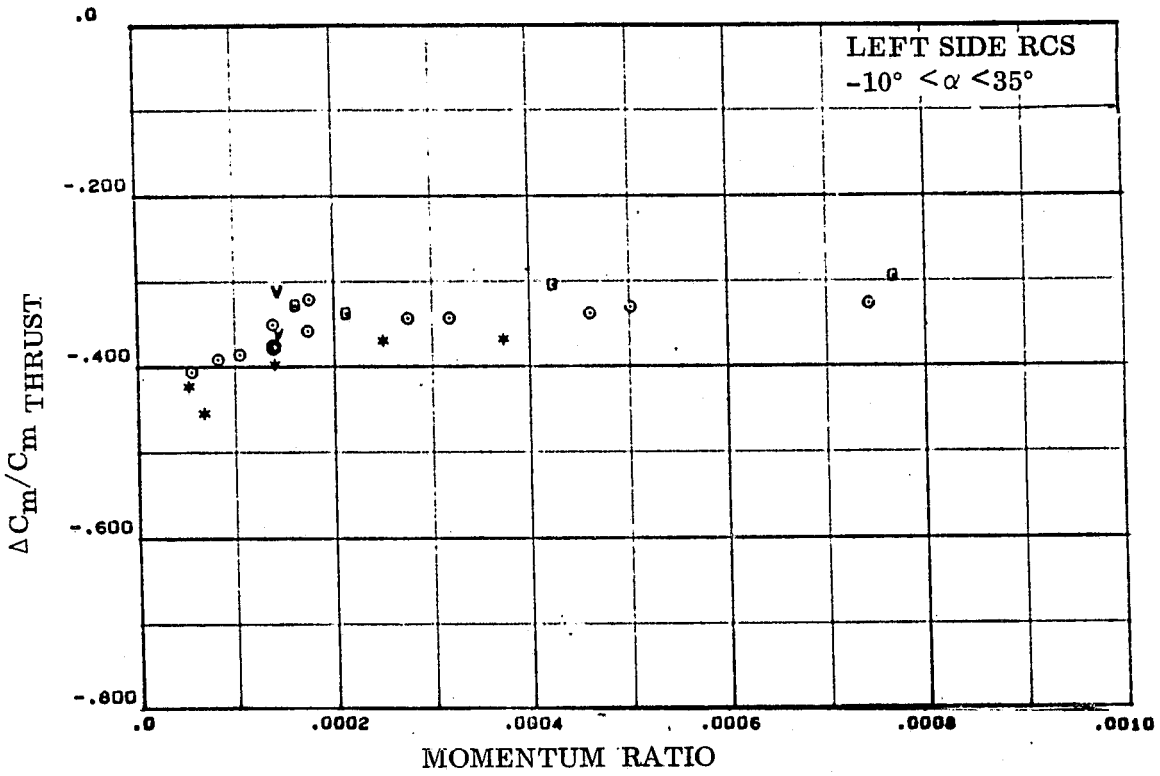

Figure 3-2. Left Side Down Data Averaged at All Angles of Attack

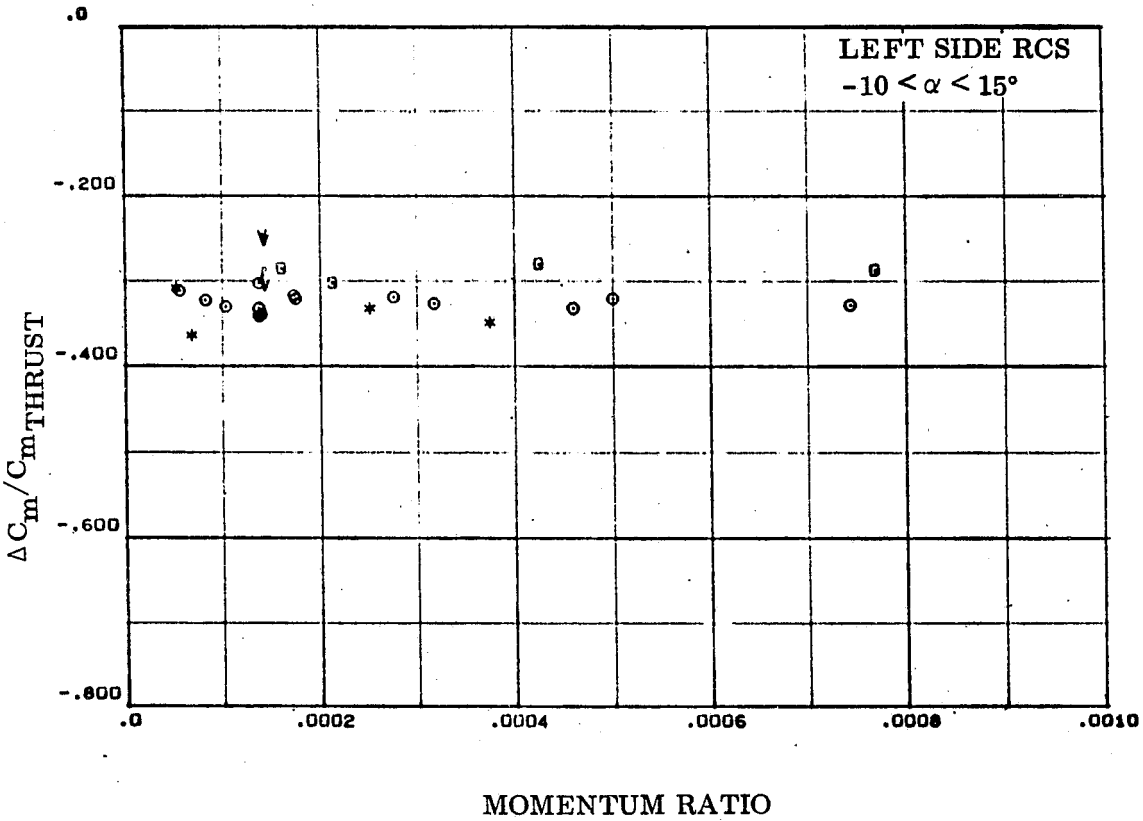

Figure 3-3. Left Side Down Data Averaged at Low Angles of Attack

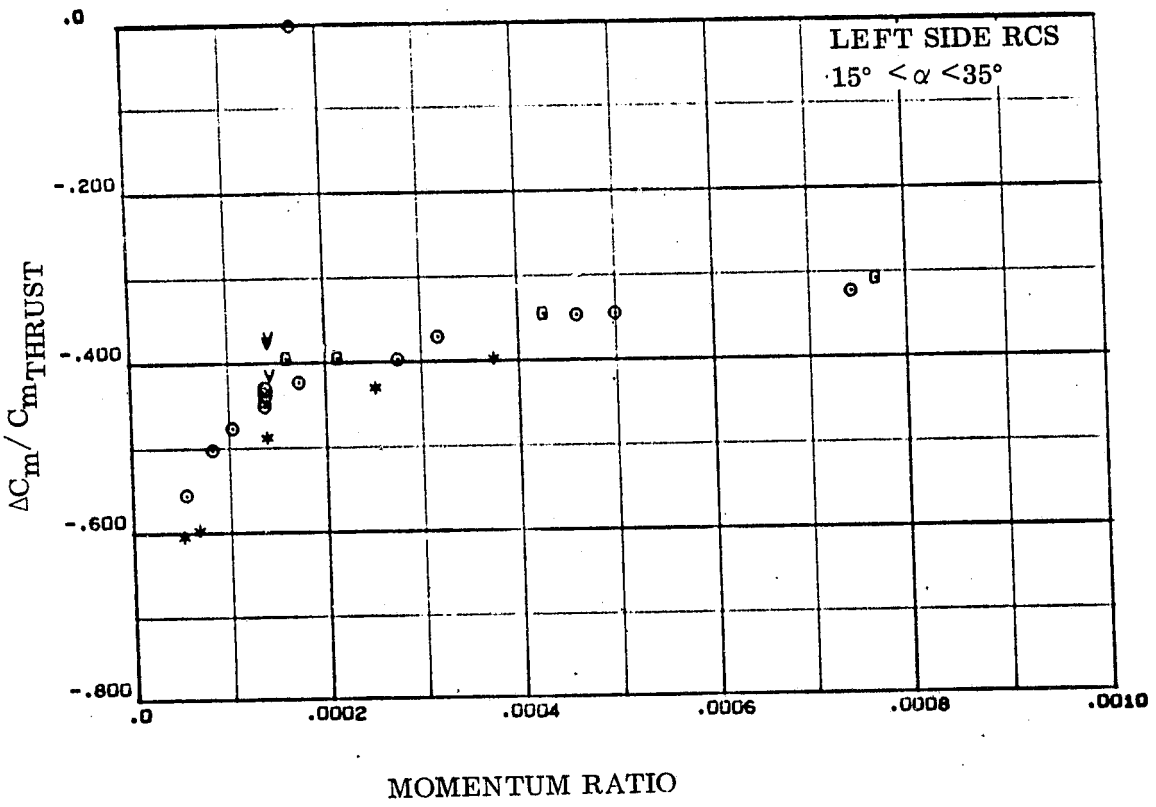

Figure 3-4. Left Side Down Data Averaged at High Angle of Attack

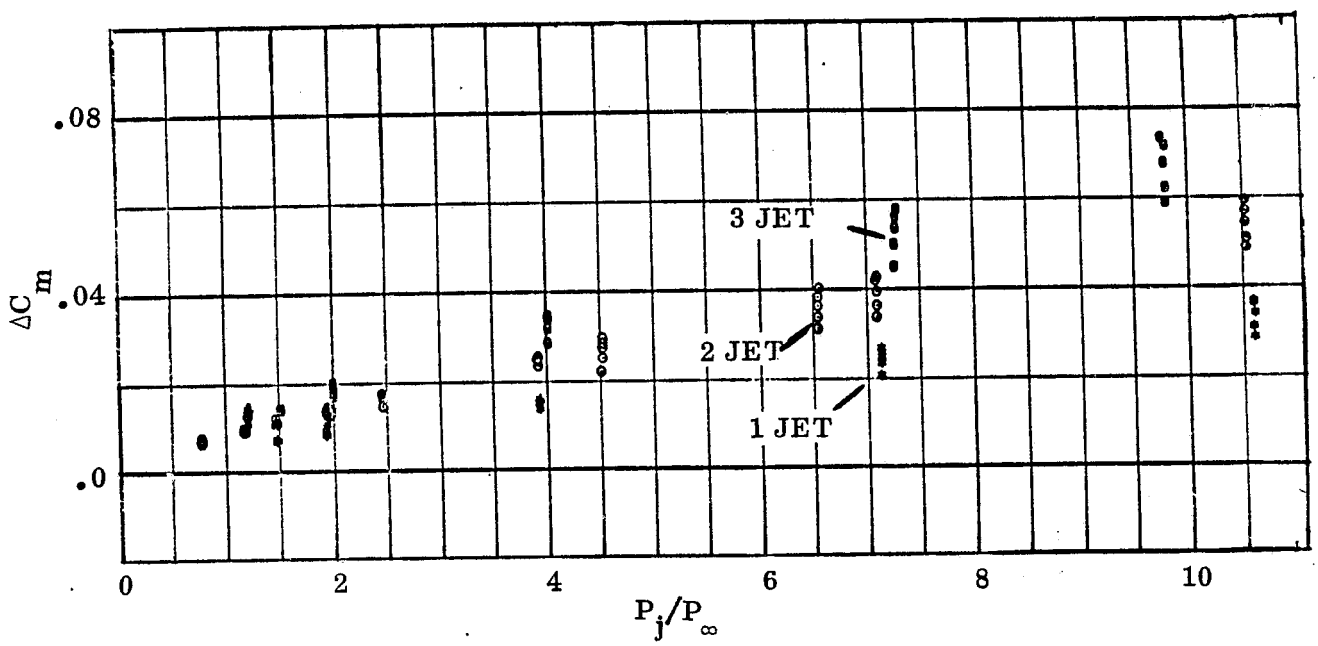

Figure 3-5. Pitch Down RCS at High Angles of Attack Correlated to Exit Pressure Ratio

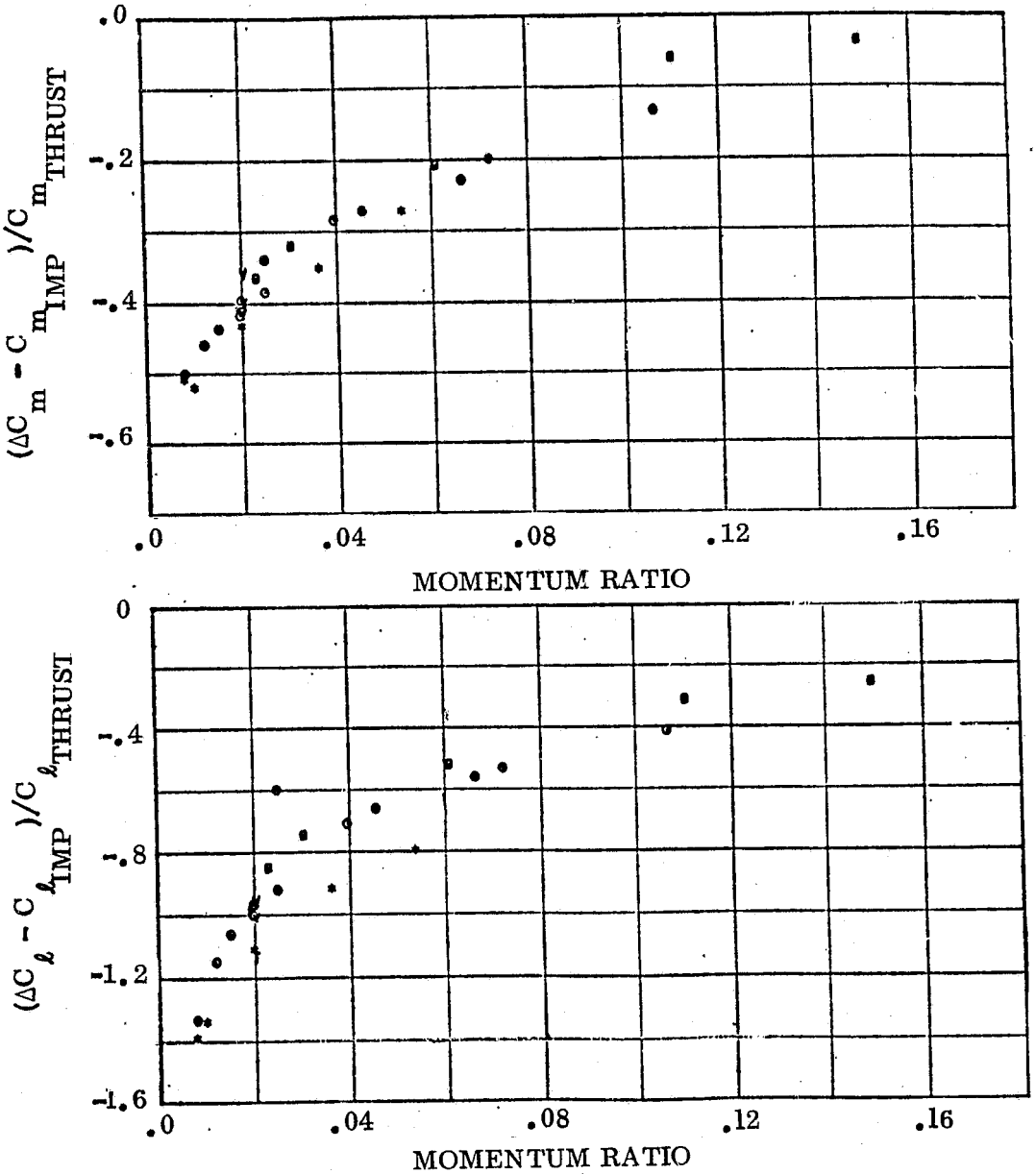

Figure 3-6. Left Side Pitch Down RCS Interaction Data Ratioed to Jet Moment

Symbol	Nozzle	Gas	Run
O	N_{49}	Air	6,30,32,38,40,42,44,45 46,47,59,60,61,62,63,64
*	N_{79}	Air	21,85,86,87,88
⊡	N_{83}	Air	23,89,90,91,92
V	N_{49}	Helium mixtures	66,74,77
f	N_{49}	Argon	71

$\alpha > 15°$

AVERAGED DATA

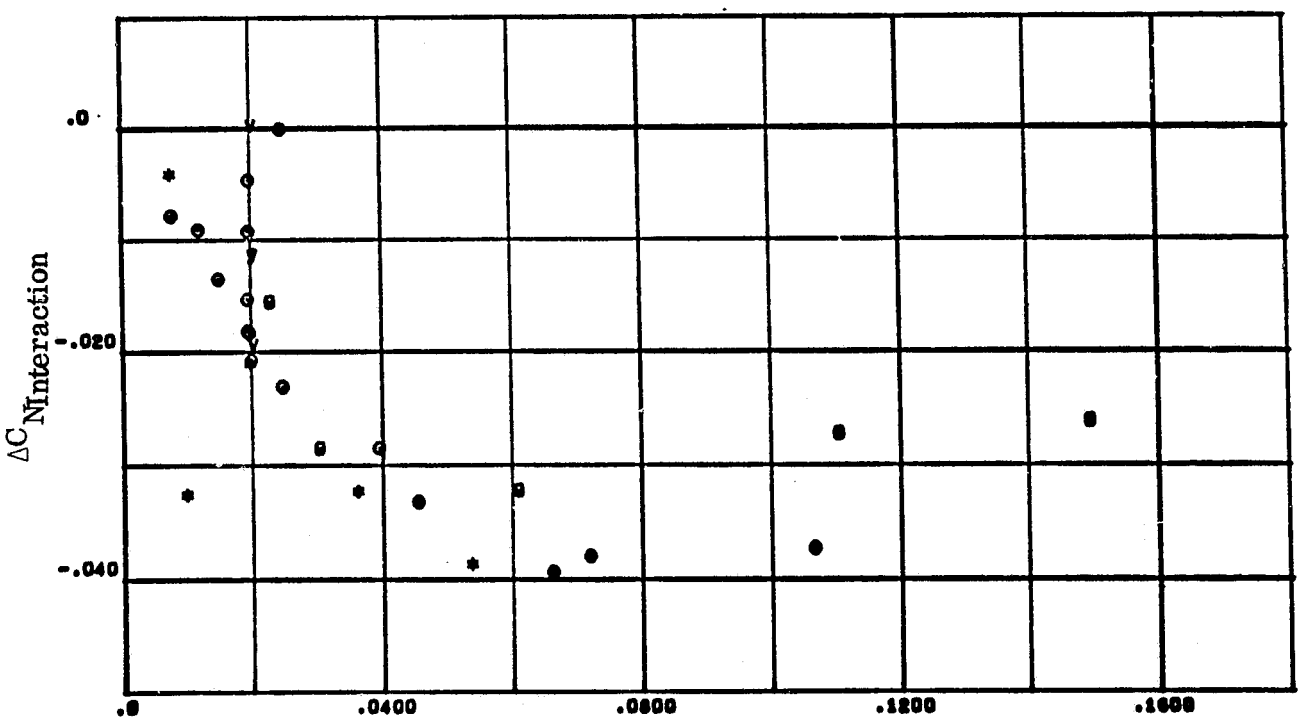

Figure 3-7. Left Side Pitch Down RCS Normal Force Interaction at High Angles ot Attack

Symbol	Nozzle	Gas	Run
O	N_{49}	Air	6, 30, 32, 38, 40, 42, 44, 45 46, 47, 59, 60, 61, 62, 63, 64
*	N_{79}	Air	21, 85, 86, 87, 88
⊡	N_{83}	Air	23, 89, 90, 91, 92
V	N_{49}	Helium mixtures	66, 74, 77
∫	N_{49}	Argon	71

$\alpha > 15°$
AVERAGED DATA

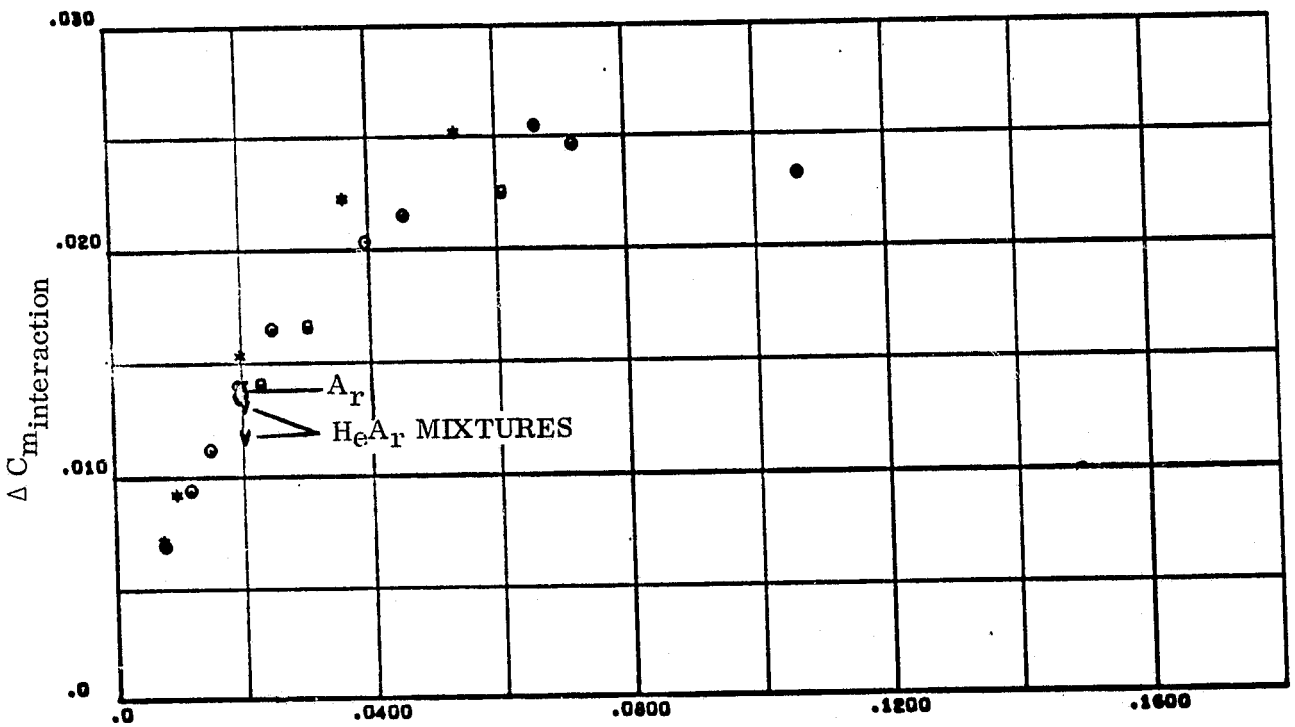

Figure 3-8. Left Side Pitch Down RCS Pitching Moment Interaction at High Angles of Attack

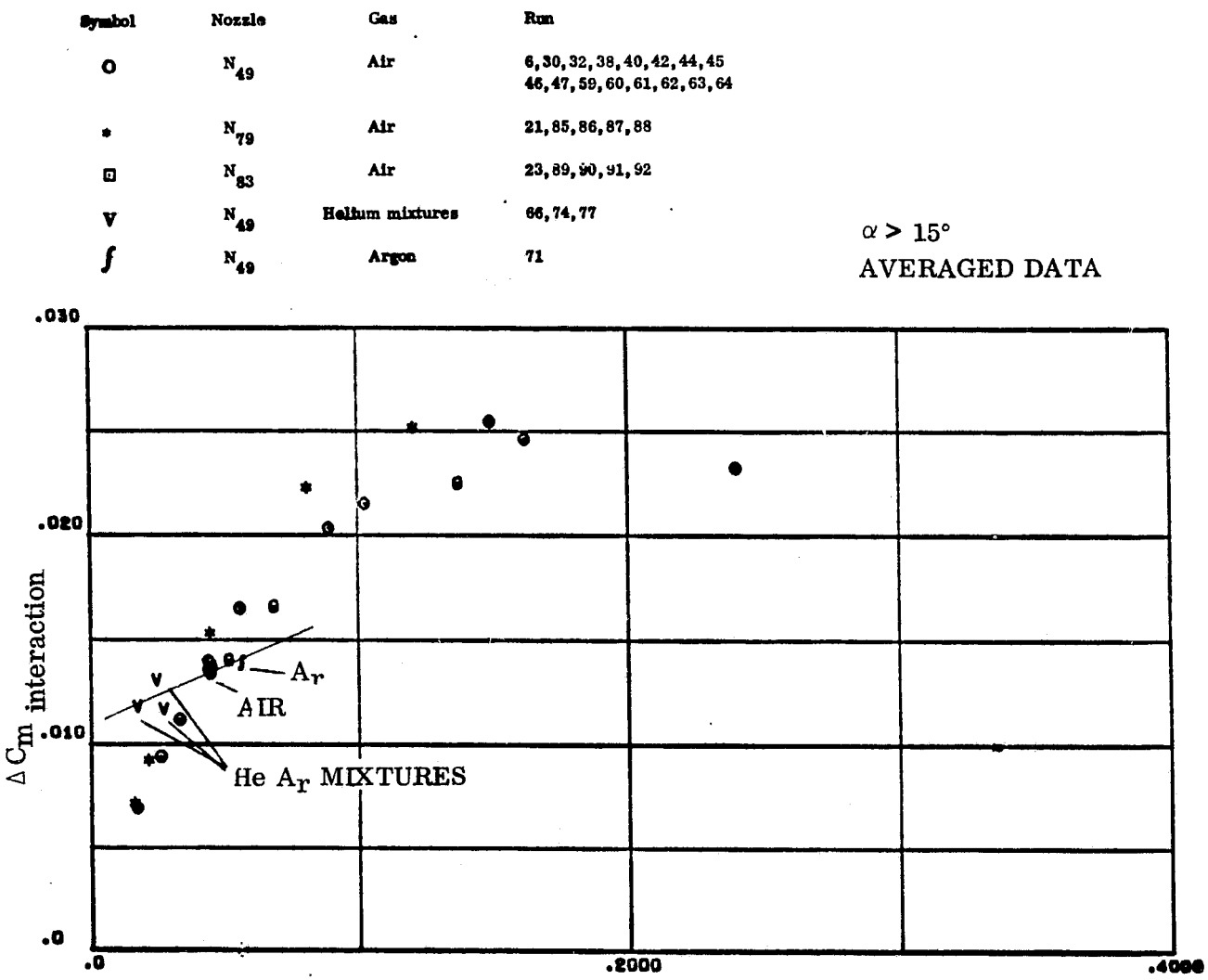

Figure 3-9. Left Side Pitch Down RCS Pitch Interaction Increment Correlated to Mass Flow Ratio

Symbol	Nozzle	Gas	Run
O	N_{49}	Air	6,30,32,38,40,42,44,45 46,47,59,60,61,62,63,64
*	N_{79}	Air	21,85,86,87,88
⊡	N_{83}	Air	23,89,90,91,92
V	N_{49}	Helium mixtures	66,74,77
∫	N_{49}	Argon	71

$\alpha > 15°$
AVERAGED DATA

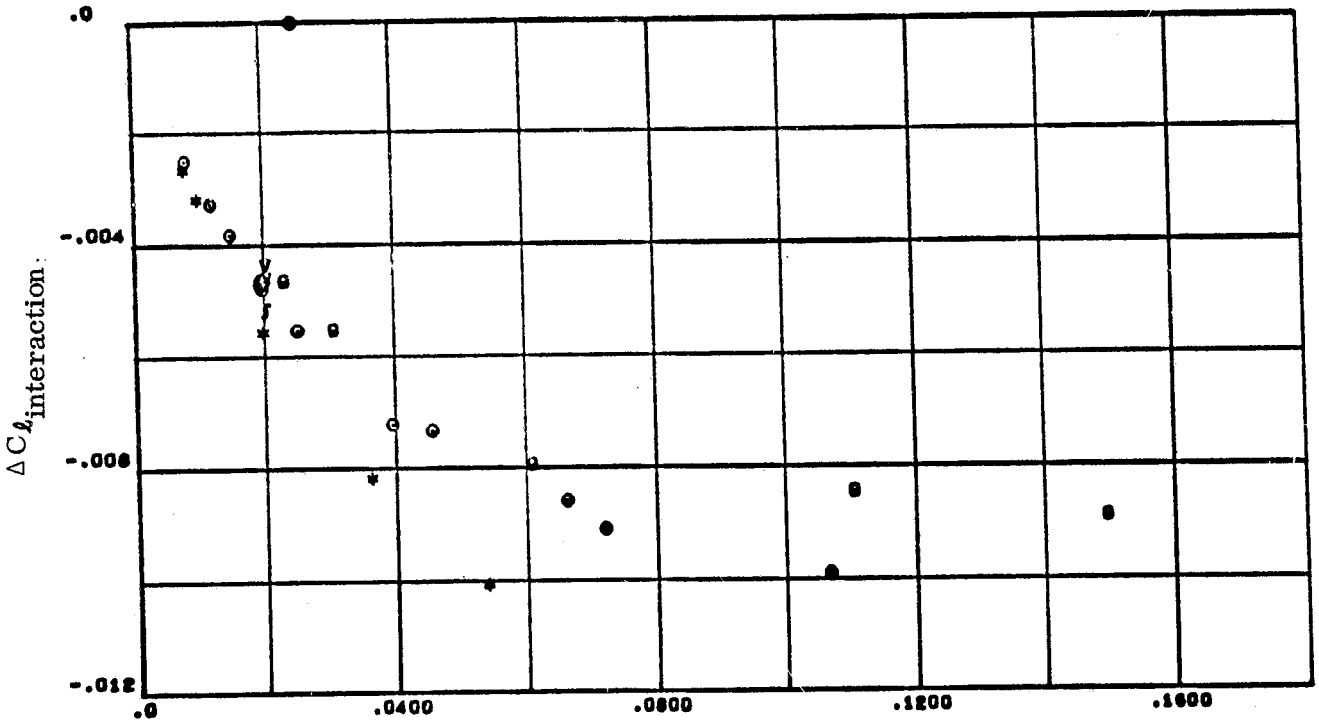

Figure 3-10. Left Side Pitch Down RCS Rolling Moment Interaction at High Angles of Attack

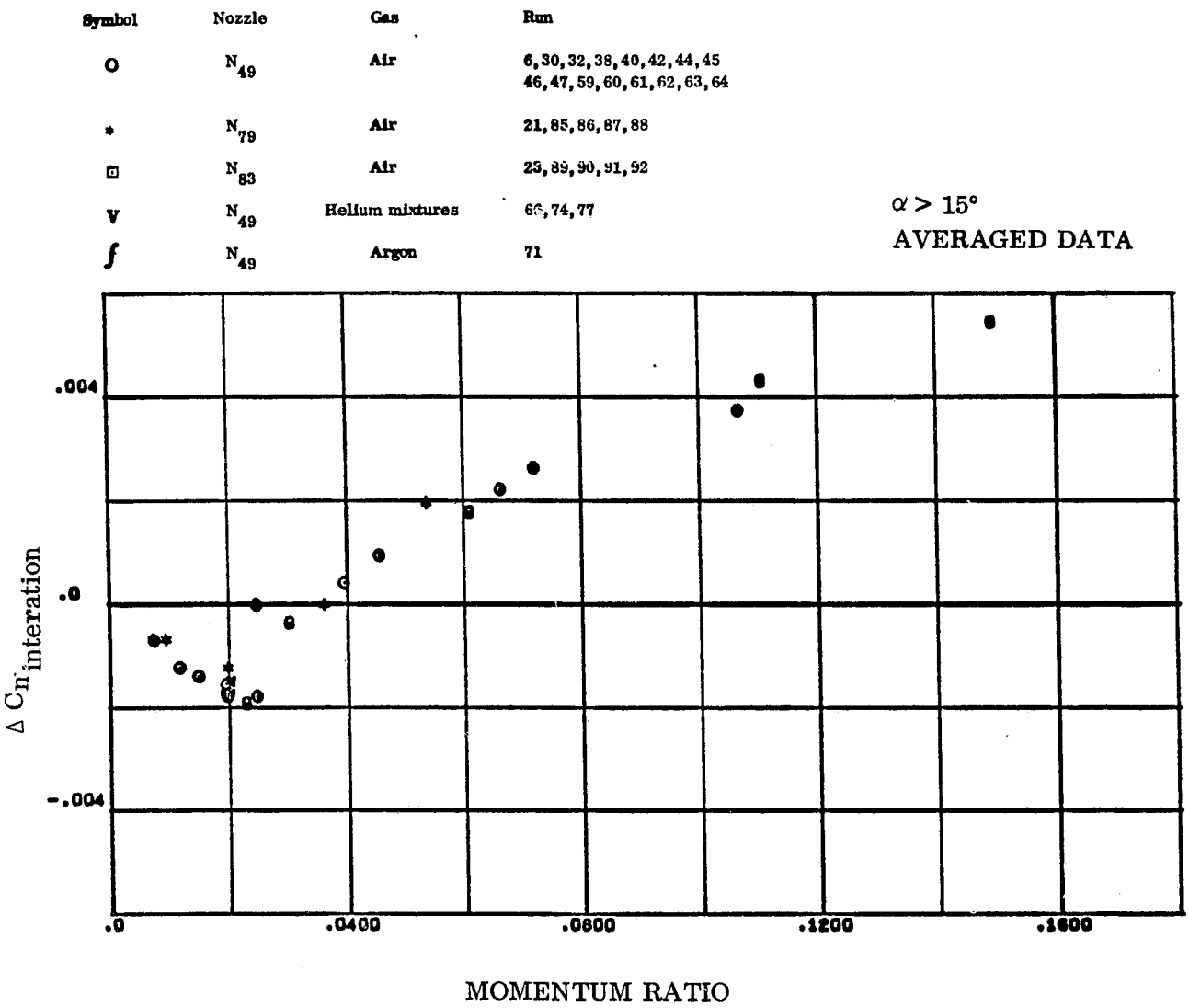

Figure 3-11. Left Side Pitch Down RCS Yawing Moment Interaction at High Angles of Attack

Symbol	Nozzle	Gas	Run
○	N_{49}	Air	6, 30, 32, 38, 40, 42, 44, 45 46, 47, 59, 60, 61, 62, 63, 64
*	N_{79}	Air	21, 85, 86, 87, 88
□	N_{83}	Air	23, 89, 90, 91, 92
▽	N_{49}	Helium mixtures	66, 74, 77
∫	N_{49}	Argon	71

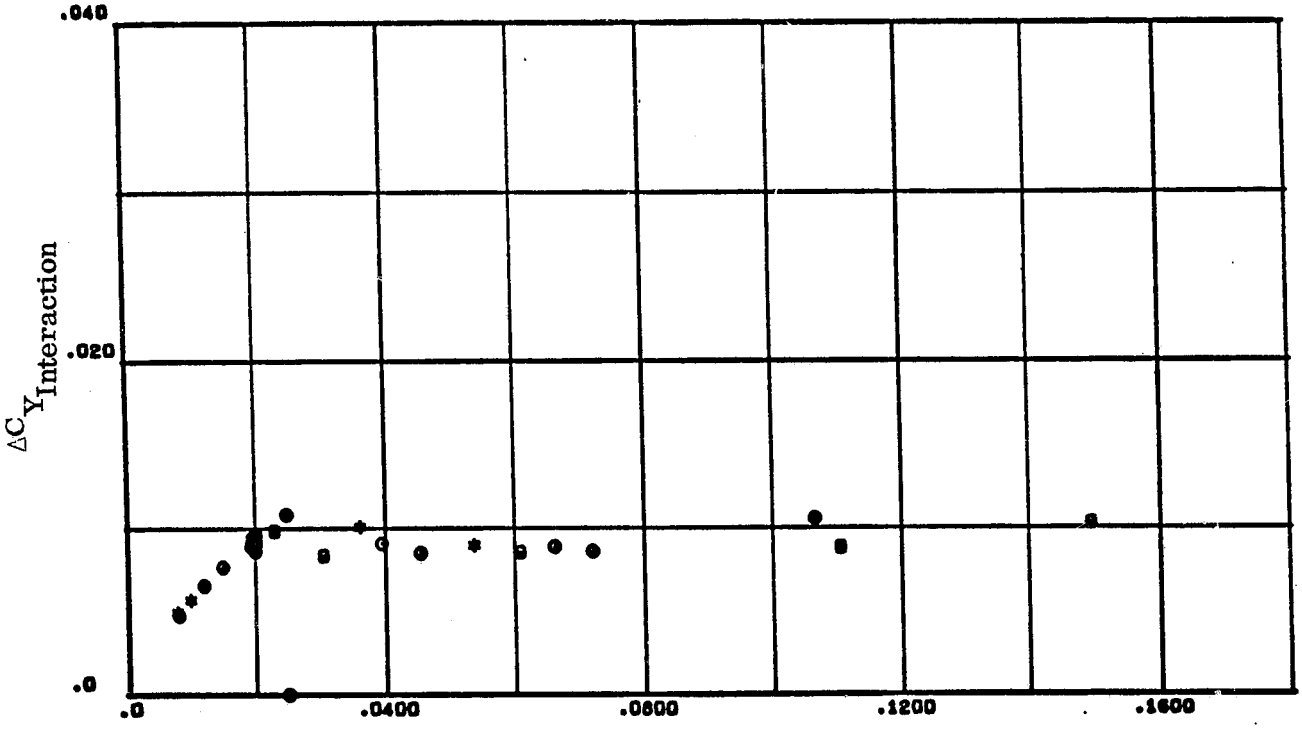

Figure 3-12. Left Side Pitch Down RCS Side Force Interaction at High Angles of Attack

Symbol	Nozzle	Gas	Run
O	N_{49}	Air	6,30,32,38,40,42,44,45 46,47,59,60,61,62,63,64
*	N_{79}	Air	21,85,86,87,88
⊡	N_{83}	Air	23,89,90,91,92
V	N_{49}	Helium mixtures	66,74,77
∫	N_{49}	Argon	71

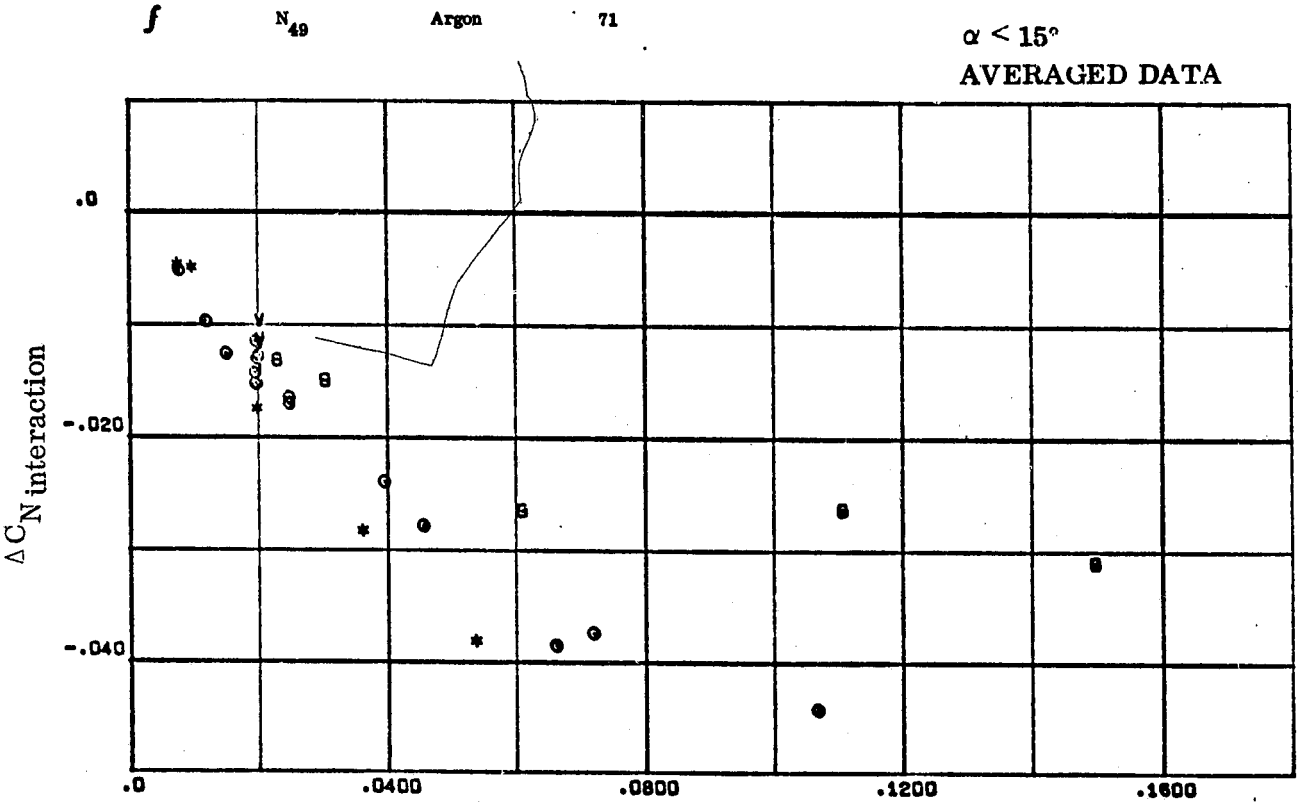

Figure 3-13. Left Side Down RCS Interaction Normal Force at Low Angle of Attack

Symbol	Nozzle	Gas	Run
O	N_{49}	Air	6,30,32,38,40,42,44,45 46,47,59,60,61,62,63,64
*	N_{79}	Air	21,85,86,87,88
⊡	N_{83}	Air	23,89,90,91,92
V	N_{49}	Helium mixtures	66,74,77
f	N_{49}	Argon	71

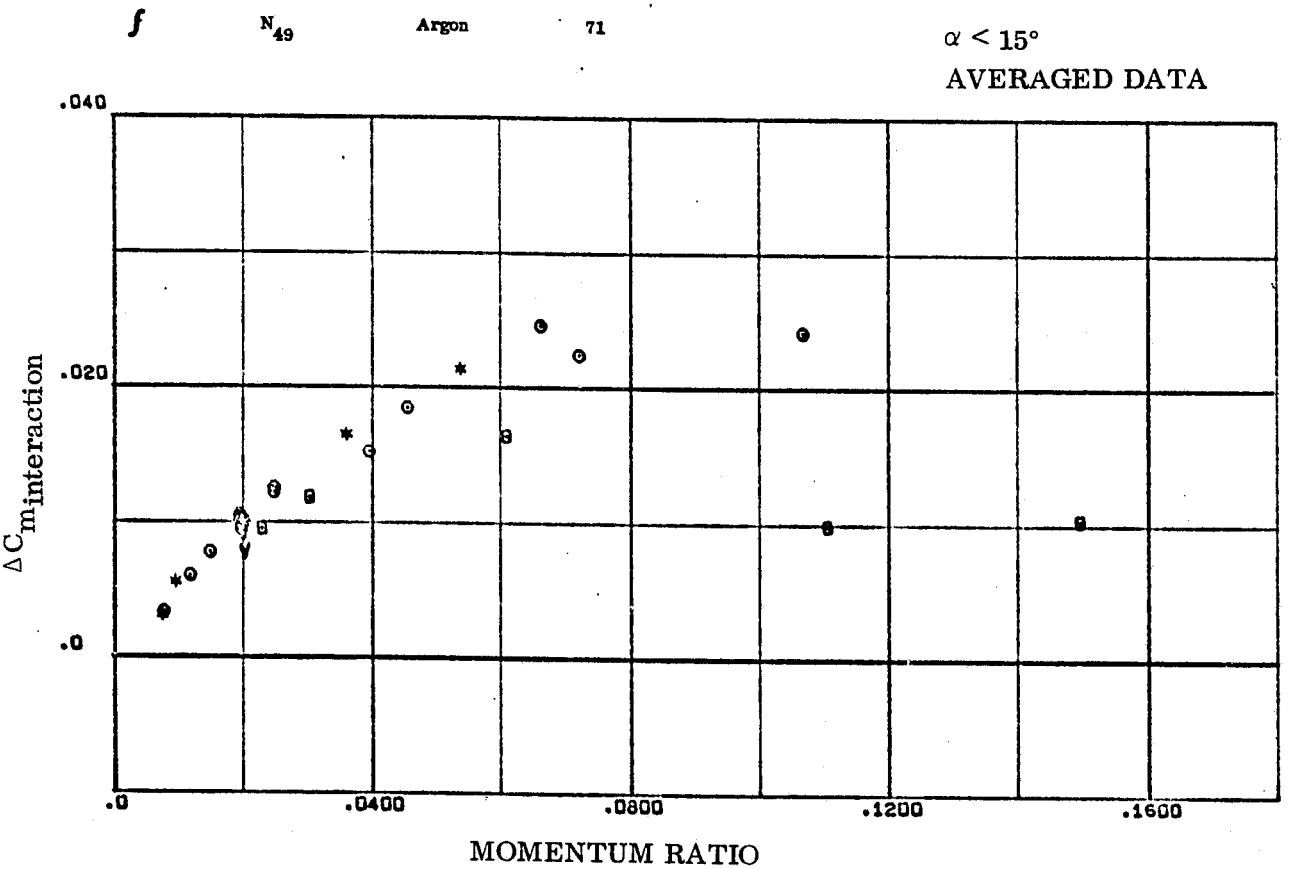

Figure 3-14. Left Side Down RCS Interaction Pitching Moment at Low Angles of Attack

Symbol	Nozzle	Gas	Run
O	N_{49}	Air	6,30,32,38,40,42,44,45 46,47,59,60,61,62,63,64
*	N_{79}	Air	21,85,86,87,88
⊡	N_{83}	Air	23,89,90,91,92
V	N_{49}	Helium mixtures	66,74,77
∫	N_{49}	Argon	71

$\alpha < 15°$
AVERAGED DATA

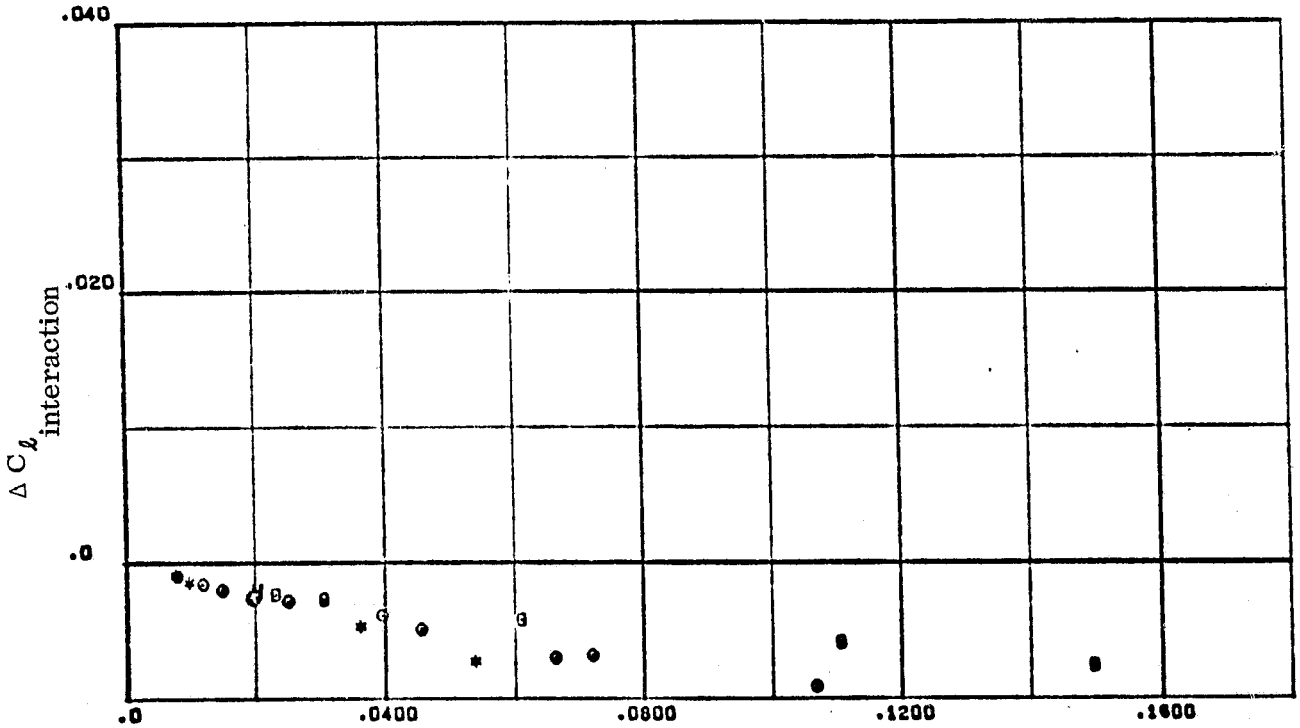

Figure 3-15. Left Side Pitch Down RCS Interaction Rolling Moment at Low Angles of Attack

Symbol	Nozzle	Gas	Run
O	N_{49}	Air	6,30,32,38,40,42,44,45 46,47,59,60,61,62,63,64
*	N_{79}	Air	21,85,86,87,88
⊡	N_{83}	Air	23,89,90,91,92
V	N_{49}	Helium mixtures	66,74,77
∫	N_{49}	Argon	71

$\alpha < 15°$
AVERAGED DATA

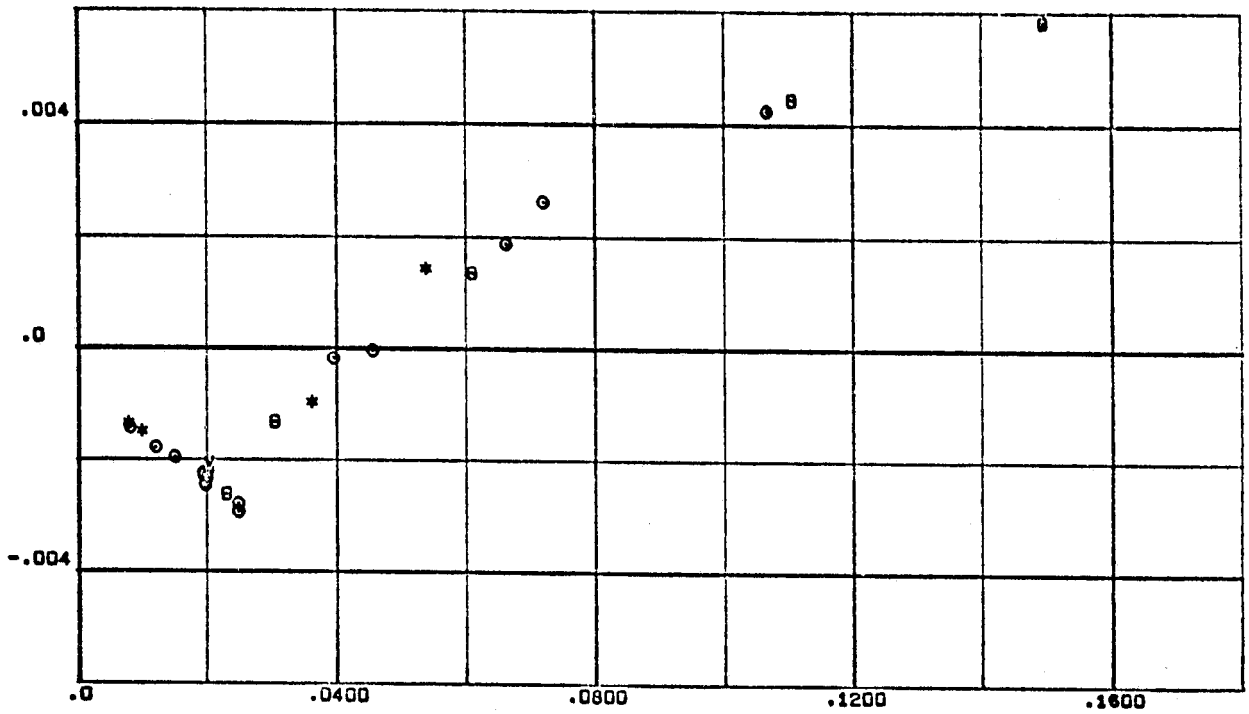

Figure 3-16. Left Side Pitch Down RCS Interaction Yawing Moment at Low Angles of Attack

Symbol	Nozzle	Gas	Run
O	N_{49}	Air	6, 30, 32, 38, 40, 42, 44, 45 46, 47, 59, 60, 61, 62, 63, 64
*	N_{79}	Air	21, 85, 86, 87, 88
⊡	N_{83}	Air	23, 89, 90, 91, 92
V	N_{49}	Helium mixtures	66, 74, 77
∫	N_{49}	Argon	71

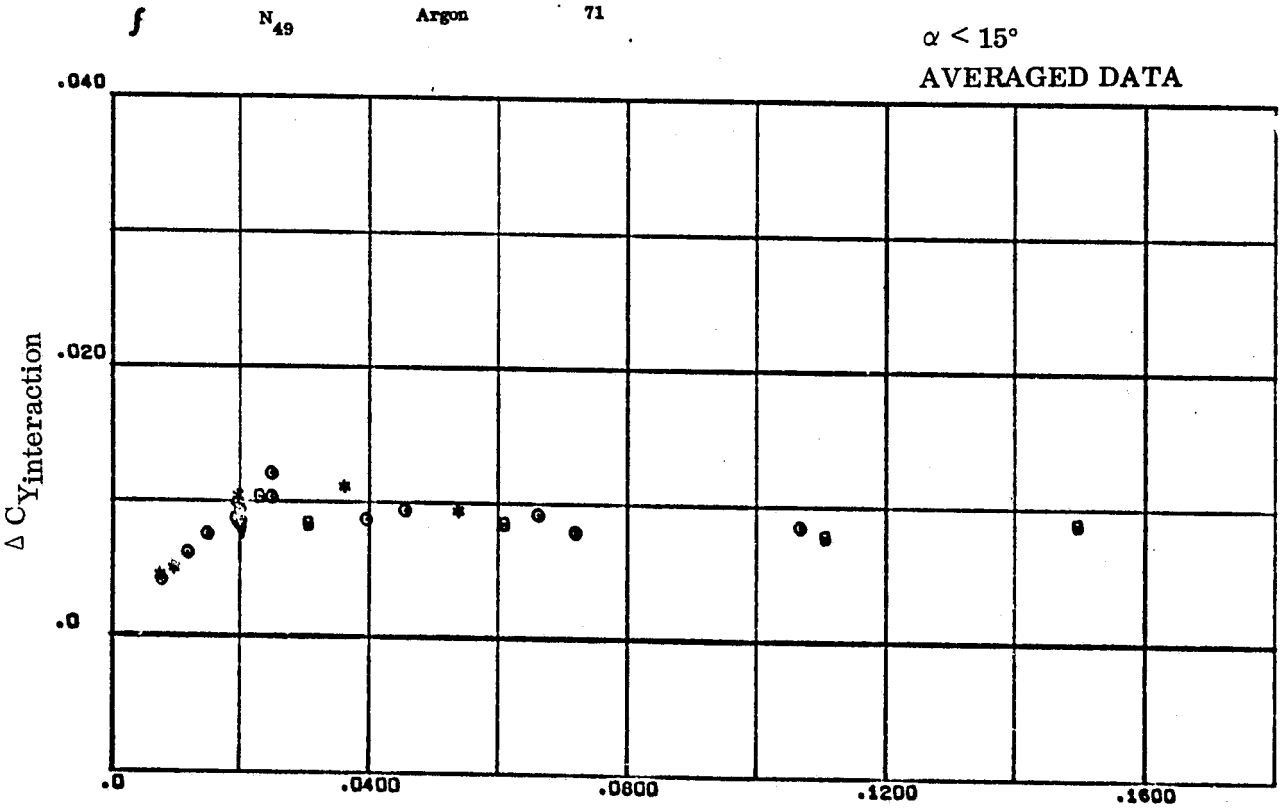

Figure 3-17. Left Side Pitch Down RCS Interaction Side Force at Low Angles of Attack

SYMBOL	RUN
◇	53
◁	34
□	55
△	56
○	57

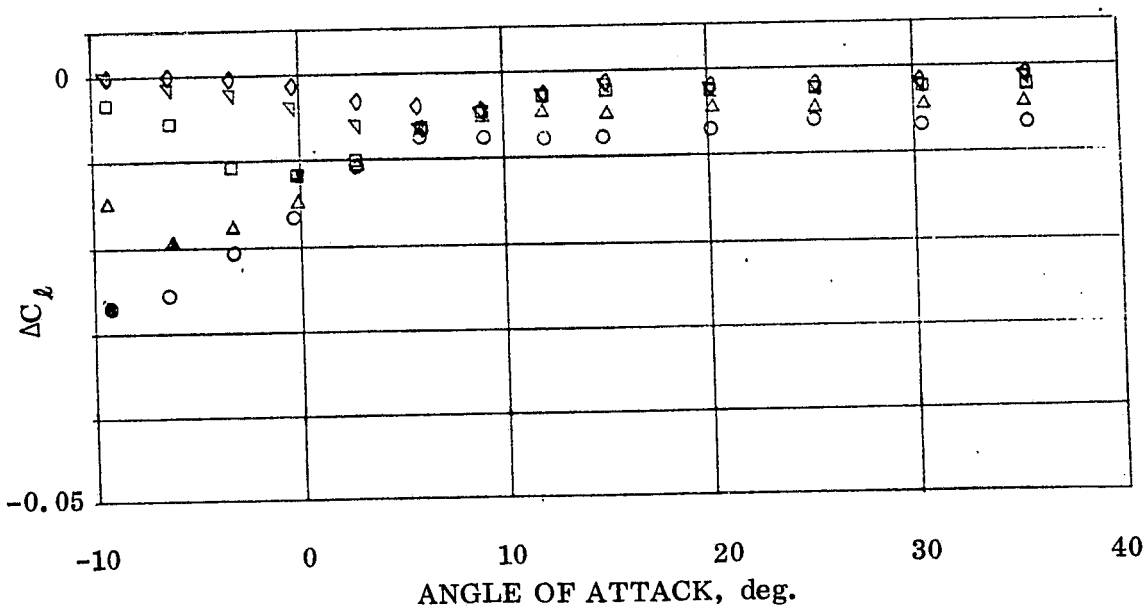

Figure 3-18. Typical Pitch Up RCS Data

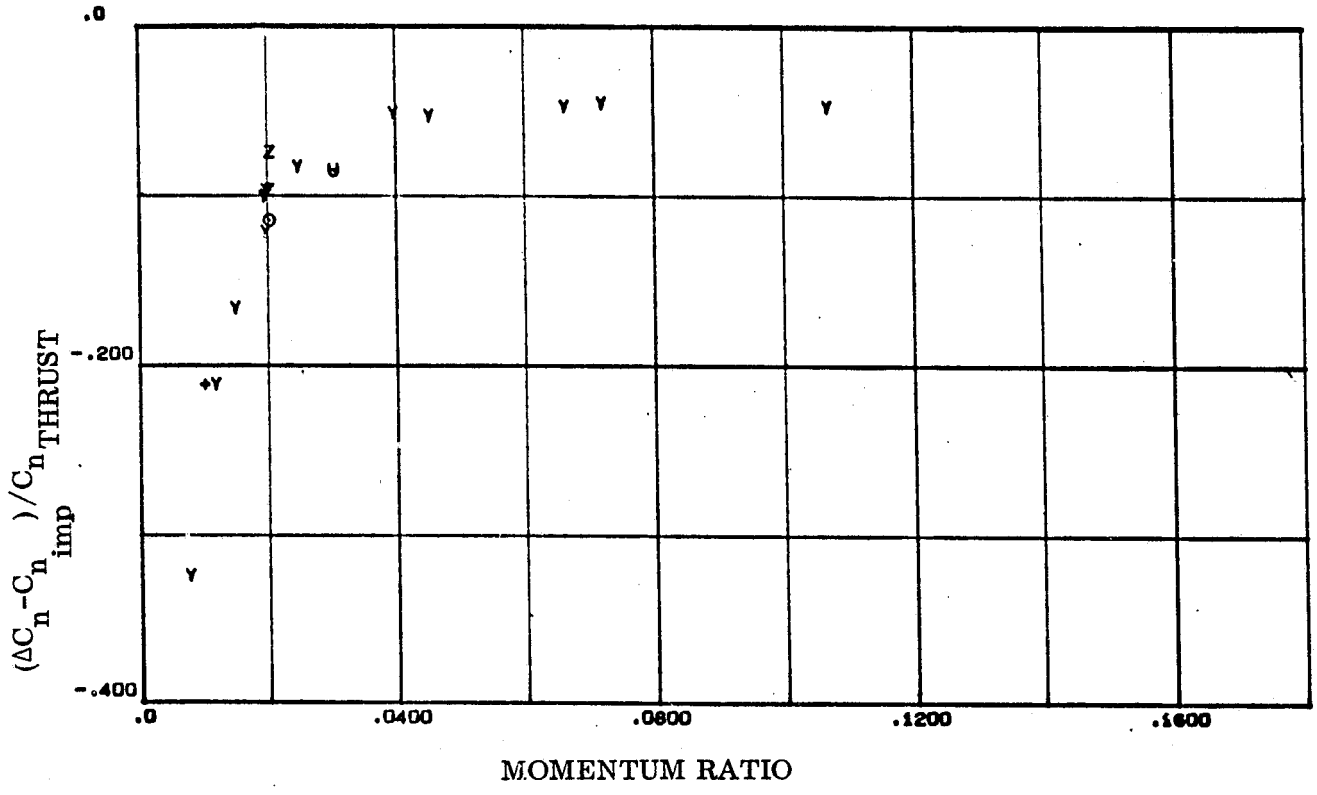

Figure 3-19a. Right Side Pitch Up RCS Interaction Moments Ratioed to Thrust Moments

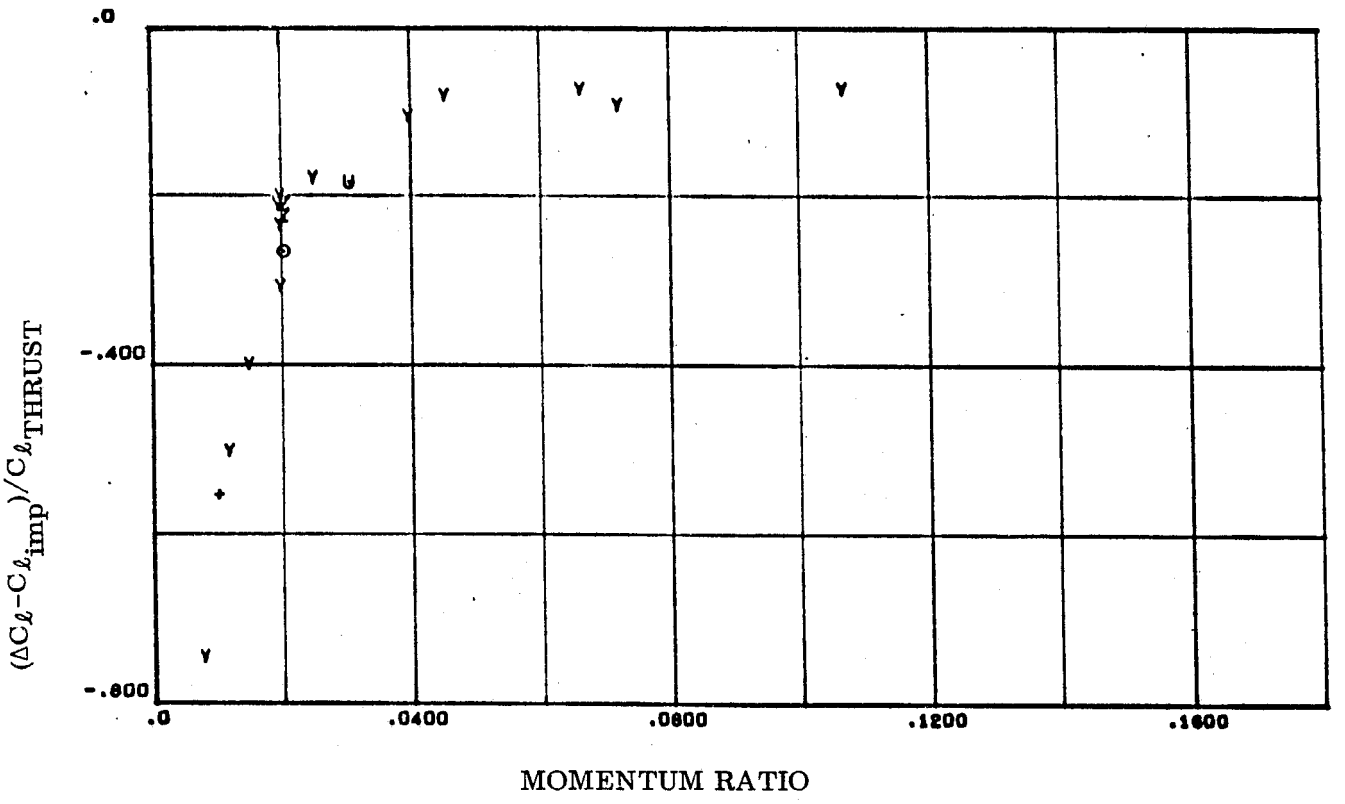

Figure 3-19b. Right Side Pitch Up RCS Interaction Moments Ratioed to Thrust Moments

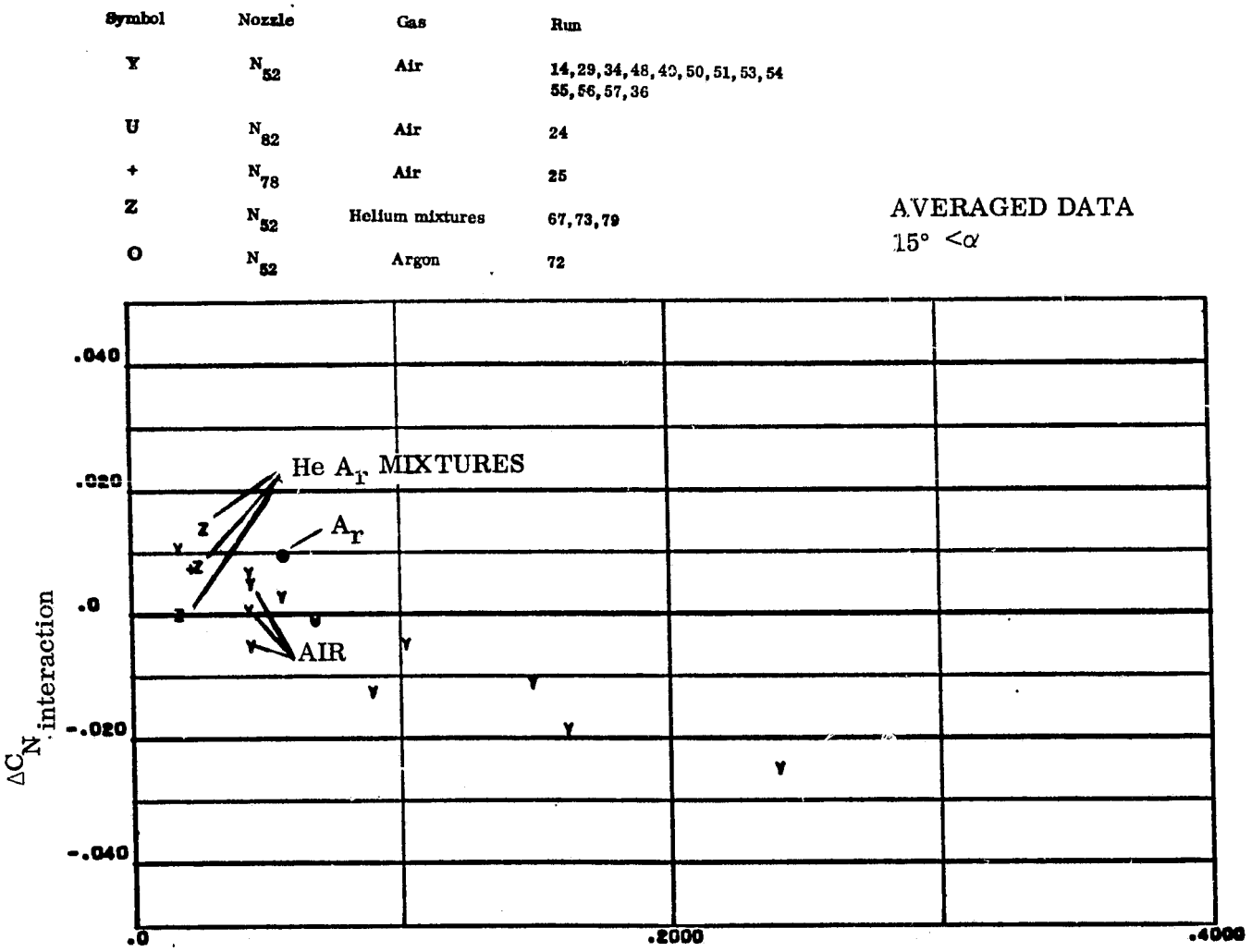

Figure 3-20. Right Side Pitch Up RCS Interaction Normal Force at High Angles of Attack

Symbol	Nozzle	Gas	Run
Y	N_{52}	Air	14,29,34,48,49,50,51,53,54 55,56,57,36
U	N_{82}	Air	24
+	N_{78}	Air	25
Z	N_{52}	Helium mixtures	67,73,79
O	N_{52}	Argon	72

AVERAGED DATA
$15° < \alpha$

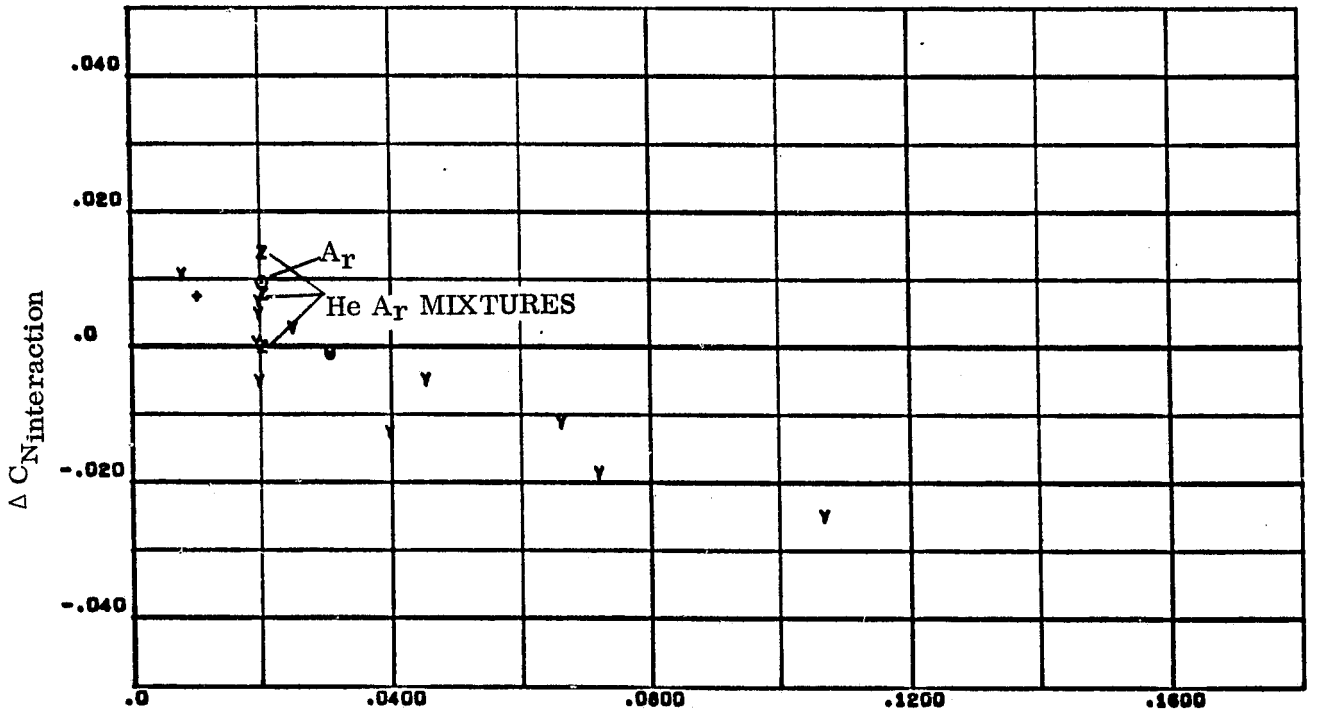

Figure 3-21. Right Side Pitch up RCS Interaction Normal Force Correlated to Momentum Ratio

Symbol	Nozzle	Gas	Run
Y	N_{52}	Air	14,29,34,48,49,50,51,53,54 55,56,57,36
U	N_{82}	Air	24
+	N_{78}	Air	25
Z	N_{52}	Helium mixtures	67,73,79
O	N_{52}	Argon	72

AVERAGED DATA
$15° < \alpha$

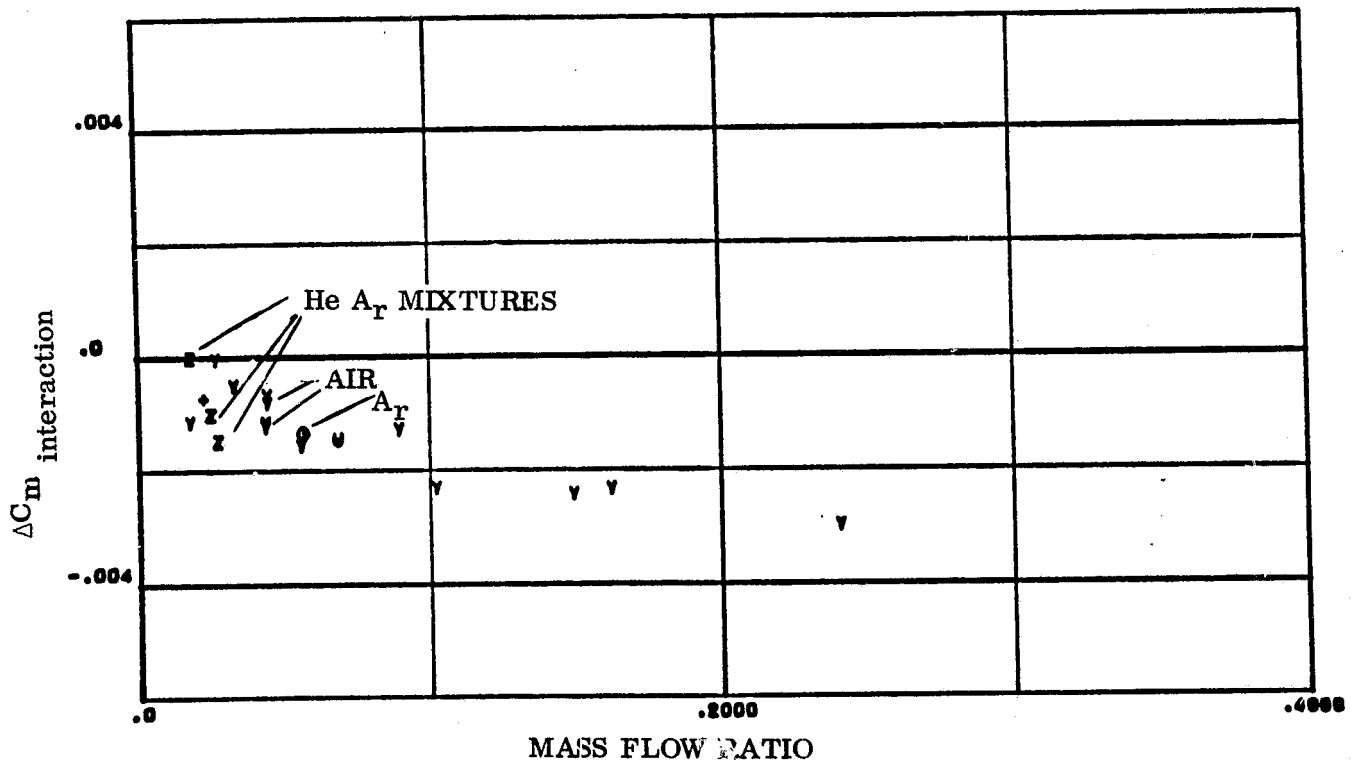

Figure 3-22. Right Side Pitch Up RCS Interaction Pitching Moment at High Angles of Attack

Symbol	Nozzle	Gas	Run
Y	N_{52}	Air	14,29,34,48,49,50,51,53,54 55,56,57,36
U	N_{82}	Air	24
+	N_{78}	Air	25
Z	N_{52}	Helium mixcures	67,73,79
O	N_{52}	Argon	72

AVERAGED DATA
$15° < \alpha$

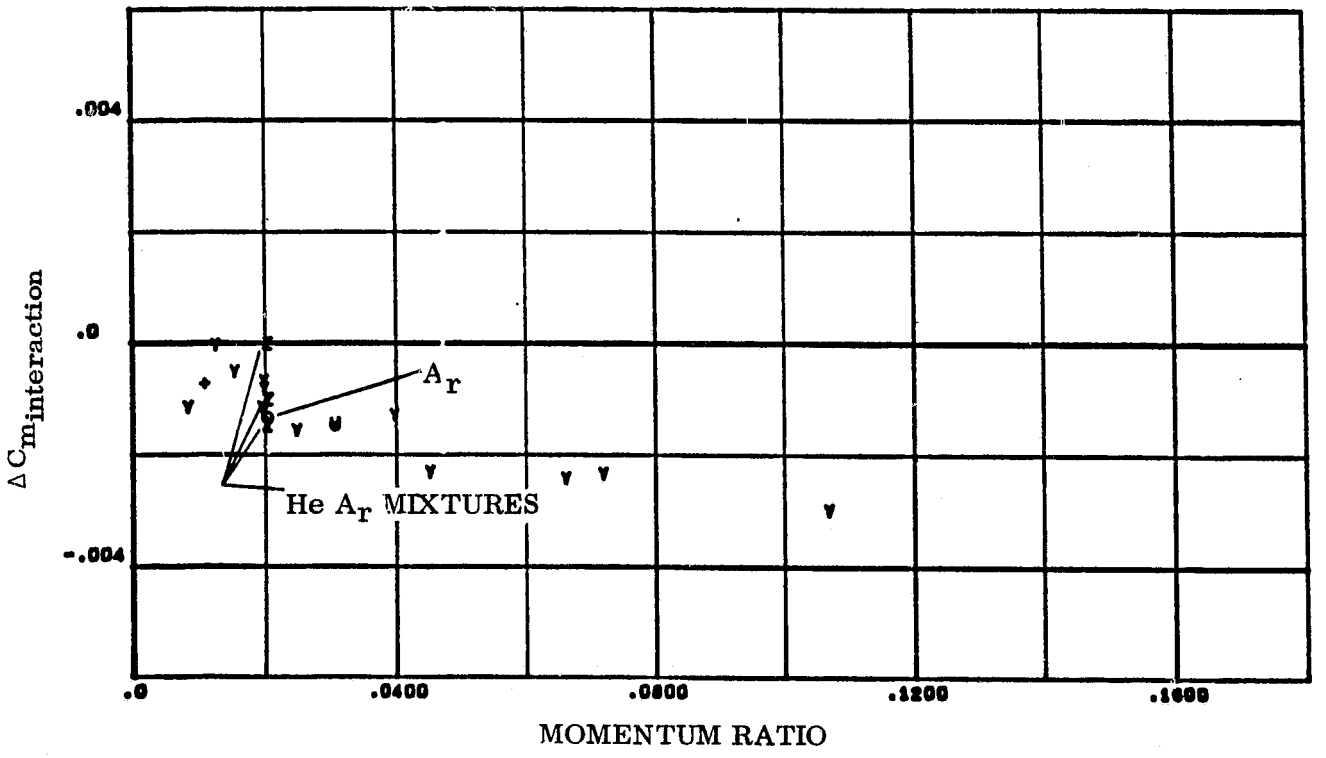

Figure 3-23. Right Side Pitch Up RCS Interaction Pitching Moment Correlated With Momentum Ratio

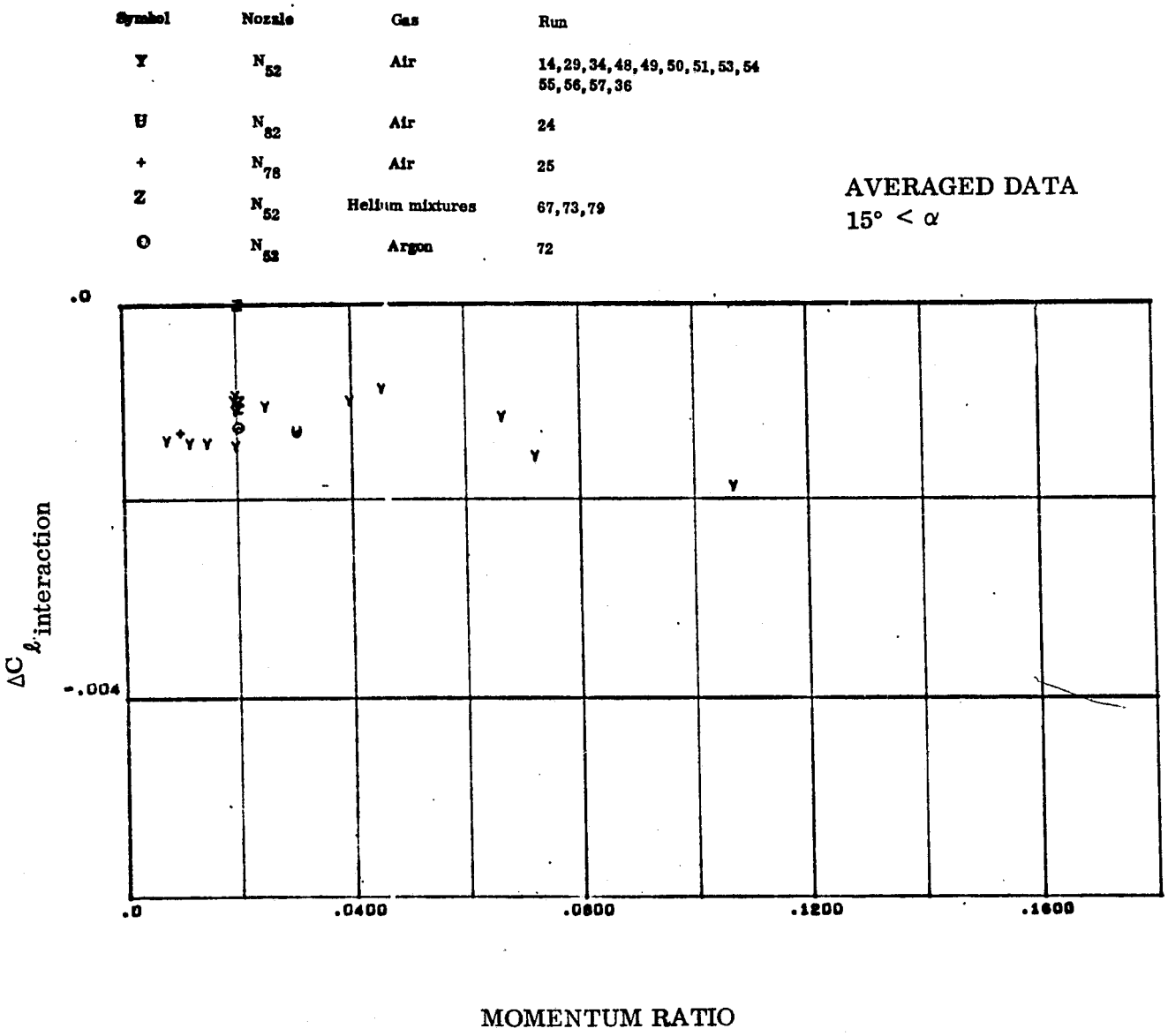

Figure 3-24. Right Side Pitch Up RCS Interaction Rolling Moment at High Angles of Attack

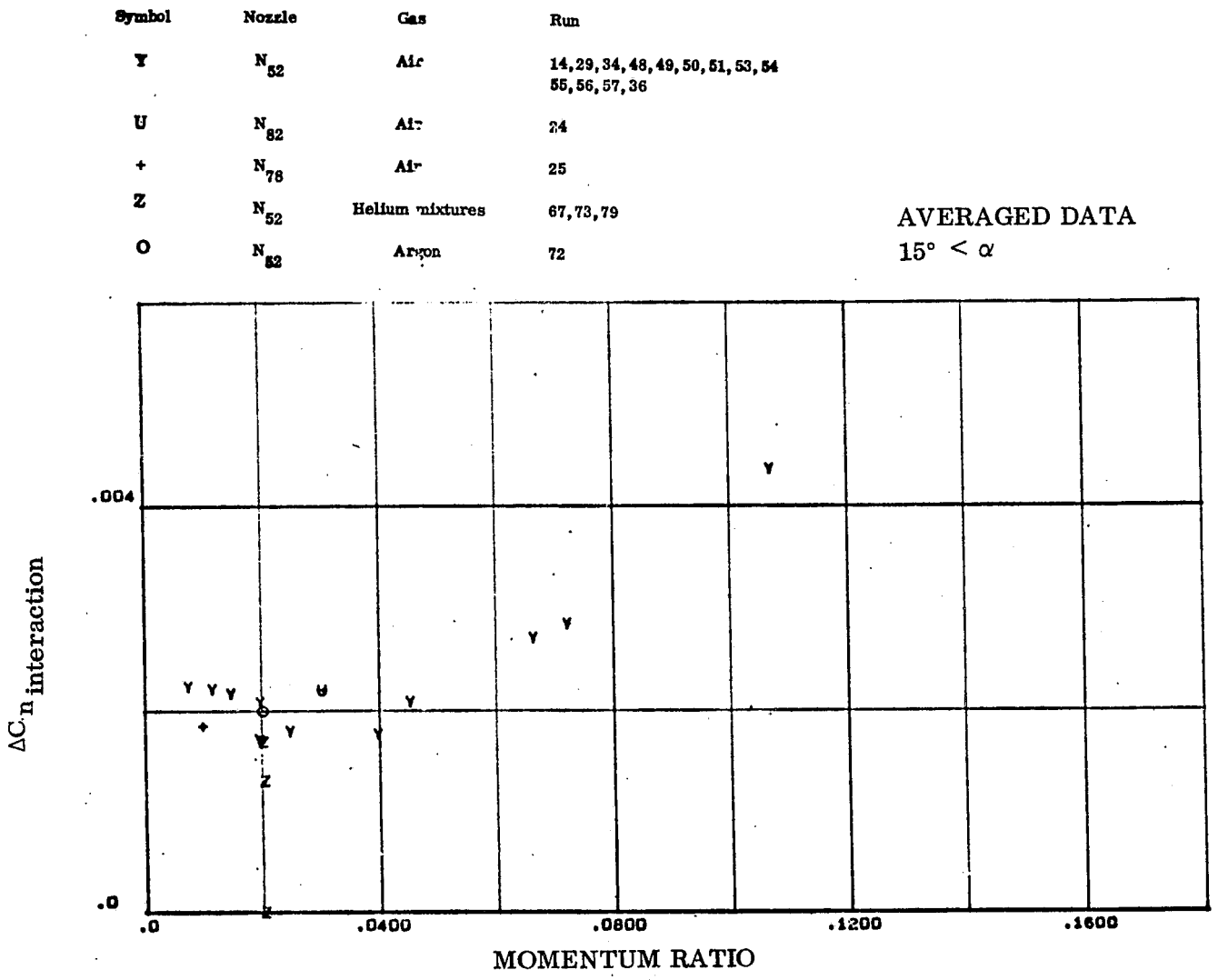

Figure 3-25. Right Side Pitch up RCS Interaction Yawing Moment at High Angles of Attack

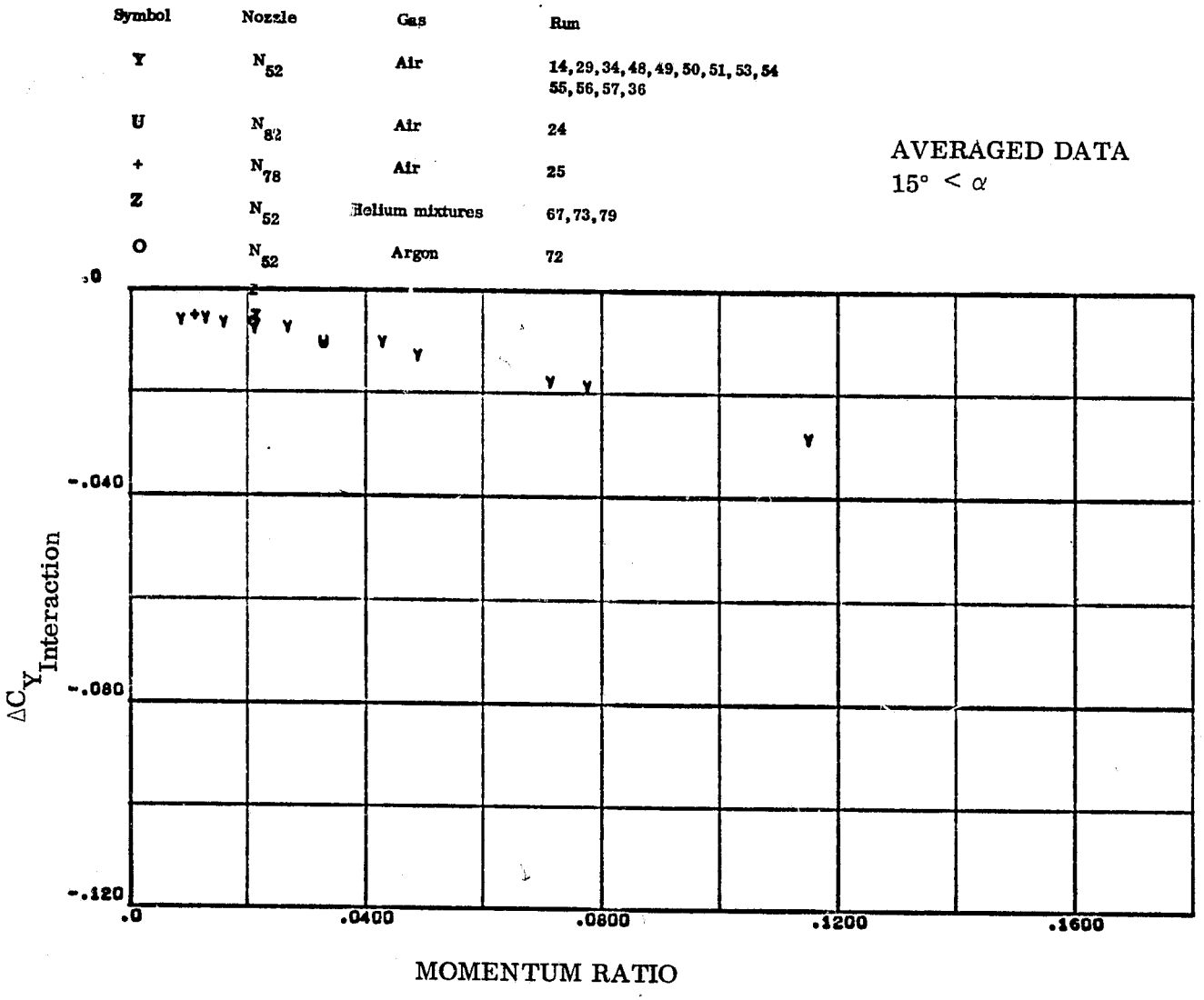

Figure 3-26. Right Side Pitch Up RCS Interaction Side Force at High Angles of Attack

Symbol	Nozzle	Gas	Run
Y	N_{52}	Air	14, 29, 34, 48, 49, 50, 51, 53, 54 55, 56, 57, 36
U	N_{82}	Air	24
+	N_{78}	Air	25
Z	N_{52}	Helium mixtures	67, 73, 79
O	N_{52}	Argon	72

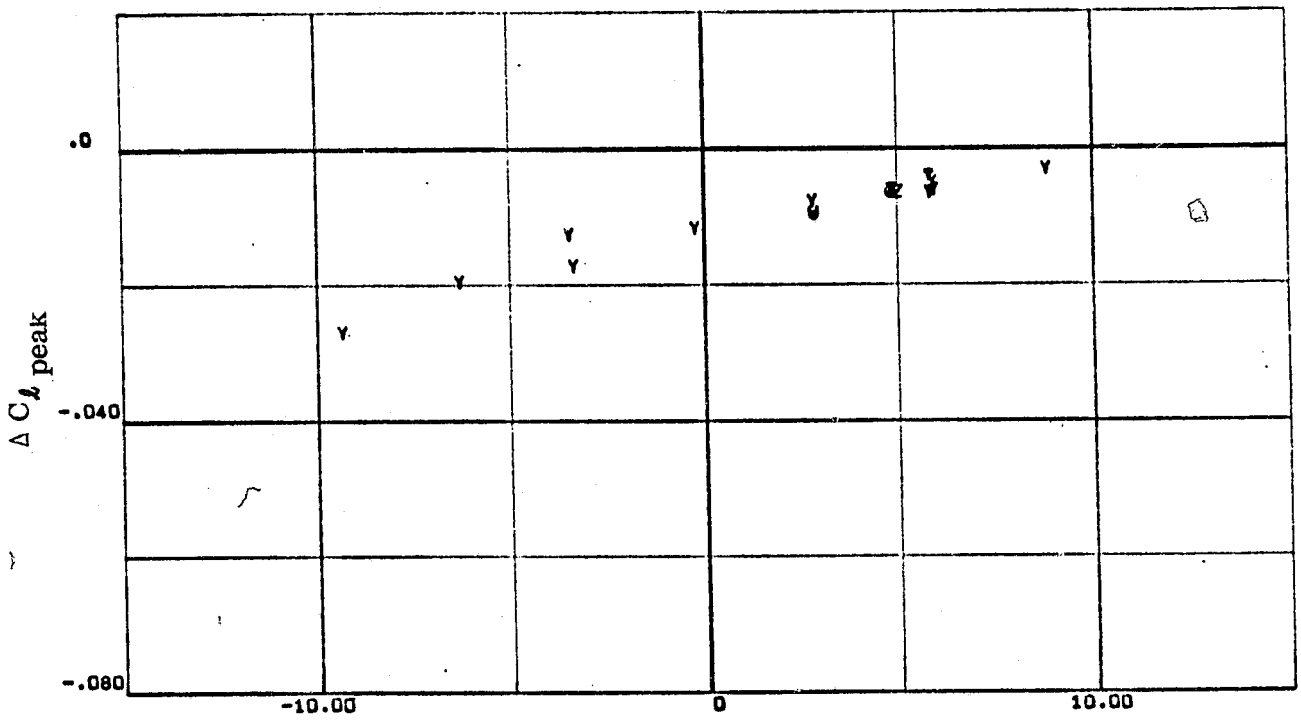

Figure 3-27. Right Side Pitch Up RCS Peak Rolling Moment Correlation

Symbol	Nozzle	Gas	Run
Y	N_{52}	Air	14, 29, 34, 48, 49, 50, 51, 53, 54 55, 56, 57, 36
U	N_{82}	Air	24
+	N_{78}	Air	25
Z	N_{52}	Helium mixtures	67, 73, 79
O	N_{52}	Argon	72

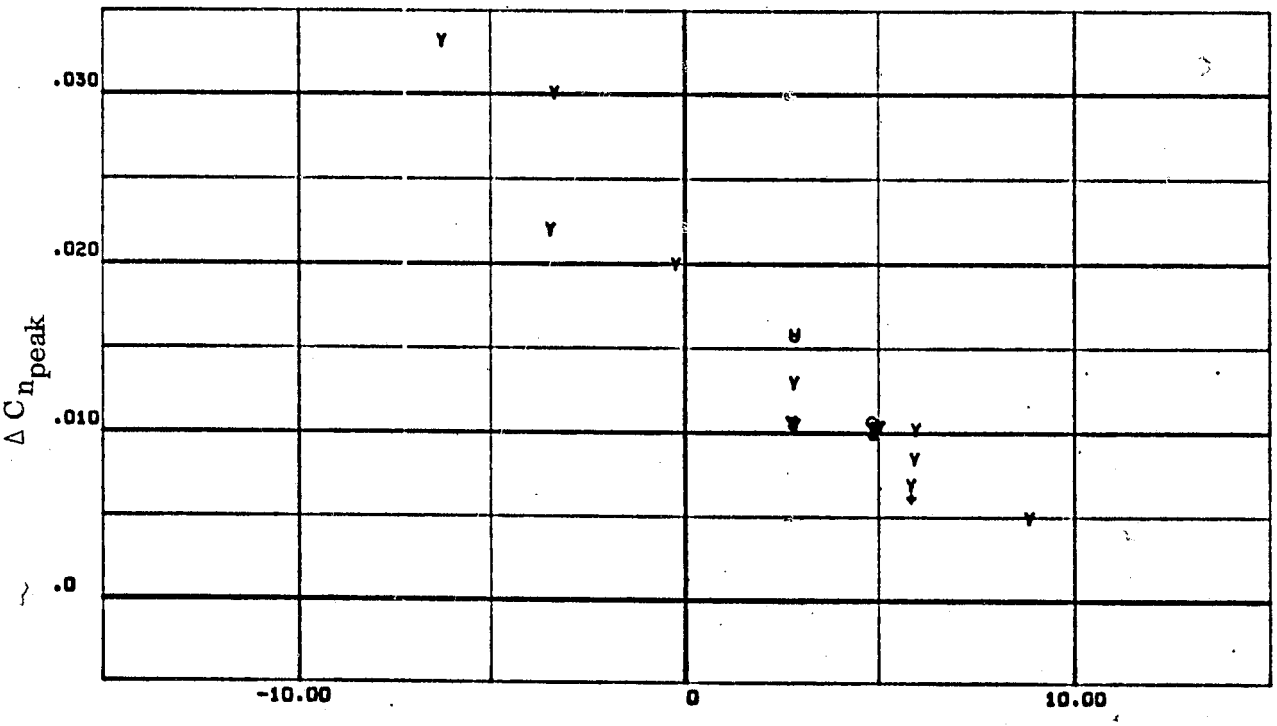

Figure 3-28. Right Side Pitch Up RCS Peak Yawing Moment Correlation

Symbol	Nozzle	Gas	Run
Y	N_{52}	Air	14,29,34,48,49,50,51,53,54 55,56,57,36
U	N_{82}	Air	24
+	N_{78}	Air	25
Z	N_{52}	Helium mixtures	67,73,79
O	N_{52}	Argon	72

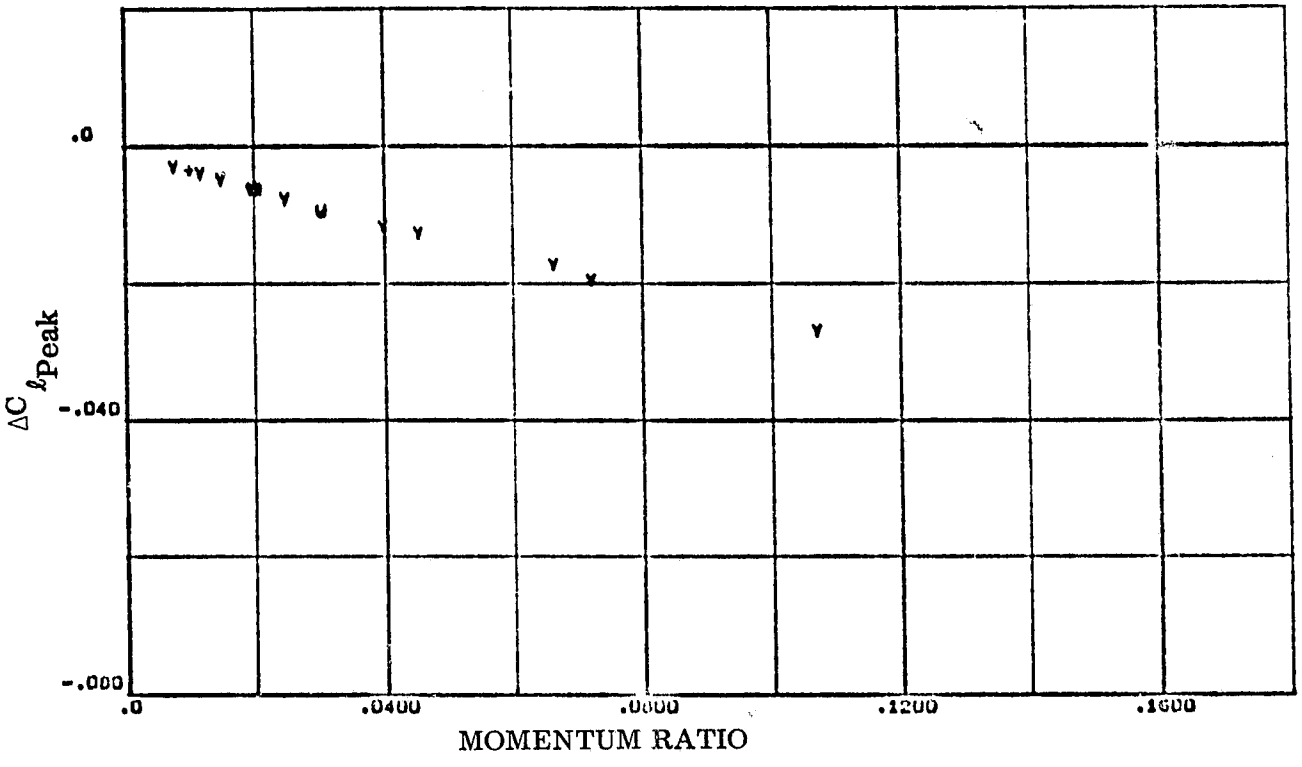

Figure 3-29. Right Side Pitch Up RCS Peak Rolling Moment Due to Interaction

Symbol	Nozzle	Gas	Run
Y	N_{52}	Air	14,29,34,48,49,50,51,53,54 55,56,57,36
U	N_{82}	Air	24
+	N_{78}	Air	25
Z	N_{52}	Helium mixtures	67,73,79
O	N_{52}	Argon	72

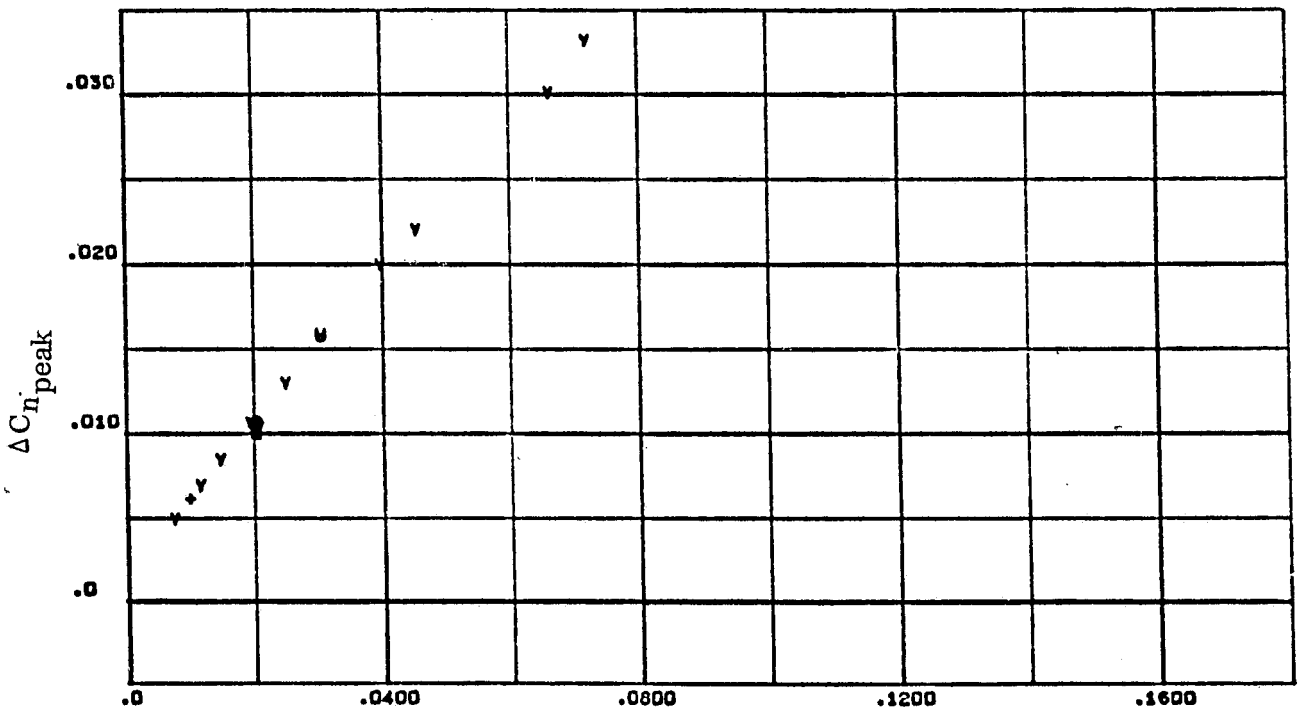

Figure 3-30. Right Side Pitch Up RCS Peak Yawing Moment Due to Interaction

Symbol	Nozzle	Gas	Run
Y	N_{52}	Air	14,29,34,48,49,50,51,53,54 55,56,57,36
U	N_{82}	Air	24
+	N_{78}	Air	25
Z	N_{52}	Helium mixtures	67,73,79
O	N_{52}	Argon	72

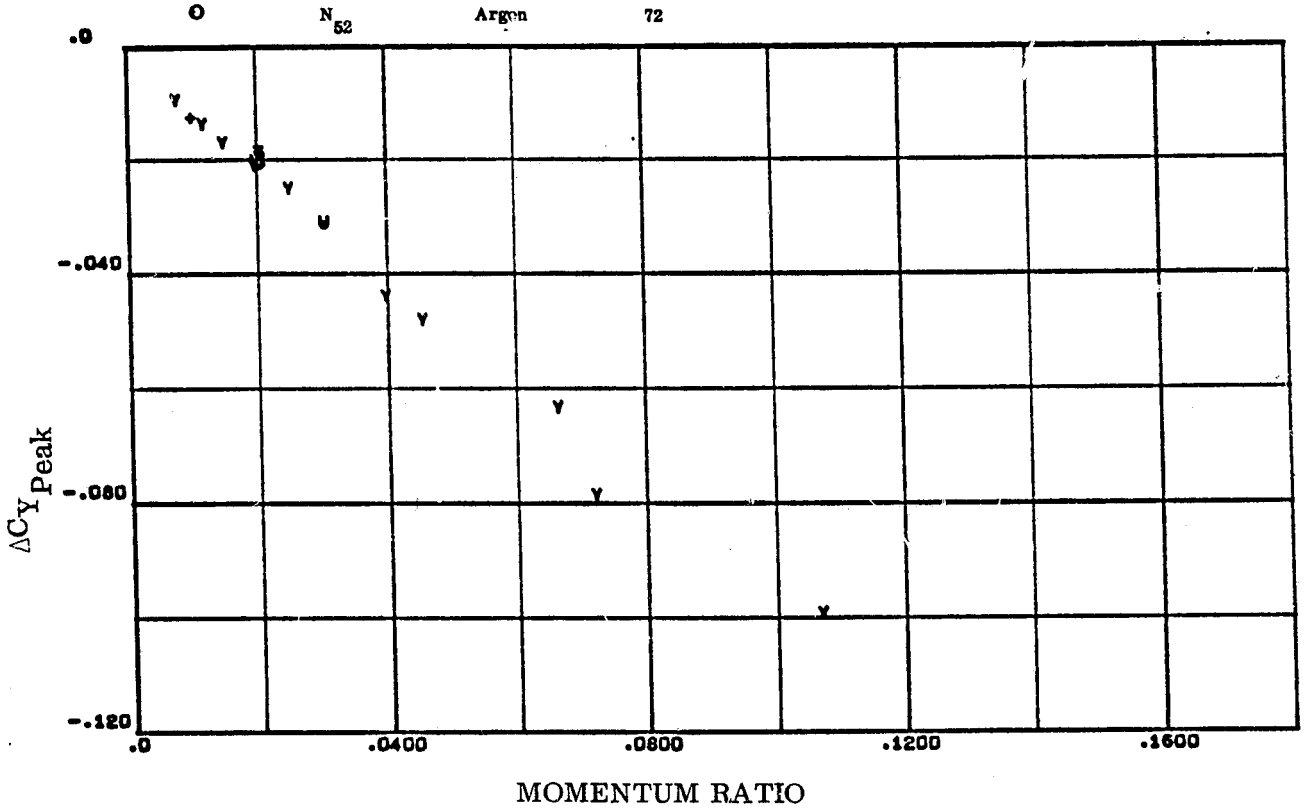

Figure 3-31. Right Side Pitch Up RCS Peak Side Force Due to Interaction

Symbol	Nozzle	Gas	Run
Y	N_{52}	Air	14,29,34,48,49,50,51,53,54 55,56,57,36
U	N_{82}	Air	24
+	N_{73}	Air	25
Z	N_{52}	Helium mixtures	67,73,79
O	N_{52}	Argon	72

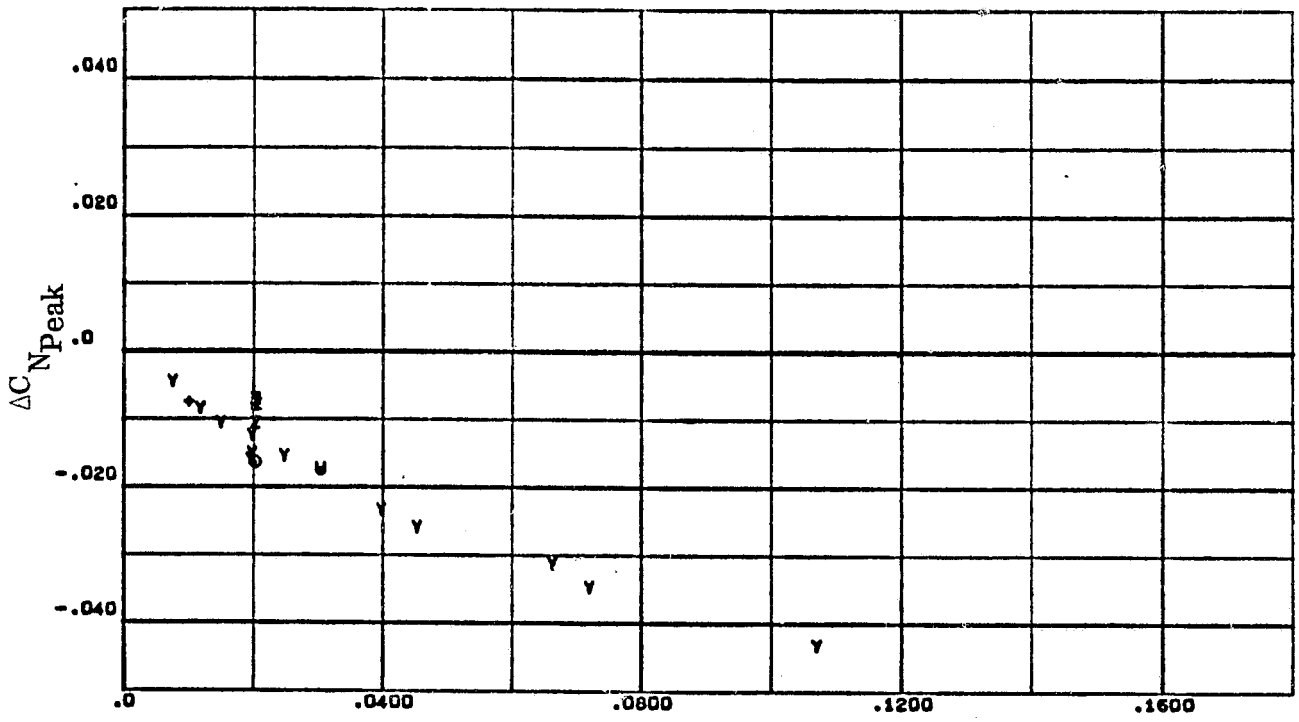

Figure 3-32. Right Side Pitch Up RCS Peak Normal Force Correlated With Momentum Ratio

Symbol	Nozzle	Gas	Run
Y	N_{52}	Air	14, 29, 34, 48, 49, 50, 51, 53, 54 55, 56, 57, 36
U	N_{82}	Air	24
+	N_{78}	Air	25
Z	N_{52}	Helium mixtures	67, 73, 79
O	N_{52}	Argon	72

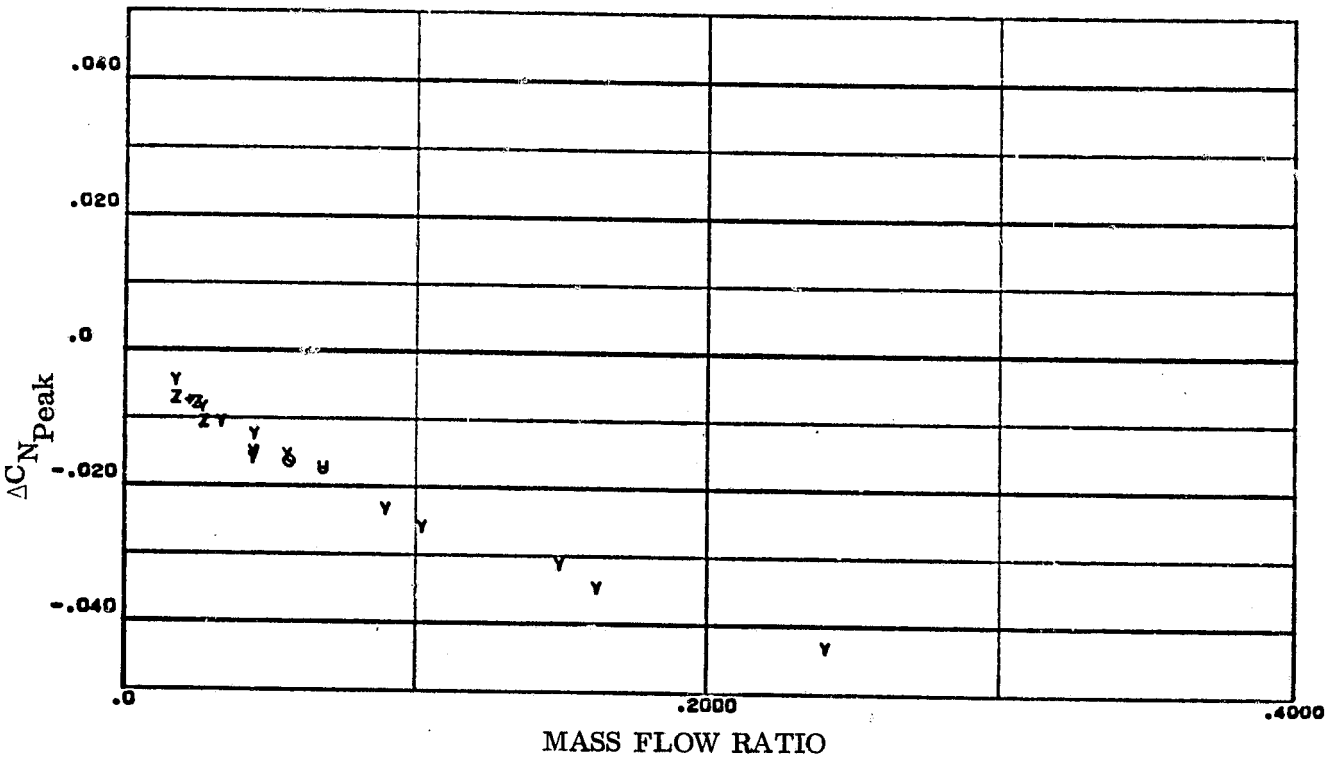

Figure 3-33. Right Side Pitch Up RCS Peak Normal Force Due to Interaction

Symbol	Nozzle	Gas	Run
Y	N_{52}	Air	14,29,31,48,49,50,51,53,54 55,56,57,36
U	N_{82}	Air	24
+	N_{78}	Air	25
Z	N_{52}	Helium mixtures	67,73,79
O	N_{52}	Argon	72

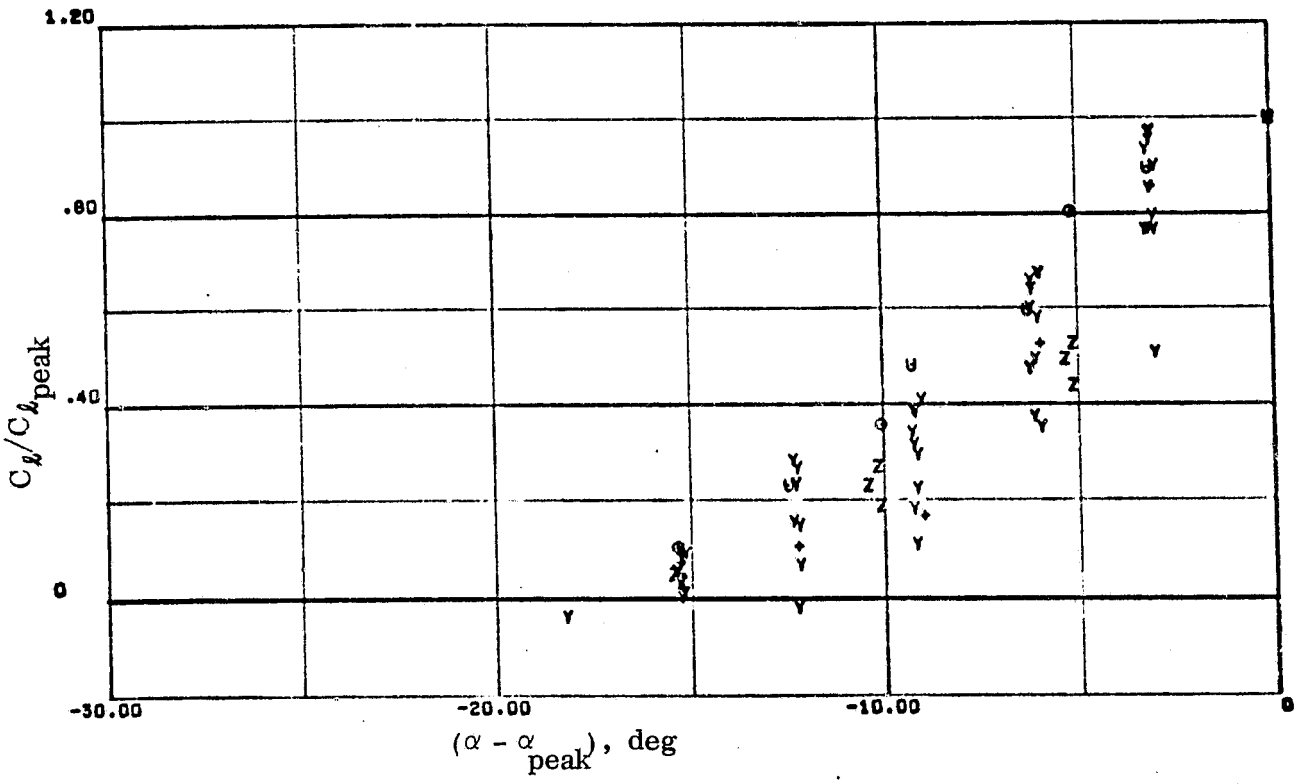

Figure 3-34. Right Side Pitch Up RCS Rolling Moment Correlation Below Peak Values

Symbol	Nozzle	Gas	Run
Y	N_{52}	Air	14, 29, 34, 48, 49, 50, 51, 53, 54 55, 56, 57, 36
U	N_{82}	Air	24
+	N_{78}	Air	25
Z	N_{52}	Helium mixtures	67, 73, 79
O	N_{52}	Argon	72

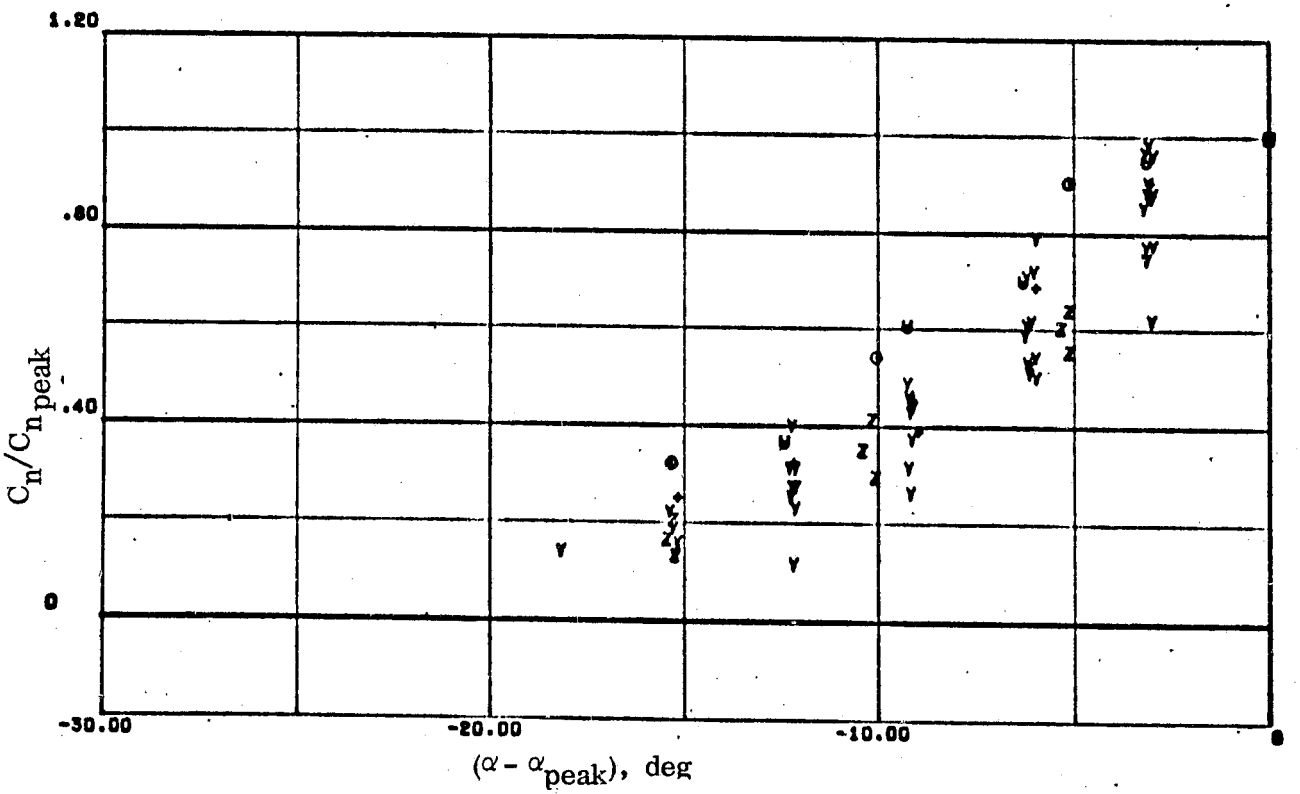

Figure 3-35. Right Side Pitch Up RCS Yawing Moment Correlation Below Peak Values

Symbol	Nozzle	Gas	Run
Y	N_{52}	Air	14,29,34,48,49,50,51,53,54 55,56,57,36
U	N_{82}	Air	24
+	N_{78}	Air	25
Z	N_{52}	Helium mixtures	67,73,79
O	N_{52}	Argon	72

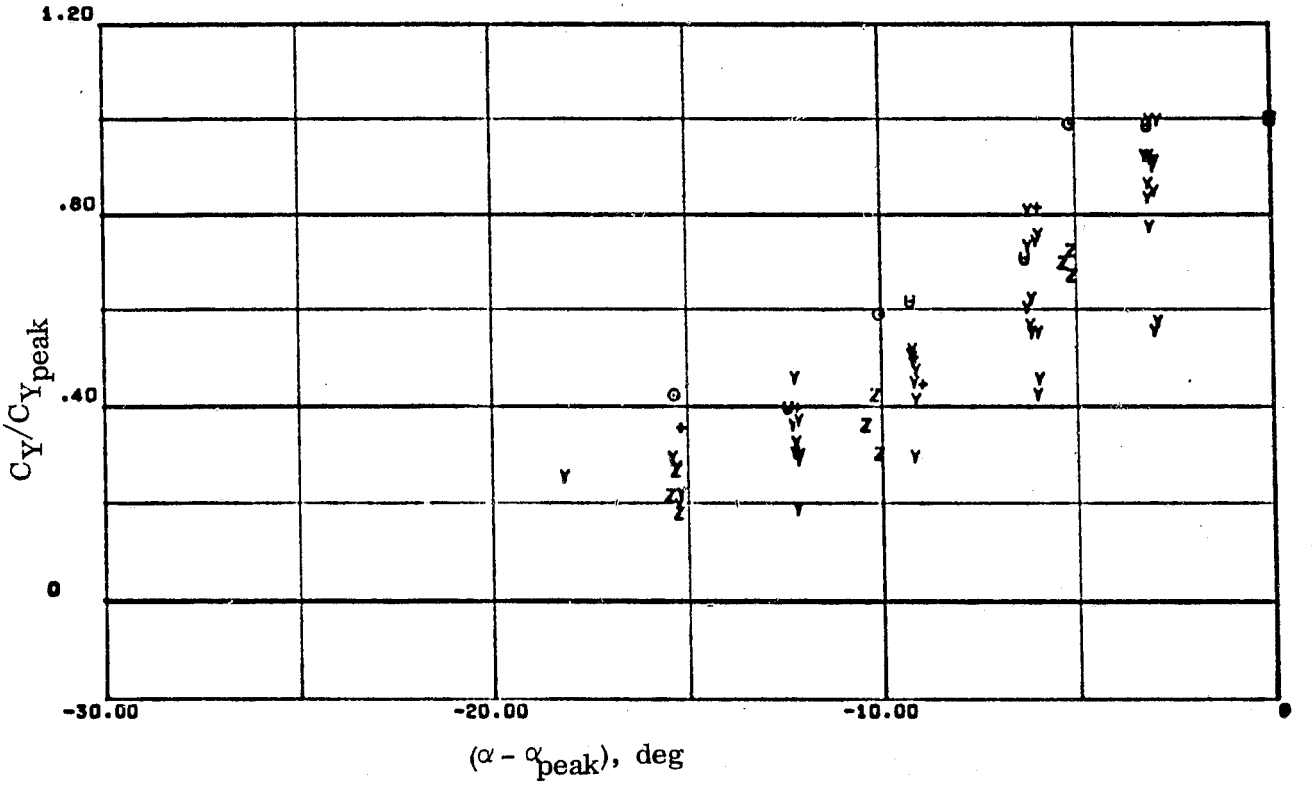

Figure 3-36. Right Side Pitch Up RCS Side Force Correlation Below Peak Values

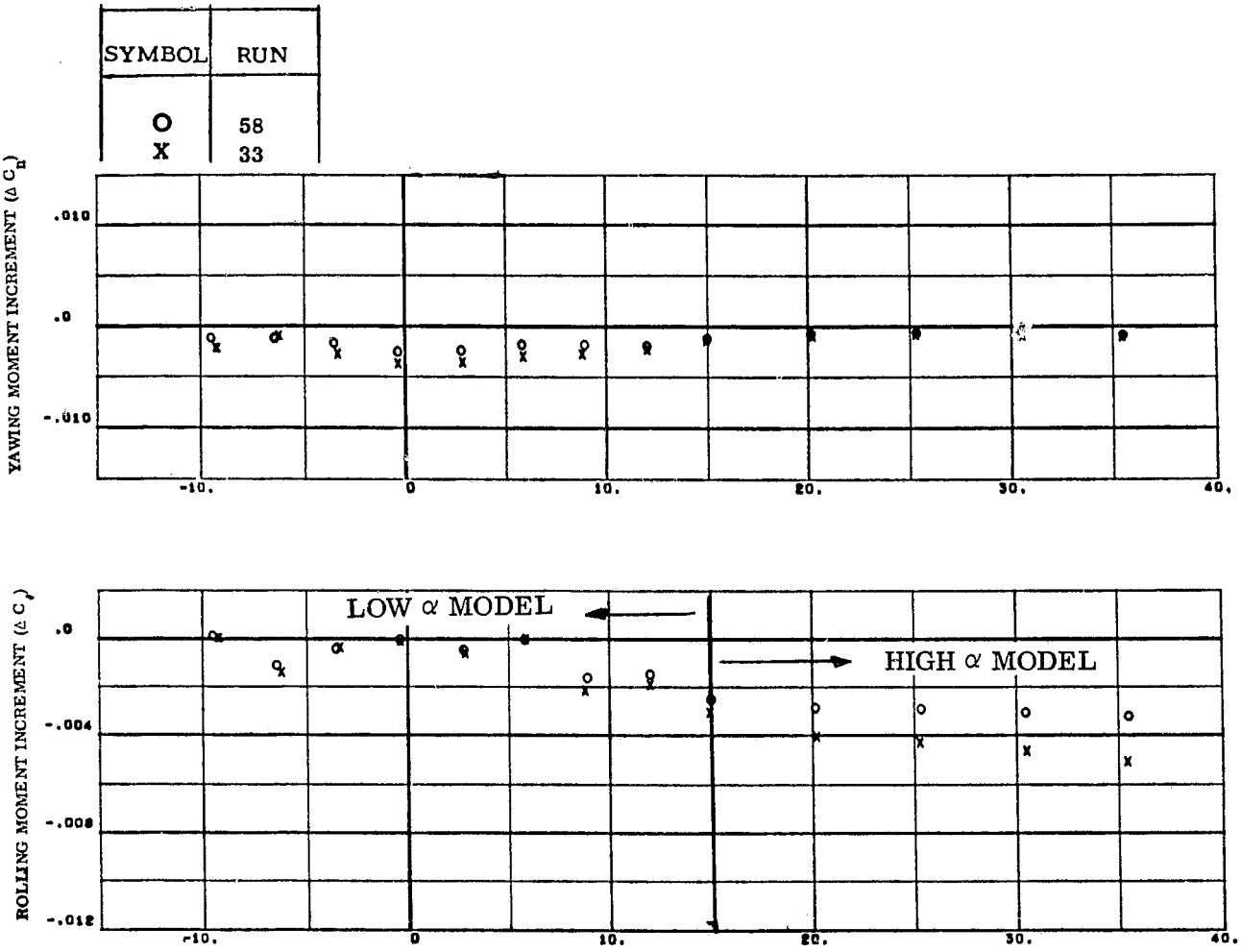

Figure 3-37. Typical Yaw RCS Data

Symbol	Nozzle	Gas	Run
■	N_{51}	Air	22
ϵ	N_{85}	Air	16, 26, 28, 33, 37, 58
⊡	N_{51}	Helium Mixtures	68, 75, 78
○	N_{51}	Argon	70

AVERAGED DATA
$15° < \alpha$

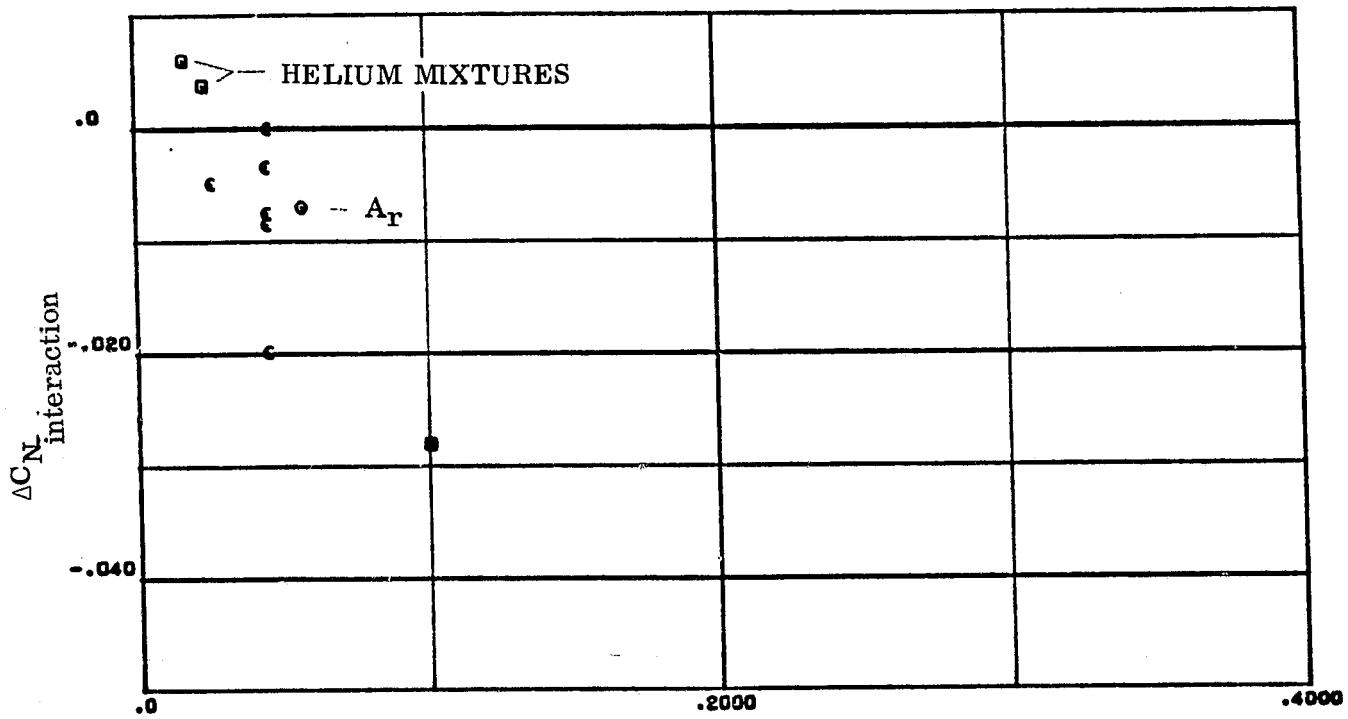

Figure 3-38. Left Side Yaw RCS Interaction Normal Force Correlation at High Angles of Attack

Symbol	Nozzle	Gas	Run
⊠	N_{51}	Air	22
⋐	N_{85}	Air	16, 26, 28, 33, 37, 58
⊡	N_{51}	Helium Mixtures	68, 75, 78
○	N_{51}	Argon	70

AVERAGED DATA
$15° < \alpha$

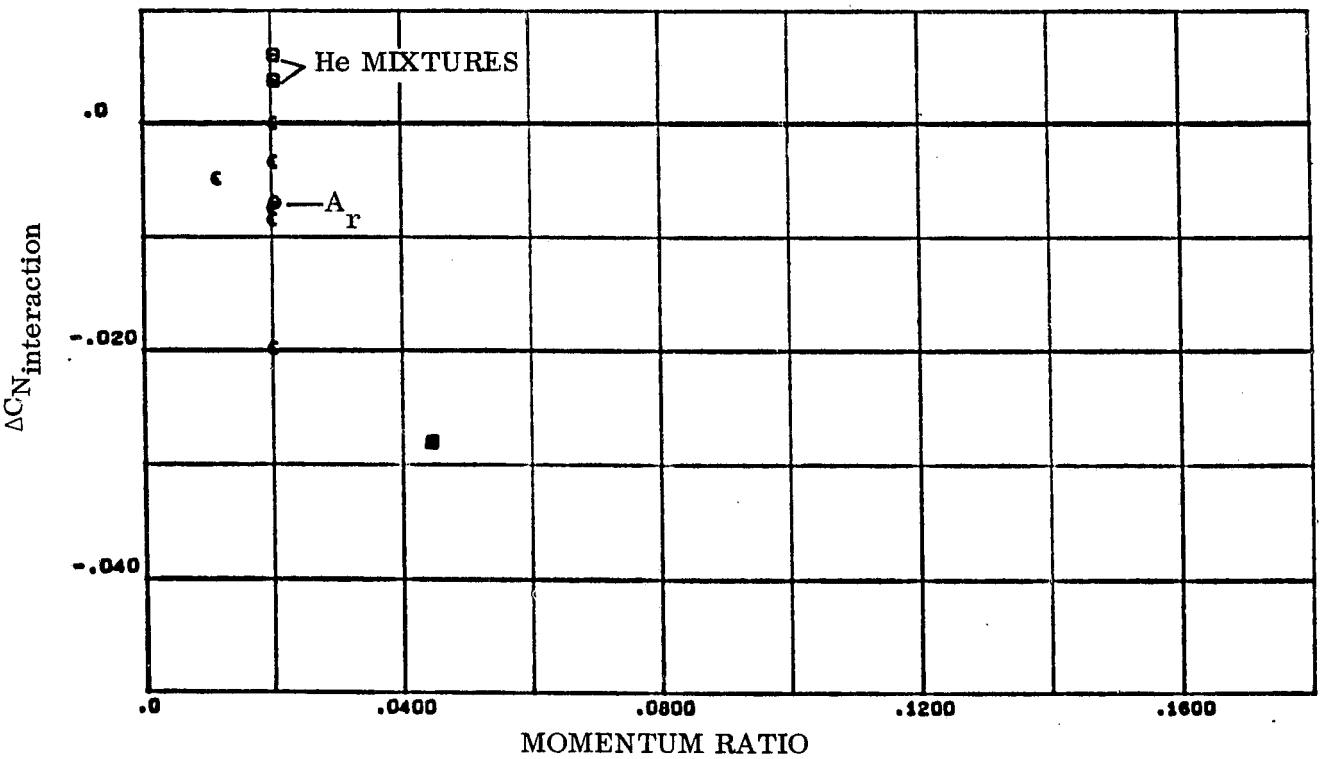

Figure 3-39. Left Side Yaw RCS Interaction Normal Force Correlation With Momentum Ratio

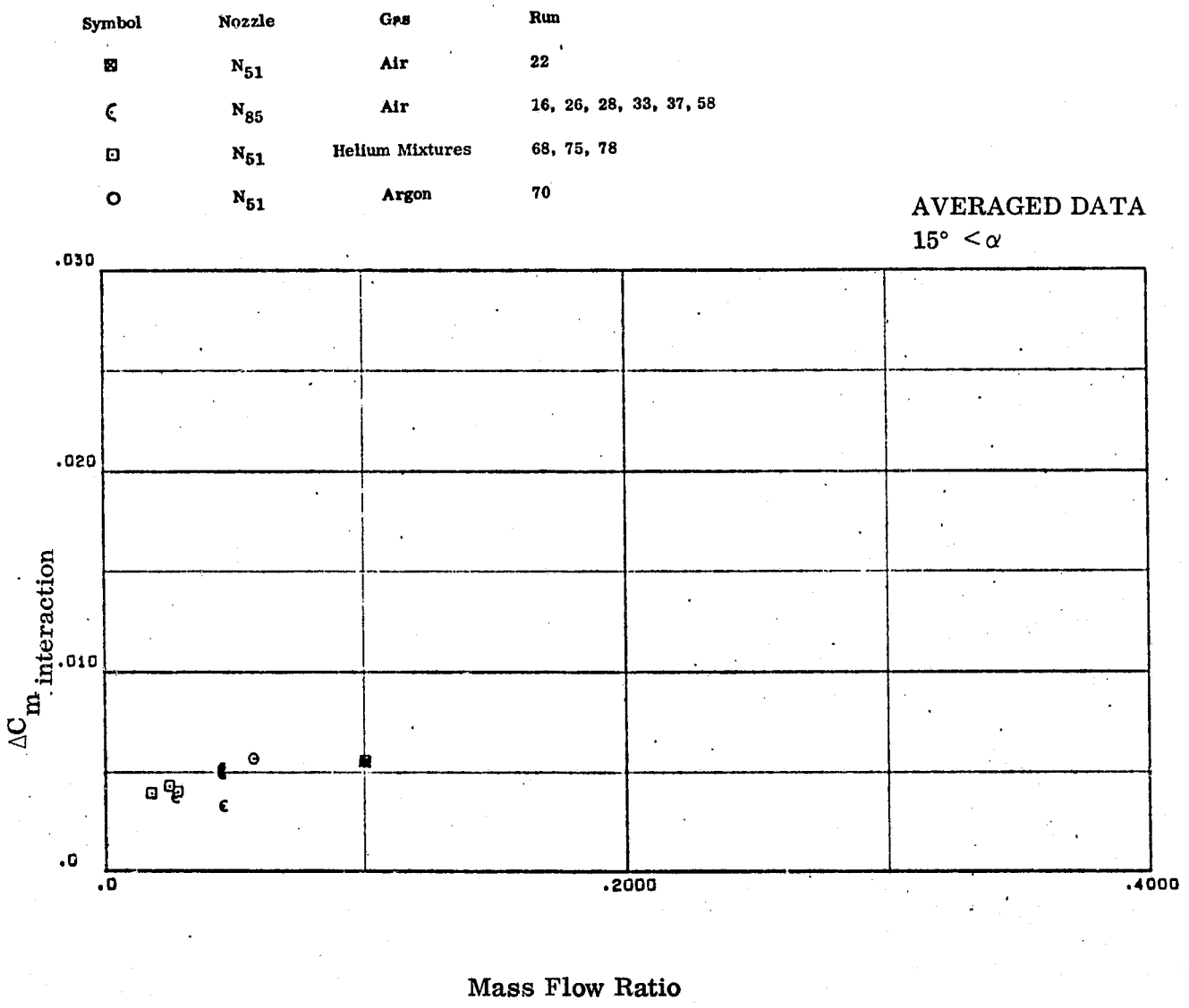

Figure 3-40. Left Side Yaw RCS Interaction Pitching Moment Correlation at High Angles of Attack

Symbol	Nozzle	Gas	Run
⊠	N_{51}	Air	22
⋐	N_{85}	Air	16, 26, 28, 33, 37, 58
⊡	N_{51}	Helium Mixtures	68, 75, 78
○	N_{51}	Argon	70

AVERAGED DATA
$15° < \alpha$

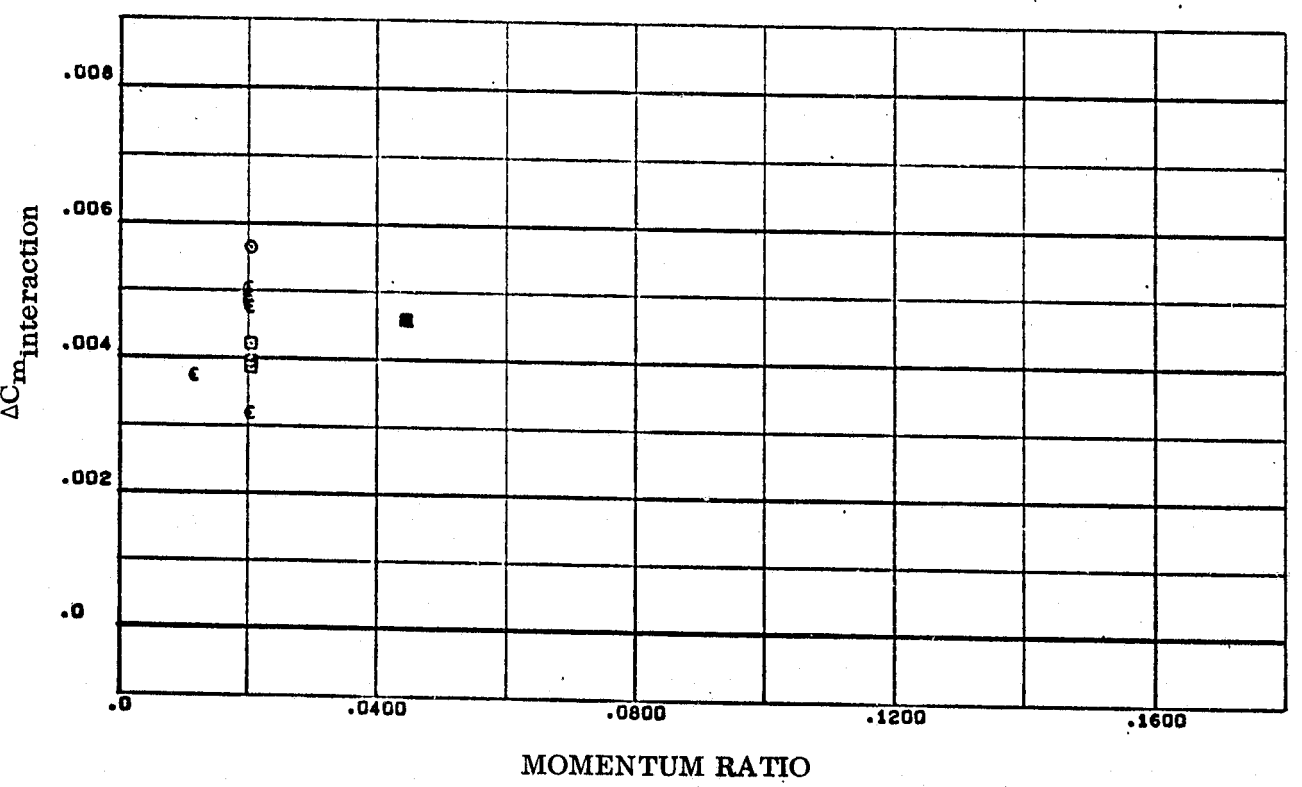

Figure 3-41. Left Side Yaw RCS Interaction Pitching Moment Correlated With Momentum Ratio

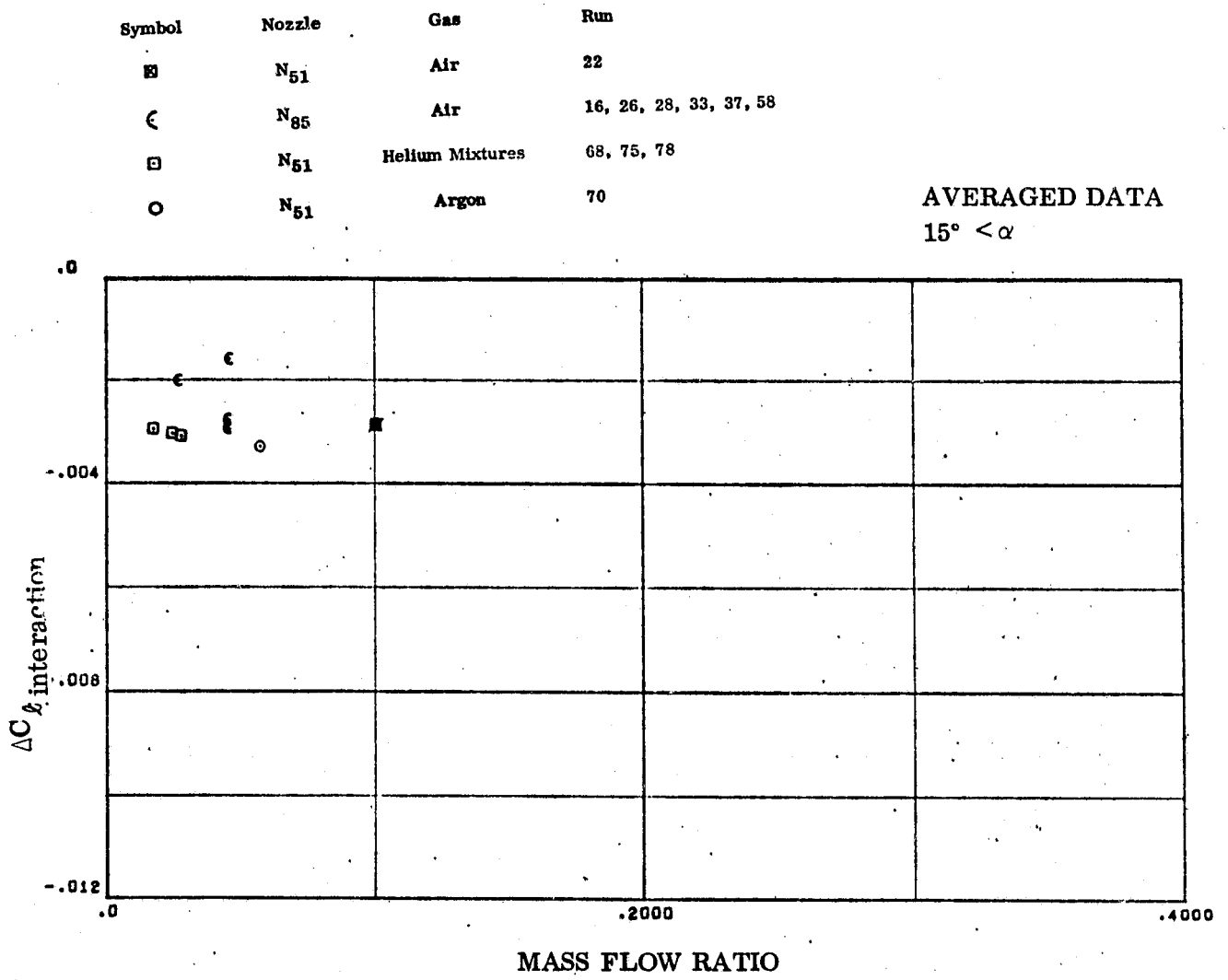

Figure 3-42. Left Side Yaw RCS Interaction Rolling Moment at High Angles of Attack

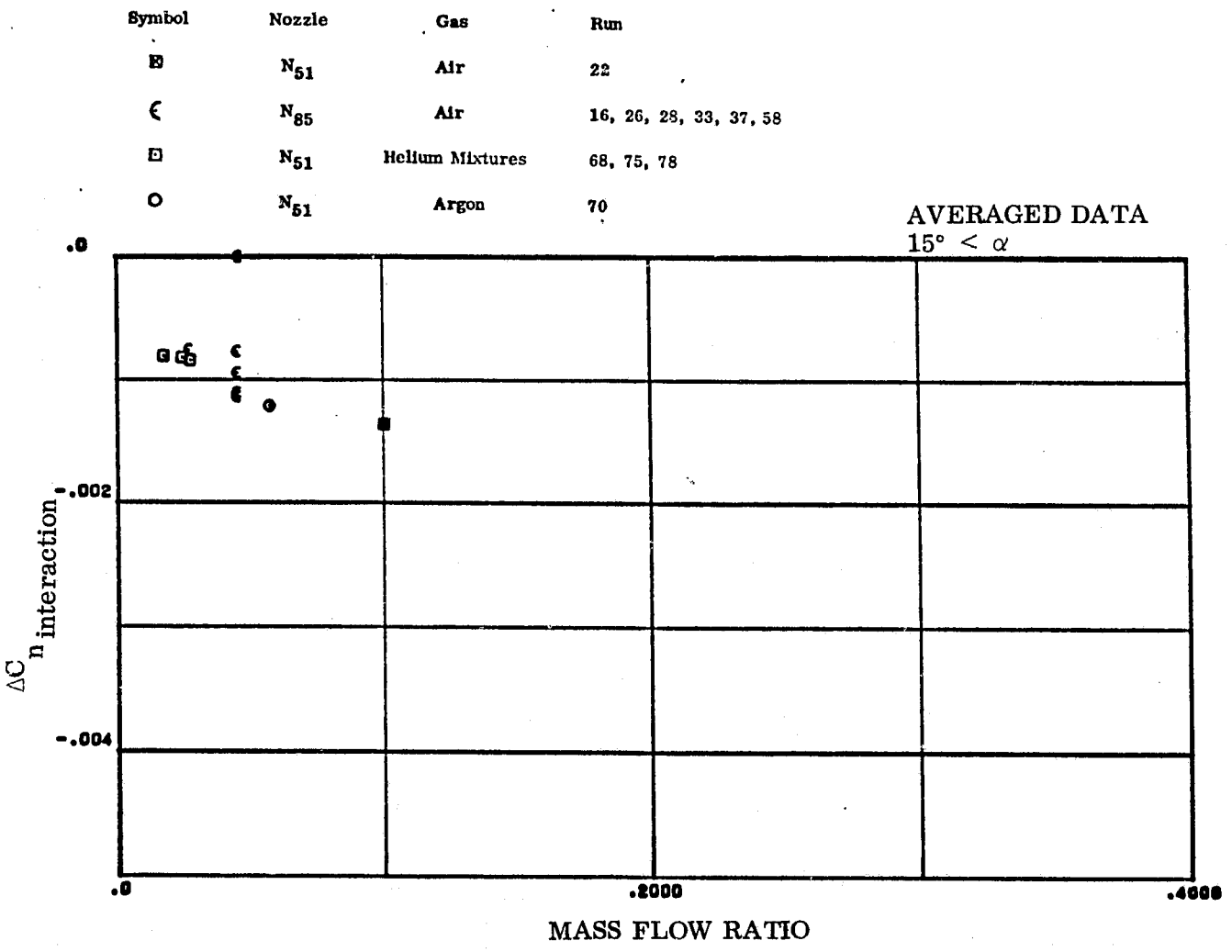

Figure 3-43. Left Side Yaw RCS Interaction Yawing Moment at High Angles of Attack

Symbol	Nozzle	Gas	Run
⊠	N_{51}	Air	22
⋐	N_{85}	Air	16, 26, 28, 33, 37, 58
⊡	N_{51}	Helium Mixtures	68, 75, 78
○	N_{51}	Argon	70

AVERAGED DATA
$15° < \alpha$

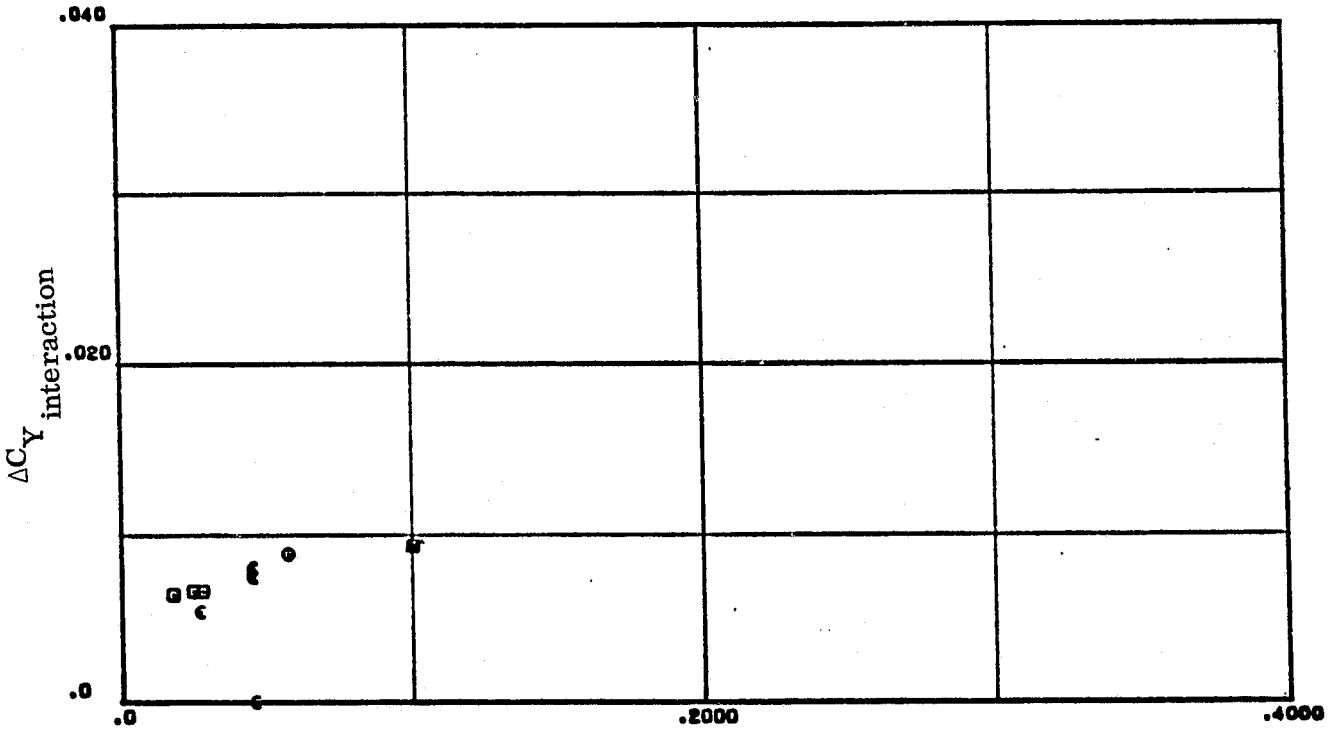

Figure 3-44. Left Side Yaw RCS Interaction Side Force at High Angles of Attack

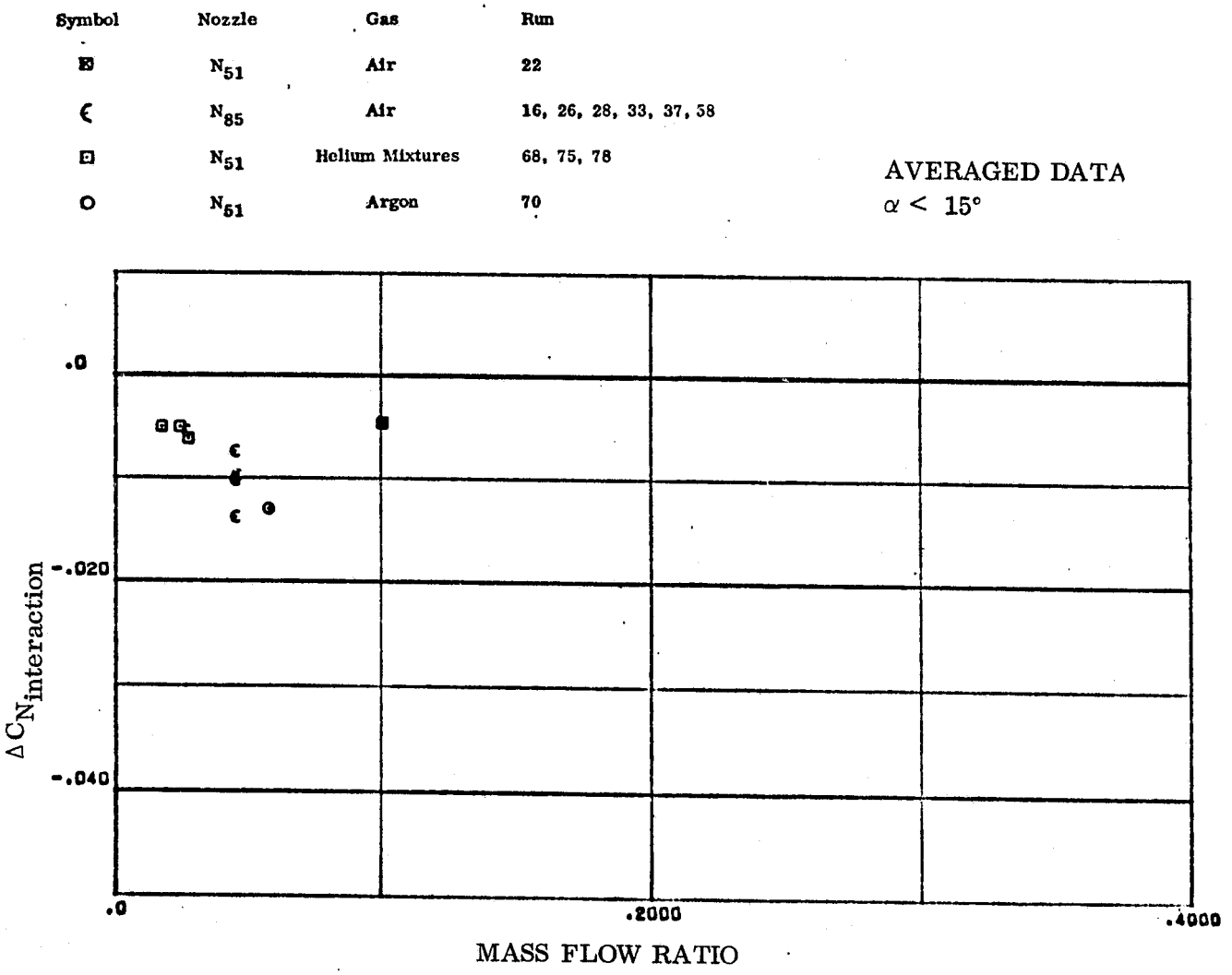

Figure 3-45. Left Side Yaw RCS Interaction, Normal Force at Low Angles of Attack

Symbol	Nozzle	Gas	Run
⊠	N_{51}	Air	22
⋐	N_{85}	Air	16, 26, 28, 33, 37, 58
⊡	N_{51}	Helium Mixtures	68, 75, 78
○	N_{51}	Argon	70

AVERAGED DATA
$\alpha < 15°$

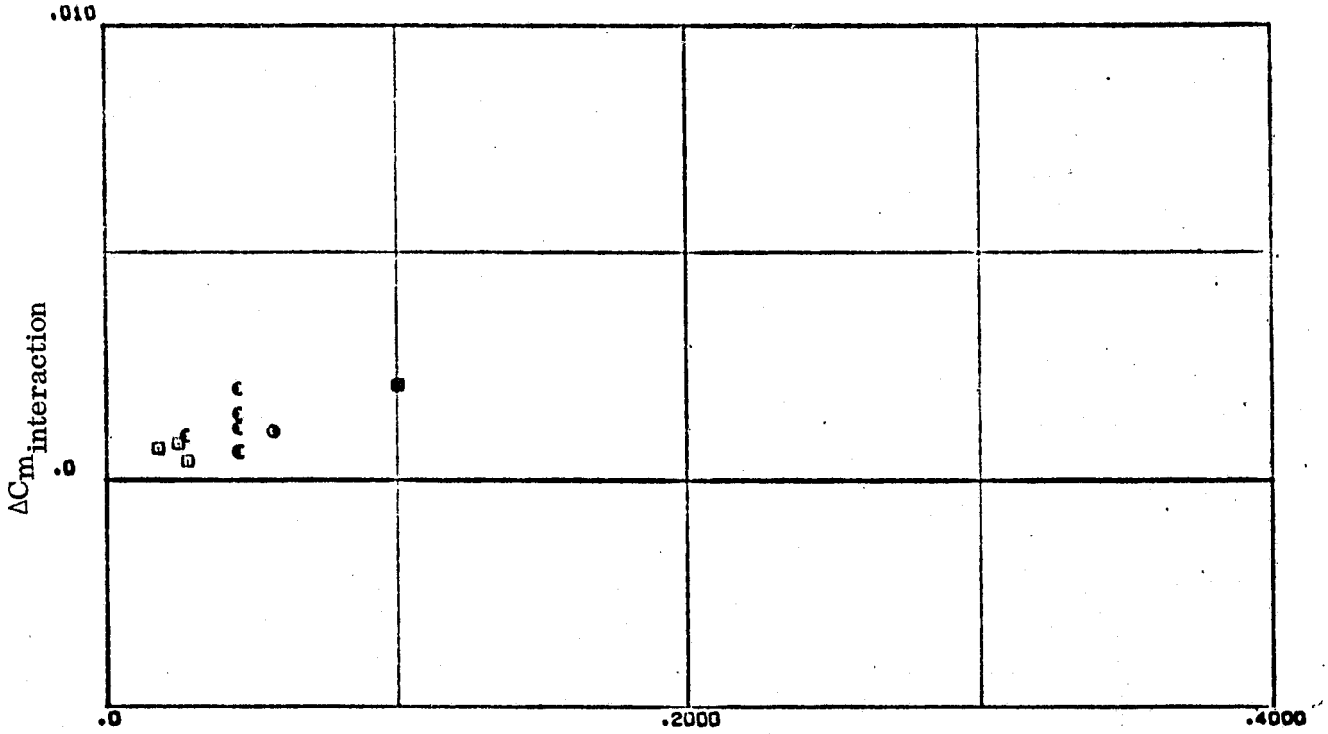

Figure 3-46. Left Side Yaw RCS Interaction, Pitching Moment at Low Angles of Attack

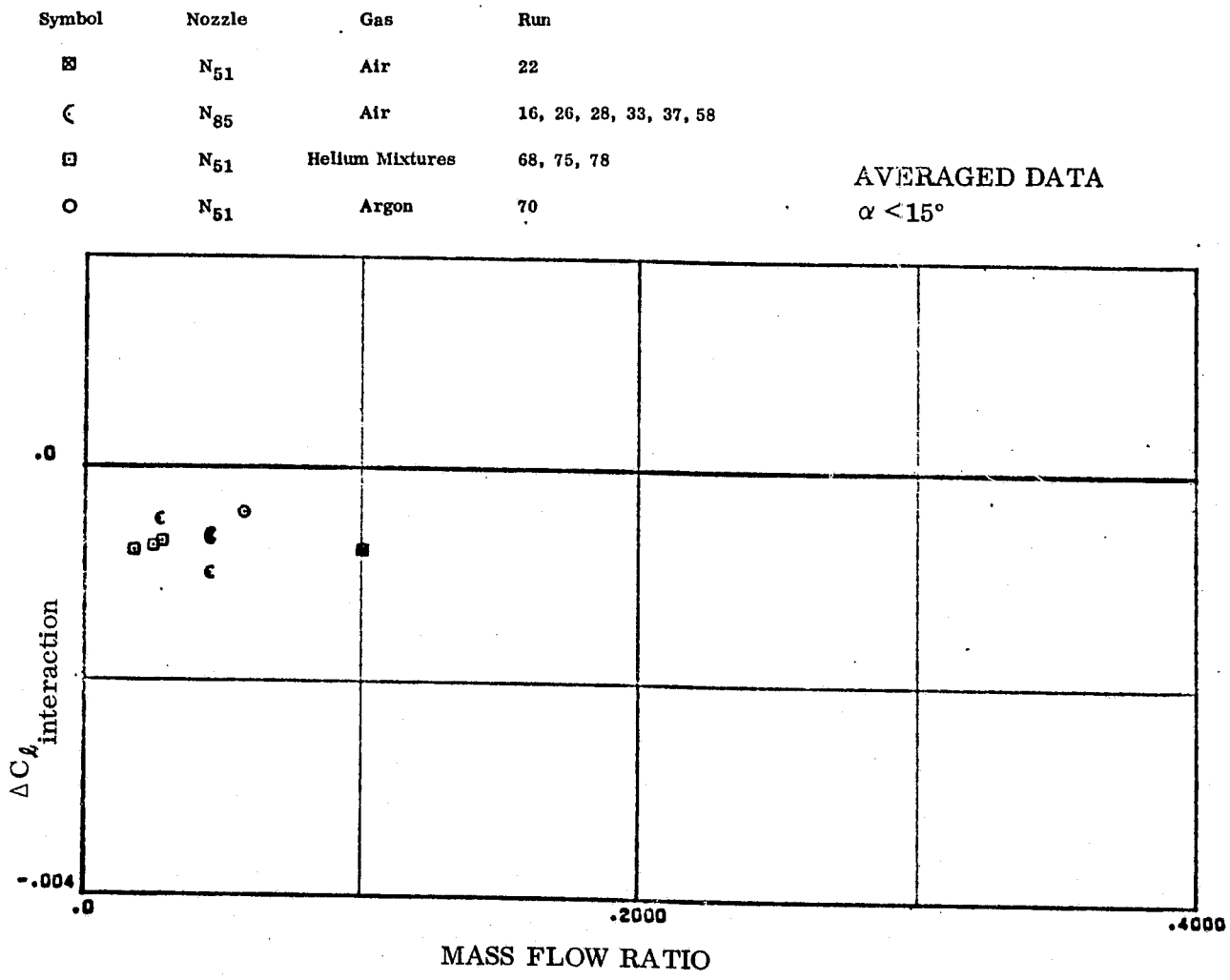

Figure 3-47. Left Side Yaw RCS Interaction Rolling Moment at Low Angles of Attack

Symbol	Nozzle	Gas	Run
⊠	N_{51}	Air	22
⋐	N_{85}	Air	16, 26, 28, 33, 37, 58
⊡	N_{51}	Helium Mixtures	68, 75, 78
○	N_{51}	Argon	70

AVERAGED DATA
$\alpha < 15°$

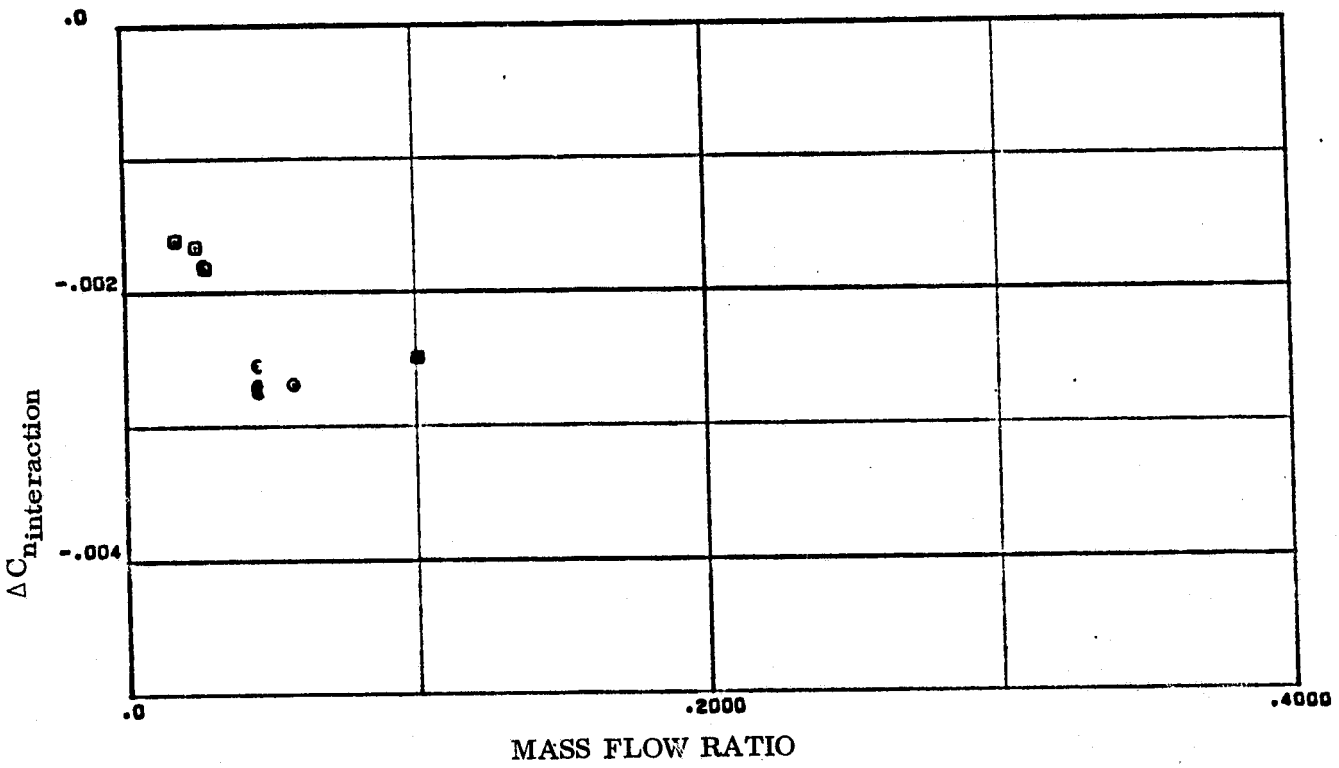

Figure 3-48. Left Side Yaw RCS Interaction Yawing Moment at Low Angles of Attack

Symbol	Nozzle	Gas	Run
⊠	N_{51}	Air	22
⊂	N_{85}	Air	16, 26, 28, 33, 37, 58
⊡	N_{51}	Helium Mixtures	68, 75, 78
○	N_{51}	Argon	70

AVERAGED DATA
$\alpha < 15°$

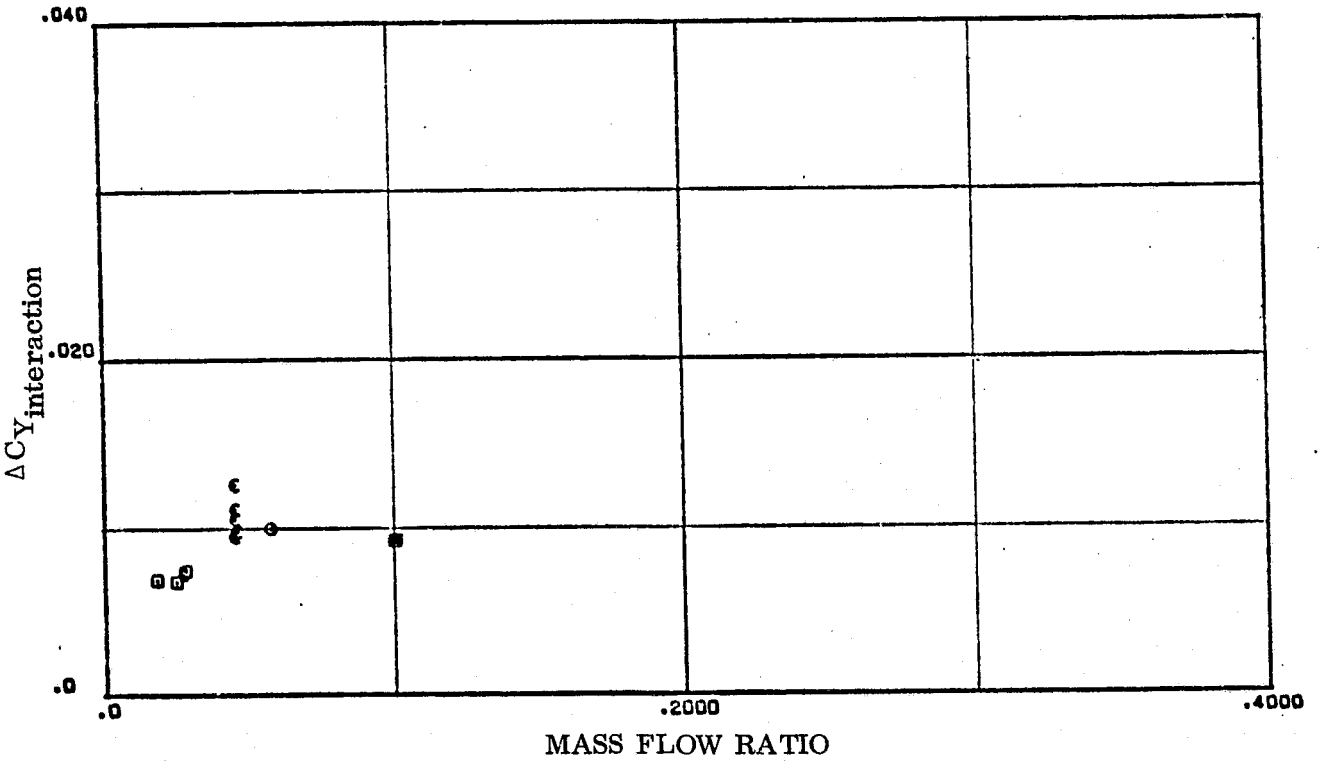

Figure 3-49. Left Side Yaw RCS Interaction Side Force at Low Angles of Attack

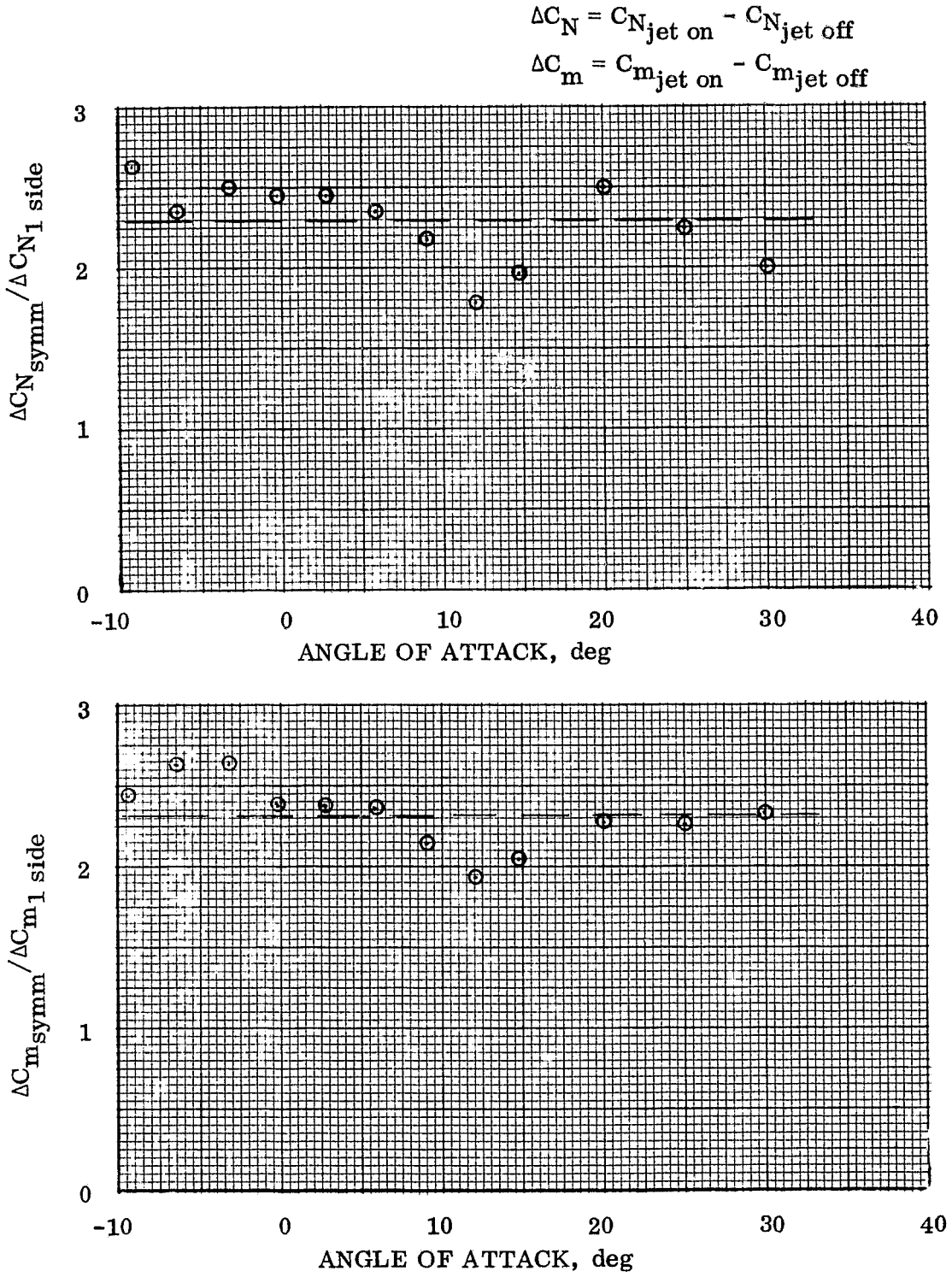

Figure 3-50. Symmetric Pitch Down Amplification

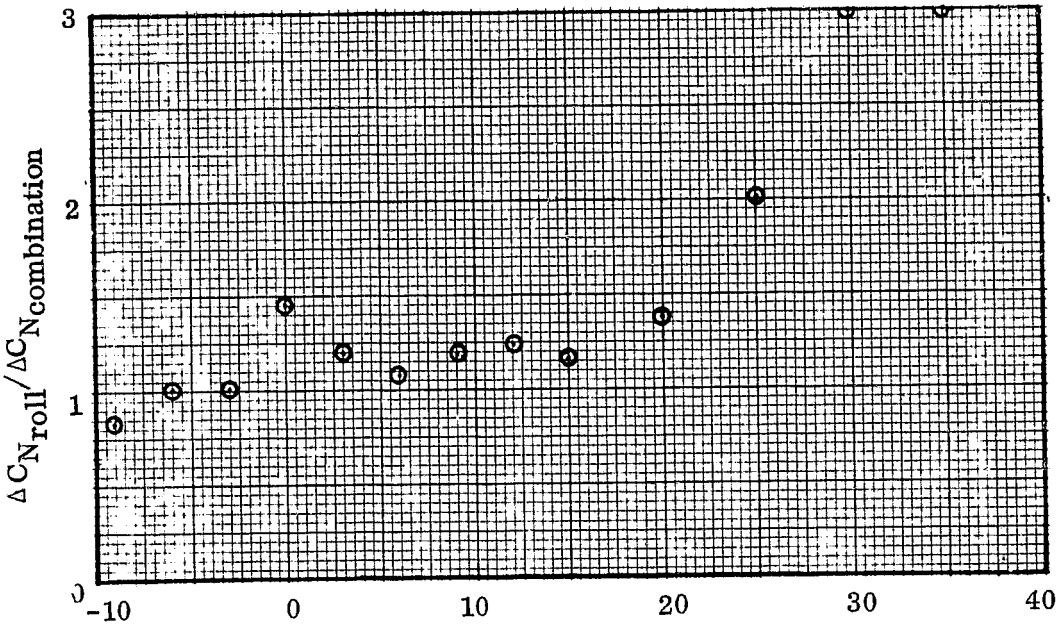

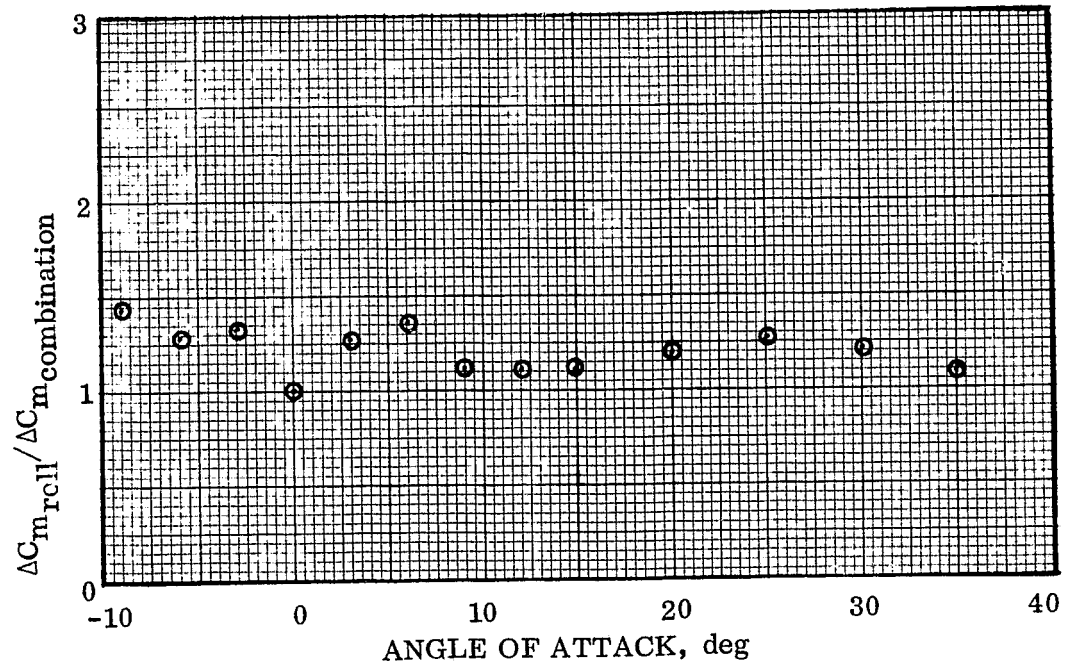

Figure 3-51a. Coupled Roll RCS Effects

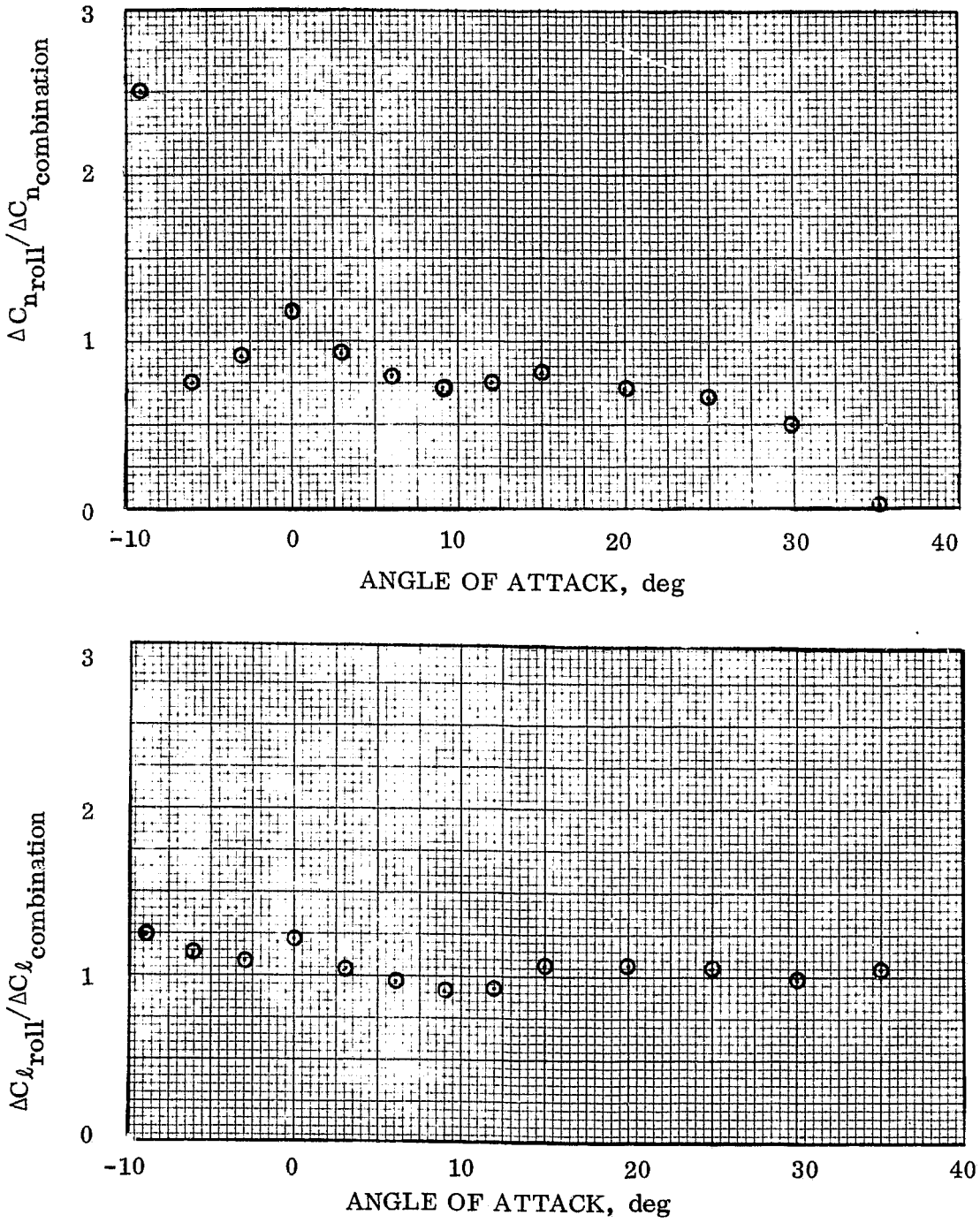

Figure 3-51b. Coupled Roll RCS Effects

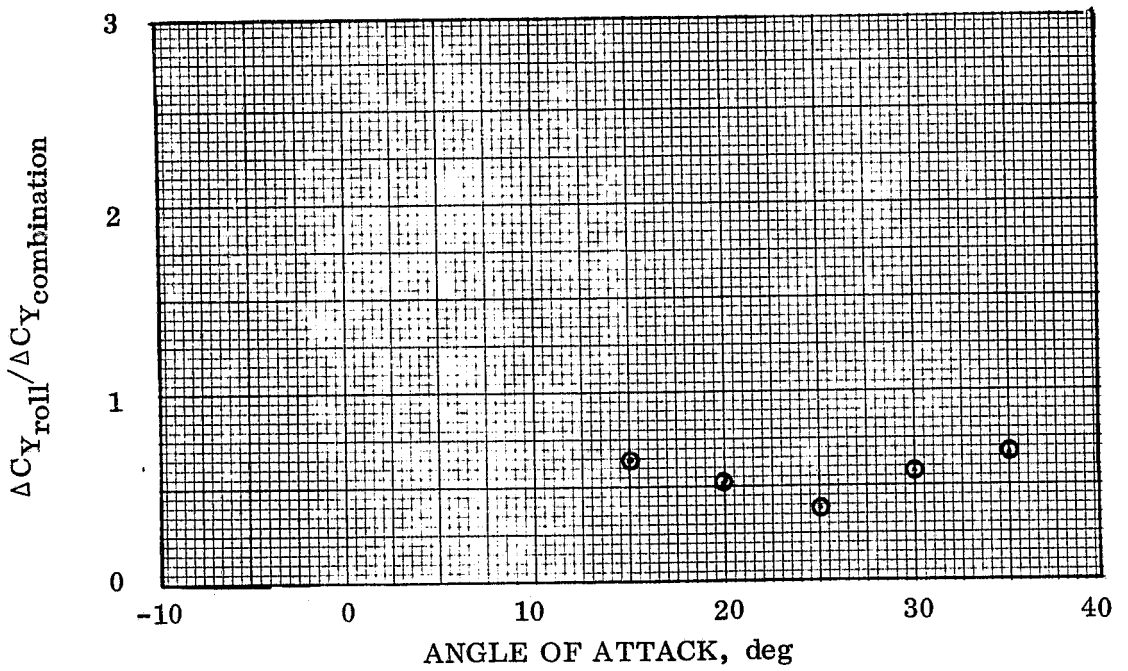

Figure 3-51c. Coupled Rolled RCS Effects

4

ANALYTIC MODEL DEVELOPMENT

4.1 GENERAL DESCRIPTION

The analysis presented in Section 3 provides the basis of the analytic model developed in this study. In general the total control effectiveness of a given control is defined as the sum of a number of parts as shown in Equation 1.

$$C_{M_{total}} = C_{M_{thrust}} + C_{M_{impingement}} + C_{M_{interaction}} + C_{M_{cross\ coupling}} \quad (1)$$

where

C_M = RCS force or moment component

and the resulting control effectiveness called control amplification is defined as an amplification factor which is the total control moment divided by the thrust moment

$$K_M = C_{M_{total}} / C_{M_{thrust}} \quad (2)$$

where

K_M = RCS force or moment amplification factor

In addition to the effects in the thrust direction, the RCS controls induce out of plane forces and moments which are the sum of some terms given in Equation 1. The data of Section 3 showed that each control generated measurable data of the five vehicle forces and moments correlated in this study and these components must be added together on each axis to determine the total value of the induced moments. It is desirable to relate these out of plane forces and moments to a thrust term in order to generate an amplification factor which is a measure of RCS effectiveness. This is done by relating the out of plane induced data to the control moment required to compensate for it. For example, rolling moment caused by yaw jets

$$K_{\ell_{yaw}} = \frac{(\Delta C_\ell)_{yaw}}{C_{\ell\ roll\ jet\ thrust}} \quad (3)$$

which is the same definition as Reference 3 . Since we wish to define amplifications for arbitrary numbers and combinations of controls, however, another definition must used for the thrust moment term. When an arbitrary combination of RCS controls is

being used and one of combination generates a control moment in the same plane as the induced moments, then that thrust moment is used in Equation 3. If none of the control combinations has a thrust term in the plane of the interaction then a two jet in plane control is used in Equation 3. For example for a single pitch up/roll nozzle being fired, the rolling moment will be related to the jet thrust roll component whereas for the rolling moment from a yaw jet firing will be related to a two jet roll nozzle combination.

The thrust moments required in Equations 1 to 3 are easily solved knowing the RCS nozzle characteristics, its location relative to the vehicle moment reference center and the mounting angle of the nozzle relative to the vehicle axis system. The interaction and cross-coupling terms were derived in Section 3 and their application in the analytic model will be described in Section 4.5. The sole remaining term which needs to be defined then is the plume impingement term.

4.2 PLUME IMPINGEMENT INCREMENTS

Figure 2-1 shows a view of the space shuttle orbiter which emphasizes the closeness of the rear RCS package to the base area of the vehicle. It is evident that the aft RCS engines will impinge heavily on the vehicle wing, vertical tail, body flap, main propulsion engine nozzles, and possible fuselage sides, depending on the nozzle set fired and on the altitude and other flight conditions affecting plume size. Reference 1 showed that plume impingement was a sizeable term for the PRR configuration while Reference 3 shows the same for the present configuration based on a vacuum chamber test (Rockwell Test OA99) and impingement predictions for the vacuum case.

Two models of plume impingement effects were developed for this prediction method and are included in the prediction computer program. The first is a vacuum data model while the second is an analtyical plume prediction model.

4.3 VACUUM TEST DATA MODEL

The first model developed is based on the assumption that the range of interest of flight conditions for full scale RCS estimation is sufficiently close to the vacuum case that the test data amplification factors from test OA99 reported in Reference 3 can be used directly from the thrust and thrust moments. Converting the data into coefficient form, the impingement increments from the pitch up jets are given in Equations 4 to 10 in body axis form:

$$\Delta C_{N_{impingement}} = -0.00086\ C_{T_{PU}} \tag{4}$$

$$\Delta C_{X_{impingement}} = 0.00246\ C_{T_{PU}} \tag{5}$$

$$\Delta C_{Y_{impingement}} = -0.06238\ C_{T_{PU}} \tag{6}$$

$$\Delta C_{\ell_{impingement}} = -0.130\ C_{\ell_{PU}} \quad (7)$$

$$\Delta C_{m_{impingement}} = 0.00078\ C_{m_{PU}} \quad (8)$$

$$\Delta C_{n_{impingement}} = 0.0593\ C_{n_Y} \quad (9)$$

where

$C_{T_{PU}}$ = (total thrust of pitch up engines)/(q S_{ref}) (10)

$C_{\ell_{PU}}$ = pitch up thrust rolling moment coefficient

C_{n_Y} = yaw thrust yawing moment coefficient

$C_{m_{PU}}$ = pitch up thrust pitching moment coefficient

The pitch down jet impingement increments are given in Equations 11 to 16:

$$\Delta C_{Z_{impingement}} = -0.27389\ C_{T_{PD}} \quad (11)$$

$$\Delta C_{X_{impingement}} = 0.10709\ C_{T_{PD}} \quad (12)$$

$$\Delta C_{Y_{impingement}} = 0.01837\ C_{T_{PD}} \quad (13)$$

$$\Delta C_{\ell_{impingement}} = -0.2312\ C_{\ell_{PD}} \quad (14)$$

$$\Delta C_{m_{impingement}} = -0.3018\ C_{m_{PD}} \quad (15)$$

$$\Delta C_{n\ impingement} = 0.01657\ C_{n_Y} \quad (16)$$

where

$C_{T_{PD}}$ = total pitch down thrust coefficient

$C_{\ell_{PD}}$ = pitch down thrust rolling moment coefficient

$C_{m_{PD}}$ = pitch down thrust pitching moment coefficient

and the yaw impingement equations are:

$$\Delta C_{Z_{impingement}} = 0.01634\ C_{T_Y} \quad (17)$$

$$\Delta C_{X_{impingement}} = 0.00288\ C_{T_Y} \quad (18)$$

$$\Delta C_{Y_{impingement}} = 0.00077\ C_{T_Y} \quad (19)$$

$$\Delta C_{\ell_{impingement}} = 0.03477\ C_{\ell_{PU}}\ C_{T_Y}/C_{T_U} \quad (20)$$

$$\Delta C_{m_{impingement}} = 0.00873\ C_{m_{PU}}\ C_{T_Y}/C_{T_U} \quad (21)$$

$$\Delta C_{n_{impingement}} = 0.0013\ C_{n_y} \quad (22)$$

where

C_{T_Y} = total yaw RCS thrust coefficient

C_{T_U} = total pitch up RCS thrust coefficient

$C_{\ell_{PU}}$ = pitch up thrust rolling moment coefficient

$C_{m_{PU}}$ = pitch up thrust pitching moment coefficient

C_{n_Y} = yaw thrust yawing moment

This model has its limitations in that it assumes that there will always be impingement, that the amount of impingement is related only to thrust, and it cannot account for nozzle or geometry variations. This last limitation was a large one because of the need to generate plume impingement corrections for the OA82 wind tunnel data which used much different nozzles and test gases than the vacuum chamber test.

This model is available in the prediction program to use if desired.

4.4 ANALYTIC PLUME IMPINGEMENT MODEL

The analytic plume impingement model of Reference 1 was compared against the OA99 vacuum chamber results and other test data and was found to underpredict the plume impingement by a significant margin and was discarded early in the data analysis and another method was sought which provided a better representation of the plume characteristics.

Simon's, Reference 4 , modeled the flow field of the RCS engines as

$$\dot{m} = 217 \frac{f(\theta)}{r^2} \quad \frac{g_{sec}}{cm^2} \tag{23}$$

where

r = radial distance from nozzle in inches

$$f(\theta) = \cos^{10}(\pi\theta/250): \; 0 < \theta < 60° \tag{24}$$

$$f(\theta) = 0.0438\,(e^{-0.064(\theta-60°)}): \; 60° < \theta \tag{25}$$

where

θ is angle from nozzle centerline in degrees

and a similar approach to the plume shape was sought for this analysis based on the assumptions that at the flight conditions of highest importance and the RCS plumes exhausting into the leeward flow over the wing at angle of attack or into the vehicle base region that the external pressure will be close to vacuum. A modified vacuum plume model would be the best representation of the RCS plume where the primary modification is to limit the plume boundary to the limit turning angle of plume flow.

Computation of plumes expanding into a vacuum by methods of characteristics (Reference 5) show that at large distances from the nozzle that the streamlines appear to emanate as radial flow from a common source point at the nozzle exit. Since the rate of mass flow through the nozzle is a constant, the mass flux ρu in the far field should vary inversely as x^2. And, since the velocity in the far field approaches the limiting velocity $\hat{u} = \sqrt{2\,h_o}$, the density variation should approach $\rho \sim x^{-2}$ as seen in Figure 4-1. Thus, one should be able to express the density distribution along the centerline $f(\theta) = 1$ in terms of the supply density as

$$\frac{\rho}{\rho_o} = B\,(x/d^*)^{-2}\; f(\theta) \tag{26}$$

where B depends on the nozzle shape and the properties of the gas. Equation 23 has this form for the centerline decay of the flow properties of the RCS engine plume but a more generalized expression was sought so that the plumes from test OA82 could also be treated in the same model. Thus Equation 26 was used where the value of B was solved in Reference 5 by using characteristics calculations of density variation along various nozzle centerlines and gas specific heats from 1.2 to 1.67.

A jet expanding into a vacuum (Figure 4-2) is bounded by a straight streamline at zero pressure and $M = \infty$. The location of this boundary, denoted as θ_∞ in Figure 4-2, will depend upon the nozzle exit lip angle θ_e, the area ratio of the nozzle A_e/A^*, and the γ of the exhausting gas. This angle θ_∞ may be determined from the Prandtl-Meyer

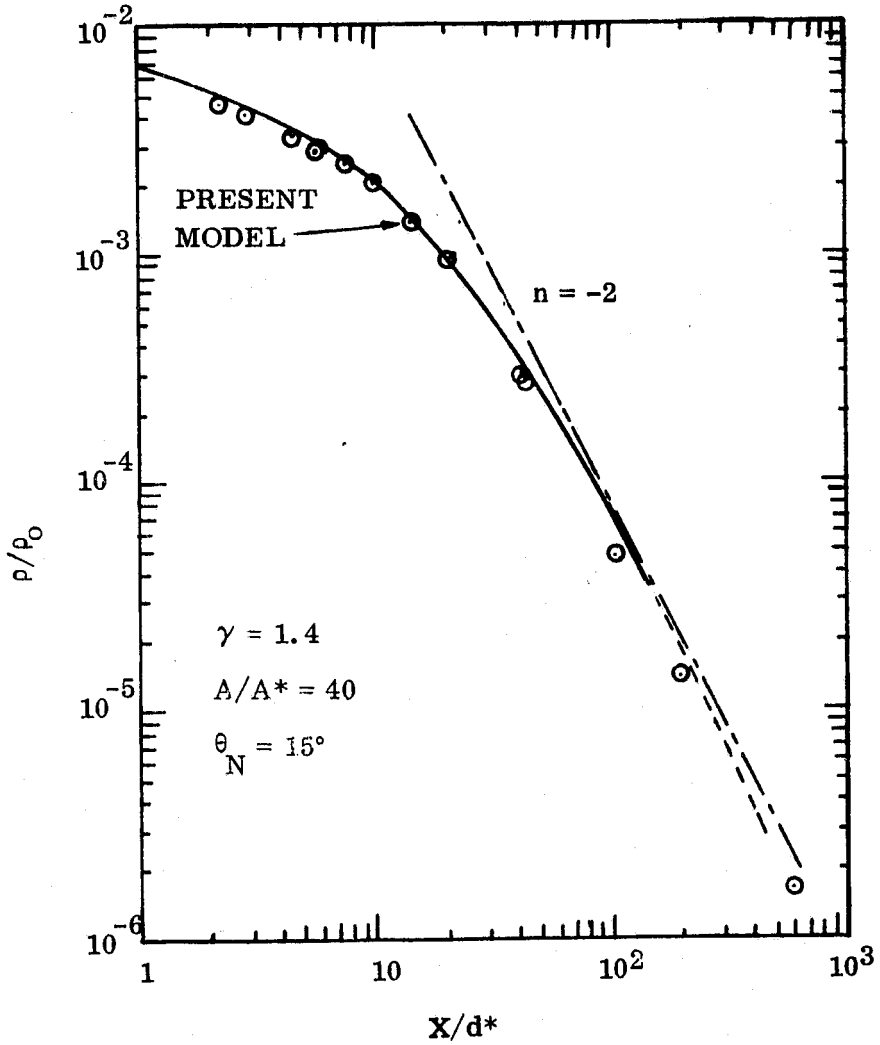

Figure 4-1. Density Distribution Along the Plume Axis

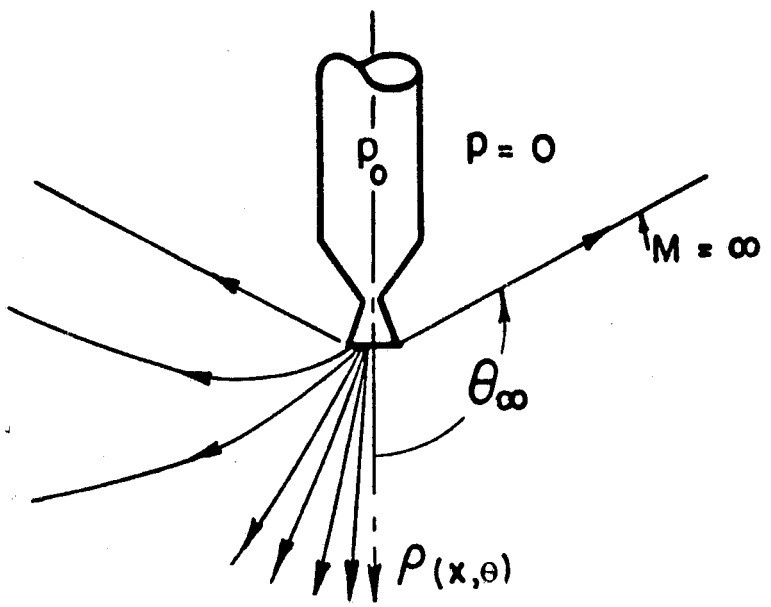

Figure 4-2. Schematic Drawing of a Jet Expanding Into a Vacuum

expansion relationship and θ_e as a function of area ratio. For other values of θ_e, the value of θ_∞ may be determined from the relationship

$$\vartheta_\infty = (\theta_\infty)_{\theta_e=0} + \theta_e \tag{27}$$

The solid angle Ψ_∞ corresponding to θ_∞ is given by

$$\Psi_\infty = 2\pi(1-\cos\theta_\infty) \tag{28}$$

The flow boundary θ_∞, and thus the limiting solid angle Ψ_∞ with increasing area ratio at a constant γ, while at a given area ratio, θ_∞ increases for decreasing value of γ.

Reference 5 showed that for a family of nozzles having the same mass flow rate the density decay along the nozzle axis is dependent upon the limiting flow angle θ_∞ as shown in Figure 4-3. The variation of B with θ_∞ for both the theoretical curves of Reference 6 and the characteristics calculations shown as symbols appear on this figure.

$$B = \frac{\text{constant}}{\Psi_\infty} = \frac{0.4\pi}{\Psi_\infty} \tag{29}$$

where the value of the constant has been chosen to fit the data of Figure 4-3. This expression assumed that the dependence of B upon specific heat ratio is small and the characteristic solution data of Figure 4-3 was recomputed to derive a new expression for B which is

$$B = \frac{K\pi}{\gamma^2\ \Psi_\infty} \tag{30}$$

and where K was defined from Figure 4-4 as

$$K = 1.24 - 0.0040894\ \theta_\infty \tag{31}$$

In these expressions θ_∞ is defined by expanding the nozzle flow to the ambient pressure of free stream or wind tunnel rather than to a vacuum angle. This approximation has been shown to cause only small errors since most of the mass and momentum within a plume are contained near the central core of the plume and truncating the vacuum plume at the angle defined by ambient pressure results in very little loss of plume mass (Ref. 7) in the conservation equations particularly where ambient pressures are low.

Figure 4-1 showed that the square power decay law does not work at distances of less than 10 to 15 throat diameters away from the nozzle exit and empirical fits were generated to cover this region using the nozzle exit density ratio as a parameter:

REFERENCE 5

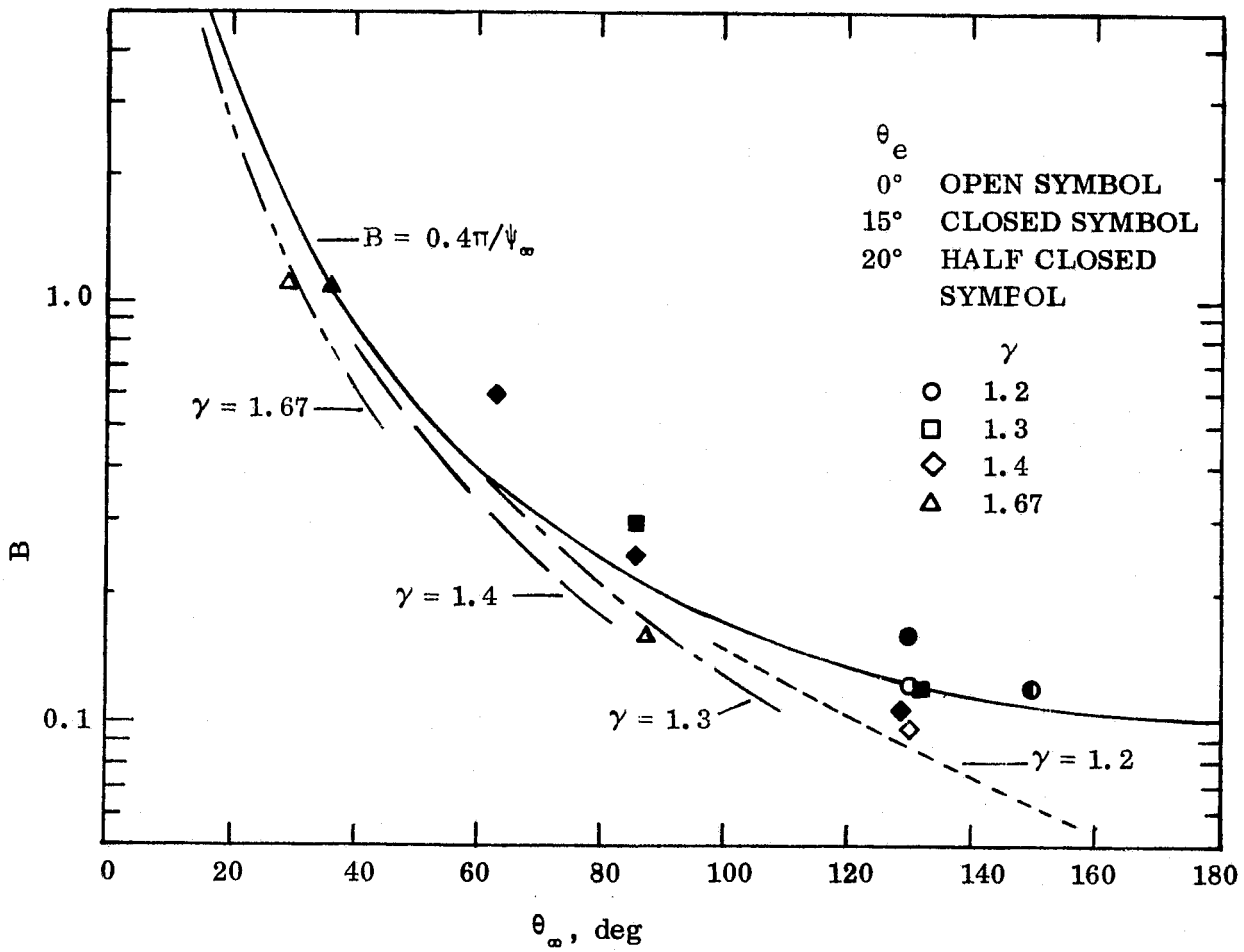

Figure 4-3. A Comparison of Density Decay and Limit- Turning Angle

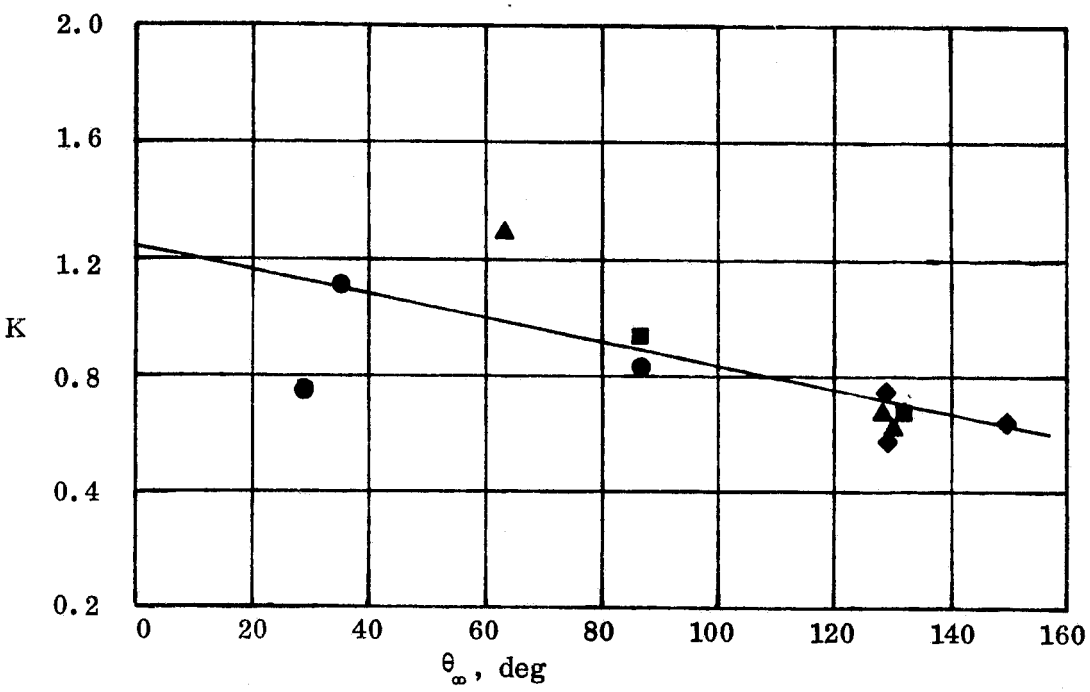

Figure 4-4. Plume Density Decay Factor Correction With Limit Turning Angle

$$\frac{\rho_j}{\rho_{o_j}} = \left[1 + \frac{\gamma_j - 1}{2} M_j^2\right]^{-1/\gamma_j - 1} \tag{32}$$

If (X/d*) was greater than $B/(\rho_j/\rho_{o_j})$ Equations 26 to 31 were used. If (X/d*) was less than the square root of $B/(\rho_j/\rho_{o_j})$ then

$$\frac{\rho}{\rho_o} = \frac{\rho_j}{\rho_{o_j}} \left(\frac{X}{d^*}\right)^{-0.5} (f(\theta) \tag{33}$$

and in between these two ends; two other expressions were used if (X/d*) were less (Equation 34) or greater (Equation 35) than $[B/(\rho_j/\rho_{o_j})]^{.67}$.

$$\frac{\rho}{\rho_o} = \frac{\rho_j}{2\rho_{o_j}} \left[\left(\frac{X}{d^*}\right)^{-0.5} + \left(\frac{X}{d^*}\right)^{-1}\right] f(\theta) \tag{34}$$

$$\frac{\rho}{\rho_o} = \frac{1}{2} \left[\frac{\rho_j}{\rho_{o_j}} \left(\frac{X}{d^*}\right)^{-1} + B\left(\frac{X}{d^*}\right)^{-2}\right] f(\theta) \tag{35}$$

In all these expressions, the variation [f (θ)] away from the plume centerline was taken from Simon's model (Equations 24 and 25). The plume Mach number, local static pressure and local dynamic pressure at a point are defined from the density ratio based on isentropic flow relations.

In the cases of the plumes firing upward past the fin (pitch up) and outward over the wing (yaw) where the plume is likely to be interacting with the flow over the vehicle, the plume is assumed to stop when the plume local dynamic pressure is less than the free stream dynamic pressure. A further limitation is placed on the plume to terminate the plume if the free stream impingement pressure coefficients are less than zero.

Multiple sets of nozzles are handled by defining a single equivalent nozzle which has the same geometric shape as the other nozzles but which has an exit area equal to the sum of the exit areas of the nozzles in the cluster. Its location is chosen as the center of the cluster. This representation of the plume from multiple sets of nozzles has been found to be a good approximation (Reference 8) and changes plume characteristics through the larger value of throat diameter in Equations 26 to 35.

4.4.1 PLUME IMPINGEMENT FORCES. The highly underexpanded flow from the nozzle expands very quickly to high Mach numbers at small distances from the exit and this supersonic flow will be undisturbed by a surface it may impinge until it is close to the surface. A detached shock wave would be formed by the high Mach number flow impinging on a surface with a region of subsonic flow between the strong

shock and the surface where the flow is turned to a direction paralleling the plate. The pressure on the surface of the vehicle was assumed to be related only to the plume conditions at the point in question and to the local slope between the surface at that point and the plume flow vector emanating from the point source at the nozzle exit (radial flow approximation). It was also assumed that the surface pressure could be predicted by a modified Newtonian pressure law because of the high plume Mach numbers and large turning angles.

$$P_{w_i} = 1.85 \frac{\gamma_j}{2} P_{j_i} M_{j_i}^2 \cos^2 \theta_i + P_{j_i} \tag{36}$$

where

P_{w_i} = plume impingement pressure at i^{th} point on body

P_{j_i} = plume ambient pressure at point i

M_{j_i} = plume Mach number at point i

θ_i = local slope between plume flow and surface at point i

The local plume impingement pressure is then converted into a pressure coefficient related to ambient flight conditions to put it into the same reference as the vehicle aerodynamic coefficients and is integrated to obtain vehicle force and moment coefficients resulting from impingement.

The integration of impingement pressures was approximated in the analytic model by breaking elements of the vehicle into flat plates of known centroid location, area, and local slope, the plume impingement pressures at each point were computed, the local force and moment cofficients computed by applying the impingement pressure across the area, and the total vehicle values obtained by summing the local values. Figures 4-5 to 4-7 present the points representing the centroids of the areas used in the determination of the plume impingement corrections to the wind tunnel data. Only one side of the vehicle is represented to increase the accuracy by having a larger number of plates which will have impingement but to reduce the computation time for plates not affected.

Figure 4-8 presents a comparison of the computed impingement force and the interaction increments for the left side pitch down jets which shows that the impingement term does not become larger than the interaction term until well past the peak interaction. Figure 4-9 presents a comparison of the impingement and interaction increments of rolling moment caused by the right side jets exhausting up past the vertical fin at high angles of attack. In this case the impingement correction never exceeds the interactions increment but they tend to parallel each other as thrust moment increases.

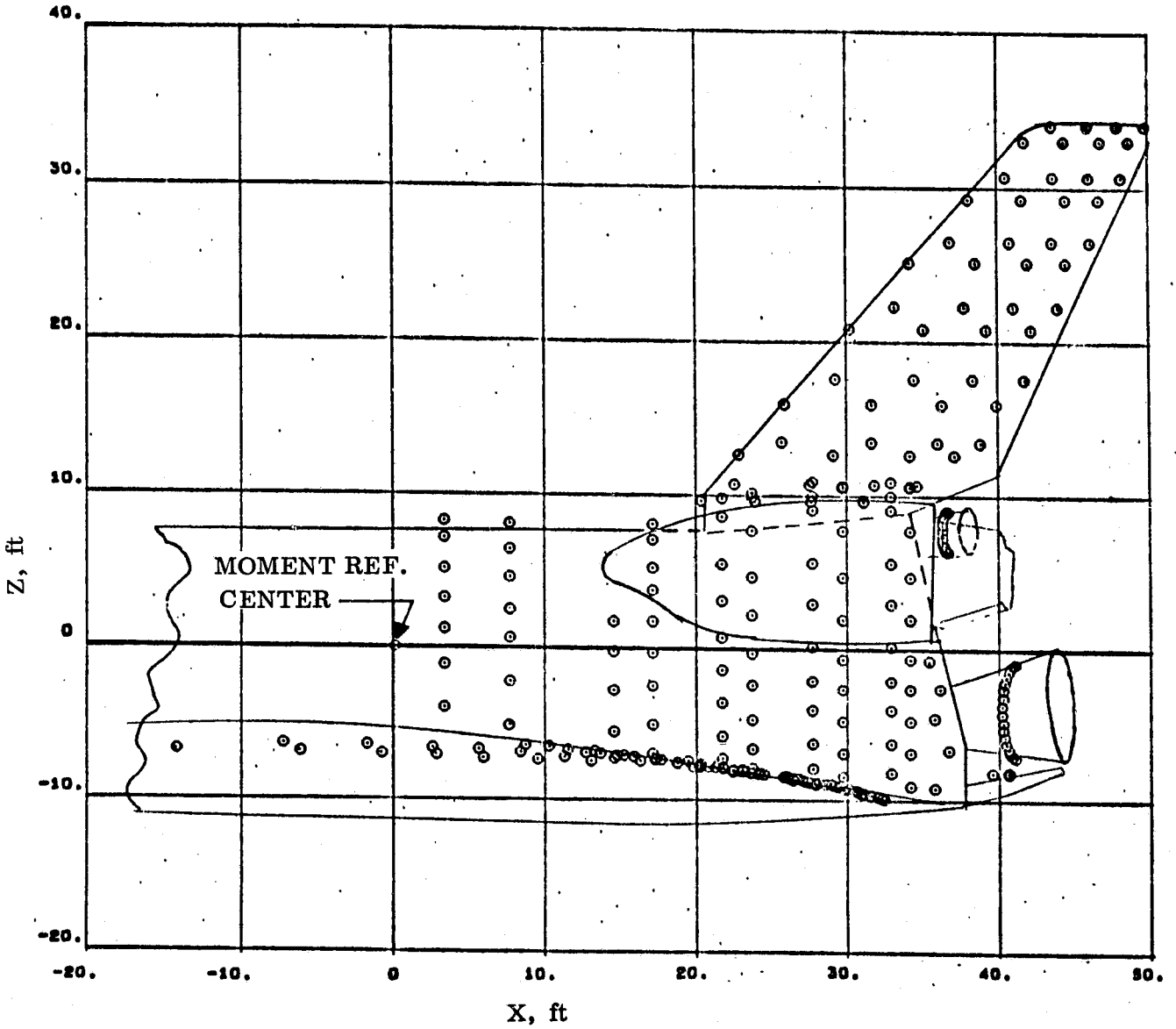

Figure 4-5. Side View of Vehicle Showing Centroids of Plates Used for Impingement

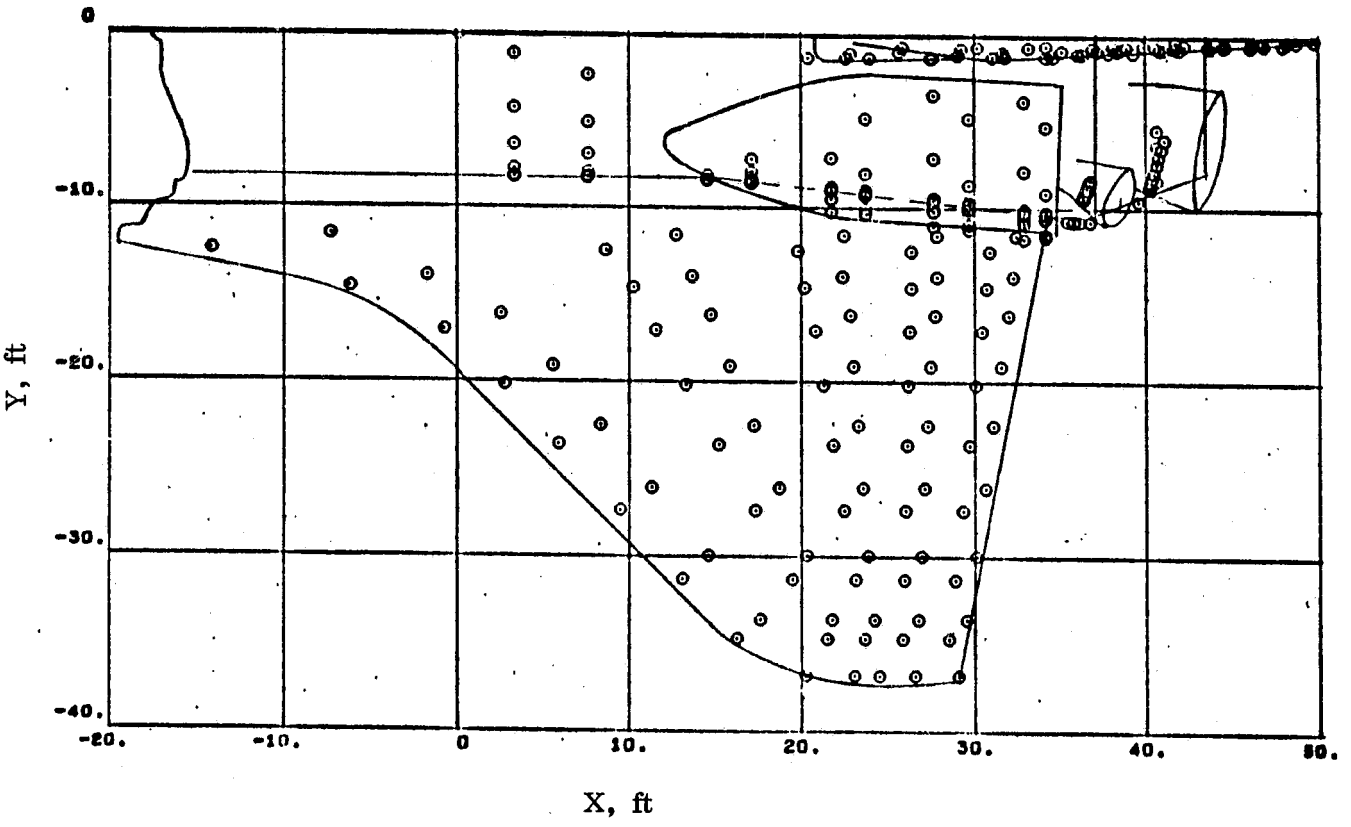

Figure 4-6. Top View of Vehicle Showing Centroids of Plates Used for Impingement

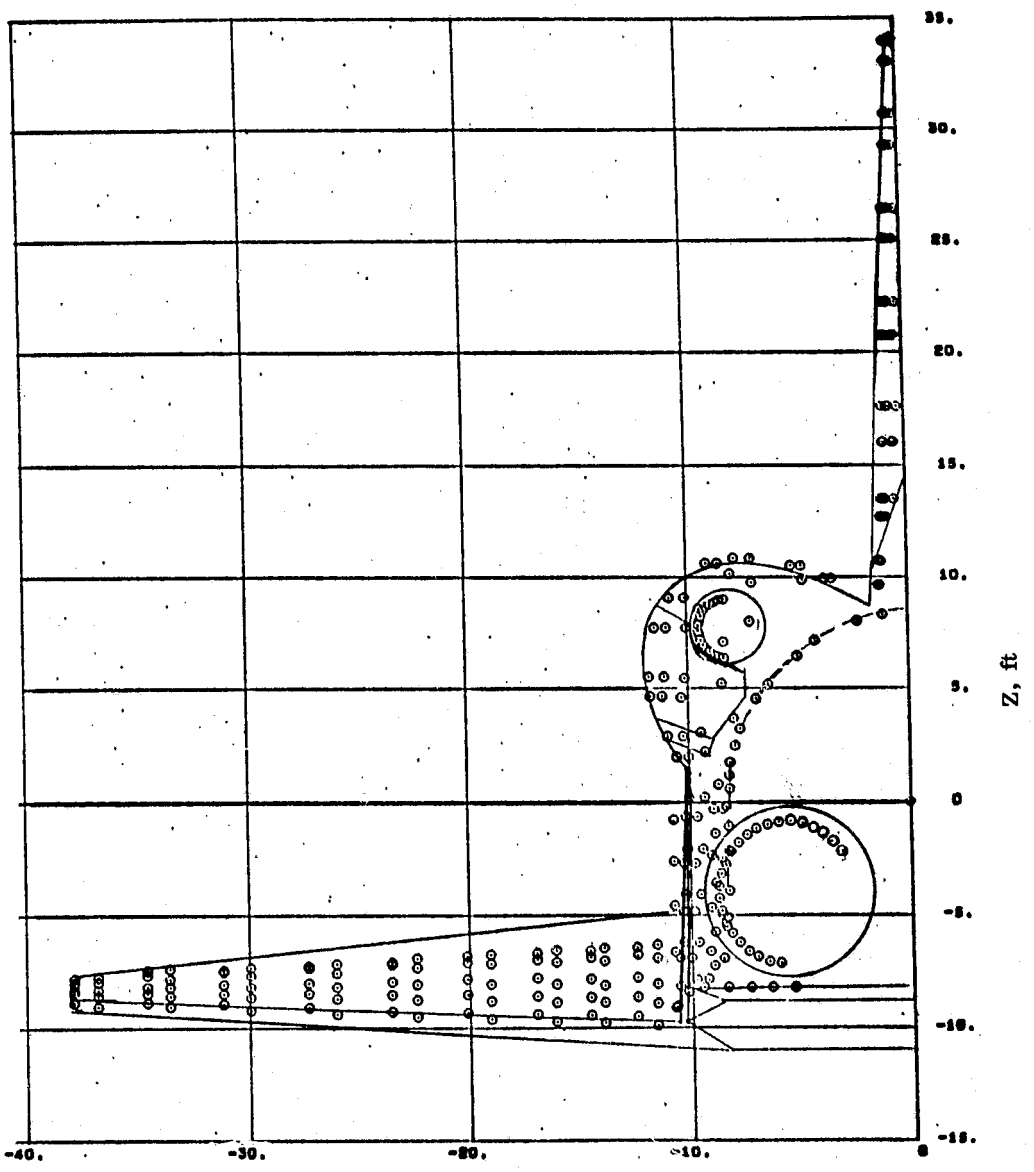

Figure 4-7. Rear End View of Vehicle Showing Centroids of Plates Used for Impingement

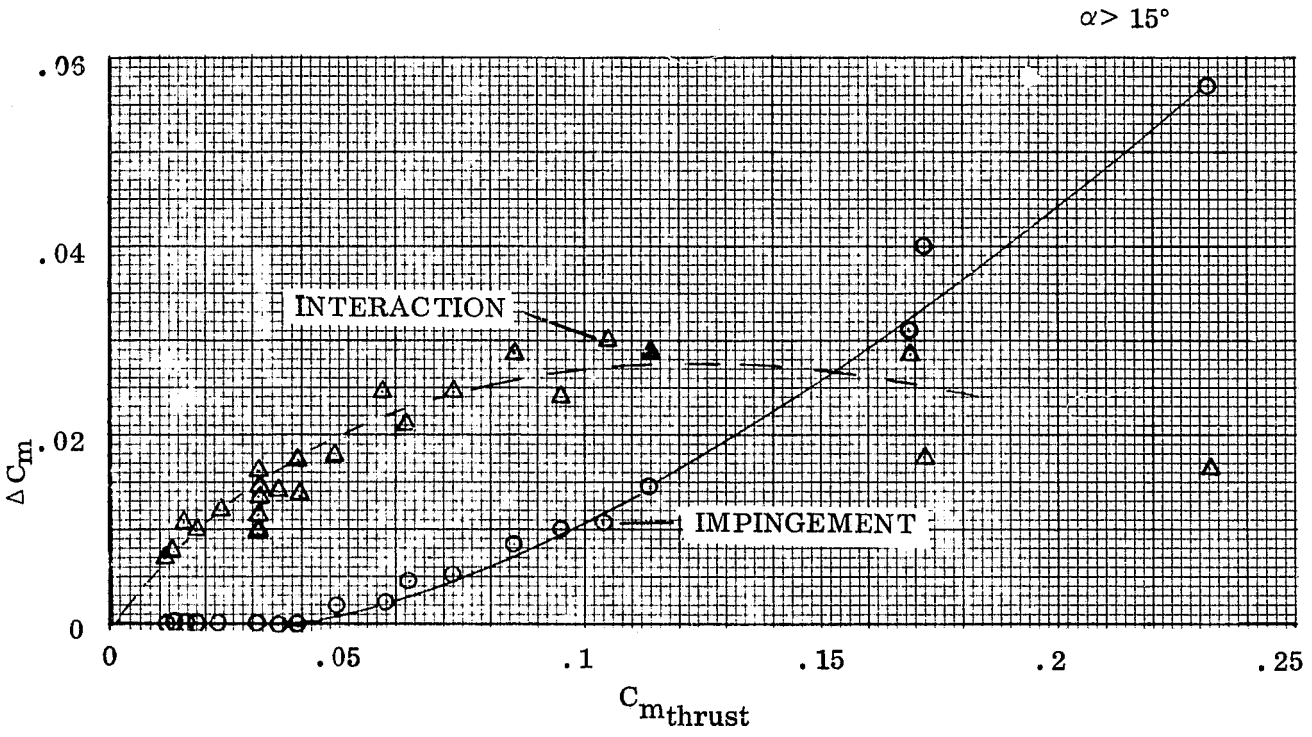

Figure 4-8. OA82 Left Side Pitch Down RCS Impingement Correction on Pitching Moment

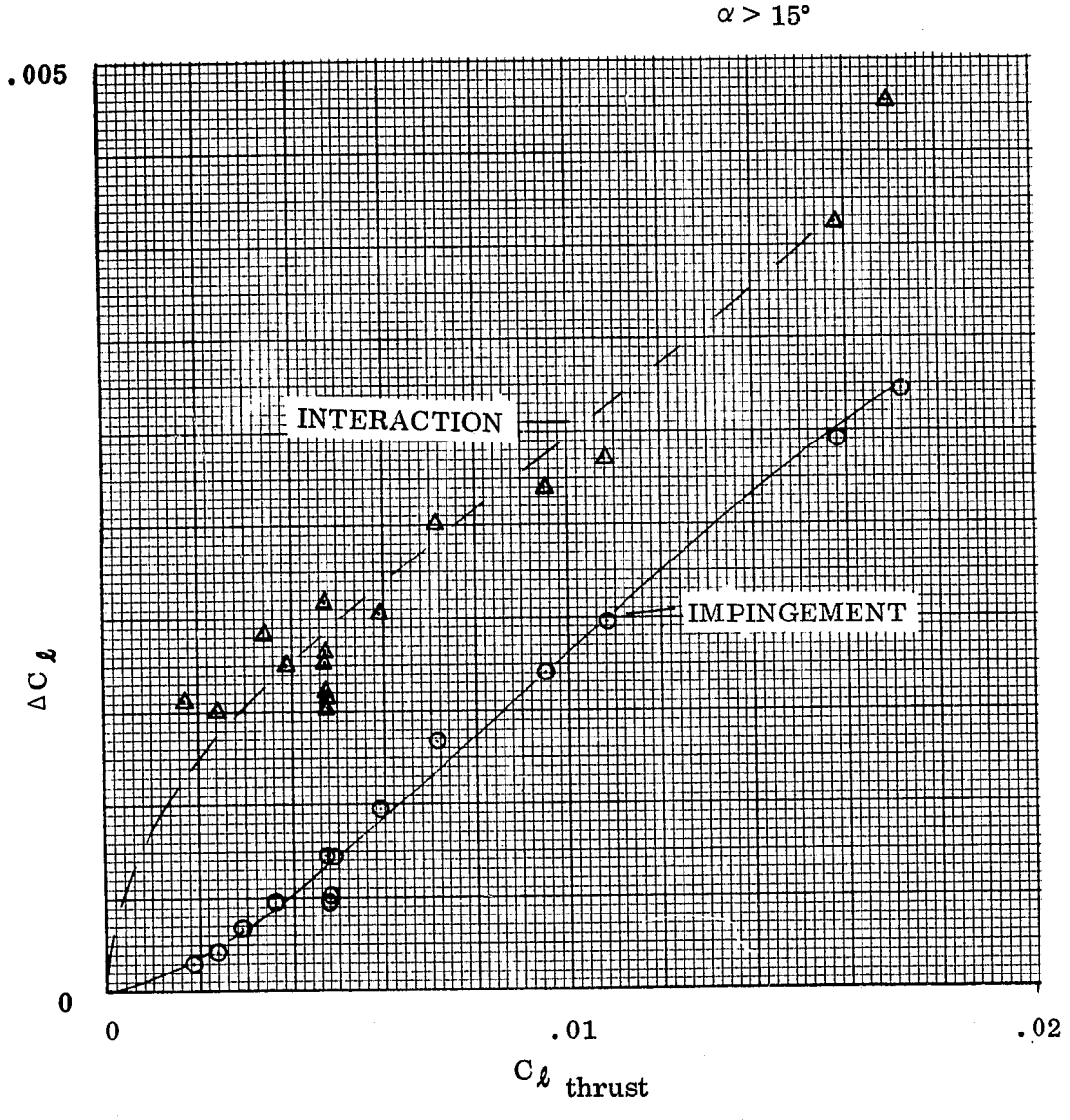

Figure 4-9. OA82 Right Side Pitch Up RCS Impingement Correction on Rolling Moment

This impingement model was checked against the method of characteristics vacuum case solution as well as the vacuum chamber test (OA99) results of Reference 3 and close agreement was obtained as shown in the table below.

Case	P_{o_j}	A/A*	θ_N	γ_j	$K_{m_{down}}$		$K_{\ell_{down}}$	
					Ref.	Computed	Ref.	Computed
OA99 Model	1000 psia	6.2	10°	1.4	0.6982	0.6479	0.6596	0.6671
Vacuum Solution	150	20	9	1.232	0.6713	0.6888	0.7085	0.7035

4.5 INTERACTION AND CROSS COUPLING MODELS

Section 3 which presents the data analysis contains within it the curve fits derived from that data analysis. These curve fits were used as the analytic model of interaction and cross coupling terms with some limitations. The limitations were generally applied in defining the upper limits of the curves. In general if a curve has a maximum or minimum value (defined in Section 3) it was only used up to the maximum (minimum) value and was assumed as a constant value beyond this mass flow or momentum ratio. When a curve fit shape is such that it has no maximum or minimum value, an arbitrary limit was applied and the data was assumed constant beyond this limit. This limit was usually taken at or near the upper value of mass flow or momentum ratio tested in test OA82.

5

ANALYTIC COMPUTER PROGRAM

5.1 GENERAL DESCRIPTION

The model of RCS control effectiveness presented in sections 3 and 4 of this report were programmed into a digital computer program named PRED which will predict reaction control system effectiveness on a space shuttle type vehicle for any combination of Rear RCS engines firing at any angle of attack and flight condition up to the vacuum case. Numbers of RCS Engine, engine size, engine operating conditions, exhaust gas properties, and nozzle geometry can be varied as input parameters. Engine location on the rear of the vehicle and cant angles can also be varied, however, the analytic models were developed from one configuration (figure 2-1) and large departures from these RCS locations will probably invalidate some of the models of interaction and cross coupling terms.

Figure 5-1 presents a flow diagram of the program which consists of a main program and 17 subroutines. The program was divided into this large number of subroutines so that modification of any part could be more easily accomplished without disrupting the whole program. The names of the subroutines are:

1. INPUTT	7. MACH	13. QUAD
2. JET	8. THR	14. KABD
3. PARCEO	9. IMPINGE	15. AKABD
4. ATMOS	10. VACPLU	16. CCOUPL
5. EXPAN	11. INTER	17. AMPL
6. SCAL	12. QUART	

The name of the main program is PRED and FORTRAN listings of all parts of the program are contained in Appendix A. Each subroutine will be briefly discussed in the sections below with the input subroutine and input key presented last.

5.2 MAIN PROGRAM PRED

Figure 5-1 shows that the function of the main program is to drive the subroutines in an orderly fashion first to obtain the input to start the problem, to define the equivalent nozzles firing upward, downward, and side ways, to define the flight conditions and resulting nozzle flow parameters for a single nozzle and then

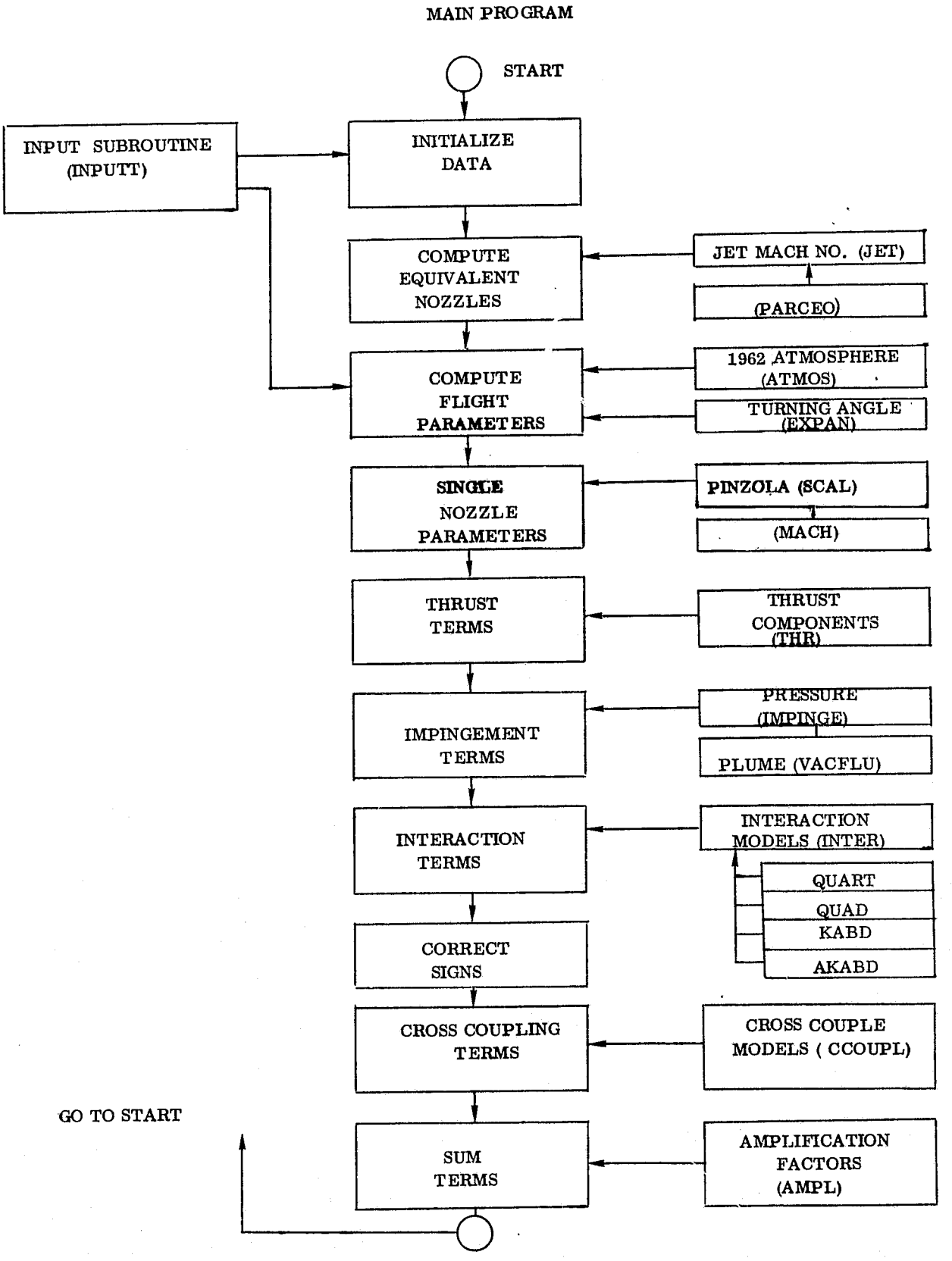

Figure 5-1. Program PRED Flow Diagram

proceed to define the various components of total RCS effectiveness for each set of equivalent nozzles fixing up, down, and sideways. These components must be corrected for the symmetric firing sets and for the side that non-symmetric sets are firing on. The cross coupling terms are then determined and all of the components of data are summed into the 6 total RCS aerodynamic force and moment coefficients and the amplification factors determined. When this occurs the program returns to the beginning to start the next case.

All input comes into the program through the INPUTT subroutine, but the main program handles most of the output printing at various stages throughout its length.

The program is set up to assume all RCS nozzles are on the left side of the vehicle when viewed from the rear looking forward in order to standardize the data for the impingement calculation and to set the signs of the interaction models. The data is corrected to the proper side of the vehicle or to symmetric firing by two input parameters for each RCS direction. The RCS directions are upward firing designated by a U as the last letter of a variable name in the listing, downward firing designated by a D as the last letter, and side firing designated by a Y as the last letter. The program always assumes that there are some upward, downward, and side firing nozzles in each problem so that all of the components are computed for all three sets before the summation of terms is made. If the number of nozzles (NONOZU, NONOZD, NONOZY) is zero those components are equal to zero. The axis system used is a body axis system shown in Figure 5-2 and the component data has these designations CX, CY, CZ, CL, CM, CN as the first two letters of the variable name where CN refers to yawing moment. Finally where the component force or moment is derived from is specified by the two middle letters of the variable names and IM is an impingement force or moment component, IN is an interaction component, and CC is a cross-coupling component. The thrust terms have no component designation and thus are 3 letter variable names while the others are 5 letter names. A typical example of a variable name is CMIMU which is the pitching moment induced by plume impingement of the upward firing nozzles.

Figure 5-3 shows that the program assumes that a downward firing set, an upward firing set, and a side firing set exit for a given problem. A set of nozzles is defined in this program as the actual number firing in a given cluster on one side of the vehicle. It is not the total number available to fire on one side nor the total number firing on both sides in a symmetric firing case.

The input data required for a first case is all of the data defining the vehicle, RCS units, and flight conditions, however, once this has been defined only the parameters which are to be changed need be input for additional cases.

5.3 COMPUTE JET EXIT MACH NUMBER(SUBROUTINES JET AND PARCEO)

After the program has received input defining the reaction control system engine in

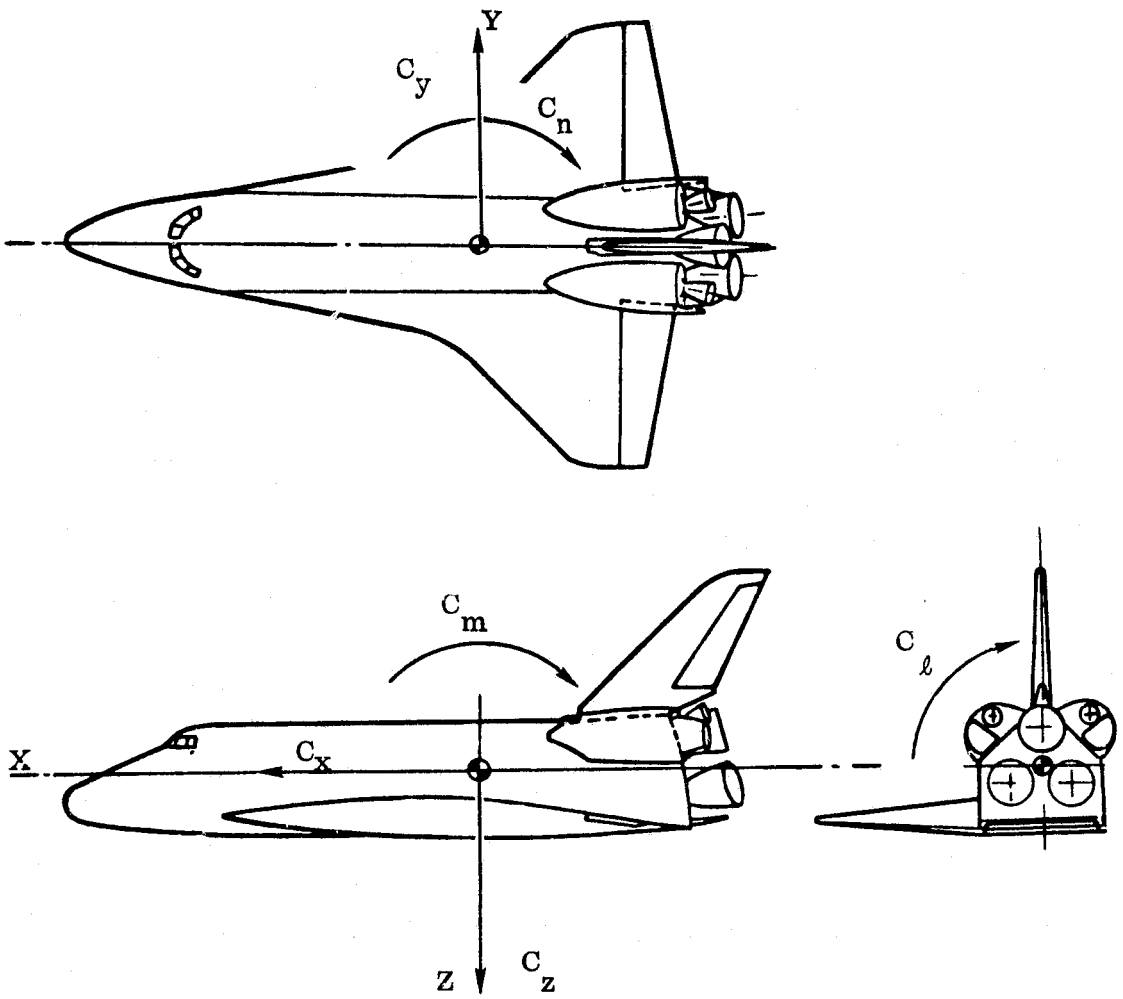

$C_N = -C_z$

$C_A = -C_x$

Figure 5-2. Body Axis Sign Convention

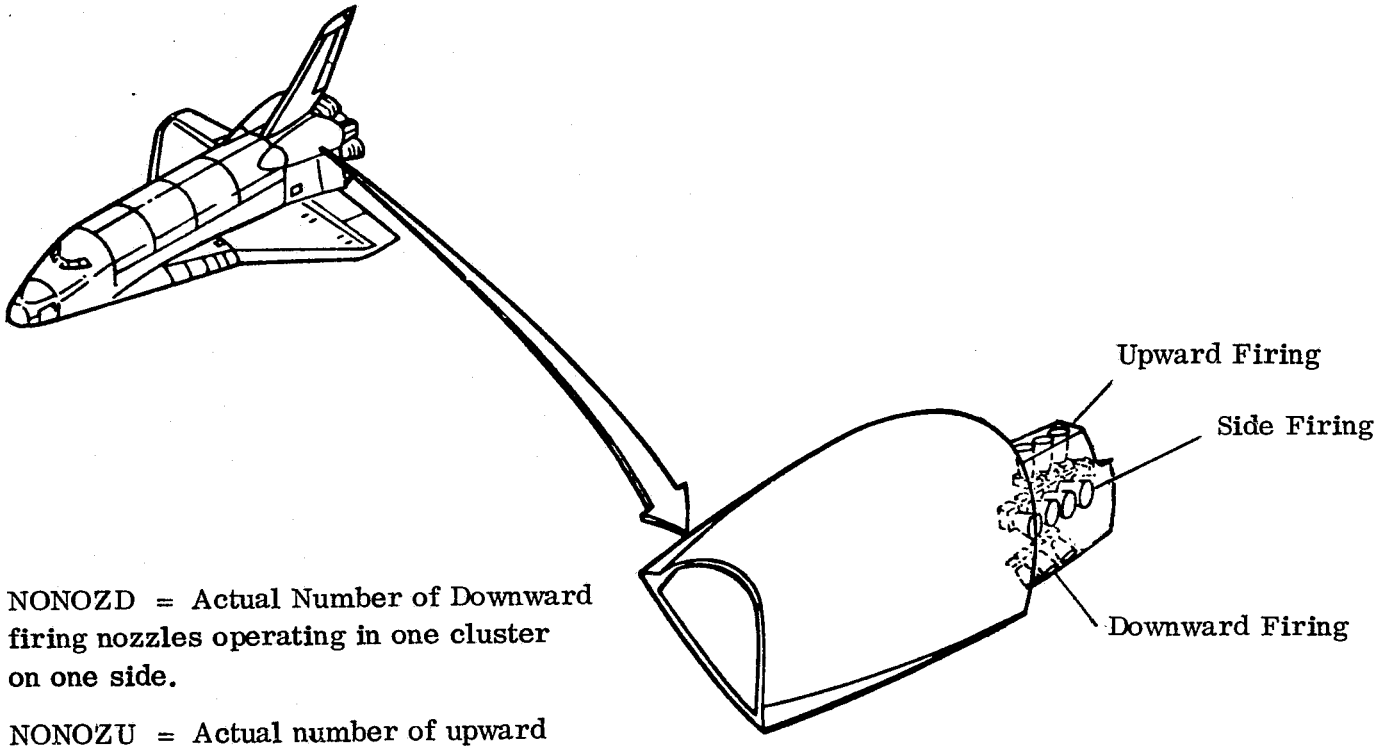

NONOZD = Actual Number of Downward firing nozzles operating in one cluster on one side.

NONOZU = Actual number of upward firing nozzles, etc.

NONOZY = Actual number of side firing nozzles, etc.

Figure 5-3. Nozzle Set Convention

terms of nozzle expansion ratio (A/A*), chamber pressure (Poj), chamber temperature (Toj), and exhaust gas specific heat ratio (γ), the subroutine JET is called to determine the nozzle exit conditions for this engine. The exit conditions are exit Mach number (Mj), static pressure (Pj) and static temperature (Tj).

Exit Mach number is computed by solving the Prandtl Meyer expansion ratio Mach number relationship (Ref. 9).

$$A/A^* = \left(\frac{\gamma_j + 1}{2}\right)^{\frac{\gamma_j + 1}{2(\gamma_j - 1)}} \quad Mj \left(1 + \frac{\gamma_j - 1)}{2} Mj^2\right)^{\frac{\gamma_j + 1}{2(\gamma_j - 1)}}$$

JET solvesthis expression by computing expansion ratio for increasing jet Mach numbers until the correct expansion ratio has been passed saving the last 3 values of each. When the correct expansion ratio is passed, JET calls the subroutine PARCEO to put a quadratic curve fit through the expansion ratio-jet Mach points and PARCEO returns the coefficients of the equation which JET then solves for jet Mach number. With jet exit Mach number determined the jet exit static pressure and temperature are computed from isontropic flow relations. In addition JET computes some constants which are related to specific heat ratio, pressure ratio, and thrust from the flow through the nozzle throat for use in later routines.

PARCEO is a standard quadratic curve jet routine which will give the coefficients for a curve through any 3 sets of points defined in the call statement . The main program defines the throat diameters of the single equivalent nozzles for each cluster of upward (DSTARU) downward, (DSTARD), and side (DSTARY) firing sets before proceeding to the definition of flight conditions

5.4 COMPUTE FLIGHT PARAMETERS (SUBROUTINE ATMOS).

The input subroutine provides data required by the program at this point to define the flight conditions in one of four allowable ways defined by an input parameter (IOPT):

a) IOPT = 1 altitude, Mach, and angle of attack specified

b) IOPT = 2 altitude, velocity, and angle of attack specified

c) IOPT = 3 altitude, freestream dynamic pressure, and angle of attack specified

d) IOPT = 4 Mach, ambient pressure, ambient temperature, and angle of attack specified

The first 3 options require an atmosphere model to define ambient pressure and ambient temperature and the program currently contains a subroutine ATMOS which provides these data from the 1962 US Standard atmosphere model. The fourth option is a means of expressing an arbitrary flight condition from some other atmosphere model or for a wind tunnel test.

Subroutine ATMOS can provide a number of flight parameters not currently used in this program including local gravity for an oblate earth model, atmosphere density, local speed of sound, dynamic pressure, absolute viscosity, kinematic viscosity, and stagnation temperature on a reference sphere. The program consists of curve fits of atmospheric properties from sea level to 230,000 meters (754,600 ft) and all conditions are set to zero above this altitude.

The vacuum case ($P_\infty = q = 0$) is treated in a special way in the program to avoid divisions by zero. A special note will be printed in the output and dynamic pressure (q) is set equal to 1 PSF. The interaction terms are not computed for the vacuum case nor are cross coupling terms which are not related to impingement. The force and moment coefficients printed are based on a q of 1 PSF while the amplification factors are independent of q.

With the flight conditions defined, all the required data is in the program and the RCS effectiveness computed. In order to do this the RCS nozzle parameters must be computed.

5.5 COMPUTE SINGLE NOZZLE PARAMETERS (SUBROUTINES EXPAN, SCAL MACH).

The nozzle parameters necessary to compute the RCS effectiveness include RCS engine thrust coefficient (TCOEF), jet exit momentum ratio (RMFS), and jet mass flow ratio (FMR). These are all computed for a single nozzle and then multiplied by the number of nozzles in each set to obtain the parameters for the three directions of firing.

Plume limit turning angle (TURN) is also required to define the plume decay characteristics as well as the extent of the plume for impingement calculations, it however is not related to the number of nozzles but rather to jet exit and freestream conditions. The limit turning angle is computed in subroutine EXPAN based on Prandtl-Meyer expansion of the flow from RCS chamber conditions to freestream ambient pressure minus the expansion in the nozzle plus the nozzle exit angle.

The Subroutine SCAL computes the nozzle exhaust scaling parameters of Pindzola (reference 10) and Herron (reference 11) for the single nozzle while the Subroutine Mach computes the Mach number of the fully expanded flow for SCAL. The program prints the flight conditions as well as a large number of nozzle parameters for the single RCS unit at this point in the main program winding up with the important nozzle interaction parameters in the three RCS directions.

5.6 COMPUTE THRUST TERMS (SUBROUTINE THR)

The thrust for a single nozzle was computed as the theoretical thrust when the other nozzle parameters were computed and the aerodynamic coefficients of thrust moment for the three RCS directions are now computed using the subroutine THR. The values of all coefficients are first set to zero to remove the data from previous cases prior to the call for THR. Subroutine THR computes the thrust coefficients for the three RCS firing directions and multiplies these by the direction cosines of the thrust vectors to obtain the thrust force coefficients. The program assumes that the nozzle clusters are all on the left side of the vehicle in determining the direction cosines of the thrust vectors and appropriate sign corrections will be made further on in the program. The nozzles are allowed an outboard and an aft cant angle in the computation of direction cosines. These are defined in figure 5-4. The direction cosines are the angles of a unit vector along the centerline of the plume in the body axis system. The thrust moments are then computed about the body reference moment center accounting for cant angles and vertical position.

5.7 COMPUTE IMPINGEMENT INCREMENTS (SUBROUTINES IMPING AND VACPLU)

The program now computes the plume impingement force and moment components from three choices based on an input parameter (IIMP):

a) No impingement

b) Vacuum data from 0A99

c) Predict plume impingement

The first option simply sets the impingement terms to zero and proceeds to the interaction computation. The second choice is a computation still in the main program which uses equations 4 to 22 in section 4 and computes the impingement increments as a function of thrust coefficient.

The third choice causes the program to make its own prediction of plume impingement by computing the pressures on the vehicle from the three direction plumes separately and integrating each pressure distribution to obtain the 6 component impingement increments. No plume/plume interaction is accounted for the three directions of RCS firing. The subroutine IMPING is called three times to integrate the pressures from each direction separately.

IMPING depends on subroutine VACPLU for its definition of plume characteristics at a given point on the vehicle by sending VACPLU the location of the point in a nozzle based ordinate system by in terms of distance from the nozzle exit plane and the angle from the centerline as well as the equivalent nozzle thrust size and the engine operating characteristics. VACPLU then computes the plume local ambient pressure, dynamic pressure, and Mach number from equations 24 to 35 of section

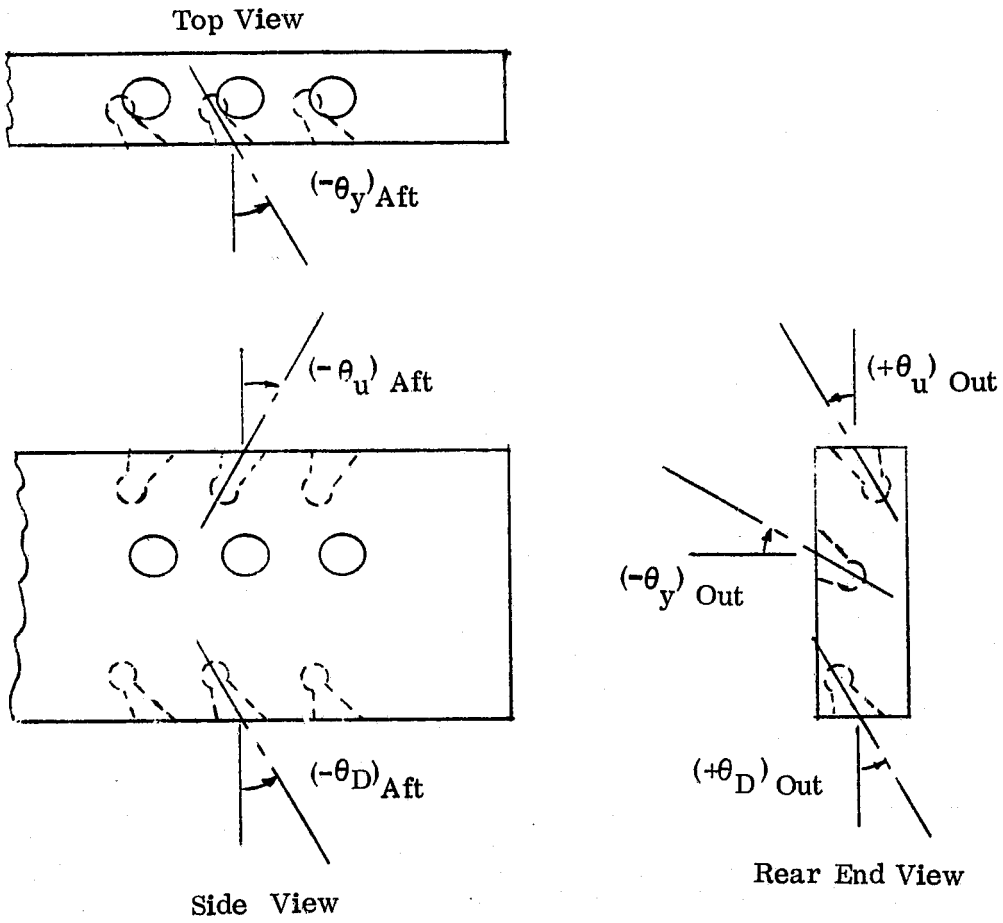

Left Side RCS Pod

Figure 5-4. Nozzle Cant Angles

4.4.1 and by assuming isentropic flow relations. If the angle from the centerline of the plume is greater than the limit turning angle the plume pressures are set to zero.

IMPING selects the correct dimensions for the nozzle set being used, zeros the total coefficients and proceeds to use VACPLU to predict the plume pressures on a set of flat plates representing the left side of the vehicle. The plume local static and dynamic pressures are used to compute the local surface pressure through a modified Newtonian pressure law and the local pressure is converted to a pressure coefficient based on free stream conditions. The pressure coefficient is multiplied by the local area and the direction cosines of the plate to obtain incremental force coefficients. The local force coefficients are used to compute local plate moments about the moment reference center and all of the local values are summed up to obtain total vehicle values.

Since this integration is accomplished by summing up local values for a series of plates, a large number of plates is desirable for good accuracy as well as to minimize the pressure change on a plate. This is one of the principal reasons for confining all predictions to one side of the plane of symmetry of the vehicle . The program presently allows a total of 300 plates to represent the vehicle. Figures 4-5 to 4-7 show the spacing of one series of approximately 280 plates representing the left side of the orbiter. Each plate is defined by 7 variables which are the location of the plate centroid from the moment reference center (X, Y, Z), the local area (SLOC), and the direction cosines of the outer unit normal vector from the plate with respect to the body axis system as is shown in Figure 5-5. The direction cosines define the local slope of the plate which combined with the angle of the plate to the nozzle determines the local slope of the surface to the flow and from equation 36 of section 4 the pressure at that point from the Newtonian pressure law.

The program assumes that the plume cannot extend beyond the point where its dynamic pressure is less than that of the free stream or where the plume induced pressure is less than ambient free stream pressure.

5.8 COMPUTE INTERACTION INCREMENTS (SUBROUTINES INTER, QUART, QUAD, KABD, ADABD).

As in the earlier terms, the program zeros the increments from a previous case and then calls the interaction subroutine INTER to compute the interaction increments for each RCS direction. The curve fit equations defined in section 3 (equations 5 through 41) are the basis of this model. The subroutine INTER contains all of the coefficients of these curves as subscripted variables defined in data statements and a namelist input option is available in the input subroutine to input changes to any or all equations. This was done to add flexibility to the program. There are three types of curves fitted to the data, a 4th power Polynominal, a 2nd power polynominal, and a hyperbolic curve. The subroutine QUART is called to evaluate the fourth

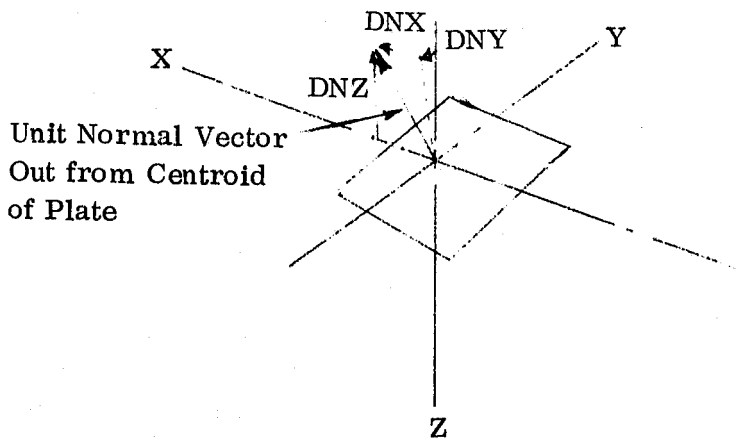

Figure 5-5. Direction Cosines of Plate on Vehicle Surface

power polynominal and the subroutine QUAD is called to evaluate the second power polynominal. These curves are fit through the interaction increments and are functions either of mass flow ratio or momentum ratio depending on the increment and RCS direction. The fourth coefficient and the sixth coefficients of the quadratic and quartic equations are upper limits beyond which a constant value of incremental force or moment is assumed. These constant values are specified as the last coefficients of a given curve fit name.

The hyperbolic curve fit is used for the pitch up RCS peak value versus angle of attack curves (section 3 equations 26 to 30) and these equations are solved by the KABD subroutine. In addition it is necessary to solve the inverse of the peak value curves and this is done by the AKABD routine.

The OA82 windtunnel data was computed in a normal force body axis system so that the sign of the normal force increment must be reversed for all RCS directions. The upward firing pitch nozzle data was generated on the right side of the vehicle in test OA82 and the lateral-directional increments must be reversed to the left side convention used in this program.

5.9 CORRECT FOR SYMMETRIC FIRING AND/OR RIGHT SIDE LOCATION.

The program has the thrust terms, the impingement increments, and the interaction increments for all nozzle sets based on one set of each on the left side of the vehicle and at this point in the main program these data are corrected to represent the actual nozzle locations. This is done by two input parameters. IBOTHA and ISIDEA for each nozzle firing direction (A = U, D, Y), with values of 0 or 1. IBOTHA is the higher order parameter of the two and if it has a value of 1 then the set firing in this direction has a symmetric set on the right side of the vehicle also. This being the case the lateral/directional turns are set to zero and the longitudinal turns are doubled. For example IBOTHU = 1 results in

CLU = 0
CNU = 0
CYU = 0
CLIMU = 0
CNIMU = 0
CYIMU = 0
CLINU = 0
CNINU = 0
CYINU = 0
CMU = 2. CMU
CXU = 2. CXU
CZU = 2. CZU

CMIMU = 2. CMIMU
CXIMU = 2. CXIMU
CZIMU = 2. CZIMU
CMINU = 2. CMINU
CXINU = 2. CXINU
CZINU = 2. CZINU

If IBOTHA is set to 1, ISIDEA is ignored, but, if IBOTHA is set to zero, then this is a non-symmetric set of nozzles and ISIDEA has meaning. If ISIDEA is set as zero then this set up of nozzles is on the left side of the vehicle and no sign changes are required. If ISIDEA is equal to 1 then this set of nozzles is on the right side of the vehicle and the signs of the lateral directional components must be reversed.

5.10 COMPUTE CROSS COUPLING INCREMENTS (SUBROUTINE CCOUPL)

The final incremental terms needed to complete the RCS effectiveness prediction are the cross coupling terms which are computed in the subroutine CCOUPL. This subroutine has only limited models because data is not available of all possible interactions between RCS units but the model is based on the models derived in section 3.5 and given in equations 42 to 54 of that section.

5.11 SUM COMPONENTS AND COMPUTE AMPLIFICATION FACTORS (SUBROUTINE AMPL)

The total RCS aerodynamic coefficients are computed as the sum of the increments from all sets of nozzles and printed out by the main program. Since it is also desirable to relate these total coefficients to RCS thrust the amplification factors as defined by equations 2 and 3 of section 4.1 are computed in the Subroutine AMPL.

Subroutine AMPL begins by computing the thrust moments for a two nozzle symmetric pitch up set, a two nozzle symmetric pitch down set, a two nozzle yaw set, and a two nozzle (one on each side) roll set by calling subroutine THR. These two nozzle thrust moments are the thrust terms which are used to compute the out of plane a amplification factors. For this reason the nozzle coordinates for all directions must be specified even if no nozzles are being used in that direction. The program will terminate if a set of nozzle specifications is missing and amplification factors will not be computed. The subroutine then proceeds to determine which types of control are being used of the twelve possible combinations:

a) symmetric pitch up
b) symmetric pitch down
c) yaw
d) pure roll
e) pitch up + Yaw

f) pitch down + yaw
g) pitch up + roll
h) pitch down + roll
i) yaw + roll
j) pitch up + yaw + roll
k) pitch down + yaw + roll
l) symmetric yaw

and a decision is reached whether to use the actual thrust moment or the two jet thrust moment to compute amplification factor. For example a yaw only case uses actual thrust side force and yawing moment to compute side force amplification and yawing moment amplification. This case, however, uses 2 jet pitch down to compute normal force and pitching moment amplification and 2 jet roll to compute roll amplification. A set of comments is printed to help clarify the definition of thrust moments used. The thrust moments used to compute amplification are also printed out and can be compared to the actual thrust moment table printed out previously.

Axial force amplification is not computed because there are no interaction or cross coupling models of these effects.

The computations are now completed and the program returns to the place specified by input parameter INEXT either for another case or to terminate the program.

5.12 PROGRAM INPUT (SUBROUTINE INPUTT)

The preceding sections have given a summary of the program operation and given a brief outline of the data required for the program to execute. This data is loaded into the program through a subroutine called INPUTT which will be briefly described in this section while a detailed description of the input data will be given in the next section.

The input subroutine is called at three different places in the main program and provides different data at each point based on a parameter INEXT. Four types of data are required for a full loading of the program:

a) vehicle surface plates
b) analytic model coefficients (namelist INCOF)
c) nozzle definitions (namelist IN)
d) flight conditions (namelist FC)

When the program is first loaded or if INEXT = 1 all of the input is required. When INEXT = 2, nozzle defintions and flight conditions changes must be input, and if INEXT = 3 only flight condition changes can be made.

The vehicle flat plate data is input using formatted read statements while the remaining data is entered through namelist. The use of namelist was made to minimize the input required for multiple cases. No input for a given variable in a namelist leaves that variable at its present value. No input should be provided for the analytic model coefficients unless changes are desired since the basic model developed in this report is already specified in data declarations in the subroutines where they are used.

Provisions have been made in INPUTT to rescale the flat plate vehicle surface data if for example model computations are to be made. The input routine also computes the direction cosines of the RCS nozzles including nozzle cant angles.

5.13 INPUT DATA DEFINITIONS

A new problem starts with first loading the vehicle flat plate surface data as formated data at a maximum of 8 words per card with an F10.3 format.

Card	Column	Variable	Description
1	1-10	SCALE	Scale factor for flat plate surface data SCALE = 1. if SCALE = 0 card must be input
2 to N-1	flat plate surface cards one plate per card up to 300 allowed at least one must be input		
	1-10	DNX(I)	X direction cosine of flat plate I. plates are counted as input is used. See figure 5-5 for definition of direction cosine.
	11-20	DNY(I)	Y direction cosine of flat plate I
	21-30	DNZ(I)	Z direction cosine of flat plate I
	31-40	X(I)	X distance of centroid of plate I from reference center. See figure 5-2 for definition of axis system. Units are feet
	41-50	Y(I)	Y distance of centroid of plate I from moment reference center. Units are feet
	51-60	Z(I)	Z distance of centroid of plate I from moment moment reference center. Units are feet
	61-70	SLOC(I)	area of plate I in square feet
N	1-10	2.0	Last card of flat plate input is signified by DNX(N) being greater than 1.1. This ends flat plate input.

The remaining input is by namelist rather than formated read and so no card can be specified . A namelist specification is made by a $ in column 2 of the first card of the list followed by the namelist name. Each variable name to be loaded must appear followed by an equal sign and the value of the input with commas separately variable specifications. The list can extend over a number of cards and is closed by a $. The order of names within a list is not important and names can be repeated if newer data becomes available. There are three namelists within INPUTT having the names INCOF, IN, and FC and they load in that order on a new job.

Namelist	Variable	Description
INCOF		Unless changes to the analytic model are to be made, do not input any data in INCOF and one card $ INCOF $ is sufficient.
INCOF	*Quatratic curve fit coefficient arrays for downward firing jets (5 coefficients) $Y = C(1) + C(2)\,x + C(3)\,x^2$	
	C (4) = limit x	
	C (5) = y value above limit x	
INCOF	CZIDL	Normal force coefficient as a function of momentum ratio at low angles of attack (below ALPHBK)
INCOF	CMIDL	Pitching moment coefficient as a function of momentum ratio at low angles of attack (below ALPHBK)
INCOF	CLIDL	Rolling moment coefficient as a function of momentum ratio at low angles of attack (below ALPHBK)
INCOF	CZIDH	Normal force coefficient as a function of momentum ratio at high angles of attack (above ALPHBK)
INCOF	CMIDH	Pitching moment coefficient as a function of momentum ratio at high angles of attack (Above ALPHBK)
INCOF	CLIDH	Rolling moment coefficient as a function of momentum ratio at high angles of attack (Above ALPHBK)
INCOF	*Quadratic curve fits coefficient arrays for upward firing jets	
INCOF	CZIUP	Peak normal force coefficient as a function of mass flow ratio at low angles of attack (Below ALPHBK)

Namelist	Variable	Description
INCOF	CYIUP	Peak side force coefficient as a function of momentum ratio at low angles of attack (Below ALPHBK)
INCOF	CMIUP	Peak pitching moment coefficient as a function of mass flow ratio at low angles of attack (Below ALPHBK)
INCOF	CNIUP	Peak yawing moment coefficient as a function of momentum ratio at low angles of attack (Below ALPHBK)
INCOF	CLIUP	Peak rolling moment coefficient as a function of momentum
INCOF	CZIUH	Normal force coefficient as a function of mass flow ratio at high angles of attack (Above ALPHBK)
INCOF	CYIUH	Side force coefficient as a function of momentum ratio at high angles of attack (Above ALPHBK)
INCOF	CMIUH	Pitching moment coefficient as a function of mass flow ratio at high angles of attack (Above ALPHBK)
INCOF	CNIUH	Yawing moment coefficient as a function of momentum ratio at high angles of attack (Above ALPHBK)
INCOF	CLIUH	Rolling moment coefficient as a function of momentum ratio at high angles of attack (Above ALPHBK)
INCOF	* Quadratic curve fit coefficient arrays for side firing jets	
INCOF	CZIYL	Normal force coefficient as a function of mass flow ratio at low angles of attack (Below ALPHBK)
INCOF	CMIYL	Pitching moment coefficient as a function of mass flow ratio at low angles of attack (Below ALPHBK)
INCOF	CLTYL	Rolling moment coefficient as a function of mass flow ratio at low angles of attack (Below ALPHBK)
INCOF	CZIYH	Normal force coefficient as a function of mass flow ratio at high angles of attack (Above ALPHBK)
INCOF	CMIYH	Pitching moment coefficient as a function of mass flow ratio at high angles of attack (Above ALPHBK)
INCOF	CLIYH	Rolling moment coefficient as a function of mass flow ratio at high angles of attack (Above ALPHBK)

Namelist	Variable	Description

INCOF * Quartic curve fit coefficient arrays for downward firing jets (7 coefficients)

$$Y = C(1) + C(2)\,X + C(3)\,X^2 + C(4)\,X^3 + C(5)\,x^4$$

C(6) = limit X

C(7) = Y value above limit X

INCOF	CYTDL	Side force coefficient as a function of momentum ratio at low angles of attack (Below ALPHBK)
INCOF	CNTDL	Yawing moment coefficient as a function of momentum ratio at low angles of attack (Below ALPHBK)
INCOF	CYIDH	Side force coefficient as a function of momentum ratio at high angles of attack (Above ALPHBK)
INCOF	CNIDH	Yawing moment coefficient as a function of momentum ratio at high angles of attack (Above ALPHBK)

INCOF * Quartic curve fit coefficient arrays for sideway firing jets

INCOF	CYIYL	Side force coefficient as a function of mass flow ratio at low angles of attack (Below ALPHBK)
INCOF	CNIYL	Yawing moment coefficient as a function of mass flow ratio at low angles of attack (Below ALPHBK)
INCOF	CYIYH	Side force coefficient as a function of mass flow ratio at high angles of attack (Above ALPHBK)
INCOF	CNIYH	Yawing moment coefficient as a function of mass flow ratio at high angles of attack (Above ALPHBK)

INCOF *KABD curve fit coefficient arrays for upward firing jets (6 coefficients)

$$Y = \frac{C(1)}{X - C(2)} + C(3) + C(4)\,X$$

C(5) - is the factor defining the proper root when computing the inverse solution of the hyperbolic curve fit (call to subroutine AKABD)

INCOF	CZAUP	Peak normal force coefficient as a function of angle of attack at low angles of attack (Below ALPHBK)
INCOF	CYAUP	Peak side force coefficient as a function of angle of attack at low angles of attack (Below ALPHBK)

Namelist	Variable	Description
INCOF	CMAUP	Peak pitching moment coefficient as a function of angle of attack at low angles of attack (Below ALPHBK)
INCOF	CNAUP	Peak yawing moment coefficient as a function of angle of attack at low angles of attack (Below ALPHBK)
INCOF	CLAUP	Peak rolling moment coefficient as a function of angle of attack at low angles of attack (Below ALPHBK)

The namelist IN defines the RCS engine, the locations of the sets and the geometry of the firing arrangement

Namelist	Variable	Description
IN	* There are no default values built in for the variables and all input must be included in the first case of a run.	
IN	* RCS Engine Characteristics	
IN	XMJ	Jet Mach number (not required, internally calculated)
IN	GJ	Specific heat of jet
IN	ARJ	Expansion ratio of jet, exit area-to-throat area
IN	AJE	Jet exit area (sq. ft.)
IN	POJ	Chamber pressure of jet (PSIA)
IN	RJ	Jet gas constant (R Air = 53.35)
IN	TOJ	Jet chamber temperature (Deg F)
IN	DEXIT	Jet exit diameter (Ft)
IN	THETA	Nozzle exit angle (angle of bell mouth nozzle wall) (Deg)
IN	*	Reference dimensions
IN	SREF	Reference area (Sq. Ft.) = wing area
IN	C	Mean aerodynamic chord (reference length) (ft)
IN	B	Wing span (reference length) (ft)
IN	*	Nozzle locations (all sets must be input and left side locations specified)

Namelist	Variable	Description
IN	XREU	X coordinate of upward firing nozzles exit plane reference center (ft)
IN	YREU	Y coordinate of upward firing nozzle exit from moment reference center (ft) (always negative)
IN	ZREU	Z coordinate of upward firing nozzle exit from moment reference center (ft)
IN	XRED, YRED, ZRED	Coordinates of downward firing jets from the moment reference center
IN	XREY, YREY, ZREY	Coordinates of sideway firing jets from the MRC (Ft)
IN	*	Input values of location even if the number of nozzles is zero, so that amplification factors can be calculated
IN	*	Nozzle angles see figure 5-4 for positive directions
IN	THAFTU	Aft cant angle of upward firing nozzle (Deg)
IN	THAFTD	Aft cant angle of downward firing nozzle (Deg)
IN	THAFTY	Aft cant angle of sideway firing nozzle (Deg)
IN	THOUTU	Outboard cant angle of upward firing nozzle (Deg)
IN	THOUTD	Outboard cant angle of downward firing nozzle (Deg)
IN	THOUTY	Upward cant angle of sideway firing nozzle (Deg)
IN	*	Input values of angles even if the number of nozzles is zero, so that amplification factors can be calculated
IN	*	Nozzle set definitions
IN	NONOZU	Number of upward firing nozzles (causing pitch up) operating in a set
IN	NONOZD	Number of downward firing nozzles (causing pitch down) operating in a set
IN	NONOZY	Number of sideway firing nozzles (causing yaw) operating in a set
IN	IBOTHU	Defines whether upward firing nozzles are operating on one or both sides of the center of gravity, = 0, Nozzles operating on one side only (set ISIDEU), = 1, Nozzles operating on both sides

Namelist	Variable	Description
IN	IBOTHD	Defines whether downward firing nozzles are operating on one or both sides of the center of gravity, = 0, Nozzles operating on one side only (set ISIDED), = 1, Nozzles operating on both sides
IN	IBOTHY	Defines whether sideway firing nozzles are operating on one or both sides of the center of gravity, = 0, Nozzles operating on one side only (set ISIDEY), = 1, Nozzles operating on both sides
IN	ISIDEU	Defines side on which upward firing nozzles are operating, = 0, Operating nozzles are on the left, = 1, Operating nozzles are on the right,
IN	ISIDED	Defines side on which downward firing nozzles are operating, = 0, Operating nozzles are on the left, = 1, Operating nozzles are on the right,
IN	ISIDEY	Defines side on which sideway firing nozzles are operating = 0, Operating nozzles are on the left, = 1, Operating nozzles are on the right,
IN	*	Impingement Selector
IN	IIMP	Defines the type of mathematical model to be used, = 1, Use the empircal impingement model, = 2, No impingement model used, = 3, Use the semi-empirical impingement model (Modified Newtonian pressures plus vacuum plume model) IIMP = 3 is the default value

The final namelist in is called FC and contains the flight conditions as well as a indicator which determines the input options on multiple cases.

Namelist	Variable	Description
FC	IOPT	Defines the flight conditions to be read = 1, Mach number, angle of attack (Deg) and altitude (Ft) must be input, all others are not used = 2, Velocity (FPS), altitude (Ft), and angle of attack (Deg) must be input = 3, Dynamic pressure (PSF), altitude (Ft), and angle of attack (Deg) must be input = 4, Ambient pressure (PSF), temperature (Deg F), Mach number and angle of attack (Deg) must be input. This is default value.
FC	MINF	Free stream Mach number
FC	PINF	Free stream ambient pressure (PSIA)
FC	TINF	Free stream ambient temperature (Deg F)
FC	QI	Free stream dynamic pressure (PSF)
FC	ALPH	Angle of Attack (Deg)
FC	HI	Altitude (Ft)
FC	VINF	Velocity (FPS)
FC	INEXT	Defines content of next set of data = 1, All data are to be read = 2, Nozzle definitions and flight conditions (namelists IN AND FC) must be read = 3, Flight conditions only (namelist FC) are to be read = 4, No more data will be read in, program stops

5.14 OUTPUT DATA DEFINITIONS

The data printed out from a sample run is shown in figure 5-6. Not shown in this figure is the listings of input which occur because of the use of the namelist input option and the names are defined in the preceding section. The output starts with a definition of the characteristics of a single RCS nozzle in lines 1 to 3.

Output Line	Word	Description
1	Nozzle Characteristics	single RCS nozzle data
2	EXIT DIA	RCS nozzle exit diameter in feet (input as DEXIT)
2	EXPANSION RATIO	RCS nozzle exit to throat area ratio (input as ARJ)
2	EXIT ANGLE	RCS nozzle exit lip angle in degrees (input as THETA)
2	NOZZLE MACH	Computed nozzle exit Mach number
3	THRUST	Computed RCS nozzle thrust in pounds
3	CHAMBER PRESSURE	RCS chamber pressure in PSIA (input as POJ)
3	EXIT PRESS	Computed static pressure at nozzle exit plane in PSIA
3	EXHAUST GAMMA	Specific heat ratio of nozzle gases (input as GJ)

The freestream flight conditions are briefly described in lines 4 and 5

4	FREESTREAM CONDITIONS	
5	P/INFINITY	Ambient pressure at flight condition either input or defined by standard atmosphere in PSIA (limited printout resolution)
5	MACH INF	freestream Mach number

XXXXXXXXXXXXXXXXXXXXXXXXXXXXXXXXXXXXXXXXXXXXXXXXXXXXXXX

XXXXXXXXXXXXXXXXXXXXXXXXXXXXXXXXXXXXXXXXXXXXXXXXXXXXXXX

(1) NOZZLE CHARACTERISTICS

(2) EXIT DIA .8000 EXPANSION RATIO 20.0000 EXIT ANGLE 9.0000 NOZZLE MACH 3.8951

(3) THRUST 925.1668 CHAMBER PRESS 150.0000 EXIT PRESS .6836 EXHAUST GAMMA 1.2320

XXXXXXXXXXXXXXXXXXXXXXXXXXXXXXXXXXXXXXXXXXXXXXXXXXXXXXX

(4) FREE STREAM CONDITIONS

(5) P INFINITY .00100 MACH INF 22.0000 GAMMA 1.4000ANGLE OF ATTACK 32.0500

(6) PRESSURE RATIO 685.1438 MOMENTUM RATIO .0035 THRUST COEFF .0071

(7) RT RATIO 6.38154 POJ/PINF 150345.79533FREE STREAM DYNAMIC PRESS 48.67493

(8) (R*TOJ)/(R*TINF) 19.26848

XXXXXXXXXXXXXXXXXXXXXXXXXXXXXXXXXXXXXXXXXXXXXXXXXXXXXXX

(9) THRUST TERMS	Ⓐ CL	Ⓑ CM	Ⓒ CN	Ⓓ CX	Ⓔ CY	Ⓕ CZ
(10) PITCH UP	-0.000000	0.000000	-0.000000	0.000000	-0.000000	0.000000
(11) PITCH DOWN	0.000000	-.025869	0.000000	.005536	0.000000	-.026044
(12) YAW	0.000000	0.000000	0.000000	0.000000	0.000000	0.000000

Figure 5-6. Sample Output

XXXXXXXXXXXXXXXXXXXXXXXXXXXXXXXXXXXXXXXXXXXXXXXXXXXXXXXX

(13) IMPINGEMENT FORCES	Ⓐ CL	Ⓑ CM	Ⓒ CN	Ⓓ CX	Ⓔ CY	Ⓕ CZ
(14) PITCH UP	-0.000000	0.000000	-0.000000	0.000000	-0.000000	0.000000
(15) PITCH DOWN	0.000000	0.000000	0.000000	0.000000	0.000000	0.000000
(16) YAW	0.000000	0.000000	0.000000	0.000000	0.000000	0.000000

XXXXXXXXXXXXXXXXXXXXXXXXXXXXXXXXXXXXXXXXXXXXXXXXXXXXXXXX

(17) INTERACTION TERMS	CL	CM	CN	CX	CY	CZ
(18) PITCH UP	0.000000	0.000000	0.000000	0.000000	0.000000	-0.000000
(19) PITCH DOWN	0.000000	.015812	0.000000	0.000000	0.000000	.015401
(20) YAW	0.000000	0.000000	0.000000	0.000000	0.000000	-0.000000

XXXXXXXXXXXXXXXXXXXXXXXXXXXXXXXXXXXXXXXXXXXXXXXXXXXXXXXX

(21) CROSS COUPLING TERMS	CL	CM	CN	CX	CY	CZ
(22) PITCH UP	0.000000	0.000000	0.000000	0.000000	0.000000	0.000000
(23) PITCH DOWN	0.000000	.002501	0.000000	0.000000	0.000000	.002191
(24) YAW	0.000000	0.000000	0.000000	0.000000	0.000000	0.000000

XXXXXXXXXXXXXXXXXXXXXXXXXXXXXXXXXXXXXXXXXXXXXXXXXXXXXXXX

(25) TOTAL VALUES	CL	CM	CN	CX	CY	CZ
(26)	0.000000	-.007555	0.000000	.005536	0.000000	-.008462

Figure 5-6. Cont'd

```
XXXXXXXXXXXXXXXXXXXXXXXXXXXXXXXXXXXXXXXXXXXXXXXXXXXXXXX
(27)THRUST MOMENTS USED FOR AMPLIFICATION FACTORS ARE DEP ENDENT ON CONTROL USED
(28)UNLESS OTHERWISE NOTED AMPLIFICATION IS BASED ON 2 ASSUMED NOZZLES IN EACH CONTROL
(29)PITCH AMP BASED ON PITCH DOWN JETS
(30)CZTH =      -.0260444CYTH =      .0141316CLTH =      .0019355CMTH  =      -.0258689CNTH =      -.0069215
(31) AMPLIFICATION FACTORS
(32)                    KL           KM           KN           KX           KY           KZ
(33) AMPLIFICATION       0.0000000    .2920568     0.0000000    0.0000000    0.0000000    .3249256
XXXXXXXXXXXXXXXXXXXXXXXXXXXXXXXXXXXXXXXXXXXXXXXXXXXXXXX
```

Figure 5-6. Cont'd

Output Line	Word	Description
5	GAMMA	freestream specific heat ratio
5	ANGLE OF ATTACK	Input angle of attack (ALPH) in degrees
Same single RCS nozzle scaling conditions are defined in lines 6 to 8.		
6	PRESSURE RATIO	Single RCS nozzle jet exit pressure ratioed to freestream pressure (P_j/P_∞
6	MOMENTUM RATIO	Single RCS Nozzle momentum ratio (equation 5) ratioed using wing area as reference. (Φ_j/Φ_∞)
6	THRUST COEFF	Single RCS nozzle thrust ratioed by dynamic pressure and wing area = T/qS
7	RT RATIO	($R_J T_J/R_\infty T_\infty$); RCS ambient temperature at exit ratioed to freestream
7	POJ/PINF	RCS chamber pressure (P_{oj}) ratioed to freestream ambient pressure (P_∞)
7	FREESTREAM DYNAMIC PRESSURE	$q_\infty = 0.7\ P_\infty\ M_\infty^2$ in PSF
8	(R*TOJ)/(R*TINF)	($R_J T_{OJ}$)/($R_\infty T_\infty$); RCS chamber temperature ratioed to freestream ambient temperature - Thayer's parameter

The program now begins a printout of all terms which are combined into total control moments and amplification. This printout is in a systematic form in which any pitch up nozzle contributions are listed first (lines 10, 14, 18, and 22); then pitch down nozzles) lines 11, 15, 19 and 23) and finally yaw nozzle contributions (lines 12, 16, 20, and 24). The data is all presented in aerodynamic coefficient form so that the force terms are non dimensionalized by dividing by dynamic pressure and wing area and additionally the moement terms by the appropriate reference length. Column A presents rolling moment (C_L), column B presents pitching moment (C_M), Column C presents yawing moment (C_N), Column D presents body axis axial force (C_X), Column E presents side force (C_Y), and Column F presents vertical force (C_Z) where figure 5-2 defines the sign convention of the force and moment coefficients.

The thrust terms are computed first and are presented first in lines 9 through 12. These thrust terms have all nozzle cant angles included in their computation. The plume impingement terms are presented in lines 13 through 16. If the input option is selected to ignore impingement a comment will be printed between lines 8 and 9. The Interaction iterms are presented in lines 17 to 20 and the cross coupling terms in lines 21 to 24. The summation of all components (equation 1 of section 4) listed in lines 9 to 24 are then obtained and printed in lines 25 and 26.

The amplification factors are then computed as described in section 4.1 and lines 27 and 28 are always printed. If data does not exist to define all nozzle locations the program will terminate at this point with a note defining this problem because the amplification factors cannot be computed without the all nozzle locations. When all nozzle locations have been defined the program goes through some logic to determine the control moments to be used to define amplication factors (see Section 4.1) and the control forces and moments used are defined in line 30. Line 29 is printed to show that the pitch down jet thrust itself is being used to compute pitch amplification Similar statements are printed if actual thrusts are used for pitch up, yaw and roll cases. Line 30 prints the actual thrust force and moment numbers used to compute the amplifications.

CZTH = control thrust vertical force coefficient

CYTH = control thrust side force coefficient

CLTH = control thrust roll moment coefficient

CMTH = control thrust pitch moment coefficient

CNTH = control thrust yaw moment coefficient

The amplification factors then are the total data from line 26 divided by the thrust terms defined in line 30. Note that where possible the actual thrust terms of lines 9 to 12 are used and only if no thrust term exists is the 2 jet assumed value used.

6

REPRESENTATIVE FLIGHT PREDICTIONS

6.1 GENERAL

The space shuttle orbiter rear RCS packages shown in Figure 1-1 have three engines for firing upward, three for firing downward, and four engines for yaw thrust on each side of the vehicle and considering that the number of RCS engines firing can be varied in addition to at least twelve combinations of combined control, the total number of predictions required becomes a very large task. The purpose of this section is rather to apply the analytic prediction method developed in this study to representative cases to illustrate the results obtained from the method. Reference 1 showed that the symmetric pitch down RCS thrust case and a pure roll thrust case were the most critical so they were chosen as representative cases. Two nozzles were assumed to be firing on each side of the vehicle in each of these cases.

6.2 ENTRY TRAJECTORY RESULTS

A representative set of flight conditions along a space shuttle orbiter entry trajectory were obtained and the flight conditions along a segment of it are shown in figure 6-1. The vehicle starts re-entry at a high angle of attack and maintains this attitude until a low Mach number transition is made. The segment shown here is at the start of reentry and the high angle of attack is maintained throughout it. The rear RCS control system starts as primary control in all axes at zero dynamic pressure and maintains control functions until dynamic pressure is high enough for the aerodynamic control surfaces to be used. Figure 1-2 shows a representative control schedule for this transfer. The area of highest interest in RCS effectiveness is the region from zero dynamic pressure to a q of 20 PSF. The single nozzle flow scaling parameters are shown in Figure 6-1 also. Predicted Control amplification factors during entry for pitch down control is shown in figures 6-2 to 6-3 while roll amplification is shown in figure 6-4. Figure 6-2 shows that the adverse effect of interaction grows with increasing dynamic pressure and causes a decreasing control amplification even if no impingement would be experienced. Figure 6-2 shows that the impingement term also causes a reduction in control amplification at the lower dynamic pressures and the total control moment at low q is very sensitive to the impingement model used. The analytic model developed in this report gives a minimum value of control amplification of about 0.21 at dynamic pressures from 2 to 4 PSF. At this low effectiveness, the question arises of how the inaccuracy in wind tunnel data will affect it. Figure 2-3 presented the error in amplification factor resulting from the wind tunnel error analysis plotted as a function of thrust coefficient. This data was applied to the pitch down and roll flight data by computing flight thrust coefficients and Figures 6-3 and 6-4 present the error envelopes on the flight predictions. Thrust coefficient increases with decreasing

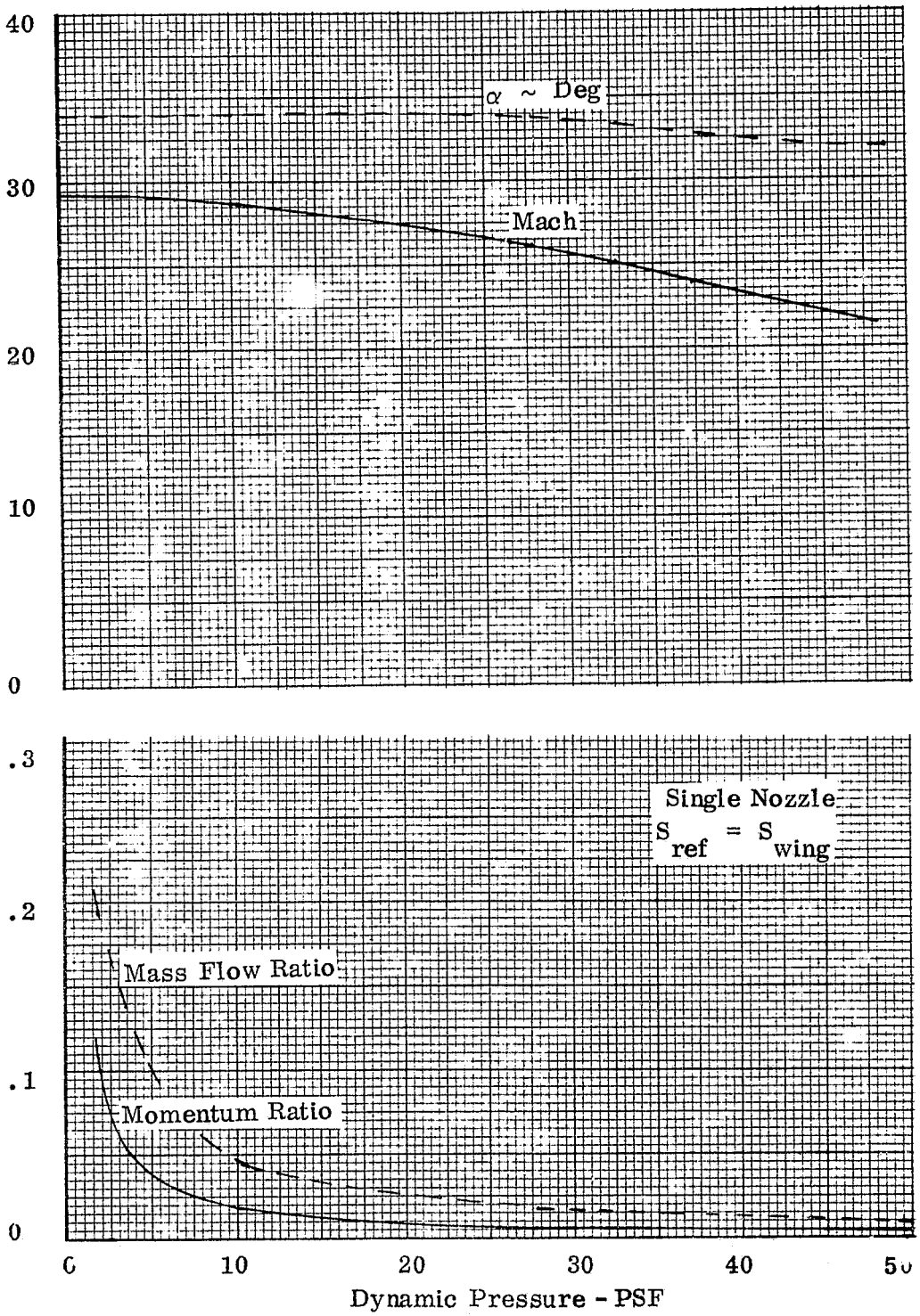

Figure 6-1. Entry Trajectory Conditions

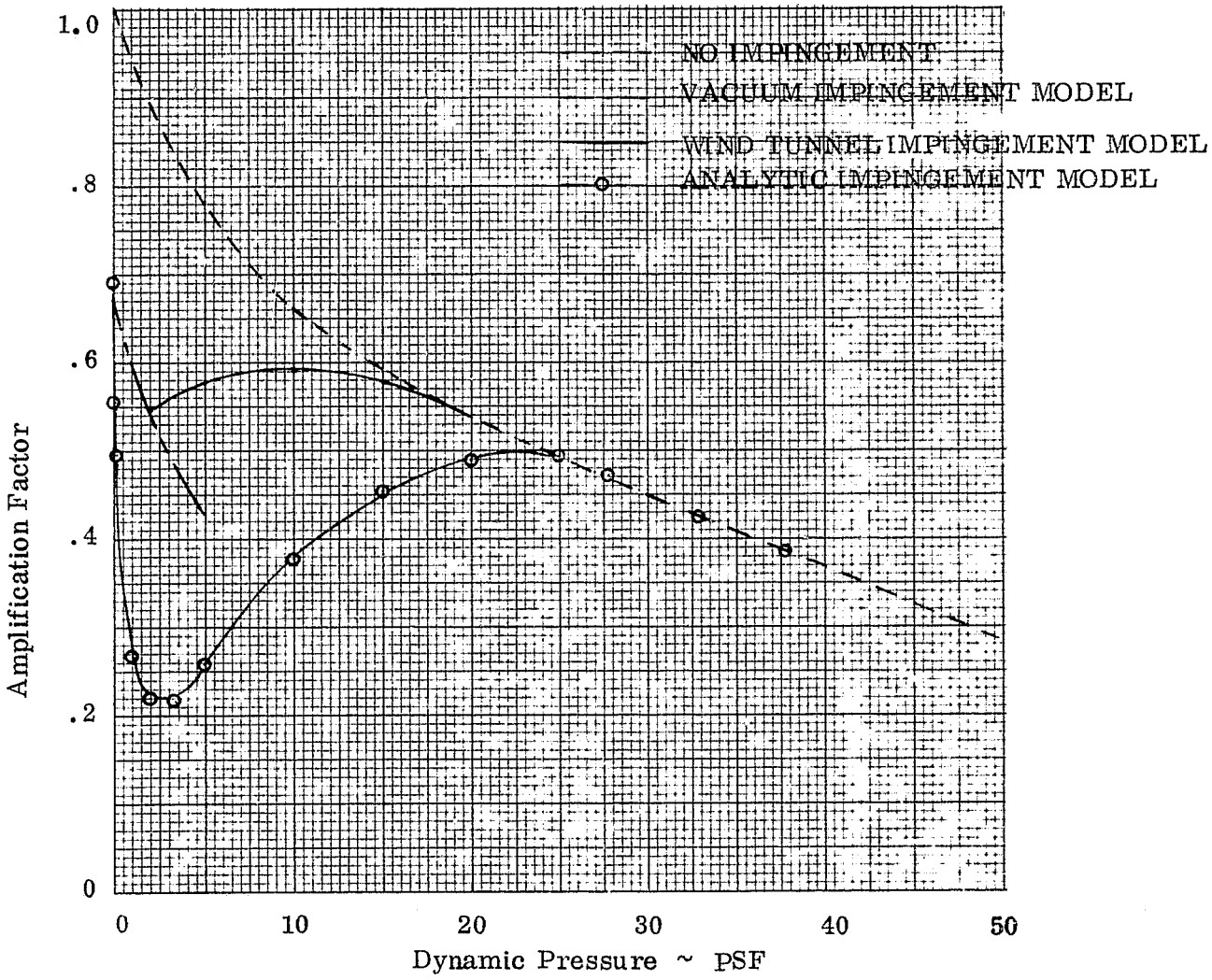

Figure 6-2. Pitch Down Control Amplification During Entry

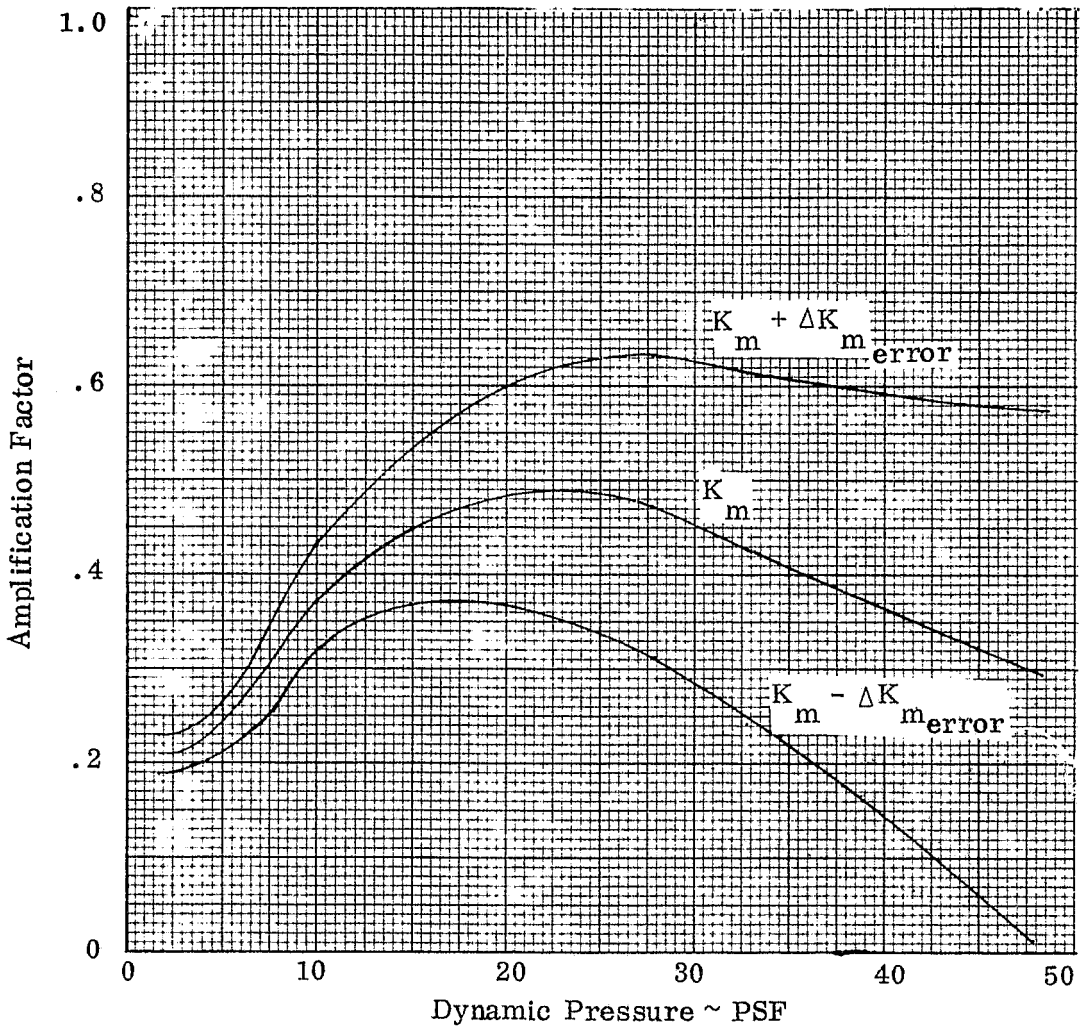

Figure 6-3. Effect of Wind Tunnel Error on Pitch Amplification During Entry

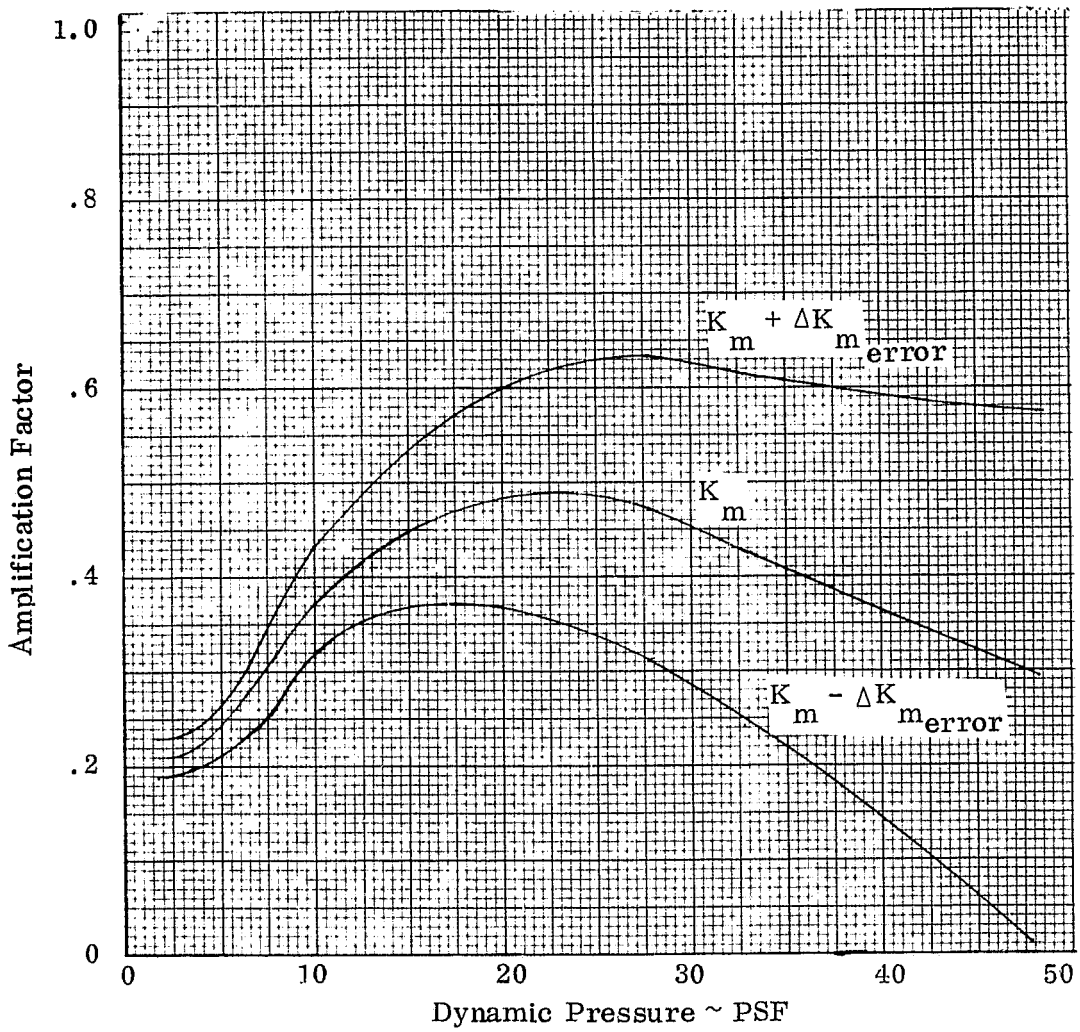

Figure 6-4. Effect of Wind Tunnel Error on Pitch Amplification During Entry

dynamic pressure so that the wind tunnel errors are only a small part of the total amplification factor in the flight range below 20 PSF dynamic pressure.

6.3 RTLS Abort Trajectory Results

Under certain abort conditions during the Space Shuttle launch, a maneuver is performed in which the orbiter jettisons the external tank and returns to the Launch site (RTLS). One critical maneuver during this abort is to jettison the tank and assume reentry attitude. The vehicle is pitched to zero angle of attack and maintains this angle until the tank separates and a pitch maneuver is started to reentry angle. Figure 6-5 present some of the flight conditions which occur during this maneuver. The vehicle starts the maneuver at the highest dynamic pressure and pitches to entry attitude at the end of the maneuver. This maneuver occurs at much lower altitude than the same dynamic pressure range during entry shown in Figure 6-1 and the Mach numbers and angles of attack are much lower.

The lower altitude effects change the plume conditions sufficiently so that much lower control is available from either pitch down or roll RCS. Figure 6-6 shows that the roll control amplification is nearly zero during the zero angle of attack portion of the maneuver. This is because the peak value of the adverse roll interaction increment on the vertical fin occurs in this range of angles. The lower altitude results in a lower plume pressure ratio and a small plume turning angle and no plume impingement occurs on the vertical fin. This lower plume turning angle, however, results in higher plume pressures on the wing and more impingement than for the entry case. When the wind tunnel error increment is applied as in section 6.2, the range of possible roll amplifications goes through zero and the RCS roll control is non existent from a 2 upfiring, 2 down firing combination. Some roll control could be obtained by firing only the upward facing engines if the pitch up moment which also results could be canceled by some other method.

The same problem of lack of control is also seen in the symmetric pitch down RCS case shown in Figure 6-7. The wind tunnel error band gives a control amplification of zero. Two terms in the the analytic model appear to dominate the adverse interaction in this figure. The first and largest is the plume impingement term. The effect of lower altitude is to reduce the plume turning angle and makes the area affected by plume impingement smaller, however, the same term enters the plume decay parameter and causes the plume to decay slower. The net result is high plume impingement pressures over the smaller area and increased impingement increments. The second term is related to plume impingement and that is the symmetric firing cross coupling increment which is a function of impingement. Figure 6-7 shows that control exists if there is no cross coupling and this term needs further definition particularly because of the sting in the base of the wind tunnel model.

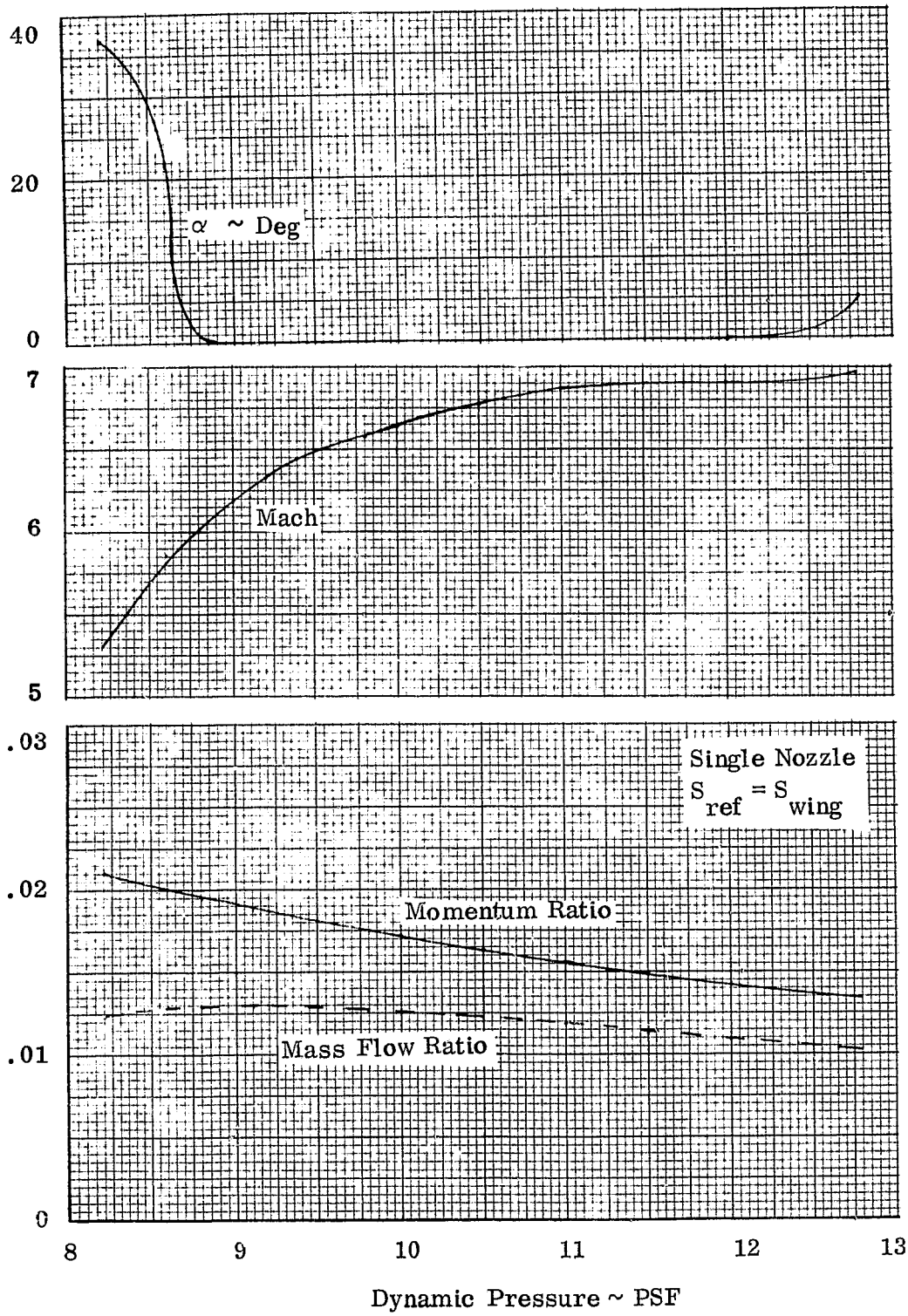

Figure 6-5. RTLS Abort Trajectory Conditions

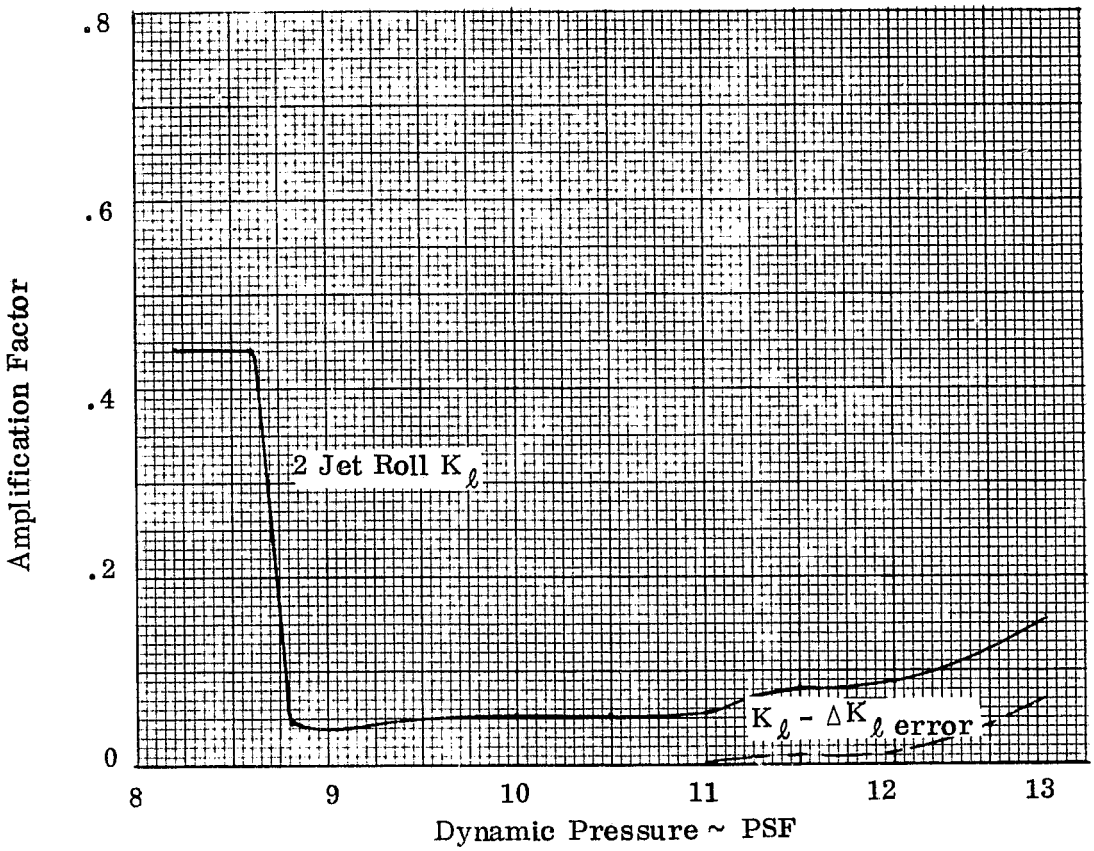

Figure 6-6. Roll Control Amplification on RTLS Abort Trajectory

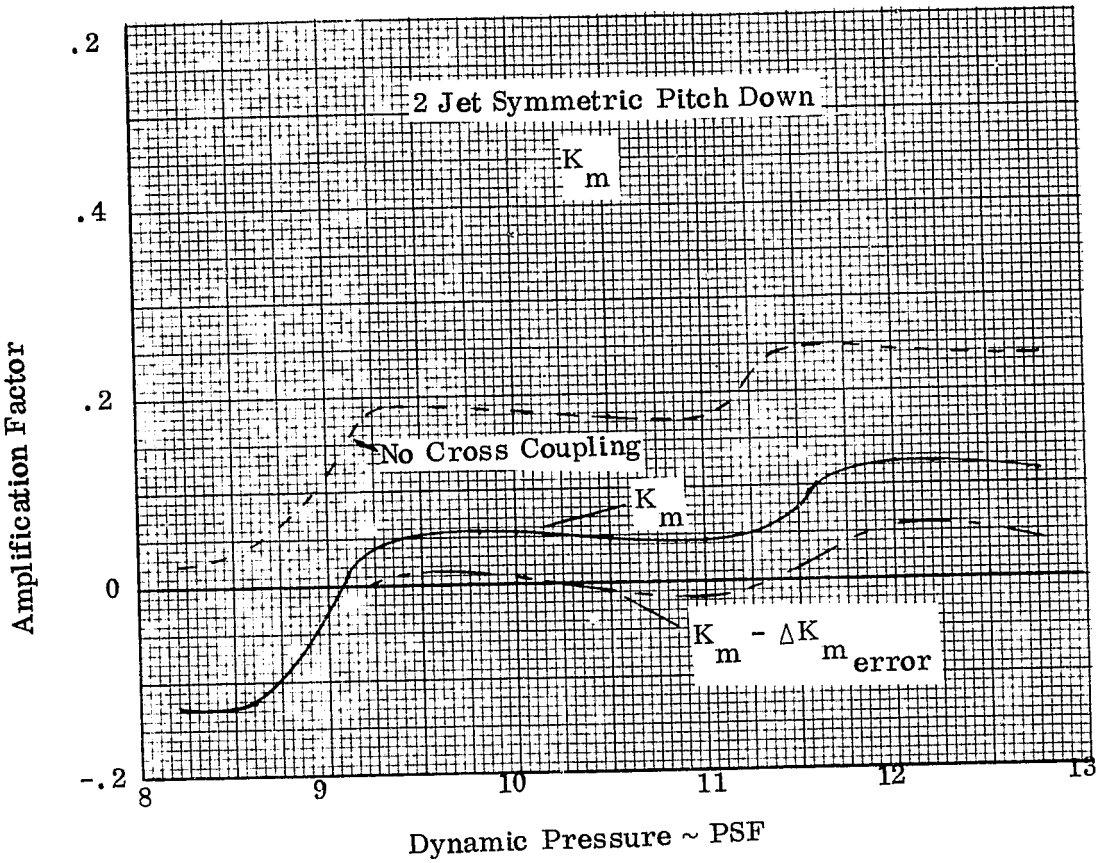

Figure 6-7. Pitch Down Control Amplification on RTLS Abort Trajectory

7

CONCLUSIONS

The interaction between the aft mounted reaction control system plumes and flow over the space shuttle orbiter vehicle is a very complex interaction and the adverse forces and moments which result are large relative to the thrust terms. An analytic model has been generated which predicts the total RCS control moment as the sum of the thrust term, an impingement term, an interaction term, and a cross coupling term. A program which incorporates this model has been written and is documented in this report.

7.1 STUDY CONCLUSIONS

1. The wind tunnel data accuracy was found to be good for all moments and the error in resulting full scale amplification was small at low dynamic pressure.

2. The interaction increments resulting from plume flow toward a surface correlated best with jet exit momentum ratio as the parameter.

3. The interaction increments resulting from plumes not flowing toward a surface correlated best with jet mass flow as a parameter.

4. Temperature ratio (RT) effects are important for those terms correlating with mass flow.

5. Additional yaw RCS simulation is desirable to improve the analytic model.

6. Combined control cross coupling is an important term and additional data is desirable.

7. Possible sting interference effects need to be resolved in the pitch down data.

8. Symmetric pitch down cross coupling needs more data to refine the model.

9. The RTLS abort maneuver appears to provide the most adverse flight conditions for RCS effectiveness.

10. Steady state simulation results are adequate for pulsing RCS controls.

7.2 STUDY RECOMMENDATIONS

1. A blade mounted model be built with a better representation of base geometry to evaluate sting interference.

2. A vacuum chamber test of symmetric pitch down RCS be performed with a good base geometry representation (no sting) to evaluate symmetric pitch down cross-coupling in the base region.

3. More wind tunnel tests be made to obtain the following data.

    a) Yaw RCS

    b) symmetric pitch down cross coupling

    c) other nozzles to verify mass flow as a parameter

    d) combined nozzles

    e) control deflection effects

SECTION 8

REFERENCES

1. Rausch, J. R. and Roberge, A. M., "RCS Jet-Flow Field Interaction Effects on the Aerodynamics of the Space Shuttle Orbiter," Convair Report CASD-NAS-73-020, November 1973.

2. Rausch, J. R. and Shih, K. T., "Space Shuttle Orbiter Reaction Control System Jet Interaction Study Interim Report," Convair Report CASD-NSC-74-009, November 1974.

3. Hayman, L. O., "Aft RCS Impingement Estimates and Comparison with OA99 Test Data," NASA Johnson Space Center aerodynamics memorandum 5437, August 20, 1974.

4. Ress, E. B., "Payload/Orbiter Contamination Control Assessment," Martin Marietta Aerospace Monthly Progress Report MCR-74-249, September 1974.

5. Sibulkin, M. and Gallaher, W. H., "Some Aspects of the Interaction of a Jet with a Dust Covered Surface in a Vacuum Environment," General Dynamics Convair Aerospace Division Report ERR-AN-244, February 1963.

6. Mirels, H. and Mullin, J. F., "Expansion of Gas Clouds and Hypersonic Jets Bounded by a Vacuum," Aerospace Corp. Report TDR-169 (3230-12) TR-1, Sept. 1962.

7. Boynton, F. P., "The Multitube Supersonic Flow Computer Code," Convair Report GDC-DBE67-003, February 1967.

8. Rausch, J. R., "Plume Impingement on a Parallel Staged Vehicle," Convair Report GDCA-ERR-1667, February 1972.

9. Ames Research Staff, "Equations, Tables, and Charts for Compressible Flow," NACA Technical Report 1135, 1953.

10. Pinzola, M., "Jet Simulation in Ground Test Facilities," NATO Advisory Group for Aeronautical Research and Development, AGARDograph 79.

11. Rausch, J. R., "A Program for Computation of Nozzle Parameters," Convair Aeroballistics Technical Note TN-72-AE-10, December 1972.

APPENDIX A PROGRAM LISTING

```
      PROGRAM PRED(INPUT,OUTPUT,TAPE5=INPUT,TAPE6=OUTPUT,TAPE48)
C
      DIMENSIONSF(15)
C
      REAL NONOZU,NONOZD,NONOZY
      REAL MINF
      COMMON/CONST/PIE,RADIAN,GI,RI,GO
      COMMON/GRP2/DNX(300),DNY(300),DNZ(300),X(300),Y(300),Z(300),SLOC(3
     100),J
      COMMON/UP/NONOZU,XREU,YREU,ZREU,DXNOZU,DYNOZU,DZNOZU,DSTARU
     1,ISIDEU,IBOTHU,RMFSU,AEXU,FMRU
      COMMON/DWN/NONOZD,XRED,YRED,ZRED,DXNOZD,DYNOZD,DZNOZD,DSTARD
     1,ISIDED,IBOTHD,RMFSD,AEXD,FMRD
      COMMON/SIDE/NONOZY,XREY,YREY,ZREY,DXNOZY,DYNOZY,DZNOZY,DSTARY
     1,ISIDEY,IBOTHY,RMFSY,AEXY,FMRY
      COMMON/FLT/MINF,PINF,TINF,ALPH,IOPT,QI,HI,VINF,THRUST,INEXT
      COMMON/REF/SREF,C,B,SCALE,XRE,YRE,ZRE,DXNOZ,DYNOZ,DZNOZ,DXNOZZ,
     1DYNOZZ,DZNOZZ
      COMMON/NOZ/XMJ,GJ,ARJ,AJE,POJ,RJ,TOJ,TURN,DSTAR,AN,THETA,DEXIT,
     1IIMP
      COMMON/A/POW,POW1,PRT,T1,PZT
      COMMON/INCOF/ CZIDL(5),CZIDH(5),CYIDL(7),CYIDH(7),CMIDL(5),
     1              CMIDH(5),CNIDL(7),CNIDH(7),CLIDL(5),CLIDH(5),ALPHBK,
     2              CZIUH(5),CYIUH(5),CMIUH(5),CNIUH(5),CLIUH(5),
     3              CZIUP(5),CYIUP(5),CMIUP(5),CNIUP(5),CLIUP(5),
     4              CZAUP(5),CYAUP(5),CMAUP(5),CNAUP(5),CLAUP(5),
     5              CZIYL(5),CZIYH(5),CYIYL(5),CYIYH(5),CMIYL(5),
     6              CMIYH(5),CNIYL(5),CNIYH(5),CLIYL(5),CLIYH(5)
      COMMON/IMCOEF/ CXIMU,CZIMU,CYIMU,CMIMU,CNIMU,CLIMU,CXIMD,CZIMD,
     1               CYIMD,CMIMD,CNIMD,CLIMD,CXIMY,CZIMY,CYIMY,CMIMY,
     2               CNIMY,CLIMY
      COMMON/INCOEF/ CXINU,CZINU,CYINU,CMINU,CNINU,CLINU,CXIND,CZIND,
     1               CYIND,CMIND,CNIND,CLIND,CXINY,CZINY,CYINY,CMINY,
     2               CNINY,CLINY
      COMMON/IHCOEF/ CXU,CZU,CYU,CMU,CNU,CLU,CXD,CZD,CYD,CMD,CND,CLD,
     1               CXY,CZY,CYY,CMY,CNY,CLY
      COMMON/TOCOEF/ CXT,CZT,CYT,CMT,CNT,CLT

      GINF=1.4
      RINF = 53.3
      PIE = 3.1415926
      RI=53.3
      GI=1.4
      RADIAN=57.2958
      GO=32.174049
      OBC=0.
      TLAI=0.
      IN=5
      IIN=1
  100 CONTINUE
      CALL INPUTT(IIN)
      IIN=2
  101 CONTINUE
      CALL INPUTT(IIN)
      AN = .7854*DEXIT**2
      CALL GET(GJ,ARJ,POJ,PJ,TOJ,TJ,XMJ,AN)
      AEXU=AN*NONOZU
      AEXD=AN*NONOZD
      AEXY=AN*NONOZY
      DSTARU=SQRT(4./PIE*AEXU/ARJ)
      DSTARD=SQRT(4./PIE*AEXD/ARJ)
      DSTARY=SQRT(4./PIE*AEXY/ARJ)
```

```
C
      IIN=5
    1 CONTINUE
C
      PRINT 4000
 4000 FORMAT (1H1)
      CALL INPUTT(IIN)
C
      GO TO (66,67,68,69),IOPT
   66 CONTINUE
      CALL ATMOS(HI,TT,PINF,RH,SOS,AQ,100.,DUM1,AM,AA,G,GO,TS,TLAT,OBC)
      PINF=PINF/144.
      TINF=TT
      VINF=MINF*SOS
      GO TO 69
   67 CONTINUE
      CALL ATMOS(HI,TT,PINF,RH,SOS,AQ,VINF,MINF,AM,AN,G,GO,TS,TLAT,OBC)
      PINF=PINF/144.
      MINF=VINF/SOS
      TINF=TT
      GO TO 69
   68 CONTINUE
      CALL ATMOS(HI,TT,PINF,RH,SOS,AQ,100.,DUM1,AM,AA,G,GO,TS,TLAT,OBC)
      PINF=PINF/144.
      QI=QI/144.
      MINF=SQRT(QI/(0.7*PINF))
      TINF=TT
   69 CONTINUE
      QI=0.7*144.*PINF*MINF**2
      IQ=0
      IF(QI.EQ.0.)IQ=1
      IF(QI.EQ.0.)QI=1.
      CALL EXPAN (GJ,POJ,PINF,XMJ,THETA,TURN)
      PR=PJ/PINF
      PRES=PR
C  JET MOMENTUM RATIO
      RMFS=GJ*PJ*XMJ**2*AN/GINF/PINF/MINF/MINF/SREF
      RMFSU=NONOZU*RMFS
      RMFSU=NONOZU*RMFS
      RMFSY=NONOZY*RMFS
      THRUST=PZT+AN*(PJ-PINF)
      TCOEF=THRUST/QI/SREF
      PRINT 3006
      PRINT 3006
      PRINT 4001
 4001 FORMAT(1H0,23H NOZZLE CHARACTERISTICS)
      PRINT4002,DEXIT,ARJ,THETA,XMJ
 4002 FORMAT(1H0,9H EXIT DIA,F12.4,16H EXPANSION RATIO,F12.4,11H EXIT AN
     1GLE,F12.4,15H NOZZLE MACH ,F15.4)
      PRINT4003,THRUST,POJ,PJ,GJ
 4003 FORMAT(1H0,7H THRUST,F12.4,14H CHAMBER PRESS,F12.4,11H EXIT PRESS,
     1F12.4,14H EXHAUST GAMMA,F12.4)
      PRINT 3006
      PRINT 4004
 4004 FORMAT(1H0,23H FREE STREAM CONDITIONS)
      PRINT4005,PINF,MINF,GINF,ALPH
 4005 FORMAT(1H0,11H P INFINITY,F13.5,9H MACH INF,F12.4,6H GAMMA,F12.4,
     115HANGLE OF ATTACK,F12.4)
      PRINT4006,PR,RMFS,TCOEF
 4006 FORMAT(1H0,14HPRESSURE RATIO,F12.4,15H MOMENTUM RATIO,F12.4,13H TH
     1RUST COEFF,F12.4)
      RTRAT=RJ*TJ/(RI*TINF)
      RTORT1=TOJ*RTRAT/TJ
      POJPIN=POJ/PINF
      PRINT4007,RTRAT,POJPIN,QI
 4007 FORMAT(10H0 RT RATIO,F13.5,9H POJ/PINF,F13.5,25HFREE STREAM DYNAMI
     1C PRESS,F13.5)
```

```
      PRINT4008,RTORT1
 4008 FORMAT(17H0(R*TOJ)/(R*TINF),F13.5)
      DO 10 IF=1,12
      CALL SCAL(PJ,GJ,XMJ,AN,TJ,RJ,PINF,GI,MINF,SREF,TINF,RI,
     1IF,ANS)
      SF(IF) = ANS
      PRINT4009,IF,SF(IF)
 4009 FORMAT(1H0,I5,5F20.6)
   10 CONTINUE
C  JET MASS FLOW RATIO
      FMR    = SF(3)
      FMRU   = NONOZU*FMR
      FMRD   = NONOZD*FMR
      FMRY   = NONOZY*FMR
      PRINT 3006
C        COMPUTE THRUST MOMENTS
      CLU=0.
      CLD=0.
      CLY=0.
      CMU=0.
      CND=0.
      CMY=0.
      CNU=0.
      CND=0.
      CNY=0.
      CXU=0.
      CXD=0.
      CXY=0.
      CYU=0.
      CYD=0.
      CYY=0.
      CZU=0.
      CZD=0.
      CZY=0.
      DO77IT=1,3
      CALL THR(IT,CXT,CYT,CZT,CLT,CMT,CNT)
      GO TO (74,75,76),IT
   74 CLU=CLT
      CMU=CMT
      CNU=CNT
      CXU=CXT
      CYU=CYT
      CZU=CZT
      GO TO 77
   75 CLD=CLT
      CMD=CMT
      CND=CNT
      CXD=CXT
      CYD=CYT
      CZD=CZT
      GO TO 77
   76 CLY=CLT
      CMY=CMT
      CNY=CNT
      CXY=CXT
      CYY=CYT
      CZY=CZT
   77 CONTINUE
C    COMPUTE PLUME IMPINGEMENT MOMENTS
      CLIMU=0.
      CLIMD=0.
      CLIMY=0.
      CMIMU=0.
      CMIMD=0.
      CMIMY=0.
      CNIMU=0.
```

```
      CNIMU=0.
      CNIMY=0.
      CXIMU=0.
      CXIMD=0.
      CXIMY=0.
      CYIMU=0.
      CYIMD=0.
      CYIMY=0.
      CZIMU=0.
      CZIMD=0.
      CZIMY=0.
      GO TO (170,180,185),IIMP
  170 CONTINUE
      CNIMU=+0.0593*CNY
      CMIMU=+0.00078*CMU
      CLIMU=-0.13*CLU
      CZIMU=-0.00086*TCOEF*NONOZU
      CXIMU=+0.00266*TCOEF*NONOZU
      CYIMU=-0.06238*TCOEF*NONOZU
      CNIMD=+0.01657*CNY
      CMIMD=-0.3018*CMD
      CLIMD=-0.2312*CLD
      CXIMD=+0.10709*TCOEF*NONOZD
      CYIMD=+0.01837*TCOEF*NONOZD
      CZIMD=-0.27369*TCOEF*NONOZD
      CNIMY=+0.0013*CNY
      CMIMY=+0.00873*TCOEF*NONOZY*XREU/C
      CLIMY=+0.03477*TCOEF*NONOZY*YREU/B
      CXIMY=0.00288*TCOEF*NONOZY
      CYIMY=+0.00077*TCOEF*NONOZY
      CZIMY=-0.01634*TCOEF*NONOZY
      GO TO 190
  180 PRINT 4010
 4010 FORMAT(28H0 IMPINGEMENT FORCE IGNORED )
      GO TO 190
  185 CONTINUE
      DO 191 IT=1,3
      CALL IMPING(IT,CXT,CYT,CZT,CLT,CMT,CNT)
      GO TO (186,187,188),IT
  186 CLIMU=CLT
      CMIMU=CMT
      CNIMU=CNT
      CXIMU=CXT
      CYIMU=CYT
      CZIMU=CZT
      GO TO 189
  187 CLIMD=CLT
      CMIMD=CMT
      CNIMD=CNT
      CXIMD=CXT
      CYIMD=CYT
      CZIMD=CZT
      GO TO 189
  188 CLIMY=CLT
      CMIMY=CMT
      CNIMY=CNT
      CXIMY=CXT
      CYIMY=CYT
      CZIMY=CZT
  189 CONTINUE
  190 CONTINUE
      CLIND=0.
      CLIND=0.
      CLINY=0.
      CMIND=0.
      CMIND=0.
```

```
      CMINY=0.
      CNIND=0.
      CNINU=0.
      CNINY=0.
      CXINU=0.
      CXIND=0.
      CXINY=0.
      CYINU=0.
      CYIND=0.
      CYINY=0.
      CZINU=0.
      CZIND=0.
      CZINY=0.
C  COMPUTE PLUME  INTERACTION MOMENTS
      IF(IQ.EQ.1)GO TO 204
      DO203IT=1,3
      CALL INTER(IT,CXB,CYB,CZB,CLB,CMB,CNB)
      GO TO (200,201,202),IT
  200 CLIND=CLB
      CMINU=CMB
      CNINU=CNB
      CXINU=CXB
      CYINU=CYB
      CZINU=CZB
      GO TO 203
  201 CLIND=CLB
      CMIND=CMB
      CNIND=CNB
      CXIND=CXB
      CYIND=CYB
      CZIND=CZB
      GO TO 203
  202 CLINY=CLB
      CMINY=CMB
      CNINY=CNB
      CXINY=CXB
      CYINY=CYB
      CZINY=CZB
  203 CONTINUE
  204 CONTINUE
      IF(IBOTHU.EQ.1)GO TO 205
      IF(ISIDEU.LT.1)GO TO 206
      CLU=-CLU
      CNU=-CNU
      CYU=-CYU
      CLIMU=-CLIMU
      CNIMU=-CNIMU
      CYIMU=-CYIMU
      CLINU=-CLINU
      CNINU=-CNINU
      CYINU=-CYINU
      GO TO 206
  205 CONTINUE
      CLU=0.
      CNU=0.
      CYU=0.
      CLIMU=0.
      CNIMU=0.
      CYIMU=0.
      CLINU=0.
      CNINU=0.
      CYINU=0.
      CMU=2.*CMU
      CXU=2.*CXU
      CZU=2.*CZU
      CMIMU=2.*CMIMU
```

```
      CXIMD=2.*CXIMD
      CZIMD=2.*CZIMD
      CMINY=2.*CMINY
      CXINY=2.*CXINY
      CZINY=2.*CZINY
  206 CONTINUE
      IF(ISYMD.EQ.1)GO TO 207
      IF(ISIDED.LT.1)GO TO 208
      CLD=-CLD
      CND=-CND
      CYD=-CYD
      CLIMD=-CLIMD
      CNIMD=-CNIMD
      CYIMD=-CYIMD
      CLINY=-CLINY
      CNINY=-CNINY
      CYINY=-CYINY
      GO TO 208
  207 CONTINUE
      CLD=0.
      CND=0.
      CYD=0.
      CLIMD=0.
      CNIMD=0.
      CYIMD=0.
      CLINY=0.
      CNINY=0.
      CYINY=0.
      CMD=2.*CMD
      CXD=2.*CXD
      CZD=2.*CZD
      CMIMD=2.*CMIMD
      CXIMD=2.*CXIMD
      CZIMD=2.*CZIMD
      CMINY=2.*CMINY
      CXINY=2.*CXINY
      CZINY=2.*CZINY
  208 CONTINUE
      IF(ISYMY.EQ.1)GO TO 209
      IF(ISIDEY.LT.1)GO TO 210
      CLY=-CLY
      CNY=-CNY
      CYY=-CYY
      CLIMY=-CLIMY
      CNIMY=-CNIMY
      CYIMY=-CYIMY
      CLINY=-CLINY
      CNINY=-CNINY
      CYINY=-CYINY
      GO TO 210
  209 CONTINUE
      CLY=0.
      CNY=0.
      CYY=0.
      CLIMY=0.
      CNIMY=0.
      CYIMY=0.
      CLINY=0.
      CNINY=0.
      CYINY=0.
      CMY=2.*CMY
      CXY=2.*CXY
      CZY=2.*CZY
      CMIMY=2.*CMIMY
      CXIMY=2.*CXIMY
      CZIMY=2.*CZIMY
      CMINY=2.*CMINY
      CXINY=2.*CXINY
```

```
      CZINY=2.*CZINY
  210 CONTINUE
C COMPUTE MULTIPLE AXES CROSSCOUPLING  TERMS
      CXCCU=0.
      CXCCD=0.
      CXCCY=0.
      CZCCU=0.
      CZCCD=0.
      CZCCY=0.
      CMCCU=0.
      CMCCD=0.
      CMCCY=0.
      CNCCU=0.
      CNCCD=0.
      CNCCY=0.
      CLCCU=0.
      CLCCD=0.
      CLCCY=0.
      CALL CCOUPL (2,CXCCD,CZCCD,CYCCD,CMCCD,CNCCD,CLCCD)
      IF(IW.EQ.1)GO TO 211
      CALL CCOUPL (1,CXCCU,CZCCU,CYCCU,CMCCU,CNCCU,CLCCU)
      CALL CCOUPL (3,CXCCY,CZCCY,CYCCY,CMCCY,CNCCY,CLCCY)
  211 CONTINUE
C COMPUTE TOTAL FORCES AND MOMENTS
      CXT=CXU+CXD+CXY+CXIMU+CXIMD+CXIMY+CXINU+CXIND+CXINY+CXCCU+
     1CXCCD+CXCCY
      CYT=CYU+CYD+CYY+CYIMU+CYIMD+CYIMY+CYINU+CYIND+CYINY+CYCCU+
     1CYCCD+CYCCY
      CZT=CZU+CZD+CZY+CZIMU+CZIMD+CZIMY+CZINU+CZIND+CZINY+CZCCU+
     1CZCCD+CZCCY
      CLT=CLU+CLD+CLY+CLIMU+CLIMD+CLIMY+CLINU+CLIND+CLINY+CLCCU+
     1CLCCD+CLCCY
      CMT=CMU+CMD+CMY+CMIMU+CMIMD+CMIMY+CMINU+CMIND+CMINY+CMCCU+
     1CMCCD+CMCCY
      CNT=CNU+CND+CNY+CNIMU+CNIMD+CNIMY+CNINU+CNIND+CNINY+CNCCU+
     1CNCCD+CNCCY
      PRINT 3001
 3001 FORMAT(14H0 THRUST TERMS)
      PRINT 3002
 3002 FORMAT (1H0,29X2HCL,16X2HCM,16X2HCN,16X2HCX,16X2HCY,16X2HCZ)
      PRINT 3003, CLU,CMU,CNU,CXU,CYU,CZU
      PRINT 3004, CLD,CMD,CND,CXD,CYD,CZD
      PRINT 3005, CLY,CMY,CNY,CXY,CYY,CZY
 3003 FORMAT(14H0 PITCH UP     ,6F18.6)
 3004 FORMAT(14H0 PITCH DOWN   ,6F18.6)
 3005 FORMAT(14H0 YAW          ,6F18.6)
      PRINT 3006
 3006 FORMAT(55H0XXXXXXXXXXXXXXXXXXXXXXXXXXXXXXXXXXXXXXXXXXXXXXXXXXXXX)
      PRINT 3007
 3007 FORMAT(21H0 IMPINGEMENT FORCES )
      PRINT 3002
      PRINT 3003, CLIMU,CMIMU,CNIMU,CXIMU,CYIMU,CZIMU
      PRINT 3004, CLIMD,CMIMD,CNIMD,CXIMD,CYIMD,CZIMD
      PRINT 3005, CLIMY,CMIMY,CNIMY,CXIMY,CYIMY,CZIMY
      PRINT 3006
      PRINT 3008
 3008 FORMAT(19H0 INTERACTION TERMS)
      PRINT 3002
      PRINT 3003, CLINU,CMINU,CNINU,CXINU,CYINU,CZINU
      PRINT 3004, CLIND,CMIND,CNIND,CXIND,CYIND,CZIND
      PRINT 3005, CLINY,CMINY,CNINY,CXINY,CYINY,CZINY
      PRINT 3006
      PRINT 3009
 3009 FORMAT (22H0 CROSS COUPLING TERMS)
      PRINT 3002
```

```
      PRINT 3003, CLCCU,CMCCU,CNCCU,CXCCU,CYCCU,CZCCU
      PRINT 3004, CLCCD,CMCCD,CNCCD,CXCCD,CYCCD,CZCCD
      PRINT 3005, CLCCY,CMCCY,CNCCY,CXCCY,CYCCY,CZCCY
      PRINT 3006
      PRINT 3010
 3010 FORMAT(14H0 TOTAL VALUES)
      PRINT 3002
      PRINT 3011, CLT,CMT,CNT,CXT,CYT,CZT
 3011 FORMAT (1H0,13X,6F18.6)
      PRINT 3006
      PRINT4100
 4100 FORMAT(1H0,*THRUST MOMENTS USED FOR AMPLIFICATION FACTORS ARE DEP
     1ENDENT ON CONTROL USED*)
C     CALCULATE AMPLIFICATION FACTORS
C     IF THE NUMBER OF NOZZLES IN ANY SET IS INPUT AS ZERO, THE THRUST
C     COEFFICIENTS FOR THAT SET TO CALCULATE AMPLIFICATION FACTORS ARE
C     COMPUTED FOR AN ASSUMED TWO NOZZLES.  NOZZLE COORDINATES MUST,
C     HOWEVER, BE INPUT FOR ALL THREE SETS.
      CALL AMPL (1,AKXU,AKZU,AKYU,AKMU,AKNU,AKLU)
      PRINT 3012
 3012 FORMAT (23H0 AMPLIFICATION FACTORS)
      PRINT 3013
 3013 FORMAT (1H0,29X2HKL,16X2HKM,16X2HKN,16X2HKX,16X2HKY,16X2HKZ)
      PRINT 3043, AKLU,AKMU,AKNU,AKXU,AKYU,AKZU
 3043 FORMAT(1H0,*AMPLIFICATION*,10X,6F18.7)
      PRINT 3006
      IIN=INEXT
      GO TO (100,101,1,61),IIN
   61 CALLEXIT
      END
```

```
      SUBROUTINE PARCEO(Y,D,COEF)
      DIMENSION Y(3), D(3), COEF(3)
C-----GIVES COEFFICIENTS FOR A PARABOLIC FIT
      X1 = Y(1)
      X2 = Y(2)
      X3 = Y(3)
      D1 = D(1)
      D2 = D(2)
      D3 = D(3)
      FACTOR = X2*X3*X3 - X2*X2*X3 - X1*X3*X3 + X1*X2*X2 + X1*X1*X3
     *       - X1*X1*X2
      A1     = X2*X3*X3 - X2*X2*X3
      A2     = X3*X1*X1 - X1*X3*X3
      A3     = X1*X2*X2 - X2*X1*X1
      B1     = X2*X2 - X3*X3
      B2     = X3*X3 - X1*X1
      B3     = X1*X1 - X2*X2
      C1     = X3 - X2
      C2     = X1 - X3
      C3     = X2 - X1
      COEF(1) = (D1*A1 + D2*A2 + D3*A3)/ FACTOR
      COEF(2) = (D1*B1 + D2*B2 + D3*B3) / FACTOR
      COEF(3) = (D1*C1 + D2*C2 + D3*C3) / FACTOR
      RETURN
      END
```

```
      SUBROUTINE JET(GAMN,ARN,PONOZ,PNOZ,TEE,TEX,MNOZ,AN)
      DIMENSION PM(3),ZM(3),COE(3)
      COMMON/A/POW,POW1,PRT,T1,PZT
      REAL MNOZ
      PM(1)=1.
      PM(2)=1.
      ZM(1)=1.
      ZM(2)=1.
      MNOZ=1.
      DM=.1
      POW=(GAMN+1.)/(2.*(GAMN-1.))
      DO111F=1,100
      MNOZ=MNOZ+DM
      AAST=((GAMN+1.)/2.)**POW
      AAST=AAST*MNOZ/((1.+0.5*(GAMN-1.)*MNOZ**2)**POW)
      AAST=1./AAST
      ZM(1)=ZM(2)$ZM(2)=ZM(3)$ZM(3)=MNOZ
      PM(1)=PM(2)
      PM(2)=PM(3)
      PM(3)=AAST
      IF(AAST.GE.ARN)GO TO 112
  111 CONTINUE
  112 CALL PARCEO(PM,ZM,COE)
      MNOZ=COE(1)+COE(2)*ARN+COE(3)*ARN**2
      AAST=((GAMN+1.)/2.)**POW
      AAST=AAST*MNOZ/((1.+0.5*(GAMN-1.)*MNOZ**2)**POW)
      AAST=1./AAST
      PNOZ=PONOZ/((1.+0.5*(GAMN-1.)*MNOZ**2)**(GAMN/(GAMN-1.)))
      POW=2.*POW
      POW1=(GAMN-1.)/GAMN
      PRT=(PNOZ/PONOZ)**POW1
      PRT=1.-PRT
      T1=((2./(GAMN+1.))**POW)*2.*GAMN**2/(GAMN-1.)
      PZT=AN/AAST*PONOZ*SQRT(T1*PRT)*144.
      TEX=TEE/(1.+0.5*(GAMN-1.)*MNOZ*MNOZ)
      RETURN
      END
```

```
      SUBROUTINE ATMOS(Z,TT,P,RHO,C,Q,V,AM,AMU,ANU,G,GO,TS,THET,OBC)
C     LATEST COMPILATION DATED    6-27-72
C     U.S. STANDARD ATMOSPHERE,1962
      ZM=Z+6.3048
      ABAR=-3.085462E-04
      BBAR=7.254E-11
      CBAR=-1.517E-17
C     GRAVITATIONAL FORCE DETERMINED FROM SMITHSONIAN POLYNOMIAL
      IF (OBC) 10,20,10
   10 THETP=90.0-THET
      THETPR=THETP/57.29578
      GO=980.665*(1.0-.002637*COS(2.0*THETPR)+.0000059*(COS(2.0*THETPR)
     1)**2)
      DBAR=-2.27E-07
      EBAR=1.0E-13
      FBAR=0.0E-20
      G=.01*(GO+(ABAR+DBAR*COS(2.0*THETPR))*ZM+(BBAR+EBAR*COS(2.0*THETPR
     1))*ZM**2+(CBAR+FBAR*COS(2.0*THETPR))*ZM**3)
      GO TO 30
   20 GO = GO*30.48
```

```
      G=0.01*(G0+ABAR*ZM+BBAR*ZM*ZM+CBAR*ZM*ZM*ZM)
   30 HM=(G0*ZM+ABAR*ZM*ZM/2.0+BBAR*ZM*ZM*ZM/3.0+CBAR*ZM*ZM*ZM*ZM/4.0)/G
     10
      G0E=G0/30.48
      AM0=28.9644
      RSM=8.31432
      IF (HM-11000.0) 40,40,50
   40 PA=101325.
      DH=HM
      TA=288.15
      DTDH=-6.5
      GO TO 190
   50 IF (HM-20000.0) 60,60,70
   60 PA=22632.
      TA=216.65
      DTDH=0.0
      DH=HM-11000.0
      GO TO 190
   70 IF (HM-32000.0) 80,80,90
   80 PA=5474.87
      TA=216.65
      DTDH=1.0
      DH=HM-20000.0
      GO TO 190
   90 IF (HM-47000.0) 100,100,110
  100 PA=868.014
      TA=228.65
      DTDH=2.8
      DH=HM-32000.0
      GO TO 190
  110 IF (HM-52000.0) 120,120,130
  120 PA=110.906
      TA=270.65
      DTDH=0.0
      DH=HM-47000.0
      GO TO 190
  130 IF (HM-61000.0) 140,140,150
  140 PA=59.0005
      TA=270.65
      DTDH=-2.8
      DH=HM-52000.0
      GO TO 190
  150 IF (HM-79000.0) 160,160,170
  160 PA=18.2099
      TA=252.65
      DTDH=-4.0
      DH=HM-61000.0
      GO TO 190
  170 IF (HM-88743.) 180,180,230
  180 PA=1.03377
      TA=180.65
      DTDH=0.0
      DH=HM-79000.0
      GO TO 190
  190 CONTINUE
      TM=TA+DTDH*DH/1000.0
      IF (DTDH) 210,200,210
  200 PPA=EXP(-G0*AM0*DH/(100000.0*RSM*TA))
      GO TO 220
  210 PPA=(TA/TM)**(G0*AM0/(100.0*RSM*DTDH))
  220 CONTINUE
      TE=TM*1.8
      TI=TE
      B = 7.3025E-07
      P = PA*PPA*2.0885468
      RHO=AM0*P/(1545.31*G0E*TE)
```

```
      AMU=B*TE**1.5/(198.72+TE)/G0E
      ANU=AMU/RHO
      C=SQRT(1.4*1545.31*G0E*TE/AMO)
      AM = V/C
      Q = 0./*P*AM*AM
      TS = (4.56E+16*SQRT(RHO/0.00238)*(V/26000.0)**3.15)**0.25
      G=G/0.3048
      GO = GO/30.48
      RETURN
  230 IF (ZM-100000.0) 240,240,250
  240 TMB=160.65
      ALM=5.0
      ZBK=90.0
      PBM = 1.6436E-03
      AMB=28.9644
      GM=-.00844
      GO TO 400
  250 IF (ZM-110000.0) 260,260,270
  260 TMB=210.65
      ALM=5.0
      ZBK=100.0
      PBM=3.0075E-04
      AMB=28.88
      GM=-.032
      GO TO 400
  270 IF (ZM-120000.0) 280,280,290
  280 TMB=260.65
      ALM=10.0
      ZBK=110.0
      PBM=7.3544E-05
      AMB=28.56
      GM=-.049
      GO TO 400
  290 IF (ZM-150000.0) 300,300,310
  300 TMB=300.65
      ALM=20.0
      ZBK=120.0
      PBM=2.5217E-05
      AMB=28.07
      GM=-.0383333
      GO TO 400
  310 IF (ZM-160000.0) 320,320,330
  320 TMB=960.65
      ALM=15.0
      ZBK=150.0
      PBM=3.0617E-06
      AMB=26.92
      GM=-.026
      GO TO 400
  330 IF (ZM-170000.0) 340,340,350
  340 TMB=1110.65
      ALM=10.0
      ZBK=160.
      PBM=1.6943E-06
      AMB=26.66
      GM=-.026
      GO TO 400
  350 IF (ZM-190000.0) 360,360,370
  360 TMB=1210.65
      ALM=7.0
      ZBK=170.0
      PBM=2.7926E-06
      AMB=26.4
      GM=-.0275
      GO TO 400
```

```
  370 IF (ZM-230000.0) 380,380,390
  380 TMB=1350.65
      ALM=5.0
      ZBK=190.0
      PBM=1.6852E-06
      AMB=25.85
      GM=-.02675
      GO TO 400
  390 CONTINUE
      Q = 0.0
      P = 0.0
      G = G/0.3048
      GO = GO/30.48
      RETURN
  400 CONTINUE
C     COMPUTE KINETIC TEMPERATURE
      ZK=ZM/1000.0
      AMRAT=((AMB+GM*(ZK-ZBK))/28.9644)
      TMOL=TMB+ALM*(ZK-ZBK)
      TT=TMOL*AMRAT*1.80
  410 CONTINUE
C     COMPUTE STATIC PRESSURE
      AP=(TMB/ALM)-ZBK
      PARTA=(ZK-ZBK)*(.625E-06*(ZK+ZBK)-.125E-05*AP-.00325)
      PARTB=(.125E-05*AP*AP+.00325*AP+9.818)*ALOG((ZK+AP)/(ZBK+AP))
      AMO=28.9644
      RSTAR=8.31432
      COEF = -ALM*RSTAR/AMO
      PRLOG=(PARTA+PARTB)/COEF
      P=2.0885468*PBM*EXP(PRLOG)
  420 CONTINUE
C     COMPUTE DENSITY, SPEED OF SOUND, DYNAMIC PRESSURE
      RHO = P*AMRAT*28.9644/(1545.31*TT*GOE)
      C=SQRT(1.4*P/RHO)
      Q=0.5*RHO*V*V
  430 CONTINUE
C     COMPUTE MACH NUMBER, GRAVITATIONAL FORCE, VISCOSITY + KIN. VISC'TY
      AM=V/C
      G = (0.125E-05)*ZK*ZK-.00325*ZK+9.818
      BETA = 7.3025E-07
      SUTH = 198.72
      AMU = BETA*SQRT(TT**3.0)/(TT+SUTH)
      ANU=AMU/RHO/GOE
      AMU=AMU/GOE
      TS = (4.56E+16*SQRT(RHO/0.00238)*(V/26000.0)**3.15)**0.25
      G=G/0.3048
      GO = GO/30.48
      RETURN
  440 FORMAT (32H0  UPPER ALTITUDE LIMIT EXCEEDED)
      END


      SUBROUTINE EXPAN(G,PT,PIT,XM,THETNO,TURN)
      IF(PT.LE.PIT)GO TO 300
      TURN=0.
      G1=(G-1.)/G
      G2=2./(G-1.)
      G3=SQRT((G+1.)/(G-1.))
      G4=SQRT((G-1.)/(G+1.))
      IF(PIT.EQ.0.)GO TO 5
      XME=SQRT(G2*((PT/PIT)**G1-1.))
      X1=SQRT(XME**2-1.)
      TURN=57.2958*(G3*ATAN(G4*X1)-ATAN(X1))
      GO TO 6
    5 TURN=90.*(G3-1.)
    6 CONTINUE
      TURNL=TURN
      XME=XM
```

```
      X1=SQRT(XME**2-1.)
      TURN=57.2958*(G3*ATAN(G4*X1)-ATAN(X1))
      TURN=TURNL-TURN+THETNO
      RETURN
  300 TURN=THETNO
      RETURN
  400 FORMAT(1H0,5F20.5)
      END


      SUBROUTINE SCAL (PJ,GJ,XMJ,AJ,TJ,RJ,PI,GI,XMI,AI,TI,RI,I,ANS)
      GO TO (10,20,30,40,50,60,70,80,90,100,110,120,130),I
   10 ANS = PJ/PI*GJ/GI*AJ/AI*((XMJ/XMI)**2)
      RETURN
   20 ANS = AJ*((PJ/PI)*(1.+GJ*XMJ**2)-1.)/(AI*GI*XMI**2)
      RETURN
   30 ANS = GJ/GI*RI/RJ*TI/TJ*((PJ*XMJ*AJ)/(PI*XMI*AI))**2
      ANS=SQRT(ANS)
      RETURN
   40 ANS = GJ/GI*RJ/RI*TJ/TI*(XMJ/XMI)**2
      RETURN
   50 ANS = GJ/GI*RJ/RI*TJ/TI*(GI-1.)/(GJ-1.)
      RETURN
   60 CONTINUE
      TMI = XMI*XMI-1.
      IF (TMI.LT.0.) TMI = -TMI
      TMJ = XMJ*XMJ-1.
      IF (TMJ.LT.0.) TMJ = -TMJ
      ANS = PJ/PI*GJ/GI*(XMJ/XMI)**2*SQRT(TMI)/(SQRT(TMJ))
      RETURN
   70 CONTINUE
      TMJ = XMJ*XMJ-1.
      IF (TMJ.LT.0.) TMJ = -TMJ
      ANS = SQRT(TMJ)/GJ/XMJ/XMJ*(1.-(PI/PJ))
      RETURN
   80 ANS = PI*AJ*(GJ**4)*(XMJ**8)*((RJ*TJ)**4)/((GI**2.5)*((RI*TI)**3.5
     1))
      RETURN
   90 ANS = PJ/PI
      RETURN
  100 ANS = PJ/(.5*GI*PI*XMI**2)
      RETURN
  110 ANS = PJ/PI*((1. + .5*(GJ - 1.)*XMJ**2)**(GJ/(GJ-1.)))
      RETURN
  120 POJ=PJ*(1.+.5*(GJ-1.)*XMJ**2)**(GJ/(GJ-1.))
      CALL MACH(POJ,PI,GJ,ANS)
      ANS=ANS/GJ
  130 RETURN
      END


      SUBROUTINE MACH(PO,PI,G,XM)
      A = (G-1.)/G
      XM=SQRT((2./(G-1.))*((PO/PI)**A-1.))
      IF (XM.LT.1) XM = -4000.
      RETURN
      END
```

```
      SUBROUTINE THR(I,CX,CY,CZ,CL,CM,CN)
      COMMON/FLT/MINF,PINF,TINF,ALPH,IOPT,QI,HI,VINF,THRUST,INEXT
      COMMON/REF/SREF,C,B,SCALE,XRE,YRE,ZRE,DXNOZ,DYNOZ,DZNOZ,DXNOZZ,
     1DYNOZZ,DZNOZZ
      COMMON/UP/NONOZU,XREU,YREU,ZREU,DXNOZU,DYNOZU,DZNOZU,DSTARU
     1,ISIDEU,IBOTHU,RMFSU,AEXU
      COMMON/DWN/NONOZD,XRED,YRED,ZRED,DXNOZD,DYNOZD,DZNOZD,DSTARD
     1,ISIDED,IBOTHD,RMFSD,AEXD
      COMMON/SIDE/NONOZY,XREY,YREY,ZREY,DXNOZY,DYNOZY,DZNOZY,DSTARY
     1,ISIDEY,IBOTHY,RMFSY,AEXY
      COMMON/NOZ/XMJ,GJ,ARJ,AJE,POJ,RJ,TOJ,TURN,DSTAR,AN,THETA,DEXIT,
     1IIMP
      REAL NONOZU,NONOZD,NONOZY
      CT1=THRUST/QI/SREF
      GO TO (1,2,3),I
    1 IF(NONOZU.EQ.0.)GO TO 5
      CT=CT1*NONOZU
      DX=DXNOZU
      DY=DYNOZU
      DZ=DZNOZU
      X=XREU
      Y=YREU
      Z=ZREU
      GO TO 4
    2 IF(NONOZD.EQ.0.)GO TO 5
      CT=CT1*NONOZD
      DX=DXNOZD
      DY=DYNOZD
      DZ=DZNOZD
      X=XRED
      Y=YRED
      Z=ZRED
      GO TO 4
    3 IF(NONOZY.EQ.0.)GO TO 5
      CT=CT1*NONOZY
      DX=DXNOZY
      DY=DYNOZY
      DZ=DZNOZY
      X=XREY
      Y=YREY
      Z=ZREY
    4 CX=-CT*DX
      CY=-CT*DY
      CZ=-CT*DZ
      CL=(CZ*Y-CY*Z)/B
      CM=(CX*Z-CZ*X)/C
      CN=(CY*X-CX*Y)/B
      RETURN
    5 CX=0.
      CY=0.
      CZ=0.
      CL=0.
      CM=0.
      CN=0.
      RETURN
      END
```

```
      SUBROUTINE WINGING(L,CXB,CYB,CZB,CLB,CMB,CNB)
      COMMON/CONST/PIE,RADIAN,GI,RI,GO
      COMMON/NOZ/XMJ,GJ,ARJ,AJE,POJ,RJ,TOJ,TURN,DSTAR,AN,THETA,DEXIT,
     1IIMF
      COMMON/UP/NONOZU,XREU,YREU,ZREU,DXNOZU,DYNOZU,DZNOZU,DSTARU
     1,ISIDEU,IBOTHU,RMFSU,AEXU,FMRU
      COMMON/DWN/NONOZD,XRED,YRED,ZRED,DXNOZD,DYNOZD,DZNOZD,DSTARD
     1,ISIDED,IBOTHD,RMFSD,AEXD,FMRD
      COMMON/SIDE/NONOZY,XREY,YREY,ZREY,DXNOZY,DYNOZY,DZNOZY,DSTARY
     1,ISIDEY,IBOTHY,RMFSY,AEXY,FMRY
      COMMON/GRP2/DNX(300),DNY(300),DNZ(300),X(300),Y(300),Z(300),SLOC(3
     100),J
      COMMON/FLT/XINF,PINF,TINF,ALPH,IOPT,QI,HI,VINF,THRUST,INEXT
      COMMON/REF/SREF,C,B,SCALE,XRE,YRE,ZRE,DXNOZ,DYNOZ,DZNOZ,DXNOZZ,
     1DYNOZZ,DZNOZZ
      GO TO (1,2,3),L
    1 IF(NONOZU.EQ.0.)GO TO 2000
      XRE=XREU
      YRE=YREU
      ZRE=ZREU
      DXNOZ=DXNOZU
      DYNOZ=DYNOZU
      DZNOZ=DZNOZU
      DSTAR=DSTARU
      AJE=AEXU
      DXNOZZ=1.
      DYNOZZ=1.
      DZNOZZ=-1.
      GO TO 4
    2 IF(NONOZD.EQ.0.)GO TO 2000
      DZNOZZ=1.
      DYNOZZ=1.
      DXNOZZ=1.
      AJE=AEXD
      DSTAR=DSTARD
      DZNOZ=DZNOZD
      DYNOZ=DYNOZD
      DXNOZ=DXNOZD
      ZRE=ZRED
      XRE=XRED
      YRE=YRED
      GO TO 4
    3 IF(NONOZY.EQ.0.)GO TO 2000
      DZNOZZ=1.
      DYNOZZ=1.
      DXNOZZ=1.
      AJE=AEXY
      DSTAR=DSTARY
      DZNOZ=DZNOZY
      DYNOZ=DYNOZY
      DXNOZ=DXNOZY
      ZRE=ZREY
      YRE=YREY
      XRE=XREY
    4 CONTINUE
      CXB=0.
      CYB=0.
      CZB=0.
      CLB=0.
      CMB=0.
      CNB=0.
C     BEGIN CALCULATIONS OF COEFFICIENTS AND DERIVATIVES
```

```
      DO 1150 I=1,5
  630 I = IC
      YQ = Y(I)
      DNQ = DNY(I)
  660 XB = X(I) / B
      XC=X(I)/C
      YB=YQ  /B
      ZB=Z(I)/B
      ZC=Z(I)/C
      SRATIO=SLOC(I)/SREF
      DX=X(I)-XRE
      DY=YQ-YRE
      DZ=Z(I)-ZRE
      DIST=SQRT(DX**2+DY**2+DZ**2)
      IF(DIST.EQ.0.)GO TO 1150
      IF(DZ.NE.0.)GO TO 6
      IF(DZNDZ.GT.0.)GO TO 1150
      GO TO 7
    6 IF(DZNDZ.LT. .)GO TO 1150
    7 CONTINUE
      DXTOT=DX/DIST
      DYTOT=DY/DIST
      DZTOT=DZ/DIST
      CETA=DXTOT*DXNDZ+DYTOT*DYNDZ+DZTOT*DZNDZ
      THET=ACOS(CETA)*RADIAN
      IF(THET.GE.TORN)GO TO 1150
      DXTOT=-DXTOT
      DYTOT=-DYTOT
      DZTOT=-DZTOT
      CETA=DXTOT*DNX(I)+DYTOT*DNQ+DZTOT*DNZ(I)
      IF(CETA.LE.0.)GO TO 1150
      CALL VACPLU(THET,DIST,XMPLUM,PLOC,QLOC)
      CPLOC=(GJ+3.)/(GJ+1.)*(1.-2./(XMPLUM**2*(GJ+3.)))*CETA**2
      IF(QLOC.LT.QI )GO TO 1150
      CPLOC=(CPLOC*QLOC+PLOC-PINF)/QI
      IF(CPLOC.LE.0.)GO TO 1150
      DELCP=-CPLOC*SRATIO
 1000 DELCX=DELCP*DNX(I)
      DELCY=DELCP*DNQ
      DELCZ=DELCP*DNZ(I)
      DELCL=DELCZ*YB-DELCY*ZB
      DELCM=DELCX*ZC-DELCZ*XC
      DELCN=DELCY*XB-DELCX*YB
      CXB=CXB+DELCX
      CYB=CYB+DELCY
      CZB=CZB+DELCZ
      CLB=CLB+DELCL
      CMB=CMB+DELCM
      CNB=CNB+DELCN
 1150 CONTINUE
      RETURN
 2000 CXB=0.
      CYB=0.
      CZB=0.
      CLB=0.
      CMB=0.
      CNB=0.
      RETURN
      END
```

```
      SUBROUTINE VACPLU(THET,RAD,XMP,PLOC,QLOC)
      COMMON/NOZ/XMJ,GJ,ARJ,AJE,POJ,RJ,TOJ,TURN,DSTAR,AN,THETA,DEXIT,
     1IIMP
      IF(THET.GT.TURN)GO TO 100
      POH=POJ*144.
      PIE=3.14159
      DSTAR=SQRT(AJE/ARJ*4./PIE)
      RHORHE=((1.+(GJ-1.)/2.*XMJ**2)**(-1./(GJ-1.)))
      BGJF=(1.24-0.0040894*TURN)/(2.*(GJ**2)*(1.-COS(TURN/57.2958)))
      XDLIM2=BGJF/RHORHE
      XDLIM3=SQRT(XDLIM2)
      XDLIM=XDLIM2**0.667
      FTHET=(COS(PIE*THET/250.))**10.
      IF(THET.LE.60.)GO TO 5
      FTHET=0.042372*EXP(-0.064*(THET-60.))
    5 CONTINUE
      POW=2.
      DCLINE=RAD/DSTAR
      IF(DCLINE.GE.XDLIM2)GO TO 10
      IF(DCLINE.LE.XDLIM3)GO TO 6
      IF(DCLINE.LE.XDLIM)GO TO 7
      RHORAT=FTHET*0.5*(RHORHE/DCLINE+BGJF/DCLINE**2)
      GO TO 11
    6 CONTINUE
      POW=0.5
      BGJF=RHORHE
      GO TO 10
    7 RHORAT=RHORHE*FTHET*0.5*(1./(SQRT(DCLINE))+1./DCLINE)
      GO TO 11
   10 CONTINUE
      RHORAT=BGJF*(DCLINE**(-POW))*FTHET
   11 IF(RHORAT.GT.RHORHE)RHORAT=RHORHE
      XMP=SQRT(2./(GJ-1.)*((RHORAT**(1.-GJ))-1.))
      PLOC=POH*((1.+(GJ-1.)/2.*XMP**2)**(GJ/(1.-GJ)))
      QLOC=GJ/2.*PLOC*XMP**2
      GO TO 101
  100 XMP=0.
      PLOC=0.
      QLOC=0.
      RHORAT=0.
  101 CONTINUE
      RETURN
  200 FORMAT(1H0,8F15.7)
      END
```

```
      SUBROUTINE AMPL (I,AKX,AKZ,AKY,AKM,AKN,AKL)
C     CALCULATES AMPLIFICATION FACTORS

      REAL NONOZU,NONOZD,NONOZY
      COMMON/UP/NONOZU,XREU,YREU,ZREU,DXNOZU,DYNOZU,DZNOZU,DSTARU
     1,ISIDEU,IBOTHU,RMFSU,AEXU,FMRU
      COMMON/DWN/NONOZD,XRED,YRED,ZRED,DXNOZD,DYNOZD,DZNOZD,DSTARD
     1,ISIDED,IBOTHD,RMFSD,AEXD,FMRD
      COMMON/SIDE/NONOZY,XREY,YREY,ZREY,DXNOZY,DYNOZY,DZNOZY,DSTARY
     1,ISIDEY,IBOTHY,RMFSY,AEXY,FMRY
      COMMON/THCOEF/ CXU,CZU,CYU,CMU,CNU,CLU,CXD,CZD,CYD,CMD,CND,CLD,
     1               CXY,CZY,CYY,CMY,CNY,CLY
      COMMON/TOCOEF/ CXT,CZT,CYT,CMT,CNT,CLT
```

```
      AKX     = 0.0
      AKZ     = 0.0
      AKY     = 0.0
      AKM     = 0.0
      AKN     = 0.0
      AKL     = 0.0
C COMPUTE THRUST MOMENTS FOR ALL CONTROLS USING 2 NOZZLE FOR EACH SIDE
   15 IF (XREU.EQ.0.0.AND.YREU.EQ.0.0.AND.ZREU.EQ.0.0)  GO TO 100
      SAVNOZ = NONOZU
      NONOZU=4.
      CALL THR (1,CXTH,CYTH,CZTH,CLTH,CMTH,CNTH)
      CMTHU=CMTH
      CZTHU=CZTH
      CLTHU=CLTH/4.
      NONOZU = SAVNOZ
   25 IF (XRED.EQ.0.0.AND.YRED.EQ.0.0.AND.ZRED.EQ.0.0)  GO TO 100
      SAVNOZ = NONOZD
      NONOZD=4.
      CALL THR (2,CXTH,CYTH,CZTH,CLTH,CMTH,CNTH)
      CMTHD=CMTH
      CZTHD=CZTH
      CLTHD=CLTH/4.
      CLTHT=CLTHD-CLTHU
      NONOZD = SAVNOZ
   35 IF (XREY.EQ.0.0.AND.YREY.EQ.0.0.AND.ZREY.EQ.0.0)  GO TO 100
      SAVNOZ = NONOZY
      NONOZY=4.
      CALL THR (3,CXTH,CYTH,CZTH,CLTH,CMTH,CNTH)
      CYTHY=CYTH/2.
      CNTHY=CNTH/2.
      NONOZY = SAVNOZ
      SIGNY=1.
      SIGNZ=1.
      SIGNL=1.
      SIGNM=1.
      SIGNN=1.
      PRINT24
      IF(CYT.NE.0.)SIGNY=CYT/ABS(CYT)
      IF(CZT.NE.0.)SIGNZ=CZT/ABS(CZT)
      IF(CLT.NE.0.)SIGNL=CLT/ABS(CLT)
      IF(CMT.NE.0.)SIGNM=CMT/ABS(CMT)
      IF(CNT.NE.0.)SIGNN=CNT/ABS(CNT)
      CZTH=CZTHD*SIGNZ
      CMTH=CMTHD*SIGNM
      CLTH=CLTHT*SIGNL
      CNTH=CNTHY*SIGNN
      CYTH=CYTHY*SIGNY
C IF REAL YAW NOZZLES EXIST USE YAW THRUST TERMS
      IF(IDUTHY.NE.0)GO TO 18
      IF(NONOZY.EQ.0.)GO TO 18
      PRINT222
      CNTH=CNY
      CYTH=CYY
   18 CONTINUE
      IF(NONOZD.EQ.0.) GO TO 20
      IF(NONOZU.EQ.0.)GO TO 30
C PITCH UP AND PITCH DOWN COMBINATIONS
      CLTH=CLU+CLD
      IF(ISIDEU.NE.ISIDED.AND.NONOZU.EQ.NONOZD)GO TO 40
      PRINT225
      CZTH=CZU+CZD
      CMTH=CMU+CMD
      GO TO 70
   20 IF(NONOZU.EQ.0.)GO TO 70
C PURE YAW BRANCHES TO 70
```

```
C PITCH UP JET ONLY COMBINATIONS
      PRINT225
      CZTH=CZU
      CMTH=CMU
      IF(IBOTHU.NE.0)GO TO 70
      CLTH=CLU
      PRINT226
      GO TO 70
   30 CZTH=CZD
C PITCH DOWN JET ONLY COMBINATIONS
      CMTH=CMD
      PRINT227
      IF(IBOTHD.NE.0)GO TO 70
      PRINT228
      CLTH=CLD
      GO TO 70
   40 PRINT229
C PURE ROLL CASE
   70 CONTINUE
      PRINT200,CZTH,CYTH,CLTH,CMTH,CNTH
  200 FORMAT(1H0,*CZTH = *,F15.7,*CYTH = *,F15.7,*CLTH = *,F15.7,*CMTH
     1= *,F15.7,*CNTH = *,F15.7)
      IF (CZTH.NE.0.0)  AKZ = CZT/CZTH
      IF (CYTH.NE.0.0)  AKY = CYT/CYTH
      IF (CMTH.NE.0.0)  AKM = CMT/CMTH
      IF (CNTH.NE.0.0)  AKN = CNT/CNTH
      IF (CLTH.NE.0.0)  AKL = CLT/CLTH
      RETURN
  100 PRINT 105, XREU,YREU,ZREU,XRED,YRED,ZRED,XREY,YREY,ZREY
  105 FORMAT (54H0 ********** NOZZLE COORDINATES NOT INPUT, IMPOSSIBLE ,
     1       45HTO CALCULATE AMPLIFICATION FACTORS **********/ 7X4HXREU,
     2        7X4HYREU,7X4HZREU,7X4HXRED,7X4HYRED,7X4HZRED,7X4HXREY,
     3        7X4HYREY,7X4HZREY/9F11.4/)
      CALL EXIT
  222 FORMAT(1H0,*YAW AMPLIFICATION BASED ON ACTUAL NOZZLES*)
  223 FORMAT(1H0,* PITCH AND ROLL AMPLIFICATION BASED ON SUM OF PITCH UP
     1 PLUS DOWN NOZZLES *)
  224 FORMAT(1H0,*UNLESS OTHERWISE NOTED AMPLIFICATION IS BASED ON 2 ASS
     1UMED NOZZLES IN EACH CONTROL*)
  225 FORMAT(1H0,*PITCH AMPLIFICATION BASED ON PITCH UP NOZZLES*)
  226 FORMAT(1H0,*ROLL AMP BASED ON PITCH UP NOZZLES*)
  227 FORMAT(1H0,*PITCH AMP BASED ON PITCH DOWN JETS*)
  228 FORMAT(1H0,*ROLL AMP BASED ON PITCH DOWN JET DATA*)
  229 FORMAT(1H0,*PURE ROLL PITCH AMP BASED ON 2 JETS PITCH DOWN*)
      END
```

```
      SUBROUTINE INTER(IT,CXB,CYB,CZB,CLB,CMB,CNB)
C     COMPUTES PLUME INTERACTION COEFFICIENTS

      REAL NONOZU,NONOZD,NONOZY
      COMMON/CONST/PIE,RADIAN,GI,RI,GO
      COMMON/A/POW,POW1,PRT,T1,PZT
      COMMON/NOZ/XMJ,GJ,ARJ,AJE,POJ,RJ,TOJ,TURN,DSTAR,AN,THETA,DEXIT,
     1111MP
      COMMON/UP/NONOZU,XREU,YREU,ZREU,DXNOZU,DYNOZU,DZNOZU,DSTARU
     1,ISIDEU,IBOTHU,RMFSU,AEXU,FMRU
      COMMON/DWN/NONOZD,XRED,YRED,ZRED,DXNOZD,DYNOZD,DZNOZD,DSTARD
     1,ISIDED,IBOTHD,RMFSD,AEXD,FMRD
      COMMON/SIDE/NONOZY,XREY,YREY,ZREY,DXNOZY,DYNOZY,DZNOZY,DSTARY
     1,ISIDEY,IBOTHY,RMFSY,AEXY,FMRY
```

```
      COMMON/FLT/MINF,PINF,TINF,ALPH,IOPT,QI,HI,VINF,THRUST,INEXT
      COMMON/INCOF/ CZIDL(5),CZIDH(5),CYIDL(7),CYIDH(7),CMIDL(5),
     1              CMIDH(5),CNIDL(7),CNIDH(7),CLIDL(5),CLIDH(5),ALPHBK,
     2              CZIUH(5),CYIUH(5),CMIUH(5),CNIUH(5),CLIUH(5),
     3              CZIUP(5),CYIUP(5),CMIUP(5),CNIUP(5),CLIUP(5),
     4              CZAUP(5),CYAUP(5),CMAUP(5),CNAUP(5),CLAUP(5),
     5              CZIYL(5),CZIYH(5),CYIYL(5),CYIYH(5),CMIYL(5),
     6              CMIYH(5),CNIYL(5),CNIYH(5),CLIYL(5),CLIYH(5)
      COMMON/ANGLES/ APKUN,APKUL
      DATA CZIDH/-0.21945636E-02,-0.81138462E+00,0.45152689E+01,
     1     0.0898489,-0.0386/,CZIDL/0.40692691E-03,-0.79586561,
     2     4.1104025,0.09e811,-0.0381174/,CMIDL/0.9995276E-03,0.50172873
     3,    -3.0783998,0.08149,0.02144292/,CMIDH/0.43873837E-02,
     4     0.52204966,-3.3771729,0.0772909,0.024562/,
     5     CLIDL/-0.33456378E-04,-0.13211043,0.56917984,0.1160533,
     6     -0.007e9938/,CLIDH/-0.1735783E-02,-0.16281436,0.80261121,
     7     0.1014278,-0.0099926/,CNIDL/0.57745228E-04,-0.2599785,
     8     9.0518929,-86.799011,265.01274,0.1,0.0042811/,
     9     CNIDH/0.34372116E-03,-0.22160433,8.0220161,-79.03936,
     *     246.34384,0.1,0.0039982/,CYIDL/-0.17442548E-03,0.75401156,
     1     -18.271309,163.01416,-481.4272,0.1,0.0073851/,
     2     CYIDH/3.67507291E-03,0.69250011,-17.07346,157.52286,
     3     -477.99347,0.1,0.0089138/
      DATA CZIUH/0.082813e1E-02,-0.15636744, 0.051909076,1.506,-0.118166
     1/,   CYIUH/-0.30982e11E-02,-0.16961923,-0.63981797,0.1,-0.0202618/
     2,    CMIUH/-0.42189836E-03,-0.016864188,0.026014049,0.324136,
     3     0.02144526/,CNIUH/0.13671134E-02,0.079588176,0.26560878,0.1,
     4     0.011962/,CLIUH/-0.10167792E-02,-0.037801275,-0.14711948,0.1,
     5     -0.0062701/
      DATA CZIUP/-0.14674243E-02,-0.28175654,0.4626589,0.30451,-0.044366
     1/,   CYIUP/0.11526641E-02,-1.1443836,1.8681083,0.30629476,
     2     -0.1741246/,CMIUP/0.11666484E-02,0.73166148E-02,0.11444519,
     3     0.30451,0.0140067/,  CNIUP/0.69952445E-03,0.50217076,
     4     -0.71851501,0.34945,0.08844/,CLIUP/-0.55440219E-03,
     5     -0.29058328,0.42193835,0.3446988,-0.05068797/
      DATA CZAUP/42.919744,91.843657,0.4351871,0.0082230815,+1.0/,
     1     CYAUP/-0.0603937,-31.841858,0.15475583,-0.0017003331,-1.0/,
     2     CMAUP/0.059078271,-16.938204,-0.0020654289,5.571072E-5,+1.0/,
     3     CNAUP/0.58634094,-18.9306,-0.01406108,-1.1173664E-04,+1.0/,
     4     CLAUP/-0.043546764,-13.273002,-0.0082230757,8.1505091E-04,
     5           -1.0/
      DATA CZIYL/0.34051625E-02,-0.4768132e,3.8111191,0.06255,-0.011507/
     1,    CYIYL/0.11121532E-02,0.30444694,-2.233286,0.0681612,
     2     0.011487866/,CMIYL/0.29195389E-03,0.02514168,-0.063726203,
     3     0.19726e3,0.0027717/,CNIYL/-0.1744416eE-03,-0.077113171,
     4     0.54073191,0.071304439,-0.002923696/,CLIYL/-0.49126038E-03,
     5     -0.86035957E-02,0.047032185,0.09146498,0.000884723/
      DATA CZIYH/0.012040164,-0.44392664,0.42364434,0.52394,-0.1042558/,
     1     CYIYH/0.27383774E-02,0.15732409,-0.92007718,0.085495,
     2     0.00946358/,CMIYH/0.15355063E-02,0.15259831,-0.99101152,
     3     0.07699184,0.0785273/,CNIYH/-0.34818231E-03,-0.019388966,
     4     0.092934704,0.104315,-0.00135946/,CLIYH/-0.17297994E-02,
     5     -0.079945247,0.57586792,0.06941279,-0.0045044/
      DATA ALPHBK/15.0/

C     APKUN     ANGLE OF ATTACK AT PEAK YAWING MOMENT COEFFICIENT FOR THE
C     APKUL     ANGLE OF ATTACK AT PEAK ROLLING MOMENT COEFFICIENT FOR
C     RMFSD     MOMENTUM RATIO FOR DOWNWARD FIRING JETS
C     RMFSU     MOMENTUM RATIO FOR UPWARD FIRING JETS
C     RMFSY     MOMENTUM RATIO FOR SIDEWAY FIRING JETS
C     FMRD      MASS FLOW RATIO FOR DOWNWARD FIRING JETS
C     FMRU      MASS FLOW RATIO FOR UPWARD FIRING JETS
C     FMRY      MASS FLOW RATIO FOR SIDEWAY FIRING JETS
```

```
      GO TO (10,65,75) IT
   10 IF (NONUZU.LE.0.0)  GO TO 65
      IF (ALPH.GT.ALPHBK)  GO TO 60
      CALL QUAD (FMRU,CZIUP,CZP)
      CALL QUAD (RMFSU,CYIUP,CYP)
      CALL QUAD (FMRU,CMIUP,CMP)
      CALL QUAD (RMFSU,CNIUP,CNP)
      CALL QUAD (RMFSU,CLIUP,CLP)
      CALL AKABD (CZP,CZAUP,APKUZ)
      CALL AKABD (CYP,CYAUP,APKUY)
      CALL AKABD (CMP,CMAUP,APKUM)
      CALL AKABD (CNP,CNAUP,APKUN)
      CALL AKABD (CLP,CLAUP,APKUL)
      IF (ALPH.LT.APKUZ)  GO TO 15
      CALL KABD (ALPH,CZAUP,CZB)
      GO TO 20
   15 CZB    = CZP*SIN(PIE/2.0*(ALPH-APKUZ+20.0)/20.0)**2.0
   20 IF (ALPH.LT.APKUY)  GO TO 25
      CALL KABD (ALPH,CYAUP,CYB)
      GO TO 30
   25 CYB    = CYP*SIN(PIE/2.0*(ALPH-APKUY+20.0)/20.0)**2.0
   30 IF (ALPH.LT.APKUM)  GO TO 35
      CALL KABD (ALPH,CMAUP,CMB)
      GO TO 40
   35 CMB    = CMP*SIN(PIE/2.0*(ALPH-APKUM+20.0)/20.0)**2.0
   40 IF (ALPH.LT.APKUN)  GO TO 45
      CALL KABD (ALPH,CNAUP,CNB)
      GO TO 50
   45 CNB    = CNP*SIN(PIE/2.0*(ALPH-APKUN+20.0)/20.0)**2.0
   50 IF (ALPH.LT.APKUL)  GO TO 55
      CALL KABD (ALPH,CLAUP,CLB)
      GO TO 90
   55 CLB    = CLP*SIN(PIE/2.0*(ALPH-APKUL+20.0)/20.0)**2.0
      GO TO 90
   60 CALL QUAD (FMRU,CZIUH,CZP)
      CALL QUAD (RMFSU,CYIUH,CYP)
      CALL QUAD (FMRU,CMIUH,CMP)
      CALL QUAD (RMFSU,CNIUH,CNP)
      CALL QUAD (RMFSU,CLIUH,CLP)
      GO TO 90
   65 IF (NONUZD.LE.0.0)  GO TO 85
      IF (ALPH.GT.ALPHBK)  GO TO 70
      CALL QUAD (RMFSD,CZIDL,CZB)
      CALL QUART (RMFSD,CYIDL,CYB)
      CALL QUAD (RMFSD,CMIDL,CMB)
      CALL QUART (RMFSD,CNIDL,CNB)
      CALL QUAD (RMFSD,CLIDL,CLB)
      GO TO 90
   70 CALL QUAD (RMFSD,CZIDH,CZB)
      CALL QUART (RMFSD,CYIDH,CYB)
      CALL QUAD (RMFSD,CMIDH,CMB)
      CALL QUART (RMFSD,CNIDH,CNB)
      CALL QUAD (RMFSD,CLIDH,CLB)
      GO TO 90
   75 IF (NONUZY.LE.0.0)  GO TO 85
      IF (ALPH.GT.ALPHBK)  GO TO 80
      CALL QUAD (RMFSY,CZIYL,CZB)
      CALL QUAD (RMFSY,CYIYL,CYB)
      CALL QUAD (RMFSY,CMIYL,CMB)
      CALL QUAD (RMFSY,CNIYL,CNB)
      CALL QUAD (RMFSY,CLIYL,CLB)
      GO TO 90
```

```
   80 CALL QUAD (RMFSU,CZIYH,CZB)
      CALL QUAD (RMFSU,CYIYH,CYB)
      CALL QUAD (RMFSU,CMIYH,CMB)
      CALL QUAD (RMFSU,CNIYH,CNR)
      CALL QUAD (RMFSU,CLIYH,CLB)
      GO TO 90
   85 CYB    = 0.0
      CZB    = 0.0
      CMB    = 0.0
      CNB    = 0.0
      CLB    = 0.0
   90 CXB    = 0.0
C     THE FOLLOWING DATA MUST BE REVERSED IN SIGN SO AS TO CORRECTLY
C     CORRELATE THE BUILT-IN CURVE FIT COEFFICIENT DATA (BASED ON WIND
C     TUNNEL TEST DATA) WITH BODY AXES CONVENTION.
      CZB    = -CZB
      IF(IT.NE.1)RETURN
      CYB    = -CYB
      CNB    = -CNB
      CLB    = -CLB
      RETURN
      END



      SUBROUTINE QUAD (X,C,Y)
C     EVALUATES AN ARRAY OF QUADRATIC CURVE FIT COEFFICIENTS AND
C     COMPUTES Y = C(1)+C(2)*X+C(3)*X**2

      DIMENSION C(1)

C     X         GIVEN INDEPENDENT PARAMETER
C     C         ARRAY OF QUADRATIC CURVE FIT COEFFICIENTS, THE FOURTH OF
C               WHICH (C(4)) IS THE UPPER LIMIT OF X FOR WHICH THE
C               COEFFICIENTS APPLY, THE FIFTH (C(5)) BEING THE Y VALUE AT
C               GREATER X VALUES
C     Y         CALCULATED DEPENDENT PARAMETER

      IF ( X.GT.C(4))  GO TO 10
      Y      = C(1)+C(2)*X +C(3)*X*X
      GO TO 20
   10 Y      = C(5)
   20 RETURN
      END



      SUBROUTINE AKABD (Y,C,X)
C     EVALUATES AN ARRAY OF HYPERBOLIC CURVE FIT COEFFICIENTS AND
C     COMPUTES THE INVERSE SOLUTION, I.E.,
C     WHERE Y = C(1)/(X-C(2))+C(3)+X*C(4), CALCULATES THE VALUE OF X FOR
C     A GIVEN VALUE OF Y

      DIMENSION C(1)

C     Y         GIVEN INDEPENDENT PARAMETER
C     C         ARRAY OF HYPERBOLIC CURVE FIT COEFFICIENTS, THE FIFTH OF
C               WHICH (C(5)) IS THE FACTOR DEFINING THE PROPER ROOT TO
C               BE USED
C     X         CALCULATED DEPENDENT PARAMETER

      DISC   = (Y-C(2)*C(4)-C(3))**2-4.0*C(4)*C(1)
      IF (DISC.LT.0.0)  GO TO 10
      A      = C(3)-C(2)*C(4)-Y
      B      = -2.0*C(4)
      X      = (A+C(5)*SQRT(DISC))/B
      RETURN
```

```
   10 PRINT 11, Y,C
   11 FORMAT (//49H********** ERROR---IMAGINARY ROOTS IN SUBROUTINE
     1        16HAKABD **********/10X3HY =,E14.7/10X3HC =,4E15.7//)
      STOP
      END



      SUBROUTINE KABD (X,C,Y)
C     EVALUATES AN ARRAY OF HYPERBOLIC CURVE FIT COEFFICIENTS AND
C     COMPUTES Y = C(1)/(X-C(2))+C(3)+X*C(4)

      DIMENSION C(1)

C     X         GIVEN INDEPENDENT PARAMETER
C     C         ARRAY OF HYPERBOLIC CURVE FIT COEFFICIENTS
C     Y         CALCULATED DEPENDENT PARAMETER

      Y       = C(3)+X*C(4)
      IF (X.NE.C(2))  Y = Y+C(1)/(X-C(2))
      RETURN
      END



      SUBROUTINE QUART (X,C,Y)
C     EVALUATES AN ARRAY OF QUARTIC CURVE FIT COEFFICIENTS, AND COMPUTES
C     Y = C(1)+C(2)*X+C(3)*X**2+C(4)*X**3+C(5)*X**4

      DIMENSION C(1)

C     X         GIVEN INDEPENDENT PARAMETER
C     C         ARRAY OF QUARTIC CURVE FIT COEFFICIENTS, THE SIXTH OF
C               WHICH (C(6)) IS THE UPPER LIMIT OF X FOR WHICH THE
C               COEFFICIENTS APPLY, THE SEVENTH (C(7)) BEING THE Y VALUE
C               AT GREATER X VALUES
C     Y         CALCULATED DEPENDENT PARAMETER

      IF ( X.GT.C(6))  GO TO 10
      Y       = C(1)+C(2)*X +C(3)*X**X  +C(4)* X**3+C(5)* X**4
      GO TO 20
   10 Y       = C(7)
   20 RETURN
      END
```



```
      SUBROUTINE CCOUPL (IT,CXC,CZC,CYC,CMC,CNC,CLC)
C     CALCULATES CROSS COUPLING NOZZLE INTERACTION COEFFICIENTS

      REAL NONOZU,NONOZD,NONOZY
      COMMON/UP/NONOZU,XREU,YREU,ZREU,DXNOZU,DYNOZU,DZNOZU,DSTARU
     1,ISIDEU,IBOTHU,RMFSU,AEXU,FMRU
      COMMON/DWN/NONOZD,XRED,YRED,ZRED,DXNOZD,DYNOZD,DZNOZD,DSTARD
     1,ISIDED,IBOTHD,RMFSD,AEXD,FMRD
      COMMON/SIDE/NONOZY,XREY,YREY,ZREY,DXNOZY,DYNOZY,DZNOZY,DSTARY
     1,ISIDEY,IBOTHY,RMFSY,AEXY,FMRY
      COMMON/ANGLES/ APKUN,APKUL
      COMMON/FLT/MINF,PINF,TINF,ALPH,IOPT,QI,HI,VINF,THRUST,INEXT
      COMMON/INCOEF/ CXIMU,CZIMU,CYIMU,CMIMU,CNIMU,CLIMU,CXIMD,CZIMD,
     1               CYIMD,CMIMD,CNIMD,CLIMD,CXIMY,CZIMY,CYIMY,CMIMY,
     2               CNIMY,CLIMY
      COMMON/INCOEF/ CXINU,CZINU,CYINU,CMINU,CNINU,CLINU,CXIND,CZIND,
     1               CYIND,CMIND,CNIND,CLIND,CXINY,CZINY,CYINY,CMINY,
     2               CNINY,CLINY
```

```
      GO TO (10,50,60) IT
   10 IF (NONOZU.LE.0.0.OR.NONOZY.LE.0.0)  GO TO 60
      IF (IBOTHU.GT.0.OR.IBOTHY.GT.0)  GO TO 20
      IF (ISIDEU.GT.0)  GO TO 15
      IF (ISIDEY.GT.0)  GO TO 60
      GO TO 20
   15 IF (ISIDEY.GT.0)  GO TO 20
      GO TO 60
   20 CXC    = 0.0
      CZC    = 0.0
      CYC    = 0.0
      IF (ALPH.GT.0.0)  CYC = -CYINY
      CMC    = -CMINU
      IF (ALPH.GT.APKUN)  GO TO 25
      CNC    = 0.5215*(CNINU+CNINY)
      GO TO 35
   25 IF (ALPH.GT.15.0)  GO TO 30
      CNC    = -0.5*(CNINU-CNINY)
      GO TO 35
   30 CNC    = -CNINY
   35 IF (ALPH.GE.APKUL)  GO TO 40
      CLC    = 0.52149*(CLINU)
      GO TO 45
   40 CLC    = 0.5*(CLINU+CLINY)
   45 CONTINUE
      GO TO 70
   50 IF (NONOZD.LE.0.0)  GO TO 60
      IF (IBOTHD.EQ.0)  GO TO 60
      CXC    = 0.0
      CYC    = 0.0
      CZC    = 0.14164*(CZIMD+CZIND)
      CMC    = 0.15818*(CMIMD+CMIND)
      CNC    = 0.0
      CLC    = 0.0
      GO TO 70
   60 CXC    = 0.0
      CZC    = 0.0
      CYC    = 0.0
      CMC    = 0.0
      CNC    = 0.0
      CLC    = 0.0
   70 RETURN
      END


      SUBROUTINE INPUTT(I1)
C     READS INPUT DATA

      REAL NONOZU,NONOZD,NONOZY
      REAL MINF
      COMMON/CONST/PIE,RADIAN,GI,RI,GO
      COMMON/GRP2/DNX(300),DNY(300),DNZ(300),X(300),Y(300),Z(300),SLOC(3
     100),J
      COMMON/UP/NONOZU,XREU,YREU,ZREU,DXNOZU,DYNOZU,DZNOZU,DSTARU
     1,ISIDEU,IBOTHU,RMFSU,AEXU,FMRU
      COMMON/DWN/NONOZD,XRED,YRED,ZRED,DXNOZD,DYNOZD,DZNOZD,DSTARD
     1,ISIDED,IBOTHD,RMFSD,AEXD,FMRD
      COMMON/SIDE/NONOZY,XREY,YREY,ZREY,DXNOZY,DYNOZY,DZNOZY,DSTARY
     1,ISIDEY,IBOTHY,RMFSY,AEXY,FMRY
      COMMON/FLT/MINF,PINF,TINF,ALPH,IOPT,WI,HI,VINF,THRUST,INEXT
      COMMON/REF/SREF,C,B,SCALE,XRE,YRE,ZRE,DXNOZ,DYNOZ,DZNOZ,DXNOZZ,
     1DYNOZZ,DZNOZZ
      COMMON/A/POW,POW1,PRT,T1,PZT
      COMMON/NOZ/XMJ,GJ,ARJ,AJE,POJ,RJ,TOJ,TURN,DSTAR,AN,THETA,DEXIT,
     1IIMP
```

```
      COMMON/INCOF/ CZIDL(5),CZIDH(5),CYIDL(7),CYIDH(7),CMIDL(5),
     1              CMIDH(5),CNIDL(7),CNIDH(7),CLIDL(5),CLIDH(5),ALPHBK,
     2              CZIUH(5),CYIUH(5),CMIUH(5),CNIUH(5),CLIUH(5),
     3              CZIUP(5),CYIUP(5),CMIUP(5),CNIUP(5),CLIUP(5),
     4              CZAUP(5),CYAUP(5),CMAUP(5),CNAUP(5),CLAUP(5),
     5              CZIYL(5),CZIYH(5),CYIYL(5),CYIYH(5),CMIYL(5),
     6              CMIYH(5),CNIYL(5),CNIYH(5),CLIYL(5),CLIYH(5)
      NAMELIST/IN/XMJ,GJ,ARJ,AJE,POJ,RJ,TOJ,NONOZU,XREU,YREU,ZREU,
     1NONOZD,THAFTU,THOUTU,IBOTHU,ISIDEU,XRED,YRED,ZRED,THAFTD,THOUTD,
     2IBOTHD,IEXIT,NONOZY,XREY,YREY,ZREY,THAFTY,THOUTY,IBOTHY,ISIDEY,
     3SREF,C,B,IIMP,THETA,ISIDED
      NAMELIST/FC/ MINF,PINF,TINF,ALPH,IOPT,QI,HI,VINF,INEXT
      NAMELIST/INCOF/ CZIDL,CZIDH,CYIDL,CYIDH,CMIDL,CMIDH,CNIDL,CNIDH,
     1                CLIDL,CLIDH,CZIUH,CYIUH,CMIUH,CNIUH,CLIUH,CZIUP,
     2                CYIUP,CMIUP,CNIUP,CLIUP,CZAUP,CYAUP,CMAUP,CNAUP,
     3                CLAUP,CZIYL,CZIYH,CYIYL,CYIYH,CMIYL,CMIYH,CNIYH,
     4                CNIYH,CLIYL,CLIYH,ALPHBK
C     INPUT DEFINITIONS
C     *****************

C              FORMATTED INPUT

C     SCALE    SCALE FACTOR FOR THE FLAT PLATE SIMULATION DATA
C     DNX, CNY, DNZ    ARRAY OF DIRECTION COSINES OF THE FLAT PLATE
C                      SIMULATION AREAS
C     X, Y, Z  ARRAY OF CENTROIDS OF THE FLAT PLATE SIMULATION AREAS
C              FROM THE CENTER OF GRAVITY, X POSITIVE FORWARD,
C              Y POSITIVE TO THE RIGHT, Z POSITIVE DOWNWARD
C     SLOC     ARRAY OF LOCAL FLAT PLATE SIMULATION AREAS (SQ FT)

C              NAMELIST INCOF (PLUME INTERACTION COEFFICIENTS)
C              NOTE---CURVE FIT DATA IS CONTAINED IN DATA STATEMENTS IN
C              SUBROUTINE INTER.  THAT DATA (BASED ON WIND TUNNEL TESTS)
C              PREDICTS COEFFICIENTS FOR CZ, CY, CN, AND CL OPPOSITE IN
C              SIGN TO THE BODY AXES CONVENTION USED HEREIN.  THE
C              INTERACTION COEFFICIENTS ARE THEN CORRECTED (SEE
C              SUBROUTINE INTER).  THUS, IF INPUTTING NEW DATA, ARRANGE
C              ACCORDINGLY.

C              QUADRATIC CURVE FIT COEFFICIENT ARRAYS
C              (FOR DOWNWARD FIRING JETS)

C     CZIDL    NORMAL FORCE COEFFICIENT AS A FUNCTION OF MOMENTUM RATIO
C              AT LOW ANGLES OF ATTACK (BELOW ALPHBK)
C     CMIDL    PITCHING MOMENT COEFFICIENT AS A FUNCTION OF MOMENTUM
C              RATIO AT LOW ANGLES OF ATTACK (BELOW ALPHBK)
C     CLIDL    ROLLING MOMENT COEFFICIENT AS A FUNCTION OF MOMENTUM
C              RATIO AT LOW ANGLES OF ATTACK (BELOW ALPHBK)
C     CZIDH    NORMAL FORCE COEFFICIENT AS A FUNCTION OF MOMENTUM RATIO
C              AT HIGH ANGLES OF ATTACK, (ABOVE ALPHBK)
C     CMIDH    PITCHING MOMENT COEFFICIENT AS A FUNCTION OF MOMENTUM
C              RATIO AT HIGH ANGLES OF ATTACK (ABOVE ALPHBK)
C     CLIDH    ROLLING MOMENT COEFFICIENT AS A FUNCTION OF MOMENTUM
C              RATIO AT HIGH ANGLES OF ATTACK (ABOVE ALPHBK)

C              (FOR UPWARD FIRING JETS)

C     CZIUP    PEAK NORMAL FORCE COEFFICIENT AS A FUNCTION OF MASS FLOW
C              RATIO AT LOW ANGLES OF ATTACK (BELOW ALPHBK)
C     CYIUP    PEAK SIDE FORCE COEFFICIENT AS A FUNCTION OF MOMENTUM
C              RATIO AT LOW ANGLES OF ATTACK (BELOW ALPHBK)
C     CMIUP    PEAK PITCHING MOMENT COEFFICIENT AS A FUNCTION OF MASS
C              FLOW RATIO AT LOW ANGLES OF ATTACK (BELOW ALPHBK)
C     CNIUP    PEAK YAWING MOMENT COEFFICIENT AS A FUNTION OF MOMENTUM
C              RATIO AT LOW ANGLES OF ATTACK (BELOW ALPHBK)
```

```
C     CLIUP   PEAK ROLLING MOMENT COEFFICIENT AS A FUNCTION OF MOMENTUM
C             RATIO AT LOW ANGLES OF ATTACK (BELOW ALPHBK)
C     CZIUH   NORMAL FORCE COEFFICIENT AS A FUNCTION OF MASS FLOW RATIO
C             AT HIGH ANGLES OF ATTACK (ABOVE ALPHBK)
C     CYIUH   SIDE FORCE COEFFICIENT AS A FUNCTION OF MOMENTUM RATIO
C             AT HIGH ANGLES OF ATTACK (ABOVE ALPHBK)
C     CMIUH   PITCHING MOMENT COEFFICIENT AS A FUNCTION OF MASS FLOW
C             RATIO AT HIGH ANGLES OF ATTACK (ABOVE ALPHBK)
C     CNIUH   YAWING MOMENT COEFFICIENT AS A FUNCTION OF MOMENTUM RATIO
C             AT HIGH ANGLES OF ATTACK (ABOVE ALPHBK)
C     CLIUH   ROLLING MOMENT COEFFICIENT AS A FUNCTION OF MOMENTUM
C             RATIO AT HIGH ANGLES OF ATTACK (ABOVE ALPHBK)
C
C             (FOR SIDEWAY FIRING JETS)
C
C     CZIYL   NORMAL FORCE COEFFICIENT AS A FUNCTION OF MASS FLOW RATIO
C             AT LOW ANGLES OF ATTACK (BELOW ALPHBK)
C     CMIYL   PITCHING MOMENT COEFFICIENT AS A FUNCTION OF MASS FLOW
C             RATIO AT LOW ANGLES OF ATTACK (BELOW ALPHBK)
C     CLIYL   ROLLING MOMENT COEFFICIENT AS A FUNCTION OF MASS FLOW
C             RATIO AT LOW ANGLES OF ATTACK (BELOW ALPHBK)
C     CZIYH   NORMAL FORCE COEFFICIENT AS A FUNCTION OF MASS FLOW RATIO
C             AT HIGH ANGLES OF ATTACK (ABOVE ALPHBK)
C     CMIYH   PITCHING MOMENT COEFFICIENT AS A FUNCTION OF MASS FLOW
C             RATIO AT HIGH ANGLES OF ATTACK (ABOVE ALPHBK)
C     CLIYH   ROLLING MOMENT COEFFICIENT AS A FUNCTION OF MASS FLOW
C             RATIO AT HIGH ANGLES OF ATTACK (ABOVE ALPHBK)
C     WHERE
C     C...(4) IS THE MAXIMUM VALUE OF THE MOMENTUM RATIO FOR WHICH THE
C             COEFFICIENTS C...(1) THRU C...(3) APPLY
C     C...(5) THE VALUE OF THE PARAMETER (CONSTANT) AT VALUES OF
C             MOMENTUM RATIO ABOVE C...(4)
C
C             QUARTIC CURVE FIT COEFFICIENT ARRAYS
C             (FOR DOWNWARD FIRING JETS)
C
C     CYIUL   SIDE FORCE COEFFICIENT AS A FUNCTION OF MOMENTUM RATIO
C             AT LOW ANGLES OF ATTACK (BELOW ALPHBK)
C     CNIUL   YAWING MOMENT COEFFICIENT AS A FUNCTION OF MOMENTUM RATIO
C             AT LOW ANGLES OF ATTACK (BELOW ALPHBK)
C     CYIUH   SIDE FORCE COEFFICIENT AS A FUNCTION OF MOMENTUM RATIO
C             AT HIGH ANGLES OF ATTACK (ABOVE ALPHBK)
C     CNIUH   YAWING MOMENT COEFFICIENT AS A FUNCTION OF MOMENTUM RATIO
C             AT HIGH ANGLES OF ATTACK (ABOVE ALPHBK)
C
C             (FOR SIDEWAY FIRING JETS)
C
C     CYIYL   SIDE FORCE COEFFICIENT AS A FUNCTION OF MASS FLOW RATIO
C             AT LOW ANGLES OF ATTACK (BELOW ALPHBK)
C     CNIYL   YAWING MOMENT COEFFICIENT AS A FUNCTION OF MASS FLOW
C             RATIO AT LOW ANGLES OF ATTACK (BELOW ALPHBK)
C     CYIYH   SIDE FORCE COEFFICIENT AS A FUNCTION OF MASS FLOW RATIO
C             AT HIGH ANGLES OF ATTACK (ABOVE ALPHBK)
C     CNIYH   YAWING MOMENT COEFFICIENT AS A FUNCTION OF MASS FLOW
C             RATIO AT HIGH ANGLES OF ATTACK (ABOVE ALPHBK)
C     WHERE
C     C...(6) IS THE MAXIMUM VALUE OF THE MOMENTUM RATIO FOR WHICH THE
C             COEFFICIENTS C...(1) THRU C...(5) APPLY
C     C...(7) THE VALUE OF THE PARAMETER (CONSTANT) AT VALUES OF
C             MOMENTUM RATIO ABOVE C...(6)
```

C-3

```
C               KABD CURVE FIT COEFFICIENT ARRAYS
C               (FOR UPWARD FIRING JETS)

C       CZAUP   PEAK NORMAL FORCE COEFFICIENT AS A FUNCTION OF ANGLE OF
C               ATTACK AT LOW ANGLES OF ATTACK (BELOW ALPHBK)
C       CYAUP   PEAK SIDE FORCE COEFFICIENT AS A FUNCTION OF ANGLE OF
C               ATTACK AT LOW ANGLES OF ATTACK (BELOW ALPHBK)
C       CMAUP   PEAK PITCHING MOMENT COEFFICIENT AS A FUNCTION OF ANGLE
C               OF ATTACK AT LOW ANGLES OF ATTACK (BELOW ALPHBK)
C       CNAUP   PEAK YAWING MOMENT COEFFICIENT AS A FUNCTION OF ANGLE OF
C               ATTACK AT LOW ANGLES OF ATTACK (BELOW ALPHBK)
C       CLAUP   PEAK ROLLING MOMENT COEFFICIENT AS A FUNCTION OF ANGLE OF
C               ATTACK AT LOW ANGLES OF ATTACK (BELOW ALPHBK)
C       WHERE
C       C...(5) IS THE FACTOR DEFINING THE PROPER ROOT WHEN COMPUTING THE
C               INVERSE SOLUTION OF THE HYPERBOLIC CURVE FIT (CALL TO
C               SUBROUTINE AKABD)

C               NAMELIST IN (NOZZLE DESCRIPTIONS)

C       NONOZU  NUMBER OF UPWARD FIRING NOZZLES (CAUSING PITCH UP)
C               OPERATING IN A SET
C       NONOZD  NUMBER OF DOWNWARD FIRING NOZZLES (CAUSING PITCH DOWN)
C               OPERATING IN A SET
C       NONOZY  NUMBER OF SIDEWAY FIRING NOZZLES (CAUSING YAW)
C               OPERATING IN A SET
C       AMJ     JET MACH NUMBER (NOT REQUIRED, INTERNALLY CALCULATED)
C       GJ      SPECIFIC HEAT OF JET
C       ARJ     EXPANSION RATIO OF JET, EXIT AREA-TO-THROAT AREA
C       AJE     JET EXIT AREA (SQ FT)
C       PCJ     CHAMBER PRESSURE OF JET (PSIA)
C       RJ      JET GAS CONSTANT (R AIR = 53.35)
C       TCJ     JET CHAMBER TEMPERATURE (DEG F)
C       XREU, YREU, ZREU    COORDINATES OF UPWARD FIRING JETS FROM THE
C                           CENTER OF GRAVITY (FT)
C               INPUT VALUES EVEN IF THE NUMBER OF NOZZLES IS ZERO, SO
C               THAT AMPLIFICATION FACTORS CAN BE CALCULATED
C       XRED, YRED, ZRED    COORDINATES OF DOWNWARD FIRING JETS FROM THE
C                           CENTER OF GRAVITY (FT)
C               INPUT VALUES EVEN IF THE NUMBER OF NOZZLES IS ZERO, SO
C               THAT AMPLIFICATION FACTORS CAN BE CALCULATED
C       XREY, YREY, ZREY    COORDINATES OF SIDEWAY FIRING JETS FROM THE
C                           CENTER OF GRAVITY (FT)
C               INPUT VALUES EVEN IF THE NUMBER OF NOZZLES IS ZERO, SO
C               THAT AMPLIFICATION FACTORS CAN BE CALCULATED
C       DEXIT   JET EXIT DIAMETER (FT)
C       SREF    REFERENCE AREA (SQ FT)
C       C       MEAN AERODYNAMIC CHORD (REFERENCE LENGTH) (FT)
C       B       WING SPAN (REFERENCE LENGTH) (FT)
C       THETA   NOZZLE EXIT ANGLE (ANGLE OF BELL MOUTH NOZZLE WALL) (DEG)
C       IIMP    DEFINES THE TYPE OF MATHEMATICAL MODEL TO BE USED,
C             = 1, USE THE EMPIRICAL IMPINGMENT MODEL,
C             = 2, NO IMPINGMENT MODEL USED,
C             = 3, USE THE SEMI-EMPIRICAL IMPINGMENT MODEL (MODIFIED
C                  NEWTONIAN PRESSURES PLUS VACUUM PLUME MODEL)
C       THAFTU  AFTWARD CANT ANGLE OF UPWARD FIRING NOZZLE (DEG)
C       THAFTD  AFTWARD CANT ANGLE OF DOWNWARD FIRING NOZZLE (DEG)
C       THAFTY  AFTWARD CANT ANGLE OF SIDEWAY FIRING NOZZLE (DEG)
C       THOUTU  OUTWARD CANT ANGLE OF UPWARD FIRING NOZZLE (DEG)
```

```
C                POSITIVE NOZZLE CANTED TO THE LEFT
C       THOUTD   OUTWARD CANT ANGLE OF DOWNWARD FIRING NOZZLE (DEG)
C                POSITIVE NOZZLE CANTED TO THE LEFT
C       THOUTY   UPWARD CANT ANGLE OF SIDEWAY FIRING NOZZLE (DEG)
C       IBOTHU   DEFINES WHETHER UPWARD FIRING NOZZLES ARE OPERATING ON
C                ONE OR BOTH SIDES OF THE CENTER OF GRAVITY,
C              = 0, NOZZLES OPERATING ON ONE SIDE ONLY (SET ISIDEU),
C              = 1, NOZZLES OPERATING ON BOTH SIDES
C       IBOTHD   DEFINES WHETHER DOWNWARD FIRING NOZZLES ARE OPERATING ON
C                ONE OR BOTH SIDES OF THE CENTER OF GRAVITY,
C              = 0, NOZZLES OPERATING ON ONE SIDE ONLY (SET ISIDED),
C              = 1, NOZZLES OPERATING ON BOTH SIDES
C       IBOTHY   DEFINES WHETHER SIDEWAY FIRING NOZZLES ARE OPERATING ON
C                ONE OR BOTH SIDES OF THE CENTER OF GRAVITY,
C              = 0, NOZZLES OPERATING ON ONE SIDE ONLY (SET ISIDEY),
C              = 1, NOZZLES OPERATING ON BOTH SIDES
C       ISIDEU   DEFINES SIDE ON WHICH UPWARD FIRING NOZZLES ARE
C                OPERATING,
C              = 0, OPERATING NOZZLES ARE ON THE LEFT,
C              = 1, OPERATING NOZZLES ARE ON THE RIGHT,
C       ISIDED   DEFINES SIDE ON WHICH DOWNWARD FIRING NOZZLES ARE
C                OPERATING,
C              = 0, OPERATING NOZZLES ARE ON THE LEFT,
C              = 1, OPERATING NOZZLES ARE ON THE RIGHT,
C       ISIDEY   DEFINES SIDE ON WHICH SIDEWAY FIRING NOZZLES ARE
C                OPERATING,
C              = 0, OPERATING NOZZLES ARE ON THE LEFT,
C              = 1, OPERATING NOZZLES ARE ON THE RIGHT,

C                NAMELIST FC (FLIGHT CONDITIONS)

C       IOPT     DEFINES THE FLIGHT CONDITIONS BEING INPUTTED,
C              = 1, MACH NUMBER, ANGLE OF ATTACK (DEG) AND ALTITUDE (FT)
C                   ARE INPUTTED,
C              = 2, VELOCITY (FPS), ALTITUDE (FT), AND ANGLE OF ATTACK
C                   (DEG) ARE INPUTTED,
C              = 3, DYNAMIC PRESSURE (PSF), ALTITUDE (FT), AND ANGLE OF
C                   ATTACK (DEG) ARE INPUTTED,
C              = 4, AMBIENT PRESSURE (PSF), TEMPERATURE (DEG F), MACH
C                   NUMBER AND ANGLE OF ATTACK (DEG) ARE INPUTTED
C       MINF     FREE STREAM MACH NUMBER
C       PINF     FREE STREAM AMBIENT PRESSURE (PSIA)
C       TINF     FREE STREAM AMBIENT TEMPERATURE (DEG F)
C       QI       FREE STREAM DYNAMIC PRESSURE (PSF)
C       ALPH     ANGLE OF ATTACK (DEG)
C       HI       ALTITUDE (FT)
C       VINF     VELOCITY (FPS)
C       INEXT    DEFINES CONTENT OF NEXT SET OF DATA,
C              = 1, ALL TYPES OF DATA ARE TO BE INPUTTED,
C              = 2, NOZZLE DEFINITIONS AND FLIGHT CONDITIONS (NAMELISTS IN
C                   AND FC) ARE TO BE INPUTTED,
C              = 3, FLIGHT CONDITIONS ONLY (NAMELIST FC) ARE TO BE
C                   INPUTTED,
C              = 4, NO MORE DATA WILL BE READ IN , PROGRAM STOPS

      GO TO (1,2,3),I1
    1 CONTINUE
      READ(5,2080)SCALE
 2080 FORMAT(8E10.3)
      IF(SCALE.EQ.0.)SCALE=1.
```

```
      J=0
  120 J=J+1
      I=J
      READ (5,2080) DNX(I),DNY(I),DNZ(I),X(I),Y(I),Z(I),SLOC(I)
      X(I)=X(I)*SCALE
      Y(I)=Y(I)*SCALE
      Z(I)=Z(I)*SCALE
      SLOC(I)=SLOC(I)*SCALE*SCALE
      IF(DNX(I).LT.1.1)GO TO 120
      J=J-1
      READ (5,INCOF)
      WRITE (6,INCOF)
      RETURN
    2 CONTINUE
      READ(5,IN)
      IF(IIMP.LE.0)IIMP=3
      IF(IIMP.GT.3)IIMP=3
      WRITE(6,IN)
      TATAFT=TAN(THAFTU/RADIAN)
      TATOUT=TAN(THOUTU/RADIAN)
      DZNOZ=-1.*COS(ATAN(SQRT(TATAFT**2+TATOUT**2)))
      DXNOZ=-1.*DZNOZ*TATAFT
      DYNOZ=-1.*DZNOZ*TATOUT
      DXNOZU=DXNOZ
      DYNOZU=DYNOZ
      DZNOZU=DZNOZ
      TATAFT=TAN(THAFTD/RADIAN)
      TATOUT=TAN(THOUTD/RADIAN)
      DZNOZ=+1.*COS(ATAN(SQRT(TATAFT**2+TATOUT**2)))
      DXNOZ=+1.*DZNOZ*TATAFT
      DYNOZ=+1.*DZNOZ*TATOUT
      DXNOZD=DXNOZ
      DYNOZD=DYNOZ
      DZNOZD=DZNOZ
      TATAFT=TAN(THAFTY/RADIAN)
      TATOUT=TAN(THOUTY/RADIAN)
      DYNOZ=-1.*COS(ATAN(SQRT(TATAFT**2+TATOUT**2)))
      DXNOZ=-1.*DYNOZ*TATAFT
      DZNOZ=-1.*DYNOZ*TATOUT
      DXNOZY=DXNOZ
      DYNOZY=DYNOZ
      DZNOZY=DZNOZ
      RETURN
    3 CONTINUE
      READ(5,FC)
      IF(INEXT.LE.0)INEXT=4
      IF(INEXT.GT.4)INEXT=4
      IF(IOPT.LE.0)IOPT=4
      IF(IOPT.GE.4)IOPT=4
      WRITE(6,FC)
      RETURN
      END
```